ONE-ELECTRON PROPERTIES OF SIMULATED NON-EMPIRICAL WAVEFUNCTIONS

A thesis presented for the degree

of

Doctor of Philosophy

in the

Department of Organic Chemistry

University of Adelaide

Bruce D. Roney, B.Sc.(Hons, Adelaide)

October, 1970.

CONTENTS

SUMMARY

One-Electron Properties of Simulated Non-Empirical Wavefunctions.

B.D. Roney: Ph.D. Thesis, University of Adelaide, 1970.

An approximate, but non-empirical, SCF LCAO-MO scheme for single-determinantal wavefunctions is developed. The formulation of this approach, Simulated Non-Empirical, or SNE, is shown to be intermediate between the NDDO method and a complete *ab initio* treatment.

The CNDO and NDDO schemes are discussed with regard to their invariance to rotation and hybridisation using matrix formulations. From the Mulliken and Ruedenberg approximations to bicentric orbital products in a Slater orbital basis, a direct relationship is established with the CNDO and NDDO methods in a basis of Löwdin orthonormalised orbitals. Expansion of second-order correction terms vindicates previously observed trends in repulsion integral values and serves a warning that errors are likely to arise in the CNDO and NDDO formalisms from failure to allow for integral modification on change of basis.

With the Ruedenberg approximation, a particularly simple transformation may be effected from the set of coulomb integrals in a Slater orbital basis to the full set of two-electron integrals in a Löwdin basis. The SNE scheme is defined in terms of this transformation, with truncation of the integral list to an effective NDDO set. One-

electron integrals are evaluated exactly, or may be approximated by Ruedenberg expansion where appropriate. Care must be excercised with Schmidt orthogonalisation outside a valence orbital basis.

The SNE scheme proves computationally economical, and some of the programming features which contribute to this favourable situation are outlined. Not least in this context is the method of integral evaluation, based on a modified C-function route, and the general features, as well as specific contributions to the evaluation of auxiliary functions, are reviewed.

Calculations on the molecular systems H_2O and NH_3 use the SNE scheme in two variants, whereby three-centre nuclear attraction integrals may be evaluated exactly, or approximated. As well, both minimal and valence orbital bases are employed. Since energy integrals are approximated in the SNE scheme, total energy is discounted as a criterion for optimisation of orbital exponents. Instead, experimental one-electron properties are taken as standards, and extensive calculations are undertaken to obtain, in each case, a set of orbital exponents which enable reproduction of those properties. Further calculations on H_2CO employ a minimal basis and exact nuclear attraction integrals.

All exponent optimisations are successful in that the required match with experimental properties could be achieved to a satisfactory degree. As a consequence, no one variant or basis set

size can be recommended as superior. Experimental error limits are sufficiently broad in most instances to preclude ultimate refinement to a unique exponent set. The functional relationships between exponents and expectation values are remarkably similar for many operators, and this fairly general characteristic also inhibits refinement to a unique set.

From a critical examination of one-electron properties for representative optimised wavefunctions, it is apparent that there exists no consistent correlation, either among the various approaches, or in comparison with *ab initio* wavefunctions. Electron density maps are in support, for, while total densities are remarkably alike, marked differences occur with partitioning to molecular orbital contributions.

Inclusion of higher excited configurations, in a configuration interaction calculation on formaldehyde, has a deleterious effect on dipole moment, and, by inference, on other optimised one-electron property expectation values. Excitation energies are in reasonable accord with observed spectral transitions.

STATEMENT

Except where otherwise stated, the work described in this dissertation is original and to the author's knowledge has not been presented in any other University, either by the author himself, or by any other person.

Bruce D. Roney.

October, 1970.

ACKNOWLEDGEMENTS

The author is glad to have the opportunity of thanking a number of people for their assistance and support.

I am particularly indebted to project supervisor Dr. T.M. Spotswood whose continued encouragement and enthusiasm have played an essential part in the completion of this work. Dr. M.L. Heffernan of Monash University has been equally unstinting in his role of external supervisor. To both I express my gratitude.

Also at Monash University, Drs. F.R. Burden, B.H. James, J.B. Peel, K.R. Roby and Mr. G. Williams have my sincere thanks for their willingness to discuss mutual problems and offer much-appreciated advice. It was Dr. James who kindly provided the integral evaluation routines which formed the prototype for my own efforts.

I am deeply grateful to Mr. W. Pearce of the University of Adelaide Computer Centre, and to Mr. J. Weyland of Control Data (Aust.) for their advice and assistance in matters computational. I would also like to thank Miss R. Coulter for typing this manuscript.

Financial support has come from the award of a Commonwealth of Australia, Department of Supply Post-graduate Studentship, and this is gratefully acknowledged.

INDEX TO TABLES

INDEX TO FIGURES

page.

page

GLOSSARY OF ABBREVIATIONS AND SYMBOLOGY

A.O.	Atomic Orbital
A.V.E.	All Valence Electron
CI	Configuration Interaction
CNDO	Complete Neglect of Differential Overlap
LCAO	Linear Combination of Atomic Orbitals
LOAO	Löwdin Orthonormalised Atomic Orbital
MO	Molecular Orbital
MSO	Molecular Spin Orbital
NDDO	Neglect of Diatomic Differential Overlap
SCF	Self-Consistent Field
SNE	Simulated Non-Empirical
STO	Slater-Type Orbital
ZDO	Zero Differential Overlap
M1	Minimal basis, version 1
M2	Minimal basis, version 2
V1	Valence basis, version 2
V2	Valence basis, version 2

Where more than one usage appears, the relevant type will be obvious from the context.

$a_{rs}^{\gamma\delta\epsilon}$	auxiliary function
A	reference point for one-electron operators, nuclear centre

$\underline{A}$	general matrix, Schmidt orthogonalisation matrix
$\underline{A}^{+}$	transpose of $\underline{A}$
$\underline{A}^{-1}$	inverse of $\underline{A}$
$\underline{A}^{D}$	diagonal of $\underline{A}$
$\underline{A}^{\circ}$	block-diagonal of $\underline{A}$
c_A	scalar quantity representing a monocentric orbital product
$\underline{c}_i$	column vector of atomic orbital coefficients
$\underline{c}$	matrix of atomic orbital coefficients
$C_{\alpha\beta}^{\gamma\delta\varepsilon}(\rho_1,\rho_2)$	C-function
$\underline{d}_i$	as for $\underline{c}_i$
$D_{ab}^{cde}(\rho_1,\rho_2)$	D-function
F	Hartree-Fock operator
$\underline{F}$	Hartree-Fock matrix
G	two-electron part of Hartree-Fock operator
$\underline{G}$	array of two-electron integrals
H	core Hamiltonian operator
$\underline{H}$	array of core Hamiltonian integrals
$\underline{I}$	identity matrix
$I_{\lambda\beta}^{\gamma\delta\varepsilon}(\rho_1,\rho_2)$	auxiliary function
J	coulomb operator

K	exchange operator
n,l,m	atomic orbital quantum numbers
N,L,M	basic charge distribution quantum numbers
$\underline{P}$	orbital population matrix of summed coefficient products
$P_n(\theta)$	auxiliary function
$Q_n(\theta)$	auxiliary function
$\underline{R}$	overlap matrix (new basis)
R	internuclear distance
$R_n(\theta)$	auxiliary function
$\underline{S}$	overlap matrix
$\underline{S}^{-\frac{1}{2}}$	inverse root of $\underline{S}$ ≡ Löwdin transformation matrix
$\underline{T}$	general transformation matrix
$T_{ij}(\rho_1,\rho_2)$	auxiliary function
$\langle x^2 \rangle$	second moment of charge distribution diagonal x component
Z	nuclear charge
z_A	dipole moment (charge centroid) from reference point (nucleus), A.

α	orbital exponent, direction component (usually Cartesian), auxiliary function parameter
β	orbital exponent, core resonance parameter, auxiliary function parameter
γ	auxiliary function parameter
δ	Kronecker delta, auxiliary function parameter
∂	differential
ε	orbital energy, eigenvalue, auxiliary function parameter
χ	atomic orbital, magnetic susceptibility
X	atomic orbital direct product
ϕ	atomic orbital, auxiliary function argument
Φ	atomic orbital direct product
Θ	molecular spin orbital, molecular quadrupole moment
ψ_o	ground state wavefunction
Ψ	determinantal wavefunction
μ	dipole moment
ρ	auxiliary function argument
σ	sigma orbital, nuclear shielding
τ	auxiliary function argument
λ	Löwdin orbital, auxiliary function parameter
Λ	Löwdin orbital direct product.
ζ	orbital exponent

CHAPTER I

THE APPROACH TO THE SIMULATED NON-EMPIRICAL METHOD

I.1. INTRODUCTION.

The decade of the sixties has been a time of increasing activity in quantum-mechanical studies of molecular electronic systems. Advances in spectrometry, exemplified by the availability of instrumentation for, *e.g.* magnetic resonance and induced electron emission studies, have generated an interest in quantum chemistry for the interpretation of the phenomena there observed. A more positive aspect of this stimulus has been the consequent accumulation of experimental data, by which the viability of various approaches to the problem of electronic structure may be assessed through their predictive properties.

The feasibility of such direct comparisons between theory and experiment has been aided by developments in quite a different field, that of computer technology. The importance of the high-speed large-memory digital computer to the quantum chemist needs no emphasis.

As computer capabilities have expanded, so too has the scope of quantum mechanical calculations. At the *ab initio* level, the ability to handle larger atomic basis sets has resulted in more accurate calculations on atoms and small molecules, as well as extending the range to more complex systems not previously amenable

to computation. The situation is by no means optimal, as the labour involved remains prohibitive for molecules of more than moderate complexity.

It is in this latter area that simplifying approximations are necessary, in order to reduce the computational effort to an acceptable level. As in the *ab initio* case, approximate techniques have been extended to studies of larger systems; but, more significant than this change in degree is a change in kind. Calculations on conjugated systems by pi-electron only methods, predominant early in the decade, have been largely superseded by techniques which take account of all bonding electrons.

A common feature in the formulation of these all-valence electron (AVE) methods is their dependence on experimental or empirical parameterisation - the advantages are two-fold, in that:

(a) computational labour is reduced by elimination of tedious integral evaluation, and

(b) the use of atomic data is some guarantee of success at the molecular level.

Against these factors must be balanced an undesirable loss in lucidity. At the *ab initio* level, the attractive, repulsive and kinetic forces which contribute to molecular stability are easily separable, but introduction of atomic ionisation spectral data inexorably mixes energy terms resulting from a process which, in itself, is imperfectly

understood. In addition, the transferability of empirical parameters from molecule to molecule is open to question, particularly in systems where large perturbations might reasonably be expected.

In the ensuing sections of this chapter, we formulate a molecular orbital (MO) treatment which retains much of the computational simplicity of AVE methods, yet, which remains essentially an *ab intio* type approach, in that no empirical parameterisation is required. Strictly speaking, the latter is untrue, both for *ab initio* treatments, and for the present approach; atomic orbital functions are themselves empirical in a molecular environment, and their exponents constitute a set of empirical parameters.

As with the majority of methods currently in use in quantum chemistry, the self-consistent field-linear combination of atomic orbitals - molecular orbitals, or SCF-LCAO-MO, scheme of Roothaan [1] forms a basis for systematic approximation and simplification. An approach similar in nature to the one developed in this work has been dubbed 'simulated non-empirical' (SNE) by its originators [2], and rather than inject a new term into an already overcrowded field, we have retained their nomenclature.

SNE is not simply an attempt to reproduce *ab initio* type results, as the name might suggest. Because total energy should not be a criterion in assessing a wavefunction in which energy integrals have been approximated, we have directed our attention towards the

reproduction of certain one-electron properties, *viz.* molecular dipole and quadrupole moments, diamagnetic susceptibilities, and nuclear diamagnetic shielding. To this end, Chapter III is devoted to an in-depth study of small molecules, which serve to characterise the properties of the SNE method in simultaneously predicting expectation values in good agreement with experiment.

I.2. THE ROOTHAAN SCF-LCAO-MO SCHEME

In 1951, Roothaan [1] formulated the solution of the Hartree-Fock equation,

$$F(1)\ \theta_i(1) = \varepsilon_i\ \theta_i(1) \qquad \underline{\text{I.2.1}}$$

for a closed shell, single determinant wavefunction in the LCAO approximation, by which a molecular orbital, ϕ_i, is expanded as a linear sum of atomic basis functions, X_k, with undetermined coefficients, c_{ki} :

$$\phi_i = \sum_k X_k\ c_{ki} \qquad \underline{\text{I.2.2}}$$

In matrix notation, X_k is a member of the row vector, $\underline{X}$, of atomic functions, and $\underline{c}_i$ is the column vector of coefficients.

$$\phi_i = \underline{X}\ \underline{c}_i \qquad \text{or} \qquad \underline{\phi} = \underline{X}\ \underline{c}$$

where $\underline{\phi}$ is the row vector of MO's and $\underline{c}$ is the complete coefficient matrix. The molecular spin orbitals, or MSO's, θ_i, are the eigenfunctions of I.2.1, and relate to the MOs through the spin functions α and β.

$$\theta_i(1) = \phi_i(1)\,\alpha(1) \qquad \alpha\text{ - spin}$$

$$\overline{\theta}_i(1) = \phi_i(1)\,\beta(1) \qquad \beta\text{ - spin}$$

The wavefunction, Ψ, for the ground state closed shell thus appears as the usual Slater determinant [4] comprising either MSO's or MO's.

$$\underline{\Psi} = \{ (2n)! \}^{-\frac{1}{2}} \mid \theta_i(1)\ \overline{\theta}_i(2) \ldots\ldots \theta_n(2n-1)\ \overline{\theta}_n(2n) \mid$$

$$= \{ (2n)! \}^{-\frac{1}{2}} \mid \phi_i(1)\,\alpha(1)\,\phi_i(2)\,\beta(2) \ldots\ldots$$

$$\phi_n(2n-1)\,\alpha(2n-1)\,\phi_n(2n)\,\beta(2n) \mid$$

The eigenvalues of I.2.1 are the Hartree-Fock orbital energies, ε_i.

Expansion of the Hartree-Fock one-electron operator $F(1)$, leads to:

$$F(1) = H(1) + G(1) \qquad \underline{\text{I.2.3}}$$

The core operator, $H(1)$, accounts for a kinetic contribution through the Laplacian operator, $-\frac{1}{2}\nabla^2 = -\frac{1}{2}(\partial^2/\partial x^2 + \partial^2/\partial y^2 + \partial^2/\partial z^2)$, plus a summation of electron-nuclear attraction potentials, over all atoms, A, of point charge, Z_A, in the molecular system, i.e.

$$H(1) = -\tfrac{1}{2}\nabla^2 + \sum_A Z_A\, r_{iA}^{-1}$$

Electron-electron repulsions are generated via the Coulomb (J_j) and Exchange (K_j) operators, which account for the interaction of the electron with the average field arising from other electrons in the

MO's, ϕ_j (or MSO's θ_j)

$$G(1) = \sum_j (J_j(1) - K_j(1))$$

$$J_j(1)\ \phi_i(1) = \int \phi_j(2)\ \phi_j(2)\ \frac{1}{r_{12}}\ \phi_i(1)\ d\tau_2$$

$$K_j(1)\ \phi_i(1) = \int \phi_i(2)\ \phi_j(2)\ \frac{1}{r_{12}}\ \phi_j(1)\ d\tau_2$$

Note that we assume both atomic and molecular orbitals in real form only. Following the linear variational treatment, I.2.1 is expanded through the LCAO approximation to yield the SCF-LCAO-MO matrix equations of Roothaan [1],

$$\underline{F}\ \underline{c_i} = \underline{S}\ \underline{c_i}\ \varepsilon_i\ , \qquad \underline{\text{I.2.4}}$$

to be solved for the orbital energies, ε_i, and coefficients, $\underline{c_i}$. The details of the expansion need not be repeated here*. The notation is, however, pertinent to our further discussion.

$\underline{F}$ is the matrix of atomic integrals over the Hartree-Fock operator. In analogy to I.2.3,

$$\underline{F} = \underline{H} + \underline{G}$$

where $\underline{H}$, the core matrix, possesses the elements

$$H_{pq} = \langle X_p \mid -\tfrac{1}{2}\nabla^2 \mid X_q \rangle - \sum_A Z_A \langle X_p \mid r_A^{-1} \mid X_q \rangle$$

---

* See, for example ref. 5 and further work cited therein

$\underline{G}$ contains the electronic interactions through

$$G_{pq} = \sum_r \sum_s P_{rs} \left[< X_p X_q \mid X_r X_s > - \tfrac{1}{2} < X_p X_r \mid X_q X_s > \right] , \quad \underline{I.2.5}$$

where $\underline{P}$, the population matrix, is defined by

$$\underline{P} = \sum_i n_i \; \underline{c}_i \; \underline{c}_i^{+} \qquad \underline{I.2.6}$$

$$\text{or} \qquad P_{rs} = \sum_i n_i \; c_{ri} \; c_{si} ,$$

with n_i the occupation number of the MO, ϕ_i

$\underline{S}$ is the matrix of overlap integrals

$$S_{pq} = < X_p \mid X_q >$$

The total electronic energy of the ground state is most conveniently calculated by

$$E_{el} = \sum_i \varepsilon_i + \underline{c}_i^{+} \; \underline{H} \; \underline{c}_i$$

To this must be added the potential energy arising from interactions among the positively charged bare nuclei, separated by the distance, R:

$$E_{nuc} = \sum_A \sum_B Z_A \; Z_B \; R_{AB}^{-1}$$

The dependence of $\underline{F}$ on the coefficients $\underline{c}$, through I.2.5 and I.2.6 necessitates an iterative solution, hence the name "Self-Consistent Field". In the brief review of nomenclature which follows, we adopt lower and upper case indices, respectively, to denote atomic orbitals and centres.

$\langle X_{pA} \mid X_{qB} \rangle \equiv S_{pA,qB}$: overlap integral, one-centre (A = B)
or two-centre (A ≠ B)

$\langle X_{pA} \mid -\frac{1}{2}\nabla^2 \mid X_{qB} \rangle$: Kinetic energy integral, one-centre,
(A = B) or two-centre (A ≠ B)

$\langle X_{pA} \mid r_C^{-1} \mid X_{qB} \rangle$: nuclear attraction - one-centre (A = B = C)
- two centre coulombic (A = B ≠ C)
- two-centre exchange (A = C ≠ B or A ≠ C = B)
- three-centre (A ≠ B ≠ C)

$\langle X_{pA}\, X_{qB} \mid X_{rC}\, X_{sD} \rangle$: electron repulsion - coulomb type
(A = B, C = D)
- non-coulomb (A ≠ B,
C ≠ D)

Subclassifications of the non-coulomb type need not concern us.

It is the evaluation of the integrals above which constitutes the greatest practical difficulty in application of the SCF-LCAO-MO scheme to complex molecular systems. With a basis set of n atomic functions, spread over N nuclei, the number of unique integrals of each type is -

n.N. (n + 1)/2	for nuclear attraction integrals
n(n + 1)/2	for other one-electron integrals
$n(n + 1)(n^2 + n + 2)/8$	for two-electron integrals

Furthermore, the integrals which are generally the most numerous, the non-coulombic repulsions and three-centre nuclear

attractions, are also the most tedious to evaluate.

Some consideration must be given to the iterative SCF stage, also. Whereas the nuclear attraction integrals are absorbed in the core-matrix, which remains constant, the assembly of the Hartree-Fock array requires the complete repulsion integral list at each cycle. Although list processing is considerably less onerous than list assembly, when taken over many iterations involving matrix diagonalisation, itself a procedure roughly proportional to n^3 in labour, the effects are significant.

Within the LCAO-SCF-MO framework, the computational problem can be approached in essentially two ways. Firstly, we can make the integrals easier to evaluate, and there exist several possibilities in this direction. The use of Gaussian functions in place of the more conventional STO's affords some advantage, but against this must be balanced an increase in the size of the basis, if comparable accuracy is to be maintained. Effectively, what is gained on the individual integral, is partially offset by the increased list size. Even contracted Gaussian sets [6], which minimise the latter complication, still require a major computational effort. As a second possibility, approximation of the more difficult integrals is attractive, and we will subsequently examine this approach more closely. Lastly, a related possibility lies in the insertion of experimental data in place of exact integrals; semi-empirical procedures of this nature are more usual in conjunction

with further approximations.

As a second approach to the computation problem, we consider truncation of the integral lists. In particular, the repulsion integrals, proportional to n^4, are of major concern, and, as previously noted, the non-coulombic type constitute the worst bottleneck. The Zero Differential Overlap, or ZDO, approximation, by equating all of the latter type to zero, effectively eliminates the problem, *i.e.*

$$< X_{pA}\, X_{qB} \mid X_{rC}\, X_{sD} > \;=\; \delta_{AB}\, \delta_{CD}$$

$$< X_{pA}\, X_{qB} \mid X_{r}\, X_{sD} > \qquad \underline{\text{I.2.7}}$$

Further, the remaining integrals are frequently replaced by experimentally derived quantities [7, 8], and, as such, form the class of semi-empirical ZDO methods [3].

A more flexible approach to the ZDO approximation can be realised through the Löwdin orthonormal transformation [9], in which the basis set of atomic orbitals $\underline{X}$, is replaced by the transformed set, $\underline{\lambda}$, through

$$\underline{\lambda} \;=\; \underline{X}\, \underline{S}^{-\frac{1}{2}} \qquad \underline{\text{I.2.8}}$$

where $\underline{S}^{-\frac{1}{2}}$ is the inverse root of the overlap matrix in the $\underline{X}$-basis. The MO's are unaffected, since

$$\underline{\phi} \;=\; \underline{X}\, \underline{c} \;=\; (\lambda\, \underline{S}^{\frac{1}{2}})\, \underline{c} \;=\; \underline{\lambda}\, \underline{d}\ ,$$

where $\underline{d} \;=\; \underline{S}^{\frac{1}{2}}\, \underline{c}$, is the coefficient matrix in the new basis. The matrix equation, I.2.4 , is simplified, for, multiplying on the left by

$\underline{S}^{-\frac{1}{2}}$ and inserting $\underline{I} = \underline{S}^{-\frac{1}{2}} \underline{S}^{\frac{1}{2}}$,

$$\underline{S}^{-\frac{1}{2}} \underline{F} (\underline{S}^{-\frac{1}{2}} \underline{S}^{\frac{1}{2}}) \underline{c}_i = \underline{S}^{-\frac{1}{2}} \underline{S} (\underline{S}^{-\frac{1}{2}} \underline{S}^{\frac{1}{2}}) \underline{c}_i \varepsilon_i$$

Hence $$(\underline{S}^{-\frac{1}{2}} \underline{F} \underline{S}^{-\frac{1}{2}}) (\underline{S}^{\frac{1}{2}} \underline{c}_i) = (\underline{S}^{-\frac{1}{2}} \underline{S} \underline{S}^{-\frac{1}{2}}) (\underline{S}^{\frac{1}{2}} \underline{c}_i) \varepsilon_i$$

and $$\underline{F}' \underline{d}_i = \underline{d}_i \varepsilon_i \qquad \text{I.2.9}$$

$\underline{F}' = \underline{S}^{-\frac{1}{2}} \underline{F} \underline{S}^{\frac{1}{2}}$ defines the transformation of one-electron integrals, so that, in the new basis,

$$\underline{H}' = \underline{S}^{-\frac{1}{2}} \underline{H} \underline{S}^{-\frac{1}{2}}$$

$$\underline{P}' = \sum_i n_i \underline{d}_i \underline{d}_i^{+} = \sum_i n_i (\underline{S}^{\frac{1}{2}} \underline{c}_i) (\underline{c}_i^{+} \underline{S}^{\frac{1}{2}})$$

$$= \sum_i n_i \underline{S}^{\frac{1}{2}} (\underline{c}_i \underline{c}_i^{+}) \underline{S}^{\frac{1}{2}} = \underline{S}^{\frac{1}{2}} \underline{P} \underline{S}^{\frac{1}{2}},$$

and for the electron repulsion integrals, the relationship

$$\langle \lambda_i \lambda_j \mid \lambda_k \lambda_l \rangle = \sum_p \sum_q \sum_r \sum_s \langle \chi_p \chi_q \mid \chi_r \chi_s \rangle$$

$$S^{-\frac{1}{2}}_{ip} S^{-\frac{1}{2}}_{jq} S^{-\frac{1}{2}}_{kr} S^{-\frac{1}{2}}_{ls} , \qquad \text{I.2.10}$$

ensures that $\underline{G}$ transforms correctly.

The relationship to the ZDO approximation lies in the form of the matrix equation, I.2.9., and the near-zero values assumed by non-coulombic repulsion integrals* in the λ-basis [10, 11, 12]. We

---

* Strictly speaking, there is no formal division into coulomb and non-coulomb type integrals in a Löwdin orthonormal basis, since each λ is, in general, a linear combination of all elements in $\underline{\chi}$. However,

defer further examination of the relationship until Section I.4.

I.3. ZERO DIFFERENTIAL OVERLAP METHODS

In the previous section we have classified, in a general way, methods by which the excessive computation associated with the *ab initio* treatment of molecular systems may be reduced. Within the class of semi-empirical ZDO methods, perhaps the best documented are the formalisms advanced by Pople et al., the Complete Neglect of Differential Overlap (CNDO), and Neglect of Diatomic Differential Overlap (NDDO) [13]. Both CNDO and NDDO have recently been extensively reviewed [3, 14, 15], and the reader is referred there for details of parameterisation, etc; our immediate concern lies with the approximations used in assembly of the electron-repulsion part of the Fock matrix. Here, and subsequently, an atomic orbital basis of Slater functions will be assumed.

In fact, it is unnecessary to consider the complete repulsion integral, $\langle X_{iA}\, X_{jB} \mid X_{kC}\, X_{lD} \rangle$, but only the overlap distribution, or orbital product, $X_{iA}\, X_{jB}$, since it is the approximation to this

---

*continued
each Lowdin orbital contains as a dominant contribution, just one STO, from which it differs only by the appearance of cusps at other orbital sites, and we classify each λ-basis integral according to the corresponding 'dominant' $\underline{X}$-basis integral.

reduced form which characterises the CNDO and NDDO schemes.

In matrix notation, $X_{iA}\, X_{jB}$ is an element of the exact product matrix,

$$\underline{X} = \underline{X}^{+}\,\underline{X} \quad , \qquad \text{I.3.1}$$

where, as previously, $\underline{X}$ is the row vector of basis functions. In the CNDO treatment, $\underline{X}$ is approximated by the diagonal matrix, $\underline{X}^{D}$, in which all products arising from orbitals on the same atom are equivalent. Hence

$$X_{ij}^{D} = \delta_{ij}\, X_{ij} \qquad \text{I.3.2}$$

is sufficient to define the diagonal nature, but not the equivalence restrictions, which are best specified by considering a local block of $\underline{X}^{D}$ containing only one-centre products,

$$\underline{X}_{A}^{D} = c_{A} \times \underline{I}_{A} \quad , \qquad \text{I.3.3}$$

with c_A a scalar quantity representing the equivalent orbital products, and $\underline{I}_A$ is the coincident block of the identity matrix, $\underline{I}$ (elements δ_{ij}). For first-row atoms, c_A is commonly chosen as the 2s self-product, or averaged over s and p distributions, although the only restriction that need be imposed on c_A is one of atom - rather than orbital-dependency. We therefore treat c_A as a scalar, atom-dependent, but otherwise undefined.

In a like manner, $\underline{X}^{\circ}$ is the NDDO approximation to $\underline{X}$ (exact), and, in matrix notation,

$$X^{o}_{iA,jB} = \delta_{AB} X_{iA,jB} \qquad \text{I.3.4}$$

indicates that all mono-centric products are retained. $\underline{X}^{o}$ is block-diagonal in structure, the dimensions of each block determined by the number of basis functions sited on the pertinent centre. Considering once more an individual local block,

$$\underline{X}^{0}_{A} = \underline{X}_{A}^{+} \underline{X}_{A} \qquad \text{I.3.5}$$

where $\underline{X}_{A}$ is the subset of $\underline{X}$ centred on atom A.

Although CNDO and NDDO were formulated with proper regard to invariance under change of orbital basis, so relevant are invariance criteria to further examination of ZDO, and, ultimately, to the evolution of SNE, that a brief review of the subject* is in order.

If the basis set, $\underline{X}$, is subjected to a linear orthogonal transformation, $\underline{T}$, then the new basis, $\underline{\phi}$, is related to the original through

$$\underline{\phi} = \underline{X}\,\underline{T} \qquad \text{I.3.6}$$

In analogy to I.3.1, the exact orbital product matrix in the new basis is given by

$$\underline{\Phi} = \underline{\phi}^{+}\,\underline{\phi}$$

---

* The particular style of matrix analysis we adopt was inspired by similar work reported by Ruttink [16]

$$= (\underline{X}\ \underline{T})^{+}\ \ (\underline{X}\ \underline{T})$$

$$= \underline{T}^{+}\ (\underline{X}^{+}\ \underline{X})\ \underline{T}$$

$$= \underline{T}^{+}\ \underline{X}\ \underline{T} \qquad \text{I.3.6}$$

Since the reduced product matrices $\underline{X}^{D}$ and $\underline{X}^{O}$ must transform in the same way, their counterparts in the $\underline{\phi}$ set are defined by

$$\underline{\Phi}^{D} = \underline{T}^{+}\ \underline{X}^{D}\ \underline{T}$$

and $$\underline{\Phi}^{O} = \underline{T}^{+}\ \underline{X}^{O}\ \underline{T}$$

Invariancy will be retained only if the approximations remain valid in the new basis (c.f. I.3.2 - 5.), ie.

$$\Phi^{D}_{iA,jB} = \delta_{ij}\ \Phi_{iA,jB} \quad \text{and} \quad \underline{\Phi}^{D}_{A} = c_{A} \times \underline{I}_{A} \qquad \text{I.3.7}$$

$$\Phi^{O}_{iA,jB} = \delta_{AB}\ \Phi_{iA,jB} \quad \text{and} \quad \underline{\Phi}^{O}_{A} = \underline{\phi}^{+}_{A}\ \underline{\phi}_{A} \qquad \text{I.3.8}$$

In essence, the structure of the approximate overlap distribution arrays must not change between bases.

Three types of linear orthogonal transformation need to be considered:-

a. Multi-centre transformations mix orbitals from different centres. Since bi-centric products must inevitably appear in $\underline{\Phi}^{D}$ and $\underline{\Phi}^{O}$, neither of the CNDO and NDDO approximations remain invariant.

b. Hybridisation confines the mixing process to orbitals on the same centre, so that $\underline{T}$ possesses the same overall block-diagonal structure as does $\underline{X}^O$. Since different blocks in $\underline{X}^O$ are not mixed, we need consider only product distributions arising from one centre, and

$$\begin{aligned} \underline{T}_A^+ \; \underline{X}_A^O \; \underline{T}_A &= \underline{T}_A^+ \; \underline{X}_A^+ \; \underline{X}_A \; \underline{T}_A \\ &= (\underline{T}_A^+ \; \underline{X}_A^+) \; (\underline{X}_A \underline{T}_A) \\ &= \underline{\phi}_A^+ \; \underline{\phi}_A \\ &= \underline{\Phi}_A^O \end{aligned}$$

as required by I.3.8. In the case of CNDO,

$$\begin{aligned} \underline{T}_A^+ \; \underline{X}_A^D \; \underline{T}_A &= \underline{T}_A^+ \; (c_A \times \underline{I}_A) \; \underline{T}_A \\ &= c_A \times (\underline{T}_A^+ \; \underline{I}_A \; T_A) \\ &= c_A \times \underline{I}_A \\ &= \underline{\Phi}_A^D \end{aligned}$$

The necessity for the equivalence restriction is apparent, since any other form for $\underline{X}_A^D$ results in off-diagonal elements appearing in $\underline{\Phi}_A^D$. Additionally, $\underline{\Phi}_A^D \equiv \underline{X}_A^D$, so that insensitivity in CNDO repulsion integrals, *ie.* non-directional character, is a direct consequence of hybridisation invariance.

c. Rotation of local axes, as with hybridisation, is confined to orbitals local to each centre, but in a more restricted manner, since components only within a particular s,p,d *etc* grouping are mixed. Consequently, the structure of $\underline{T}$ is reduced block diagonal, the dimensions of each block determined by the number of components $(2l + 1)$ within each subset. Rotational invariance will be satisfied for both $\underline{X}^D$ and $\underline{X}^O$, but we may distinguish a special case of the former, wherein the diagonal elements are equalised only within each subset. Using an obvious notation to denote blocks local to basis functions possessing the same l quantum number,

$$\underline{X}^D_{lA} = c_{lA} \times \underline{I}_{lA}$$

$$\underline{T}^+_{lA}\, \underline{X}^D_{lA}\, \underline{T}_{lA} = \underline{T}^+_{lA}\, (c_{lA} \times \underline{I}_{lA})\, \underline{T}_{lA}$$

$$= c_{lA} \times (\underline{T}^+_{lA}\, \underline{I}_{lA}\, \underline{T}_{lA})$$

$$= \underline{c}_{lA} \times \underline{I}_{lA}$$

$$= \underline{\Phi}^D_{lA} \equiv \underline{X}^D_A$$

Invariance properties and restrictions are summarised below:

Approximation	Invariant to	Restrictions on monocentric products
None	General orthogonal transformations	None
NDDO (Block-diagonal)	Hybridisation Rotation	None
CNDO/B (diagonal)	Rotation	px.px = py.py = pz.pz dxy.dxy = $dz^2.dz^2$ = dxz.dxz =dyz.dyz = $dx^2-y^2.dx^2-y^2$
CNDO/A (diagonal)	Rotation Hybridisation	As above, plus s.s = px.px. = dxy.dxy.

The CNDO/A restrictions are particularly stringent, since the same product distribution must suffice for all orbitals on a given centre. It is precisely this insensitivity to orbital variations which limits the basis to a valence orbital set (the AVE basis). While differentiation between s and p functions may not be

important for first row atoms, it has been reported necessary to distinguish 3d from 3s and 3p orbitals in elements of the second row [17, 18], i.e. to employ a CNDO/B approach.

Although hybridisation invariance criteria are relaxed in passing to CNDO/B, the loss is not serious, as hybrid orbitals, while affording some conceptual advantages, remain essentially an artifice of atomic theory, and are only approximately related to properly localised bond orbitals [19-21]. Provided that rotational invariance is satisfied, the desirable physical properties of independence to both molecular coordinate system and orientation of local axes are retained. Furthermore, CNDO/B possesses sufficient flexibility to admit extension beyond the AVE restriction to minimal (including inner-shell) and expanded (multiple-zeta, promoted AO's) bases.

Quite a different type of partitioning has been advocated by Jug [22] for planar conjugated systems, viz. between orbitals which contribute exclusively to either σ or π MO's. On the premise that $\pi(pz)$ - type functions belong to a symmetry class separate from those of $\sigma(sp^2)$ - type, Jug suggested that the hybrid distributions, $\sigma\sigma$ and $\pi\pi$, should form the diagonal basis for the CNDO approximation, and further, what they should be parametrised differently.* The resultant loss of invariance to both hybridisation and rotation makes the latter

---

* In a related context, differentiation between $\sigma\sigma$ and $\pi\pi$ core resonance parameters has been introduced into excited state calculations [23-25].

a drastic step.

Unless a completely empirical approach to parameterisation is employed, there will always exist some integrals which will have to be initially evaluated in a pure s, p basis, and, therefore, the transformation to the hybrid set must be exactly specified. More correctly for this particular example, specification need be precise only to the orientation of the pz-orbital, since the $\sigma\sigma$ distribution is spherically symmetrical. Provided that this condition is satisfied, invariance losses introduce no special problems beyond those of accounting exactly for off-diagonal overlap distributions which appear on change of basis.

The potential weakness of Jug's approach lies in extension to molecular systems wherein pz-orientation cannot be unambiguously determined, as in non-planar conjugated molecules. Under these circumstances, an inappropriate choice among various possibilities may well be reflected in the quality of the final results.

A more natural approach to the problem of σ-π differentiation is evident through CNDO/B. As an example, we consider the projection of a simple 2s, 2p valence basis of nodeless Slater functions, $\underline{X}$, into the trigonal hybrid set $\underline{\phi}$. We also distinguish between the 2s orbital exponent, α, and 2p exponent, β. Thus

$$\underline{X} = \{ 2s(\alpha) , 2px(\beta), 2py(\beta), 2pz(\beta) \}$$

As a preliminary step, the diagonal products of the CNDO/B

type matrix, $\underline{X}^D$ are expanded in basic charge distributions [26] -

$$2s(\alpha).2s(\alpha) \equiv {}^3S(\alpha)$$

The 2p self-products are made equivalent by trace-averaging ie.

$$2px.2px = 2py.2py = 2pz.2pz$$

$$= \tfrac{1}{3} \mathrm{Tr}\,[\underline{X}^{+}_{2p(\beta)}\ \underline{X}_{2p(\beta)}]$$

$$= \tfrac{1}{3}\,[2px(\beta).2px(\beta) + 2py(\beta).2py(\beta) + 2pz(\beta).2pz(\beta)]$$

$$= \tfrac{1}{3}\,[{}^3S - (\tfrac{3}{2})\,{}^3D\Pi + (3\sqrt{3}/2).{}^3D\Delta + {}^3S - (\tfrac{3}{2}).{}^3I\Pi - (3\sqrt{3}/2).{}^3D\Delta + {}^3S + (3)\,{}^3D\Delta]$$

$$= {}^3S(\beta)$$

$$\equiv 2s(\beta).2s(\beta)$$

From the above, it is evident that trace-averaging over the local block of 2p distributions is exactly equivalent to the self product arising from a 2s function with exponent β. Furthermore, the reason for using the 2s.2s product as an approximation to c_A in I.3.3 is also apparent, since equalising the orbital exponents, α and β, ensures identity with the averaged 2p.2p distributions*, and

---

* This conclusion is true only in the particular basis specified above, ie. nodeless Slater functions. If the 2s orbital is in Schmidt-orthogonalised form, and hence contaminated by inner-she l 1s contributions, the expansion into basic charge distributions is not

hence, equality among the diagonal elements of $\underline{X}^D$.

Using an obvious notation for the hybrid basis,

$$\phi = \{\sigma_1, \sigma_2, \sigma_3, \pi\}$$

is related through $\phi = \underline{X}\,\underline{A}$, where

$$A = \begin{bmatrix} 1/\sqrt{3} & 1/\sqrt{3} & 1/\sqrt{3} & 0 \\ \sqrt{2/3} & -1/\sqrt{6} & -1/\sqrt{6} & 0 \\ 0 & 1/\sqrt{2} & -1/\sqrt{2} & 0 \\ 0 & 0 & 0 & 1 \end{bmatrix}$$

The products in the new basis are:-

$$\sigma_1\sigma_1 = \sigma_2\sigma_2 = \sigma_3\sigma_3 = \tfrac{1}{3} \cdot 3S(\alpha) + \tfrac{2}{3} \cdot 3S(\beta)$$

$$\sigma_1\sigma_2 = \sigma_1\sigma_3 = \sigma_2\sigma_3 = \tfrac{1}{3} \cdot 3S(\alpha) - \tfrac{1}{3} \cdot 3S(\beta)$$

$$\sigma_1\pi = \sigma_2\pi = \sigma_3\pi = 0$$

$$\pi\pi = 3S(\beta)$$

---

* Continued
simply to $3S(\alpha)$, and therefore, $\alpha = \beta$ is not sufficient to ensure identity among the overlap distributions. If the nodeless 2s self product is used to approximate c_A, then it is not truly representative of the orthogonalised 2s orbital in the basis. On the other hand, trace-averaging over all exact distributions introduces 1s character into what are meant to be 2p.2p products. We conclude that this dilemna is best resolved by avoiding it altogether, and maintaining a pure valence basis.

Thus differentiation between 2s and 2p exponents in the original basis has the desired effect in the hybrid basis, since the $\sigma\sigma$ distribution differs from $\pi\pi$ by the admixture of $\frac{1}{3}$. $3S(\alpha)$ in place of $\frac{1}{3}$. $3S(\beta)$. The rotational invariance of this CNDO/B approach is evinced by the spherical symmetry of all products in both bases. As well, the relationship to CNDO/A is apparent through the orbital exponents, whereby all off-diagonal products vanish and identity among the diagonal distributions is regained simply by equating α and β.

Whereas Jug's approach requires an *a priori* decision as to the 'best' hybrids, the CNDO/B treatment affords a rotationally invariant s,p basis which can be projected, *a posteriori*, into an optimum hybrid set *eg.* via Wiberg's bond indices [21, 27]. The advantage of CNDO/B, as we see it, lies in its ability to provide all the properties associated with the hybrid set without forsaking rotational invariance.

The success of CNDO is predicting reasonable ground-state geometries is well-established [17, 18, 28 - 31]. Dipole moments, also, are in reasonable accord with experimental data, provided that an approximate ZDO-type formula is used in their calculation. A reparameterisation of CNDO by Brown and Burden [32], based on a least-squares fit to observed dipole moments has proved successful in further dipole calculations, although some exceptions were noted.

Significantly different dipole moments can be obtained if the CNDO vectors are transformed from the assumed Löwdin basis to the STO set, and used in conjunction with theoretically determined dipole length integrals [33, 34]. In view of this duality, it would appear that the electron distribution is not as well represented by CNDO as approximate dipole calculations suggest. The ZDO-type formula is the more questionable because estimation of other one-electron properties will almost certainly have to proceed via exact integrals and a properly transformed basis.

McWeeny et al [2] have criticised the CNDO and NDDO procedures on the grounds that integrals derived in an STO basis are inserted directly into the approximate Löwdin basis of ZDO. Their objection is not to the omission of significant STO integrals, but to neglect of integral modification in the change of basis. Table I.3.1 is illustrative of the observed trends, whereby one-centre repulsions are generally increased, and two-centre coulomb integrals are decreased. In keeping with the ZDO assumptions, repulsion integrals which involve a bicentric charge distribution assume near-zero values in the Löwdin basis, as previously noted.

McWeeny suggested that certain integrals should be scaled by predetermined average-magnitude-change scale factors to compensate for the basis transformation, but we consider that such a procedure would be too general. Reference to Table I.3.1. indicates that the

Table I.3.1. Repulsion Integrals in STO and LOAO Bases

Integral (a,b)	STO	LOAO	Scale = $\frac{\text{LOAO}}{\text{STO}}$
(kk/kk)	3.81250	3.81968	1.002
(ss/ss)	0.66076	0.78517	1.188
(yy/yy)	0.64582	0.70519	1.092
(zz/zz)	0.64582	0.67152	1.040
(kk/ss)	0.93370	1.04197	1.116
(kk/yy)	0.82064	0.86971	1.060
(kk/zz)	0.82064	0.84018	1.024
(ss/yy)	0.62730	0.70810	1.129
(ss/zz)	0.62730	0.68900	1.098
(yy/zz)	0.57621	0.60250	1.046
(hh/hh)	0.62500	0.68963	1.103
(kk/hh)	0.48772	0.41420	0.849
(ss/hh)	0.44884	0.41169	0.917
(yy/hh)	0.46122	0.41273	0.895
(zz/hh)	0.43625	0.40918	0.938
(h_1h_1/h_2h_2)	0.33684	0.29164	0.866
(kh/kh)	0.00594	0.00012	0.020
(sh/sh)	0.19202	0.00244	0.013
(yh/yh)	0.11265	0.00069	0.006
(zh/zh)	0.05198	0.00092	0.018
(h_1h_2/h_1h_2)	0.07205	0.00263	0.037
(sy/yz)	0.00000	-.00275	∞
(sy/yy)	0.00000	0.00307	∞
(sz/zz)	0.00000	-.04334	∞

a. Integrals for NH_3. The orbital basis is (k,s,x,y,z) on N, h on H.

b. Non-Coulombic integrals in the STO basis are estimated by Ruedenberg approximation [35]. All integrals in the Löwdin basis were obtained from the partially approximated STO set; while there will undoubtedly be some error involved, the scaling factors should be reasonably representative.

scaling factors are far from consistent, and note particularly the incidence of integrals in the Löwdin basis whose STO counterparts are zero by atomic symmetry*.

In the next section the ZDO approximation is formulated in a manner which enables further insight into the problems of basis choice and integral modification.

1.4. OVERLAP EXPANSION APPROXIMATIONS AS A BASIS FOR ZDO

According to Ruedenberg [35], the bicentric overlap distribution, $X_{iA}\, X_{jB}$, may be expanded as a linear sum of one-centre products,

$$X_{iA}\, X_{jB} \simeq \tfrac{1}{2}\, [\, \sum_{k}^{A} S_{kA,jB}\, X_{iA}\, X_{kA} + \sum_{l}^{B} S_{iA,lB}\, X_{jB}\, X_{lB}\,] \qquad \underline{\text{I.4.1.}}$$

where $S_{kA,jB}$ is an element of the overlap matrix, $\underline{S}$, in the X-basis, and the summations extend over all orbitals resident on atoms A and B, as indicated. Whereas I.4.1 is formally exact if the expansion extends over a complete orbital set, we shall be concerned with a restricted basis, and I.4.1 then defines the Ruedenberg approximation.

---

* These integrals are not spurious, but arise from the 'other atom' contributions to each Löwdin orbital, so that the symmetry of nominally mono-centric integrals is not determined by the atomic pure rotation groups, but by molecular symmetry.

If all but leading terms in the summations are omitted, the expansion above reduces to the Mulliken approximation [36] -

$$X_{iA}\, X_{jB} \simeq \tfrac{1}{2} S_{iA,jB} (X_{iA}\, X_{iA} + X_{jB}\, X_{jB}) \qquad \underline{\text{I.4.2}}$$

With the notation of the previous section, wherein $\underline{X}^{O}$ and $\underline{X}^{D}$ are, respectively, block-diagonal and diagonal orbital product matrices, I.4.1 and I.4.2 appear in equivalent matrix form as

$$\underline{X} \simeq \tfrac{1}{2} (\underline{S}\, \underline{X}^{O} + \underline{X}^{O}\, \underline{S}) \qquad \underline{\text{I.4.3}}$$

$$\underline{X} \simeq \tfrac{1}{2} (\underline{S}\, \underline{X}^{D} + \underline{X}^{D}\, \underline{S}) \qquad \underline{\text{I.4.4}}$$

Ruttink [16] has examined the invariance restrictions imposed on the Mulliken and Ruedenberg approximations by localised orthogonal transformation, and shown them to be identical to those found in the CNDO and NDDO formalisms.

Orthogonality of all orbitals on the one centre is implicit in I.4.3 and I.4.4, since otherwise the approximations do not properly reduce to the mono-centric orbital product. This is a point of some consequence in a basis set of Slater functions (as assumed), since orbitals of the same defining l and m quantum numbers, and on the same centre, are not orthogonal, and some procedure must be adopted to make them so. This condition applies not only to the inner-shell interactions of minimal atomic bases, but also to intra-shell conflicts in expanded sets eg. of the multiple-zeta type, wherein complete orthogonality of all orbitals on the same centre must be enforced.

A common procedure, and the one we follow, is the Schmidt method. Despite its name, the Schmidt orthogonalisation procedure is not itself an orthogonal transformation, since, in matrix form, the inverse and transpose are not identical, ie. $\underline{A}^{-1} \neq \underline{A}^{+}$ and $A^{+}\underline{A} \neq \underline{A}\underline{A}^{+} \neq \underline{I}$. The non-orthogonality of $\underline{A}$ is easily illustrated in the case of a simple atomic basis of $\underline{X} = \{1s, 2s\}$ in transformation to the orthogonalised set, $\phi = \{1s', 2s'\}$, by $\underline{\phi} = \underline{X}\,\underline{A}$. Here,

$$\underline{A} = \begin{bmatrix} 1 & -S_{12} & (1 - S_{12}^2)^{-\frac{1}{2}} \\ 0 & & (1 - S_{12}^2)^{-\frac{1}{2}} \end{bmatrix}$$

with S_{12} as the overlap integral $S_{1s,2s}$

$$\underline{A}^{-1} = \begin{bmatrix} 1 & S_{12} \\ 0 & (1 - S_{12}^2)^{\frac{1}{2}} \end{bmatrix}$$

$$\underline{A}^{+} = \begin{bmatrix} 1 & 0 \\ -S_{12}\,(1 - S_{12}^2)^{-\frac{1}{2}} & (1 - S_{12}^2)^{-\frac{1}{2}} \end{bmatrix}$$

and $$\underline{A}^{+}\underline{A} = \begin{bmatrix} 1 & -S_{12}\,(1 - S_{12}^2)^{-\frac{1}{2}} \\ -S_{12}\,(1 - S_{12}^2)^{-\frac{1}{2}} & (1 + S_{12}^2)\,(1 - S_{12}^2)^{-1} \end{bmatrix} \neq \underline{I}$$

We now examine the consequences of non-orthogonality in the Schmidt transformation, $\underline{A}$. The exact orbital product matrix, $\underline{\Phi}$, in the new basis, is given by

$$\underline{\Phi} = \underline{\phi}^{+}\underline{\phi} = \underline{A}^{+}\underline{X}^{+}\underline{X}\underline{A} = \underline{A}^{+}\underline{X}\underline{A} \qquad \text{I.4.5}$$

Hence, the overlap matrix in the ϕ-basis,

$$\underline{R} = \underline{A}^{+}\underline{S}\,\underline{A} ,$$

since all products are exact in the integrals of $\underline{R}$ and $\underline{S}$. The transformation of the Ruedenberg approximation follows from I.4.3 and I.4.5:-

$$\Phi \simeq \underline{A}^{+}\,[\tfrac{1}{2}\,(\underline{S}\,\underline{X}^{o} + \underline{X}^{o}\,\underline{S})]\,\underline{A}$$

$$\simeq \tfrac{1}{2}\,[\underline{A}^{+}\underline{S}\,\underline{X}^{o}\,\underline{A} + A^{+}\,\underline{X}^{o}\,\underline{S}\,\underline{A}]$$

Inserting $\underline{I} = \underline{A}\,\underline{A}^{-1} = (\underline{A}^{+})^{-1}\,\underline{A}^{+}$ into the above,

$$\underline{\Phi} \simeq \tfrac{1}{2}\,[\underline{A}^{+}\underline{S}\,\{\,\underline{A}\,\underline{A}^{-1}\}\,\underline{X}^{o}\underline{A} + \underline{A}^{+}\underline{X}^{o}\,\{\,(\underline{A}^{+})^{-1}\,\underline{A}^{+}\,\}\,\underline{S}\,\underline{A}]$$

$$\simeq \tfrac{1}{2}\,[\{\,\underline{A}^{+}\underline{S}\,\underline{A}\,\}\,\{\,\underline{A}^{-1}\underline{X}^{o}\underline{A}\,\} + \{\,\underline{A}^{+}\underline{X}^{o}\,(\underline{A}^{+})^{-1}\,\}\,\{\,\underline{A}^{+}\underline{S}\,\underline{A}\,\}]$$

$$\simeq \tfrac{1}{2}\,[\underline{R}\,\{\,\underline{A}^{-1}\underline{X}^{o}\underline{A}\,\} + \{\,\underline{A}^{+}\underline{X}^{o}\,(\underline{A}^{+})^{-1}\,\}\,\underline{R}]$$

Invariance requires that

$$\underline{\Phi}^{o} = \underline{A}^{-1}\,\underline{X}^{o}\,\underline{A} = \underline{A}^{+}\underline{X}^{o}(\underline{A}^{+})^{-1}, \qquad \text{I.4.6}$$

for then,

$$\underline{\Phi} \simeq \tfrac{1}{2}\,[\underline{R}\,\underline{\Phi}^{o} + \underline{\Phi}^{o}\underline{R}]$$

Clearly, I.4.6 will be satisfied only if $\underline{A}^{-1} = \underline{A}^{+}$, a condition which is not met in this case. Thus the Ruedenberg approximation is not invariant to Schmidt orthogonalisation; nor, analogously, is the Mulliken approximation.

As a consequence, some care must be excercised in using overlap expansion approximations of this type. Not only is an orthogonalised basis necessary to ensure correct mono-centric reduction, but the Schmidt transformation should be made prior to approximation. We emphasize this point because it is frequently more convenient to orthogonalise after integral lists have been assembled in an unmodified STO basis. A case in point is the core matrix, $\underline{H}$, which, in a non-exact method might be expected to contain both theoretical and approximate integrals. Whereas the demands of computational efficiency argue for *a posteriori* orthogonalisation of the entire assemblage of kinetic energy and nuclear attraction terms, the overlap expansion approximations require that all exact integrals occurring in the mono-centric products should be properly orthogonalised beforehand. The formal correspondence between exact and approximated product distributions, as contained in I.4.3 and I.4.4, is otherwise lost.

Having established the correct basis, we now consider transformation to the assumed ZDO set of Löwdin orthonormalised atomic orbitals (LOAO). The transformation matrix, $\underline{S}^{-\frac{1}{2}}$, is neither local nor orthogonal, and therefore, the overlap expansion approximations will not remain invariant.

Without loss of generality, we choose $\underline{X}$ as the Schmidt-orthogonalised STO basis. Following the notation of section I.2.,

$$\underline{\lambda} = \underline{X}\,\underline{S}^{-\frac{1}{2}}$$

defines the transformation to the Löwdin basis. Hence, for exact orbital products,

$$\underline{\Lambda} = \underline{S}^{-\frac{1}{2}}\,\underline{X}\,\underline{S}^{-\frac{1}{2}}$$

and, taking the Ruedenberg approximation as example,

$$\begin{aligned}\underline{\Lambda} &\simeq \underline{S}^{-\frac{1}{2}}\,[\tfrac{1}{2}\,(\underline{S}\,\underline{X}^{o} + \underline{X}^{o}\,\underline{S})]\,\underline{S}^{-\frac{1}{2}} \\ &\simeq \tfrac{1}{2}\,[\underline{S}^{-\frac{1}{2}}\,\underline{S}\,\underline{X}^{o}\,\underline{S}^{-\frac{1}{2}} + \underline{S}^{-\frac{1}{2}}\,\underline{X}^{o}\,\underline{S}\,\underline{S}^{-\frac{1}{2}}] \\ &\simeq \tfrac{1}{2}\,[\underline{S}^{\frac{1}{2}}\,\underline{X}^{o}\,\underline{S}^{-\frac{1}{2}} + \underline{S}^{-\frac{1}{2}}\,\underline{X}^{o}\,\underline{S}^{\frac{1}{2}}] \qquad \text{I.4.7}\end{aligned}$$

In accord with the original Löwdin definition [7], we write $\underline{S} = \underline{\Delta} + \underline{I}$, where $\underline{\Delta}$ corresponds to the overlap matrix with zeroes along the diagonal. In binomial expansion,

$$\begin{aligned}\underline{S}^{\pm\frac{1}{2}} &= [\underline{I} + \underline{\Delta}]^{\pm\frac{1}{2}} \\ &= \underline{I} \pm \tfrac{1}{2}.\underline{\Delta} + \tfrac{3}{8}\,.\,\underline{\Delta}^{2} \pm \tfrac{5}{16}\,\underline{\Delta}^{3} + \cdots\cdots\end{aligned}$$

and substituting into I.4.7

$$\underline{\Lambda} \simeq \underline{X}^{o} + \tfrac{3}{8}\,[\underline{\Delta}^{2}\,\underline{X}^{o} + \underline{X}^{o}\underline{\Delta}^{2}] - \tfrac{1}{4}\,\underline{\Delta}\,\underline{X}^{o}\underline{\Delta} + R_4 \qquad \text{I.4.8}$$

$$\simeq \underline{X}^{o} + R_2 \qquad \text{I.4.9}$$

where R_n represents additional terms nth order and greater in overlap ($\underline{\Delta}$).

From I.4.9 it is evident that the NDDO approximation to overlap distributions is correct to first order in overlap, within the accuracy of the Ruedenberg approximation. Interchange of $\underline{X}^{o}$ and $\underline{X}^{D}$ enables a similar conclusion to be reached for CNDO, with respect to the Mulliken approximation.

The relationship between NDDO and the Ruedenberg approximation, and again, between CNDO and the Mulliken approximations has been previously recorded [10], but not, to our knowledge, in such a direct manner.

A semi-quantitative estimate of the behaviour of two-electron integrals on change of basis can be made via expansion of the second order terms in I.4.8. We have p reviously noted this behaviour in an actual example in Table I.3.1. For the sake of simplicity, we consider the Mulliken approximation ($\underline{X}^{o} \rightarrow \underline{X}^{D}$), and factor out the identical elements within each local atomic block as X_A (c.f. previous notation as c_A).

For the distinguishable types of product that appear in the Löwdin basis approximate overlap distributions, i.e. bi-centric, mono-centric off-diagonal and diagonal, we may write

$$\Lambda_{iA,jB} = \sum_{C \neq A,B} (\tfrac{3}{8} X_A + \tfrac{3}{8} X_B - \tfrac{1}{4} X_C) \sum_{p}^{c} \Delta_{iA,pC} \, \Delta_{jB,pC}$$

$$\Lambda_{iA,jA} = \sum_{C \neq A} (\tfrac{3}{4} X_A - \tfrac{1}{4} X_C) \sum_{p}^{c} \Delta_{iA,pC} \cdot \Delta_{jA,pC}$$

$$\Lambda_{iA,iA} = \sum_{C \neq A} (\tfrac{3}{4} X_A - \tfrac{1}{4} X_C) \sum_{p}^{c} \Delta^2_{iA,pC} + X_A$$

Whereas sign variation in the overlap ($\underline{\Delta}$) elements may be expected to result in some cancellation, and hence dimunition in the off-diagonal distributions, the summation terms in the diagonal product are invariably positive, and hence ultimate behaviour rests with the relative magnitudes of X_A and X_c. We may see this more clearly if the atomic basis is reduced to two centres, A and B.

$$\Lambda_{iA,jB} = 0$$

$$\Lambda_{iA,jA} = (\tfrac{3}{4} X_A - \tfrac{1}{4} X_B) \sum_p^B \Delta_{iA,pB}\, \Delta_{jA,pB}$$

$$\Lambda_{iA,iA} = (\tfrac{3}{4} X_A - \tfrac{1}{4} X_B) \sum_p^B \Delta^2_{iA,pB} + X_A$$

Two electron integrals $\langle \underline{\Lambda} | \underline{\Lambda} \rangle$ are the direct product of the individual overlap distributions, hence -

$$\langle \Lambda_{iA,jB} \mid \Lambda_{kC,lD} \rangle = 0 \qquad \text{for } A \neq B \text{ and/or } C \neq D$$

To a good approximation, all non-Coulombic integrals should vanish.

$$\langle \underline{\Lambda}_{iA,jA} \mid \underline{\Lambda}_{kB,lB} \rangle = [\tfrac{5}{8} \langle X_A | X_B \rangle - \tfrac{3}{16} \{ \langle X_A | X_A \rangle + \langle X_B | X_B \rangle \}] \sum_q^A \sum_p^B \Delta_{kB,qA} \cdot \Delta_{lB,qA} \cdot \Delta_{iA,pB} \cdot \Delta_{jA,pB}$$

Whatever the consequences of the summation, and we can reasonably expect some cancellation to occur, the terms in square brackets will generally be of comparable magnitude, with the one-centre contributions probably slightly larger. Overall, Löwdin basis repulsion integrals of this type will be rather small.

$$\langle \Lambda_{iA,jA} \mid \Lambda_{kA,lA} \rangle = [\tfrac{9}{16} \langle X_A \mid X_A \rangle + \tfrac{1}{16} \langle X_B \mid X_B \rangle$$

$$- \tfrac{3}{8} \langle X_A \mid X_B \rangle] \sum_{p}^{B} \sum_{q}^{B} \Delta_{iA,pB} \cdot \Delta_{jA,pB} \cdot \Delta_{kA,qB} \cdot \Delta_{lA,qB}$$

We note that cancellation within the square brackets will not be as effective as in the previous example, and, therefore, integrals of this type should be small, but possibly significant*.

$$\langle \Lambda_{iA,iA} \mid \Lambda_{kB,kB} \rangle = \langle X_A \mid X_B \rangle + [\tfrac{5}{8} \langle X_A \mid X_B \rangle - \tfrac{3}{16} \{ \langle X_A \mid X_A \rangle$$

$$+ \langle X_B \mid X_B \rangle \}] \sum_{q}^{A} \sum_{p}^{B} \Delta^2_{kB,qA} \cdot \Delta^2_{iA,pB}$$

In contrast to the integral $\langle \Lambda_{iA,jA} \mid \Lambda_{kB,lB} \rangle$, that above must be positive in its summations, and any departure from $\langle X_A \mid X_B \rangle$ will be determined solely by the relative magnitudes of the mono-centric and bi-centric terms. At normal bonding distances, and definitely for larger separations, we anticipate a nett negative result in the bracketed contributions, and hence a decrement from $\langle X_A \mid X_B \rangle$.

---

* Integrals of this type are retained in the Intermediate Neglect of Differential Overlap, or INDO, formalism [37], which we have not yet had occasion to mention. Since INDO contains features common to both CNDO and NDDO, it introduces no new issues to the discussion.

$$\langle \Lambda_{iA,iA} \mid \Lambda_{kA,kA} \rangle = [\tfrac{9}{16} \langle X_A \mid X_A \rangle + \tfrac{1}{16} \langle X_B \mid X_B \rangle - \tfrac{3}{8} \langle X_A \mid X_B \rangle] \sum_{p}^{B} \sum_{q}^{B} \Delta^2_{iA,pB} \cdot \Delta^2_{kA,qB} + \langle X_A \mid X_A \rangle$$

A similar expression holds for the case $i = k$. As previously, the summations are positive, as should be the resultant of the bracketed terms. Consequently, the STO integral value, $\langle X_A \mid X_A \rangle$, will be incremented.

In its qualitative aspects, the foregoing illustrates the essential validity of the CNDO formalism, with the possible exception of significant mono-centric integrals which should be accounted. If the conclusions above are generalised to larger atomic bases and the Ruedenberg approximation, then observed trends in integral values upon change of basis are fully substantiated (c.f. Table I.3.1).

While I.4.9 ensures the validity of the 'mixed' bases criticised by McWeeny et al [2], their comments on integral modification are undoubtedly relevant if accuracy beyond the first order in overlap is desired. To this end, one could estimate second-order corrections in a manner similar to that above, but, in terms of computational effort, there is little extra involved in working directly with the transformation I.4.7. If the Löwdin orbital products are fully simulated by this latter procedure, only those deficiencies inherent in the Ruedenberg or Mulliken approximations will produce departures from the exact distributions.

I.5. FORMULATION OF THE SIMULATED NON-EMPIRICAL SCHEME

Development of a reasonable approximation to exact overlap distributions in a Löwdin orbital basis has been discussed in the previous section. In particular, the modifications necessary to compensate for change of basis are exactly expressible, via the Ruedenberg approximation, for two-electron integrals as

$$\langle \lambda_{iA}\,\lambda_{jB} \mid \lambda_{kC}\,\lambda_{lD}\rangle \simeq \tfrac{1}{4} \sum_{M}\sum_{N} \sum_{p}^{M}\sum_{q}^{M}\sum_{r}^{N}\sum_{s}^{N} \langle \chi_{pM}\,\chi_{gM} \mid \chi_{rN}\,\chi_{sN}\rangle$$

$$\cdot\left(S^{\frac{1}{2}}_{iA,pM}\cdot S^{-\frac{1}{2}}_{jB,qM} + S^{-\frac{1}{2}}_{iA,pM}\cdot S^{\frac{1}{2}}_{jB,qM}\right)\left(S^{\frac{1}{2}}_{kC,rN}\cdot S^{-\frac{1}{2}}_{lD,sN} + S^{-\frac{1}{2}}_{kC,rN}\cdot S^{\frac{1}{2}}_{lD,sN}\right) \qquad \text{I.5.1}$$

Furthermore, we anticipate that the approximation, $\underline{\Lambda} = \underline{\Lambda}^{o}$, whereby all bicentric products vanish is reasonable in view of the deficiencies likely to occur in I.5.1. Hence, for repulsion integrals,

$$\langle \lambda_{iA}\,\lambda_{jB} \mid \lambda_{kC}\,\lambda_{lD}\rangle \simeq 0 \quad \text{for } A \neq B \text{ and/or } C \neq D.$$

In matrix notation, the direct product matrix ($\underline{\Lambda}^{o} \times \underline{\Lambda}^{o}$) defines the array of non-vanishing repulsion integrals.

We believe that the SNE treatment of repulsion integrals, as defined above through I.5.1 and I.5.2, should be superior to that of NDDO, wherein no compensation is allowed for the Löwdin-type ZDO basis. In addition, our formulation of the SNE approach has an advantage over that proposed by McWeeney in that integral modifications

are directly dependent on the features of the overlap distribution, as opposed to predetermined average scaling factors.

The SNE approximation introduces considerable simplification into the generation and handling of repulsion integrals. Not only is exact calculation of the most difficult integrals avoided (which would be true of any approximation), but the integral list in both initial STO and transformed LOAO bases comprises only coulomb-type repulsions.

Among non-empirical methods, the latter property is apparently unique to SNE. Whereas omission of non-coulombic integrals in the Löwdin basis is a direct consequence of near-zero values, other integral approximations require a complete list in the initial Slater set, followed by the transformation I.2.17. However, the SNE scheme allows transition from truncated STO set to truncated LOAO set without that intermediate expansion, and consequently, with a significant reduction in effort. The innermost terms in the summations of I.5.1 are scarcely more tedious than those arising in the complete transformation, I.2.17, while summation ranges, involving, at most, orbitals from two atomic centres, are substantially contracted.

One-electron core integrals we evaluate as they occur in the Hamiltonian. Of these, only three-centre nuclear attractions are at all tedious to evaluate from first principles, and we have therefore treated them at two levels - by Ruedenberg approximation and by

an exact procedure. In contrast to our treatment of two-electron integrals, the core integrals are more conveniently transformed to the Löwdin basis *in toto* from the entire assemblage in the orthogonalised STO set.

The decision to treat the core matrix elements as we do was not taken lightly, since the inclusion of valence-state atomic ionisation data in preference to exact integrals is undoubtedly responsible for the success enjoyed by semi-empirical schemes. On the otherhand, the existing spectral constants do not easily lend themselves to the parameterisation of expanded orbital bases. As well, the ubiquity of the β-parameter formulation in π-only treatments foreshadows similar difficulties in extension to an all-electron method. At this stage of development, a formal treatment of the core matrix appears desirable.

We therefore place the simulated Non-Empirical method as intermediate in complexity between semi-empirical ZDO formalisms and the *ab initio* type. Table I.5.1 lists the main features in compasison with other treatments.

While SNE wavefunctions will be less flexible with parameterisation only through orbital exponents, optimisation to agreement with experimental one-electron properties should be a practical proposition, provided that individual calculations are not too laborious. Exponent variation of this kind introduces problems not encountered in the more conventional orbital exponent optimisation

Table I.5.1. Heirarchy of SCF-MO Methods

Type	Basis		Core Integrals	Repulsion Integrals		
	Initial	Final		Exact	Approxi-mate	In Basis Trans-formation
ab initio	STO	LOAO	Exact	All	-	All
	STO	STO	Exact	All	-	-
Near *ab initio* (Alternative Approximations)	STO	LOAO	Exact	Coulomb-Type	All Others	All
	STO	STO	Exact	Coulomb-Type	All Others	-
SNE - this work	STO	LOAO	Exact or Approxi-mate	Coulomb-Type	-	Coulomb-Type
SNE - McWeeny	STO	LOAO	Exact	Coulomb-Type	-	Scaled to Simulate
NDDO	STO	ZDO	Semi-empirical	Coulomb-Type	-	-
CNDO	STO	ZDO	Semi-empirical	S-type Coulomb	-	-

procedure of energy minimisation. By this latter method, orbital exponents should always reduce to an unique set, i.e. with zero degrees of freedom remaining at optimisation, but, using one-electron properties as criteria, one can hope, at best, to lose just one degree of freedom per operator, and, perhaps, not even this should the functional variations of two or more expectation values exhibit near-linear dependence as they approach the experimental ranges. As well, insensitivity to exponent variations, coupled with large experimental error bounds, can do much to reduce the effectiveness of the optimisation procedure.

However, energy minimisation should not be used as an optimisation procedure where Hamiltonian integral approximations exist, as they do in the SNE scheme, unless the energy differences thereby introduced remain reasonably constant. Since it is our experience that errors arising from Ruedenberg approximation are quantitatively unpredictable, there appears no alternative to one-electron property optimisation*, despite the restrictive features which we have outlined above. Therefore, we have concentrated our

---

* One might also argue that even *ab initio* calculations in the SCF LCAO-MO approach make no account of electron correlation energy. While this error should be unimportant for one-electron properties at or near the Hartree-Fock limit, minimal bases such as we envisage are usually not flexible enough to bridge the gap to that limit. Since the energy errors arising therefrom may have a deleterious effect on

efforts on exponent variation to reproduce available experimental data, and it is on the degree of success achieved in this enterprise that we base our assessment of the SNE formalism as a viable molecular orbital method.

---

* continued
electron distribution, and hence on one-electron properties, we feel that our attempt to directly duplicate experimental data should produce a more realistic distribution.

II. THE MECHANICS OF THE SIMULATED NON-EMPIRICAL METHOD

II.1 GENERAL CONSIDERATIONS

In the previous chapter we have concentrated our attention on reduction in computational effort through systematic approximation within the theoretical framework. However, in this age of high-speed digital computers, concern is not so much with the amount of labour involved as with the consequences of that effort, viz. the cost. The personal effort in preparation of input is not substantially different between a simple Hückel and a highly sophisticated *ab initio* program. But the economics of the subsequent computations are highly significant. So spectacular have been the recent improvements in electronic data processing capabilities that computer technology is rapidly approaching a stage where processing cost is the ultimate justification for the retention of approximate methods. However, until sufficient time and resources become more generally available, *ab initio* calculations cannot reasonably be extended into those domains where empirical and semi-emprical schemes are predominantly employed.

Even at the same level, order of magnitude differences may exist between programs designed to carry out identical calculations, simply through the use of computational algorithms well adapted to source language and hardware features.

This is not to say that the program should assume an importance approaching that of the method upon which it is based, but, if a particular theoretical formalism is to achieve its full potential, then the methods by which optimum performance can be realised merit some consideration. The importance of efficient computational routes and overall program design have been adequately covered by Clementi [38] and others [39, 40]. At a more basic level, an appreciation of the relationships between source language and machine code operations is essential if proficiency in the former is to be realised.

However, we do not intend a treatise on programming technique, but rather to emphasize the considerations which led us to incorporate certain features into our master program system. From our experiences with external programs disseminated through Quantum Chemistry Program Exchange, it would appear that the combination of features, if not some of the ideas themselves, are novel. We present below only a few of the more isolated aspects - a more general description is to be found in Appendix A.2.

a. Source Language

FORTRAN was the obvious choice, primarily because it is a high-level arithmetic-oriented language which is almost universally transferrable among computer installations. Object code (COMPASS, in our case) affords greater flexibility and efficiency, but, as a

register operation language, is distinctly more cumbersome, and, furthermore, local to the particular computer type. We did, however, adapt certain FORTRAN sections to the COMPASS language when the original versions proved inefficient, on occasion using substantially different algorithms more suited to the extra features of object code.

b. Overlay* Program Structure

Recourse to a linked program structure proved a matter of necessity, purely through the sheer bulk of coding (some 14,000 statements). While computational economy is little affected by this procedure, code modification can usually be performed within the local substructure, independently of the major portion of the total program system.

c. Storage/Output

Apart from essential information, which may be selectively printed, most of the intermediate items, integral arrays etc., are stored on magnetic tape, from which they may be extracted, or used in

---

* The Control Data 6400 Scope 2 Operating System offers two alternatives for program sequencing. SEGMENT employs relocatable code and performs linkage at execution time i.e. dynamic loading. OVERLAY mode generates absolute code prior to execution, and program sequencing therefore requires only a very elementary (and fast) loading operation.

a subsequent RESTART operation, such as initialisation or extension of configuration interaction. Recognition of tape-stored data is facilitated by an extended sequence of double records, the first of which contains a (maximum) 10-character mnemonic for the type (e.g. OVERLAPS, EXPONENTS, F-MATRIX), plus the word length of the succeeding data record.

d. Lower Triangle Linear Arrays

All symmetric matrices, including the super-matrix of Coulomb repulsion integrals, are stored in linear form as the lower triangle packed by rows. The location of the square matrix element (i,j) is found in the linear sequence by $j + i(i-1)/2$ for $i > j$. Not only does this procedure avoid redundancies in core storage, but it also speeds up matrix manipulation, since FORTRAN is not particularly efficient at handling double (and higher order) indexing.

e. 'Reverse' Matrix Assembly

We use the term 'reverse' in the sense that the computational procedure is not that implied by the algebraic statement. In particular, the algebraic formula for the repulsion elements of the F-matrix is (c.f. Section I.2).

$$F_{ij} = (H_{ij}) + \sum_k \sum_l P_{kl} \, [(ij/kl) - \tfrac{1}{2} (ik/jl)]$$

implying that the elements of F are formed over the ranges of i and j

by 'inner' summation over the indices k and l. Instead we process the unique repulsion integral list over the proscribed ranges of i,j,k and l, and, using index permutations, insert into the proper F-array location the corresponding product of P-element and repulsion integral.

e.g.

Indices of* Integral	Permuted† Indices	F-element	Term added to F-element
(ij/kl)	(ij/kl)	F_{ij}	$2\ P_{kl}$ (ij/kl)
	(kl/ij)	F_{kl}	$2\ P_{ij}$ (kl/ij)
	(ij/kl)	F_{ik}	$-\frac{1}{2}\ P_{jl}$ (ij/kl)
	(ji/kl)	F_{ik}	$-\frac{1}{2}\ P_{il}$ (ji/kl)
	(ij/lk)	F_{il}	$-\frac{1}{2}\ P_{jk}$ (ij/lk)
	(ji/lk)	F_{jl}	$-\frac{1}{2}\ P_{ik}$ (ji/lk)

* We have outlined above only the most general case for i,j,k and l all different. If equalities exist among the indices, fewer permutations are required and the numerical coefficients in the final column may change. At the other extreme, for example, where i=j=k=l, the term added to the unique element F_{ii} is $\frac{1}{2}\ P_{ii}$ (ii/ii).

† Note that not all permutations need to be considered. Since the repulsion integrals are stored uniquely as the (super-matrix) lower triangle, as are $\underline{F}$ and $\underline{P}$, it is immaterial whether the formal element F_{ij} or F_{ji} is formed, provided that only one of the pair is processed.

We consider that those features above, and our techniques of integral evaluation to be described in the next section, have been highly successful in maintaining computational effort at a very reasonable level. For small molecular systems, such as valence basis H_2O where we have achieved execution times of the order 1 - 2 seconds*, our SNE calculations are hardly less economical than CNDO-type, despite a substantial difference in the complexity of the underlying formalisms.

II.2 EVALUATION OF ATOMIC INTEGRALS†

The general remarks of the previous section apply equally to the evaluation of atomic integrals. While the essentially manipulative features described therein contribute considerably to our favourable computational times, the part played by integral evaluation routines deserves some mention.

As we have approached the problem, integral determination divides naturally into two stages.

---

* The operations span for that execution time covers initial input of atom coordinates, requested orbital types and control variables through integral generation and iteration to final output of the SCF wave-function and calculated dipole moment.

† For the C-function route we are indebted to B.H. James, who brought to our attention the Russian literature [46,47] and provided us with his prototype routines.

a. Evaluation of basic integrals is accomplished in rectangular diatomic axes, consisting of parallel right-handed Cartesian systems with common Z-axis connecting the two atomic centres*. The limiting case of one-centre orbital products occurs when the two axis systems coincide.

We have followed the C-function route [41-43], utilising a combination of the analyses presented by Fraga [44,45] and Klimenko and Dyatkina [46,47]. For a general one-electron operator, P, the one-electron integral appears as

$$\langle X_A \mid P \mid X_B \rangle = k_A . k_B . \nu^{(n_A+\frac{1}{2})} . \nu^{-\omega} . F(\phi)\ D_{ab}^{cde}\ (\rho_A, \rho_B)$$

In the usual prolate spheroidal coordinates [26], ξ, η, ϕ

$$P = (R/2)^{\omega}\ (\xi+\eta)^{\alpha'}\ (\xi-\eta)^{\beta'}\ (1+\xi\eta)^{\gamma'}\ (1-\xi\eta)^{\delta'}\ (\xi^2-1)^{\varepsilon'}$$

$$(1+\eta^2)^{\varepsilon'}\ f(\phi)$$

R is the internuclear distance

---

* Our system differs slightly from the conventional choice [26], in which the second set of axes are in a left-handed arrangement. We consider the completely parallel arrangement more natural, since it reduces without axis reversal to the one-centre example. Integrals in the two systems are related through orbital quantum numbers on the second centre by $(-1)^{l+|m|}$.

$$F(\phi) = \int_0^{2\pi} f(\phi).g_A(\phi).g_B(\phi).d\phi$$

where $g_A(\phi)$ is the ϕ-dependent part of the orbital on centre A.

Fraga [45] has tabulated $F(\phi)$ vs. $f(\phi)$ for complex spherical harmonics; for the real orbitals in use here, our tabulation in Appendix A-1 should be consulted.

$$k = \frac{2^{n-l-\frac{1}{2}} \cdot (2l)!\ (2l+1)^{\frac{1}{2}}.}{1!\ [(2n)!\ (l-|m|)!\ (l+|m|)!]^{\frac{1}{2}}}$$

$$\nu = \zeta_A/\zeta_B \qquad \rho_A = \zeta_A.R \qquad \rho_B = \zeta_B.R$$

$$D_{ab}^{cde}(\rho_A,\rho_B) = \sum_p \sum_q c_p.c_q\, C_{\alpha+2p,\ \beta+2q}^{\gamma-2p,\ \delta-2q,\ \varepsilon}(\rho_A,\rho_B)$$

$$c_0 = 1$$

$$c_p = \frac{(l-|m|)\ (l-|m|-1)....(l-|m|-2p+1) \cdot (-1)^p}{2^1.2^2.2^3...2^p \cdot (2l-1)(2l-3)....(2l-2p+1)}$$

$$\alpha = n_A - l_A + \alpha'$$

$$\beta = n_B - l_B + \beta'$$

$$\gamma = l_A - |m_A| + \gamma'$$

$$\delta = l_B - |m_B| + \delta'$$

$$\varepsilon = \tfrac{1}{2}(|m_A| + |m_B|) + \varepsilon'$$

$$\rho = \tfrac{1}{2}(\rho_A + \rho_B)$$

$$\tau = (\rho_A - \rho_B) / (\rho_A + \rho_B)$$

Thus the parameters of the C-function are directly related to the orbital quantum numbers and the defining exponents of the operator, P. In its analytical form

$$C_{\alpha\beta}^{\gamma\delta\varepsilon}(\rho_A,\rho_B) = (\rho_B/2)^{\alpha+\beta+\gamma+\delta+2\varepsilon+1} \int_1^{\infty} d\xi \int_{-1}^{1} e^{-\rho\xi-\eta\rho\tau}$$

$$(\xi+\eta)^{\alpha}(\xi-\eta)^{\beta}(1+\xi\eta)^{\gamma}(1-\xi\eta)^{\delta}(\xi^2-1)^{\varepsilon}(1-\eta^2)^{\varepsilon}\, d\eta$$

For the one-electron integrals of interest, we may write

$a = n_A - l_A$, $b = n_B - l_B$, $c = l_A - |m_A|$, $d = l_B - |m_B|$, $e = |m_A| = |m_B|$

and hence, [41,47]

(1) Overlap

$$\langle X_A|X_B\rangle = 2k_A.k_B\, \nu^{n_A+\frac{1}{2}}\, D_{ab}^{cde}(\rho_A,\rho_B)$$

(2) Kinetic Energy

$$\langle X_A|-\tfrac{1}{2}\nabla^2|X_B\rangle = -\zeta^2.k_A.k_B\,\{\nu^{n_A+\frac{1}{2}}\, D_{ab}^{cde}(\rho_A,\rho_B)$$

$$-2n_A\,\nu^{n_A-\frac{1}{2}}\, D_{a-1,b}^{cde}(\rho_A,\rho_B) + (n_A+l_A)(n_A-l_A-1)\, D_{a-2,b}^{cde}(\rho_A,\rho_B)\}$$

(3) Exchange Nuclear Attraction

$$\langle X_A|-Z_A r_A^{-1}|X_B\rangle = -2Z_A.k_A.k_B\,\nu^{n_A-\frac{1}{2}}\, D_{a-1,b}^{cde}(\rho_A,\rho_B)$$

$$\langle X_A|-Z_B r_B^{-1}|X_B\rangle = -2Z_B.k_A.k_B\,\nu^{n_A-\frac{1}{2}}\, D_{a,b-1}^{cde}(\rho_A,\rho_B)$$

Further expansion of the C-function leads to [46]

$$C_{\alpha\beta}^{\gamma\delta\varepsilon}(\rho_A,\rho_B) = \rho_B^{\alpha+\beta+\gamma+\delta+2\varepsilon+1} \sum_{r=0}^{\gamma+\delta+2\varepsilon} \sum_{s=0}^{\gamma+\delta+2\varepsilon-r} a_{rs}^{\gamma\delta\varepsilon} \cdot T_{\alpha+2r,\beta+2s}(\rho_A,\rho_B)$$

$$a_{rs}^{\gamma\delta\varepsilon} = (-1)^{\varepsilon} \frac{\gamma!\delta!\varepsilon!}{2^{\gamma+\delta+2\varepsilon}} \sum_{\gamma_2=0}^{\gamma} \sum_{\gamma_3=0}^{\gamma-\gamma_2} \sum_{\delta_2=0}^{\delta} \sum_{\delta_3=0}^{\delta-\delta_2} \sum_{\varepsilon_2=0}^{\varepsilon} \sum_{\varepsilon_3=0}^{\varepsilon-\varepsilon_2}$$

$$\sum_{\varepsilon_4=0}^{\varepsilon-\varepsilon_2-\varepsilon_3} \sum_{\varepsilon_5=0}^{\varepsilon-\varepsilon_2-\varepsilon_3-\varepsilon_4} \sum_{\varepsilon_6=0}^{\varepsilon-\varepsilon_2-\varepsilon_3-\varepsilon_4-\varepsilon_5}$$

$$\frac{(-1)^{\gamma_3+\delta_2+\varepsilon_2+\varepsilon_3+\varepsilon_4}\, 2^{\varepsilon_2+\varepsilon_3+\varepsilon_4}}{\gamma_1!\gamma_2!\gamma_3!\delta_1!\delta_2!\delta_3!\varepsilon_1!\varepsilon_2!\varepsilon_3!\varepsilon_4!\varepsilon_5!\varepsilon_6!}$$

with $\gamma_1 + \gamma_2 + \gamma_3 = \gamma$

$\delta_1 + \delta_2 + \delta_3 = \delta$

$\varepsilon_1 + \varepsilon_2 + \varepsilon_3 + \varepsilon_4 + \varepsilon_5 + \varepsilon_6 = \varepsilon$

$r = \gamma_2 + \delta_2 + \varepsilon_2 + \varepsilon_4 + 2\varepsilon_5$

$s = \gamma_3 + \delta_3 + \varepsilon_3 + \varepsilon_4 + 2\varepsilon_6$

Thence,

$$T_{ij}(\rho_A,\rho_B) = j! \sum_{k=0}^{j} \sum_{l=0}^{j-k} \frac{1}{\rho_B^{k+1}\cdot l!(j-k-l)!} \{(-1)^{j-k-l} e^{\rho_B} P_{i+l}(\rho_A+\rho_B)$$

$$+ e^{-\rho_B} (-1)^l R_{i+l}(\rho_A-\rho_B) - e^{-\rho_B} Q_{i+l}(\rho_A+\rho_B)\}$$

Finally the P,Q and R functions above are expressed as

$$P_n(\theta) = \frac{1}{2^{n+1}} \int_2^{\infty} e^{-\theta x/2} x^n \, dx$$

$$Q_n(\theta) = \frac{1}{2^{n+1}} \int_0^{\infty} e^{-\theta x/2} \; x^n \; dx$$

$$R_n(\phi) = \frac{1}{2^{n+1}} \int_0^{2} e^{-\theta x/2} \; x^n \; dx$$

with $\theta = \rho_A + \rho_B$ and $\phi = \rho_A - \rho_B$

While most of the preceding formulations have appeared previously in the literature, we felt it worthwhile to collate the extremely elegant analysis of Fraga [44,45], relating operator form (through the exponents α',β' etc) to C-function parameters, with the equally elegant work of Klimenko and Dyatkina [46] in overcoming the convergence difficulties which have plagued C-functions since their inception by Ruedenberg and co-workers [41] almost a decade earlier. In the form above, the C-functions provide a general scheme for most one-electron operators, and further, one that is ideally set up for automatic digital processing.

As well, the Fraga-type analysis may be extended to the two-electron repulsion integrals to give a more general formulation than that described by Klimenko and Dyatkina, and earlier, by Ruedenberg et al.

$$\langle X_A X'_A \mid X_B X'_B \rangle = W_A . W_B . \sum (N_A+L_A+1)! \; (N_B+L_B+1)! \; a_{LM_A} . a_{LM_B} .$$

$$[NLM_A \mid NLM_B] \; \delta_{M_A, M_B}$$

$$W = \frac{(1+\tau)^{n+\frac{1}{2}} \cdot (1-\tau)^{n'-\frac{1}{2}}}{[(2n)!\ (2n')!]^{\frac{1}{2}}}, \qquad \tau = \frac{\zeta - \zeta'}{\zeta + \zeta'}$$

$$N = n + n' - 1$$

The form of the basic charge distributions and coefficients a_{LM} are conveniently taken from Table I of ref. 46.

$$[NLM_A|NLM_B] = K_{AB}\,\bar{\zeta}_B^{\,} \sum_p \sum_q c_p \cdot c_q \; I^{\gamma-2p,\ \delta-2q,\ \varepsilon}_{\lambda+2p,\ \beta+2q} (\rho_A, \rho_A^*, \rho_B)$$

$$K_{AB} = \frac{(2L_A)!\ (2L_B)!\ (2L_B+1)}{L_A!\ L_B!\ (N_B+L_B+1)!\ [(L_A-M_A)!\ (L_A+M_A)!\ (L_B-M_B)!\ (L_B+M_B)!]^{\frac{1}{2}}}$$

$$\bar{\zeta} = \tfrac{1}{2}(\zeta + \zeta')$$

c_p as previously, using L, M in place of l, m.

$$\rho_A = 0, \quad \rho_A^* = 2\bar{\zeta}_A R, \quad \rho_B = 2\bar{\zeta}_B R$$

$$\lambda = -2L_A, \ \beta = N_B - L_B, \ \gamma = L_A - |M_A|, \ \delta = L_B - |M_B|, \ \varepsilon = |M_A| = |M_B|$$

And, to completely detail the further expansion into C-functions,

$$I^{\gamma\delta\varepsilon}_{\lambda\beta} (\rho_A, \rho_A^*, \rho_B) = (2\mu)^{-L_A} \{C^{\gamma\delta\varepsilon}_{\lambda\beta} (\rho_A, \rho_B) - \sum_{m=0}^{N_A+L_A} u_m (2\mu)^m C^{\gamma+m,\ \delta,\ \varepsilon}_{\lambda,\ m,\ \beta} (\rho_A^*, \rho_B)\}$$

$$\mu = \frac{\rho_A^* - \rho_A}{2\rho_B}$$

$$u = 1/m! \quad \text{for} \quad 0 \leq m \leq 2L$$

$$= 1/m! - (N-L)!/[(N+L+1)!\ (m-2L-1)!] \quad \text{for} \quad 2L+1 \leq m \leq N+L$$

Apart from the practical effort in programming the procedures above for general evaluation of one-electron and two-electron coulomb integrals*, our contribution lies with the P,Q and R functions, which, in the form given by Klimenko and Dyatkina, are numerically unstable over all but a fairly confined range of the arguments θ and ϕ. We have investigated this problem for n in the range -8 and 18 (sufficient up to 3d atomic orbitals), and θ, ϕ in the range 0 to $\pm$100. The methods outlined below are the fastest we could find [48], consistent with an error not greater than 1 in the 11th decimal figure, 3 less than the maximum for the 48 binary bit coefficient of the single precision CDC6400 word.

$P_n(\theta)$ $n \geq 0$ All θ - Forward recurrence from $P_o(\theta) = e^{-\theta}\,\theta^{-1}$

$$P_n = \theta^{-1}\,(e^{-\theta} + P_{n-1})$$

$n < 0$ $0<\theta<4$ - Forward recurrence from $P_{-1}(\theta) = E_i(-\theta)$

$$E_i(-\theta) = \gamma + ln\theta + \sum_{p=1}^{\infty} (-\theta)^p/p.p!$$

γ = Euler's constant = 0.5772156649....

$$P_{n-1} = n^{-1}\,(\theta P_n - e^{-\theta})$$

$\theta \geq 4$ - Back recurrence from $P_m(\theta)$ [m = Min(n)]

$P_m(\theta)$ by continued fraction $= e^{-\theta}\left(\frac{1}{\theta-}\,\frac{m}{1+}\,\frac{1}{\theta-}\,\frac{m-1}{1+}\,\frac{2}{\theta-}\ldots\right)$

$$P_n = \theta^{-1}\,(nP_{n-1} + e^{-\theta})$$

---

* These routines are available as QCPE # 131 [84].

$Q_n(\theta)$ $n \geq 0$ all θ - Forward recurrence from $Q_o(\theta) = \theta^{-1}$

$$Q_n = nQ_{n-1}\theta^{-1}$$

$n < 0$ all θ - Dyatkina formula

$$Q_n(\theta) = -\frac{(-\theta)^{-n-1}}{(-n-1)!}\{\gamma+\ln\theta + \sum_{p=o}^{-n-2}\frac{1}{n+p+1}\left(1+\frac{(-n-1)!\,(-\theta)^{n+p+1}}{p!}\right)\}$$

$R_n(\phi)$ $n \geq 0$ $\phi \geq 80$ - $R_n(\phi) = Q_n(\phi)$ (c.f. $Q_n(\theta)$, $n \geq 0$; $\theta \leftrightarrow \phi$)

$9 \leq \phi < 80$ and $-40 < \phi \leq -8$ - Forward

recurrence from $R_o(\phi) = \phi^{-1}(1-e^{-\phi})$

$$R_n = \phi^{-1}(nR_{n-1}-e^{-\phi})$$

$-8 < \phi < 9$, $\phi \neq 0$ - Back recurrence from

$R_m(\phi)$ $[m = \text{Max.}(n)]$

$$R_m(\phi) = \frac{m!e^{-\phi}}{\phi^{m+1}}\sum_{p=m+1}^{\infty}\frac{\phi^p}{p!}$$

$$R_{n-1} = n^{-1}(\phi R_n + e^{-\phi})$$

$\phi = 0$ $R_n(o) = (n+1)^{-1}$

$\phi \leq -40$ $R_n(\phi) = -P_n(\phi)$ (c.f. $P_n(\theta)$, $n \geq o$; $\theta \leftrightarrow \phi$)

$R_n(\phi)$ $n < o$ $\underline{\phi > 40}$ $R_n(\phi) = Q_n(\phi)$ (c.f. $Q_n(\theta)$, $n<o$; $\theta-\phi$)

$\underline{2<\phi<40}$ Dyatkina formula

$$R_n(\phi) = \frac{-(-\phi)^{-n-1}}{(-n-1)!} \{\gamma + \ln|\phi| - E_i(-\phi)$$

$$+ \sum_{p=o}^{-n-2} [\frac{1}{n+p+1} (1 + \frac{(-n-1)!\ (-\phi)^{n+p+1}}{p!}$$

$$+ e^{-\phi} (-n-p-2)!\ (-\phi)^{n+p+1})]\}$$

$E_i(\phi)$ by continued fraction $= -e^{-\phi}(\frac{1}{\phi+} \frac{1}{1+} \frac{1}{\phi+} \frac{2}{1+} \frac{2}{\phi+} ..)$

$n < o$ $\underline{-2<\phi<2}$ $\phi \neq o$

$$R_n\phi = \sum_{p=-n}^{\infty} (-\phi)^p / p!(n+p+1)$$

$\underline{\phi=o}$ $R_n(o) = 0$

$\underline{-40<\phi<-2}$

Series expansion, as above for $-2<\phi<2$, is stable but slowly convergent as $|\phi|$ increases. In this range of ϕ, Q_n is stable, as is P_n to forward recurrence, but not backwards. We generate $R_m(\phi)$, [m = Min(n)], through series expansion, followed by $Q_n(\phi)$ for all $n<o$. From $P_m(\phi) = Q_m(\phi) - R_m(\phi)$, forward recurrence gives all P-functions in the desired range by a stable method. Individual

$R_n(\phi)$ $n < o$ are formed from the difference of the corresponding P and Q functions. Despite its apparent complexity, this approach is considerably faster than series expansion for each n.

$\underline{\phi<-40}$

$R_n(\phi) = -P_n(\phi)$ (c.f. $P_n(\theta)$, $\theta \gtrsim 4$; $\theta \backsim \phi$)

Several possibilities exist for increasing computational efficiency, principally by external projection of functions likely to be encountered frequently within an individual integral. Most obvious are the $a_{rs}^{\gamma\delta\varepsilon}$ functions, which involve a complex summation best performed external to the entire integral evaluation procedure. Since the parameters are determined solely by the participant orbital quantum numbers, we have found it convenient to enter the range of a-functions into a data array, from which they may be referenced as required. The complete list of 1229 unique functions, sufficient to evaluate all one and two-electron integrals over orbitals up to d-type, does not overly strain core storage allocations during execution.

As well, we have chosen in our programs to form the arrays of P, Q and R functions at the earliest possible stage, i.e. when all parameters and maxima and minima of the ranges have been determined. By this procedure, integral evaluation consists

essentially of manipulating pre-calculated auxiliary functions, (P, Q, R, $a_{rs}^{\gamma\delta\varepsilon}$, exponentials and factorials), thus eliminating repetition of the 'heavy' calculations, although possibly introducing a few redundancies by way of unwanted 'once-only' function generation. Nevertheless, the advantages far outweigh minor side effects of that nature.

b. Transformation to the molecular axis system of all integrals evaluated in rectangular diatomic coordinates is accomplished by standard rotation matrices*. Three-centre nuclear attraction integrals we evaluate directly in the molecular axis system by the Gaussian transform procedure [50,51], adapted from a general integral evaluation program disseminated through QCPE[52]. The average timing of 200-300 msec per integral constitutes the worst bottleneck encountered in the SNE method; for larger molecules, of the order of pyrrole and pyridine, the major processing effort is expended in evaluating these nuclear attraction integrals. By contrast, the C-function route to two-electron coulomb repulsion integrals has proven highly efficient, averaging at 6-8 msec each, including the transformation to molecular axes.

For integrals over other one-electron operators, except dipole length where the C-function approach was employed, we have

---

* Using a two-angle rotation suggested by F. Burden [49].

continued with the Gaussian transform method. It was with these atomic integrals that the one-electron property expectation values recorded in the next chapter were obtained.

III. APPLICATION OF THE SIMULATED NON-EMPIRICAL SCHEME

III.1 PRELIMINARY CONSIDERATIONS TO ORBITAL EXPONENT OPTIMISATION

In view of the problems likely to be encountered in exponent optimisation to one-electron properties, we have concentrated more on extensive calculations on a very few molecular systems, rather than the reverse. Some 1,300 wavefunctions were generated for the molecules water, ammonia and formaldehyde, and, of that number, approximately 1000 were further continued to the calculation of one-electron properties.

The one-electron properties were*:

Dipole moment

$$\mu_\alpha(A) = \sum_N Z_N (R_{NA})_\alpha - \langle\psi_o|\sum_{iA} (r_{iA})_\alpha|\psi_o\rangle$$

Diagonal components of the molecular quadrupole tensor

$$\theta_{\alpha\alpha}(A) = \tfrac{1}{2}\sum_N Z_N [3(R_{NA})^2_\alpha - R^2_{NA}] - \tfrac{1}{2}\langle\psi_o|\sum_i [3(r_{iA})^2_\alpha - r^2_{iA}]|\psi_o\rangle$$

Components of diamagnetic susceptibility

$$\chi^d_{\alpha\alpha} = -(e^2N/4mc^2)\langle\psi_o|\sum_i [(r_{iA})^2 - (r_{iA})^2_\alpha]|\psi_o\rangle$$

---

* See reference 73 for an excellent listing.

Average diamagnetic susceptibility

$$\chi^{d}_{av} = (-e^2N/2mc^2) \langle\psi_o|\sum_i r^2_{iA}|\psi_o\rangle$$

Average diamagnetic shielding

$$\sigma^{d}_{av}\ (A) = (e^2/3mc^2) \langle\psi_o|\sum_i r^{-1}_{iA}|\psi_o\rangle$$

Here, the summations are over nuclei, N, and electrons, i, with $(R_{NA})_\alpha$ and $(r_{iA})_\alpha$ the components along the Cartesian axis α (= X, Y or Z) connecting the nucleus and electrons to the reference point, A. Z_N is the nuclear charge on atom N, and ψ_o is the ground state wavefunction. The reference point, A, differs for each operator. For the dipole moment, the nett expectation value is independent of origin, and we have arbitrarily selected the first row atom of least atomic number (O in H_2O, N in NH_3, C in H_2CO).

Molecular quadrupole moments are origin dependent if the system possesses a permanent dipole moment, as occurs in all three molecules considered here. The conventional choice of reference point is then the centre of nuclear mass, and all quadrupole moments and diamagnetic susceptibilities have been calculated from this origin. Finally, the chemical shielding at nucleus A must obviously be estimated with A as reference point.

Three operator types need to be considered for the one-electron properties above; they are $(r_{iA})_\alpha$, $(r_{iA})^2_\alpha$ and $(r_{iA})^{-1}$.

All atomic integrals over these operators were evaluated by exact methods, (c.f. Section II.3) irrespective of approximations employed in the generation of parent wavefunctions.

Within the SNE approximation, various procedures with respect to core integral evaluation and basis set size may be followed. We have distinguished procedures in which 3-centre nuclear attraction integrals are formed by Ruedenberg approximation (Version 1), and by exact calculation (Version 2), in each of minimal, (M), and valence, (V), basis sets. Thus our four procedures, in obvious notation, we label M1, M2, V1 and V2.

The number of individual calculations required for the optimisation procedure depends on two factors. Firstly, the relationships between one-electron property expectation values and orbital exponents must be established for each orbital in the basis. For graphical methods, a minimum of 3 points, and preferably 4, should be sufficient to interpolate and/or extrapolate with reasonable accuracy. Secondly, dimensionality will obviously be dependent on the number of orbitals within which variation of orbital exponent values is allowed. Thus, a system characterised by n independent exponent variations entails a minimum of 3^n individual calculations, equivalent to an n-dimensional grid containing 3 nodal points per axis. Although there need be no restrictions on value intervals along any particular axis of exponent variation, we have adhered to regular decimal increments as the simplest procedure.

In the case of the water and ammonia systems, grid dimensionality was reduced to variation of valence atomic orbital exponents only; inner shell oxygen and nitrogen 1s exponents were maintained at, respectively, 7.66 and 6.7 throughout. First row atom 2s and 2p exponents were each permitted 4 values, and the hydrogen 1s orbital, 6 values, thus characterising the final grid as 3-dimensional, with 96 nodal points. We used this same grid structure in each of the four procedures M, M2, V1 and V2 for both molecules.

Formaldehyde was treated rather more harshly, in that all 1s orbital exponents, including that on H, were 'frozen' for the grid calculations, while the 2s and 2p exponents were each allowed only 3 values. Even so, the exponent grid is 4-dimensional with 81 nodal points, and, with a basis set nearly twice the size of the H_2O and NH_3 molecules, we confined our investigations solely to the M2 procedure.

III.2 ORBITAL EXPONENT OPTIMISATION TO ONE-ELECTRON PROPERTIES

In this section, we describe our calculations on H_2O, NH_3 and H_2CO through to the actual determination of orbital exponents, optimised to reproduce, as far as possible, experimental data for the various one-electron properties. Although the greater part of our computational effort was expended at this stage, the grid calculations are relevant only insofar as they provided the numbers from which preliminary expectation value-orbital exponent relationships could be

established. We therefore treat them rather sketchily. In particular, the operational details of the optimisation process need be described but once, since the same basic pattern of refinement was a common feature throughout.

Finally, the orbital exponents determined as optimum in each procedure are examined for their consistency in reproduction of experimental one-electron property values. We defer discussion beyond the gross one-electron properties level to Section III.3, where the optimised wavefunctions are examined in terms of total energy, ionisation potentials, and electron density distribution.

III.2.A H_2O - M1

Calculated one-electron properties over the M1 grid are listed in the first column of Table III.2.1 as maxima and minima of the complete range. It is unfortunate that space considerations limit tabulation to this form, because the distribution of values within the extrema has some bearing on the argument which follows.

Although the calculated multipole moments and diamagnetic shieldings are spread well beyond the experimental limits (last column), this is not true for diamagnetic susceptibility components. In particular the minimum calculated value for X^d_{yy}, -15.44×10^{-6}erg G^{-2} $mole^{-1}$ falls only just below the lower experimental limit of -15.22×10^{-6}erg G^{-2} $mole^{-1}$. While other susceptibility components show greater deviations in their calculated values, their distribution

Table III.2.1. Exponents and Expectation Value Variation in Grid Calculations - H_2C

Type	M1		M2	
	Min.	Max.	Min.	Max.
$\zeta 2s(0), \zeta 2p(0)$	2.0	2.3	2.0	2.3
$\zeta 1s(H)$	1.0	1.5	1.0	1.5
μ (Debyes)	0.40	3.15	2.24	4.65
θ_{xx} (Buckinghams)	-2.55	0.17	-3.30	-1.52
θ_{yy} "	-.64	2.70	1.40	3.35
θ_{zz} "	-.16	0.40	-.14	0.18
χ^d_{xx} ($\times 10^{-6}$ erg G^{-2} $mole^{-1}$)	-19.58	-14.57	-15.55	-13.80
χ^d_{yy} ($\times 10^{-6}$ erg G^{-2} $mole^{-1}$)	-15.44	-11.45	-13.18	-11.16
χ^d_{zz} ($\times 10^{-6}$ erg G^{-2} $mole^{-1}$)	-17.75	-12.87	-14.26	-12.39
χ^d_{av} ($\times 10^{-6}$ erg G^{-2} $mole^{-1}$)	-17.56	-12.97	-14.16	-12.47
$\sigma^d_{av}(0)$ (ppm)	401.4	418.8	410.0	421.4
$\sigma^d_{av}(H)$ (ppm)	100.4	106.9	97.2	104.6

Table III.2.1. Cont. Exponent and Expectation Value Variation in Grid Calculations - H_2O(a)

Type	V1		V2		Expt.	
	Min.	Max.	Min.	Max.	Min.	Max.
ζ2s(O),ζ2p(O)	2.0	2.3	2.0	2.3		
ζ1s(H)	1.0	1.5	1.0	1.5		
μ (Debyes)	0.09	2.53	0.30	2.80	1.83	1.87(b)
θ_{xx} (Buckinghams)	-2.42	-.26	-2.59	-.73	-2.57	-1.39(c)
θ_{yy} "	-.26	2.52	0.40	2.62	0.97	2.15(c)
θ_{zz} "	-.10	0.42	-.03	0.32	0.06	0.78(c)
χ^d_{xx} ($\times 10^{-6}$ erg G^{-2} $mole^{-1}$)	-18.06	-14.68	-17.49	-14.50	-18.01	-13.55(c)
χ^d_{yy} ($\times 10^{-6}$ erg G^{-2} $mole^{-1}$)	-14.70	-11.31	-13.94	-11.21	-15.22	-10.76(c)
χ^d_{zz} ($\times 10^{-6}$ erg G^{-2} $mole^{-1}$)	-16.58	-12.98	-15.66	-12.98	-16.84	-12.64(c)
χ^d_{av} ($\times 10^{-6}$ erg G^{-2} $mole^{-1}$)	-16.45	-12.99	-15.48	-12.92	-16.40	-12.60(c)
σ^d_{av}(O) (ppm)	400.7	415.3	403.7	415.6		
σ^d_{av}(H) (ppm)	100.1	108.2	99.0	108.0	100.8	103.2(d)

(a) Atom coordinates (au) - O(0,0,0), H_1(0,1.43153, 1.10941), H_2(0,-1.43153, 1.10941)

(b) Ref. 53

(c) Calculated from data in Refs. 54,55

(d) Refs. 56,57

within the extrema approximates a Gaussian shape, with the consequence that many more values fall within the experimental limits than is indicated by our method of tabulation. Therefore, diamagnetic susceptibilities are practically useless as optimisation criteria, which thereby suffer a drop in number from 9 to 5. One further is eliminated as a result of linear dependence among the components of the molecular quadrupole tensor, for, by definition, $\theta_{zz} = -(\theta_{xx}+\theta_{yy})$. As we shall subsequently elucidate, such a dramatic reduction in the number of effective criteria has a profound effect on the selectivity of the optimisation procedure.

For the following description of operational details in the optimisation process, we have selected the quadrupole moment component, θ_{yy}, as a representative example. Fig. III.2.1.a depicts the interpolated plot of θ_{yy} *vs* 02s exponent at various nodal points in the plane of 02p and Hls variation. Upper and lower limits to the experimental value are shown as solid horizontal lines. In Fig. III.2.1.b, we have displayed the limits of 02s and 02p exponent variation (at each value interval in the Hls exponent) wherein calculated values of θ_{yy} lie within the experimental bounds. The limits were obtained from Fig. III.2.1.a (and a complementary plot of θ_{yy} *vs* 02p exponent, at nodal points in the 02s - Hls plane) by interpolation and extrapolation to the upper and lower experimental bounds. For instance, an intersection with the lower bound occurs at grid coordinate (02s = 2.1, 02p = 2.3, Hls = 1.3). The inter-

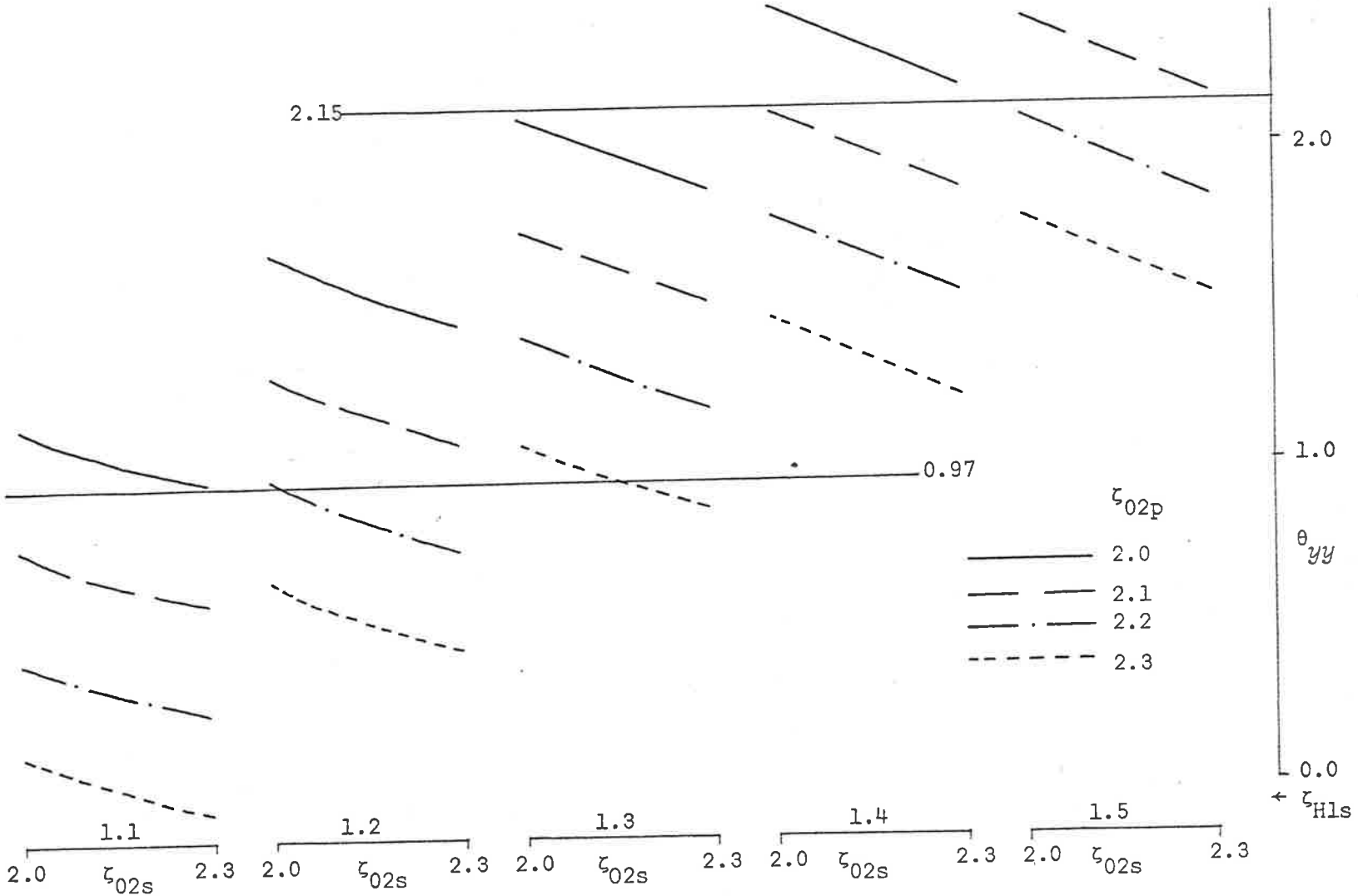

Figure III.2.1.a. θ_{yy} *vs* exponents, H_2O-M1

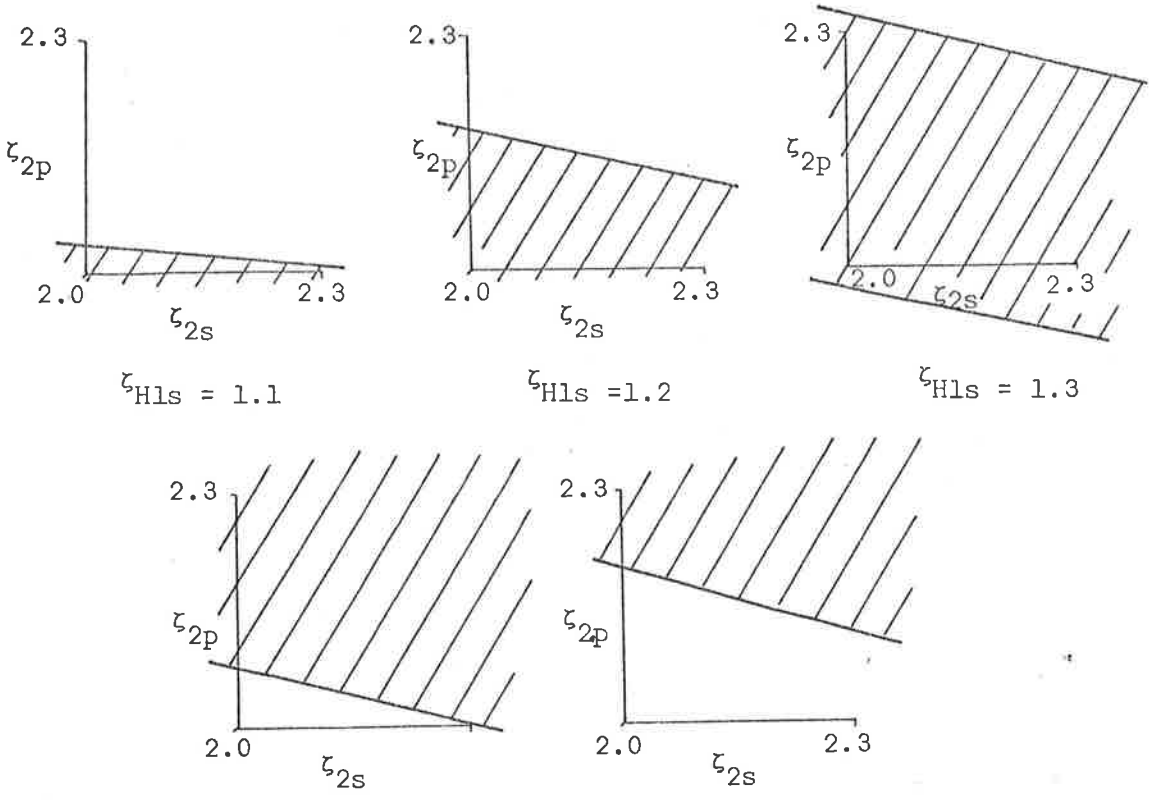

Figure III.2.1.b. Bounded areas for θ_{yy} calc., exponent variation, H_2O-M1

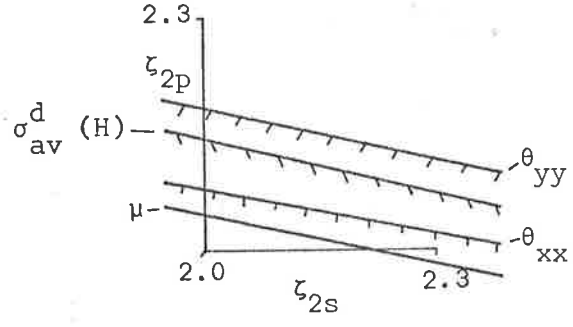

Figure III.2.1.c. Superposition of bounded areas for one-electron properties. All except μ represent upper bounds.

section coordinates were then laid out in the 02s-02p exponent plane, at each Hls exponent value, as shown. These plots may be visualised as a 3-D representation by stacking one on top of the other at the proper intervals. The broadness of the bounded areas in Fig. III.2.1.b are typical of those properties which exhibit large experimental error limits; in view of this complicating factor, we did not attempt to refine Hls exponent values beyond the decimal intervals of the original grid axis.

It is obvious that the optimised exponent region is that common to all such bounded areas when the above process has been applied to all other one-electron properties, and the results superimposed. In this particular example, a common overlap area was manifest only in the superposition at Hls exponent 1.2, and we have depicted the end-result in Fig.III.2.1.c. Furthermore, we ignored completely the small experimental error in dipole moment, so that the optimised exponents were finally determined along the locus of μ.

Had we accounted this error, the region of optimised exponents would have finalised as a narrow planar strip. Note also that our summary restriction on Hls variation ignores completely the extra dimension available to the optimised exponent region.

Fig. III.2.1.c is illustrative of the pseudo-linear dependence which appears to be a common feature of this particular set of one-electron operators, despite individual differences in direction, origin and exponent. Apart from a purely displacement

term, functional dependence on orbital exponents is close to identical in every case, as evinced by the nearly parallel boundaries.

Representative combinations of optimised exponents are listed in Table III.2.2, together with calculated one-electron properties. Small departures in the calculated dipole moments from the experimental value of 1.85D are due to minor interpolation errors during the optimisation process, and should be discounted. It is noteworthy that the total variation in other calculated one-electron properties are considerably less than the ranges of experimental errors. For example, the experimental range of θ_{yy} is approximately 2 orders of magnitude greater than the total span of calculated values. It is apparent that stratification in expectation values is a further facet of pseudo-linear dependence among one-electron operators.

The exponent values deserve further comment. It would appear that one-electron properties are not particularly sensitive to the 02s exponent, but permit only very small variations in 02p value. The median of 02p combinations, at 2.025, is closer to the Burns value of 1.975 [74] than to either of the Slater [75] or Clementi [76] exponents, respectively 2.275 and 2.212. By comparison, Aung, Pitzer and Chan [57] report an energy-optimised value of 2.21 for the 02p exponent; however, quadrupole moments calculated with their *ab initio* wavefunction were unsatisfactory.

Table III.2.2. H_2O - One-electron Properties and Optimised Exponents in the M1 and M2 Sets.

Exponents			μ	θ_{xx}	χ^d_{xx}	χ^d_{av}	$\sigma^d_{av}(O)$
O1s = 7.66				θ_{yy}	χ^d_{yy}		$\sigma^d_{av}(H)$
O2s	O2p	H1s		θ_{zz}	χ^d_{zz}		
2.00	2.05 (M1)	1.20	1.84	-1.50	-17.14	-15.59	405.4
				1.48	-14.03		102.4
				0.02	-15.59		
2.05	2.035 (M1)	1.20	1.84	-1.51	-17.11	-15.56	405.8
				1.50	-14.01		102.4
				0.01	-15.55		
2.10	2.02 (M1)	1.20	1.85	-1.52	-17.08	-15.54	406.2
				1.50	-14.00		102.4
				0.02	-15.53		
2.15	2.01 (M1)	1.20	1.85	-1.52	-17.06	-15.51	406.7
				1.52	-13.98		102.4
				0.00	-15.50		
2.20	2.00 (M1)	1.20	1.85	-1.52	-17.04	-15.49	407.3
				1.53	-13.96		102.4
				- '01	-15.47		
2.00	2.40 (M2)	1.20	2.13	-1.36	-15.42	-13.78	418.4
				1.35	-12.15		102.9
				0.01	-13.77		
2.05	2.39 (M2)	1.20	2.10	-1.36	-15.36	-13.78	418.9
				1.35	-12.08		103.0
				0.01	-13.77		

Table III.2.2 (Cont'd)

Exponents			μ	θ_{xx}	χ^d_{xx}	χ^d_{zv}	$\sigma^d_{av}(O)$
O1s = 7.66				θ_{yy}	χ^d_{yy}		$\sigma^d_{av}(H)$
O2s	O2p	H1s		θ_{zz}	χ^d_{zz}		
2.10	2.38 (M2)	1.20	2.08	-1.35 1.34 0.01	-15.30 -12.02 -13.66	-13.66	419.3 103.0
2.15	2.37 (M2)	1.20	2.06	-1.35 1.34 0.01	-15.25 -11.97 -13.60	-13.61	419.8 103.1
2.20	2.36 (M2)	1.20	2.06	-1.35 1.34 0.01	-15.21 -11.92 -13.56	-13.56	420.3 103.1
2.25	2.35 (M2)	1.20	2.05	-1.35 1.34 0.01	-15.17 -11.89 -13.52	-13.52	420.7 103.1
2.30	2.34 (M2)	1.20	2.05	-1.36 1.35 0.01	-15.13 -11.86 -13.48	-13.49	421.2 103.1
2.35	2.33 (M2)	1.20	2.06	-1.36 1.35 0.01	-15.10 -11.83 -13.45	-13.46	421.6 103.1
2.40	2.32 (M2)	1.20	2.06	-1.37 1.36 0.01	-15.07 -11.81 -13.42	-13.43	422.0 103.1

III.2.B H_2O - M2

In qualitative aspects, this series of grid calculations hardly differ from those previously described. Extrema of calculated one-electron property expectation values fall closer to the experimental range, and in the case of diamagnetic susceptibilities, overlap is almost complete (Table III.2.1). It is noteworthy that the calculated ranges are displaced from those in the M1 series, a difference that is reflected in the values of optimised exponents and attendant one-electron properties in Table III.2.2.

Exponent optimisation proved less successful, in this instance, due to our inability to locate an area of experimental agreement common to all one-electron properties, at any Hls exponent interval. Accordingly, the dipole moment was sacrificed to ~10% error in order to achieve agreement with other experimental values. Apparently there is insufficient flexibility within the basis set and approximations to accommodate complete matching.

Among the one-electron operators, pseudo-linear dependence is again evident in the individual expectation values, for they show very little overall variation relative to the span of experimental error. It is significant that molecular quadrupole moments and diamagnetic susceptibilities are considerably different from those calculated in the M1 set. The magnitude of the absolute variations in each (~1.1 Buckinghams in θ, ~1·8erg G^{-2} $mole^{-1}$ in X) stem, in the first instance, from a fairly constant difference of 0.35 in the

optimised 02p exponents, but, in reality, this is no more than a reflection of more subtle differences between Version 1 and Version 2. It would appear therefore, that approximation of nuclear attraction integrals has a profound effect on the resultant wavefunction in a minimal basis.

As previously observed, expectation values are not greatly dependent on the 02s exponent, but remain highly sensitive to 02p values. In this instance, there is a tendency to group at a somewhat higher level, 2.32 to 2.40, than the Slater exponent (2.275).

III.2.c H_2O - V1

It should be emphasized that our valence bases differ from the preceding minimal bases not only by collapse of the oxygen K-shell into the atomic nucleus, but also in the form of the valence 2s orbital. In this respect, the 2s function has been chosen to correspond to a CNDO-type valence orbital in its nodeless non-Schmidt orthogonalised character. Proper invariance to Ruedenberg approximation will be maintained in the absence of explicit consideration of the oxygen inner-shell 1s orbital.

One-electron property expectation values calculated over the exponent grid correspond quite closely to the extrema observed in the M1 series. In most instances, the ranges are more contracted, and we take this as an indication that the valence basis affords

Table III.2.3 H_2O - One-electron Properties and Optimised Exponents in the V1 and V2 Sets.

Exponents			μ	θ_{xx} θ_{yy} θ_{zz}	χ^d_{xx} χ^d_{yy} χ^d_{zz}	χ^d_{av}	$\sigma^d_{av}(O)$ $\sigma^d_{av}(H)$
O2s	O2p	H1s					
2.00	2.01 (V1)	1.20	1.82	-1.81 1.81 0.00	-16.67 -13.93 -15.28	-15.29	401.9 102.0
2.01	2.00 (V1)	1.20	1.82	-1.82 1.82 0.00	-16.68 -13.96 -15.30	-15.31	401.8 102.0
2.02	2.06 (V1)	1.30	1.83	-1.85 1.90 -.05	-15.98 -13.32 -14.58	-14.63	404.2 103.2
2.04	2.04 (V1)	1.30	1.83	-1.88 1.93 -.05	-16.00 -13.38 -14.62	-14.67	404.0 103.2
2.06	2.02 (V1)	1.30	1.83	-1.92 -.05	-16.02 -14.67	-14.71	403.7
2.08	2.00 (V1)	1.30	1.82	-1.96 2.00 -.04	-16.05 -13.51 -14.73	-14.76	403.4 103.0

Table III.2.3. (Cont'd)

Exponents			μ	θ_{xx} θ_{yy} θ_{zz}	χ^d_{xx} χ^d_{yy} χ^d_{zz}	χ^d_{av}	$\sigma^d_{av}(O)$ $\sigma^d_{av}(H)$
O2s	O2p	H1s					
2.00	2.17 (V2)	1.10	1.83	-1.64 1.57 0.07	-16.22 -13.24 -14.78	-14.75	407.6 101.4
2.05	2.12 (V2)	1.10	1.84	-1.77 1.68 0.09	-16.14 -13.30 -14.78	-14.74	407.1 101.2
2.10	2.07 (V2)	1.10	1.86	-1.90 1.80 0.10	-16.09 -13.39 -14.81	-14.76	406.6 101.0
2.15	2.03 (V2)	1.10	1.84	-1.98 1.87 0.11	-16.08 -13.48 -14.86	-14.81	406.2 100.9
2.00	2.16 (V2)	1.20	1.86	-1.74 1.71 0.03	-15.83 -12.99 -14.42	-14.42	407.4 102.4
2.05	2.12 (V2)	1.20	1.82	-1.81 1.76 0.05	-15.80 -13.03 -14.44	-14.42	407.1 102.3

Table III.2.3. (Cont'd)

Exponents			μ	θ_{xx} θ_{yy} θ_{zz}	χ^d_{xx} χ^d_{yy} χ^d_{zz}	χ^d_{av}	$\sigma^d_{av}(0)$ $\sigma^d_{av}(H)$
O2s	O2p	H1s					
2.10	2.07 (V2)	1.20	1.82	-1.93 1.86 0.07	-15.78 -13.14 -14.50	-14.47	406.5 102.1
2.12	2.06 (V2)	1.20	1.83	-1.96 1.89 0.07	-15.78 -13.18 -14.53	-14.50	406.4 102.0
2.15	2.02 (V2)	1.20	1.83	-2.04 1.95 0.09	-15.80 -13.28 -14.60	-14.56	406.0 101.8
2.10	2.09 (V2)	1.30	1.84	-1.95 1.90 0.05	-15.40 -12.80 -14.13	-14.11	407.3 103.2
2.15	2.04 (V2)	1.30	1.84	-2.05 1.98 0.07	-15.43 -12.94 -14.23	-14.20	406.7 102.9
2.19	2.00 (V2)	1.30	1.84	-2.13 2.04 0.09	-15.49 -13.08 -14.35	-14.30	406.2 102.7

greater stability in the calculation of one-electron properties, at least within Version 1. This premise is supported by the optimised exponent values of Table III.2.3, where the additional freedom allowed in the H1s exponent is reflected in the range of values 1.2 to 1.3. Conversely, there would appear to be less latitude in the choice of O2s exponent, since the span there is 2.02 to 2.08, while the O2p exponent optimises once more over a very narrow range.

The effect of a decimal increment in the hydrogen exponent is most apparent in the expectation values for chemical shielding, where a jump from 102.0 to 103.2 ppm may be observed. Less dramatic is the increase of ~0·6 x 10^{-6}erg G^{-2} $mole^{-1}$ in diamagnetic susceptibilities, but still in excess of the total span at constant H1s exponent. The situation with regard to molecular quadrupole moment is not as well-defined, and it would appear that this property, at least, remains relatively insensitive to exponent changes, provided that the dipole moment is unaffected.

In comparison with the M1 results at H1s exponent 1.2, marked differences occur in the molecular quadrupole moment, with V1 values consistently greater in absolute magnitude by ~0·3 Buckinghams. Of the diamagnetic susceptibility components, both X^{d}_{xx} and X^{d}_{yy} show greater deviations between the two sets than within each set. In view of the similarity in orbital exponents, (e.g. M1-2.0, 2.05, 1.20 *vs* V1-2.0, 2.10, 1.20) we must attribute these discrepancies entirely to omission of the inner shell O1s function, and attendant nodeless

2s orbital in the V1 basis.

III.2.D H_2O - V2

Examination of the extrema listed in Table III.2.1 reveals that grid calculations performed with the Version 2 valence basis classify less readily than those previously described. Whereas both orbital bases in Version 1 produce comparable groupings in one-electron properties, our V2 results occupy an intermediate position, biased more towards the V1 set rather than M2. Calculated dipole moments constitute the most striking example, wherein the minimum V2 value of 0.30D is to be compared with 2.24D in M2, and 0.09D in V1. Diamagnetic susceptibilities, also, are inclined to fall between the two sets.

As observed with the V1 series, hydrogen 1s orbital exponents optimise over an extended range (1.1 to 1.3), but it is apparent, also, that considerable latitude exists for the 02s and 02p orbitals where the exponents span, respectively, 2.00 to 2.15 and 2.03 to 2.17 (Table III.2.3). Once more, the effects of variation in the hydrogen orbital exponent are most marked in chemical shielding values, with an increase of ~1ppm in σ^{d}_{av}(H); diamagnetic susceptibilities show only a small decrease in absolute value, while variations in molecular quadrupole mom ent are quite minor, in agreement with V1 behaviour.

It is in comparison with expectation values for the minimal basis wavefunctions in Version 2 that the V2 set departs from the

uniformity exhibited by the Version 1 results. The dipole moment error in the M2 expectation values was a matter of necessity, and we discount the difference there between M2 and V2. However, substantial differences are evident in other properties, e.g. $\Delta\theta_{xx} \simeq \Delta\theta_{yy} \simeq 0.35$ in quadrupole moments, and $\Delta X^{d}_{av} \simeq 0{\cdot}7$ is representative for diamagnetic susceptibilities. Undoubtedly, the differences above stem from an expanded O2p distribution in the V2 set, relative to M2; we cannot credit such behaviour simply to the absence of an orthogonalising node in the 2s function.

III.2.E H_2O - A Summary

There can be no doubt that the calculations on H_2O were successful in the stated objective of defining a set of orbital exponents which adequately reproduce experimental values of one-electron properties. If anything, this phase of the project proved too successful, in that the very ubiquity of optimum exponent combinations prevented definition of an 'absolutely best' unique set. While such a 'failure' is irrelevant in the context of this work, future application of the SNE principle to more complex molecules will undoubtedly depend on the successful transfer of exponent combinations established by pilot calculations, such as these, on smaller systems. Unless unique exponent values are then available, there can be little hope of efficient performance. Unfortunately, orbital exponents obtained from purely atomic calculations are not

directly extensible to molecular systems, simply because the SNE approximation reduces to exact when only one centre is involved.

Our results have shown also that size of basis set, and approximation of three-centre nuclear attraction integrals have a direct bearing on relative magnitudes of calculated one-electron properties and, perforce, on optimised exponent values. In qualitative aspects, all four procedures appear more sensitive to the oxygen 2p exponent than to either of 2s or hydrogen 1s values, but the ranges established by optimisation differ in each case.

While we find the M2 procedure intuitively the most appealing, incorporating as it does a full basis set and approximation only in electron repulsion integrals, it was, perhaps, a little less successful than the other methods in its ability to correctly reproduce the complete range of one-electron properties.

Neglect of the oxygen inner shell in Version 2 has a greater effect than occurs in Version 1, where M1 and V1 were in fair agreement with respect to exponents and expectation values. Why there should be such a discrepancy between M2 and V2 is not altogether clear, since the major difference lies ultimately in the number of terms within the Ruedenberg expansion of bicentric orbital products - overlap integrals and mono-centric coulomb distributions involving the O1s orbital are absent in a valence basis. On theoretical grounds, approximations should be less with larger basis sets, but it is

possible that our bases are too small for any improvement from this source, and, therefore, both bases must be viewed with equal caution. We postulate that the uniformity in the Version 1 values stems from a compensatory effect i.e. errors in approximated repulsion integrals are effectively cancelled by errors of similar magnitude, but opposite sign, in approximated attractive potentials.

In summary, we have found no basis for selecting any one of our four procedures as superior to the remainder. Furthermore, we consider it unlikely, in view of the pseudo-linear dependence complication, that additional one-electron properties with the same coarse errors in experimental data would enable either sharper definition of orbital exponents, or establishment of a clear superiority in method.

In turning to our calculations an ammonia, we make prior emphasis that in qualitative aspects, they differ but little from our preceding observations on the water molecule. For the most part, a few necessary numerical and descriptive alterations to the foregoing would suffice to report and summarise our work on NH_3, so remarkable is the degree of parallelism. We therefore report only the essentials of the ammonia optimisation, and take the inferences arising therefrom as read.

III.2.F NH_3 - M1

One real difference between the NH_3 and H_2O grid calculations lies in the number and quality of experimentally-determined one-electron properties. Whereas the H_2O series were characterised by a wealth of relatively coarse experimental measurements, there are only a few properties available for NH_3, but these, fortunately, are known to fair accuracy (Table III.2.4).

Error spread in measured diamagnetic susceptibility, -21.0 to -19.4 x 10^{-6}erg G^{-2} $mole^{-1}$, for example, may be compared with the corresponding quantity for H_2O, -16.4 to -12.6$^{\times 10^{-6}}$erg G^{-2} $mole^{-1}$. Due to this fortuitous balance of availability and precision, the actual refinement of exponent grid values to optimum followed the same pattern as previously described in III.2.A.

Listed in the first column of Table III.2.4 are the extrema of one-electron property expectation values calculated from grid wavefunctions in the M1 approach. Both dipole moments (-.34 to 2.30D) and diamagnetic shielding), (93.1 to 100.5 ppm) show a characteristic spread well beyond the experimental bounds, 1.48D and 94.0 to 96.92 ppm, respectively. Although this behaviour was present in the H_2O series, calculated diamagnetic susceptibilities in NH_3 exhibit a definite contrast, for they span a range sufficiently beyond experimental limits to ensure their inclusion among the effective optimisation criteria.

Table III.2.4. Exponents and Expectation Value Variation in Grid Calculations - NH_3

Type	M1		M2	
	Min.	Max.	Min.	Max.
$\zeta 2s(N), \zeta 2p(N)$	1.75	2.05	1.75	2.05
$\zeta 1s(H)$	1.0	1.5	1.0	1.5
μ (Debyes)	- .34	2.30	1.44	3.67
θ_{zz} (Buckinghams)	- 2.76	0.78	- 3.29	- 1.16
χ^d_{xx} ($\times 10^{-6}$ erg G^{-2} $mole^{-1}$)	-24.04	-17.23	-19.82	-16.64
χ^d_{zz} ($\times 10^{-6}$ erg G^{-2} $mole^{-1}$)	-28.13	-20.10	-22.87	-19.13
χ^d_{av} ($\times 10^{-6}$ erg G^{-2} $mole^{-1}$)	-25.30	-18.22	-20.82	-17.51
$\sigma^d_{av}(N)$ (ppm)	342.8	360.1	353.3	362.3
$\sigma^d_{av}(H)$ "	93.1	100.5	91.2	99.2

Table III.2.4. Cont. Exponent and Expectation Value Variation in Grid Calculations - NH_3(a)

Type	V1		V2		Expt.	
	Min.	Max.	Min.	Max.	Min.	Max.
ζ2s(N), ζ2p(N)	1.75	2.05	1.75	2.05		
ζ1s(H)	1.0	1.5	1.0	1.5		
μ (Debyes)	-.26	2.12	0.13	2.60	1.48(b)	
θ_{zz} (Buckinghams)	-2.76	0.30	-2.96	-.29		
χ^d_{zz} ($\times 10^{-6}$ erg G^{-2} $mole^{-1}$)	-22.65	-16.89	-20.69	-16.72		
χ^d_{zz} ($\times 10^{-6}$ erg G^{-2} $mole^{-1}$)	-26.28	-19.83	-24.68	-19.58		
χ^d_{av} ($\times 10^{-6}$ erg G^{-2} $mole^{-1}$)	-23.72	-17.89	-22.02	-17.75	-21.0	-19.4(c)
σ^d_{av}(N) (ppm)	342.8	356.9	347.7	357.5		
σ^d_{av}(H)	92.9	100.9	92.1	100.6	94.0	96.9(c)

(a) Atom coordinates (au) - N(0,0,0), H_1(0,1.77595, -.71960), H_2(1.53802, -.88798, -.71960), H_3(1.53802, -.88798, -.71960)

(b) Ref. 58

(c) Ref. 56

The M1 set was to prove the only case in which an unique set of exponents was obtained, and these are listed in Table III.2.5, together with attendant one-electron properties. It is to be noted that optimised exponent values for N2s and N2p orbitals, viz. 1.84 and 1.75, lie closer to the Burns exponents, 1.88 and 1.65, than to either of the Slater, 1.95 and 1.95, or Clementi values, 1.92, 1.88. (c.f. III.2.A). At 1.3, the hydrogen exponent optimised decimally above the corresponding H_2O - M1 value.

III.2G NH_3 - M2

Extrema of grid expectation values in the M2 set (Table III.2.4) follow the previously established pattern in their relationship to the M1 set; the ranges are generally narrower, and displaced in the same manner as observed for H_2O. In this instance, the optimisation procedure proved less selective, and the final exponent combinations span a large range of values: 1.75 to 2.05 for 2s orbital, 2.11 to 2.03 for 2p and 1.1 to 1.2 for H1s (Table III.2.3). Fortunately, the loci of 2s and 2p combinations are very nearly identical at both H1s exponents, and comparison between the two is particularly simple.

Taking the first combination of each as example, we can summarise the changes on increasing the H1s exponent, as follows: θ_{zz}, -1.2 to -1.4; χ^{d}_{yy}, -19.4 to -18.8x10^{-6}erg G^{-2} $mole^{-1}$;

Table III.2.5. NH_3 - One-electron Properties and Optimised Exponents in the M1 and M2 Sets.

Exponents N1s = 6.70			μ	θ_{zz}	χ^d_{yy} χ^d_{zz}	χ^d_{av}	$\sigma^d_{av}(N)$ $\sigma^d_{av}(H)$
N2s	N2p	H1s					
1.84	1.75 (M1)	1.30	1.43	-1.99	-20.14 -22.62	-20.97	349.5 96.1
1.75	2.11 (M2)	1.10	1.51	-1.22	-19.40 -22.55	-20.45	356.6 94.9
1.80	2.10 (M2)	1.10	1.49	-1.21	-19.31 -22.48	-20.37	357.1 94.9
1.85	2.09 (M2)	1.10	1.48	-1.21	-19.24 -22.41	-20.30	357.5 95.0
1.90	2.07 (M2)	1.10	1.51	-1.25	-19.16 -22.29	-20.21	357.8 94.9
1.95	2.06 (M2)	1.10	1.51	-1.25	-19.11 -22.24	-20.16	358.2 95.0
2.00	2.05 (M2)	1.10	1.52	-1.26	-19.07 -22.20	-20.11	358.6 95.0
2.05	2.04 (M2)	1.10	1.52	-1.26	-19.03 -22.15	-20.07	358.9 95.0

Table III.2.5. (Cont'd)

Exponents N1s = 6.70			μ	θ_{zz}	χ^d_{yy} χ^d_{zz}	χ^d_{av}	$\sigma^d_{av}(N)$ $\sigma^d_{av}(H)$
N2s	N2p	H1s					
1.75	2.11 (M2)	1.20	1.49	-1.36	-18.77 -21.80	-19.78	356.9 96.1
1.80	2.09 (M2)	1.20	1.51	-1.39	-18.68 -21.68	-19.68	357.3 96.1
1.85	2.07 (M2)	1.20	1.53	-1.42	-18.60 -21.58	-19.59	357.6 96.1
1.90	2.06 (M2)	1.20	1.53	-1.42	-18.54 -21.52	-19.53	358.0 96.1
1.95	2.05 (M2)	1.20	1.52	-1.41	-18.49 -21.48	-19.49	358.4 96.1
2.00	2.04 (M2)	1.20	1.52	-1.41	-18.45 -21.44	-19.45	358.8 96.2
2.05	2.03 (M2)	1.20	1.52	-1.41	-18.42 -21.41	-19.42	359.1 96.2

χ^{d}_{zz}, -22.6 to -21.8 x 10^{-6}erg G^{-2} $mole^{-1}$; σ^{d}_{av} (H), 94.9 to 96.1 ppm. Apart from a more measurable effect on the quadrupole moment, these are almost identically the magnitude changes found for H_2O - V2. We note a further parallel in the magnitude decrease of one-electron properties in passing from the M1 to M2 procedures.

III.2.H NH_3 - V1

In a qualitative sense, there is little to say about this set of calculations that has not already been covered in our record of the M1 series. Maxima and minima in the grid calculations (Table III.2.4) correspond quite closely to the M1 extrema, while optimised exponent values and attendant one-electron properties are not significantly different (Table III.2.6). Although we have quoted two combinations in the optimised exponents, the limits of variation are small indeed, again in accord with the M1 series, where only a single combination was observed.

This very marked similarity between the valence and minimal bases affords support for our contention that a self-cancelling mechanism operates in the Version 1 procedure.

III.2.I NH_3 - V2

As previously recorded in the H_2O series, V2 calculations classify as intermediate between valence basis results in Version 1,

Table III.2.6. NH_3 - One-electron Properties and Optimised Exponents in the V1 and V2 Sets.

Exponents			u	θ_{zz}	χ^d_{yy} χ^d_{zz}	χ^d_{av}	$\sigma^d_{av}(N)$ $\sigma^d_{av}(H)$
N2s	N2p	H1s					
1.75	1.77 (V1)	1.30	1.48	-2.19	-19.80 -22.10	-20.56	346.4 96.0
1.77	1.75 (V1)	1.30	1.46	-2.22	-19.85 -22.12	-20.60	346.3 95.9
1.75	1.98 (V2)	1.20	1.50	-1.62	-19.14 -21.94	-20.08	350.7 95.8
1.80	1.91 (V2)	1.20	1.50	-1.77	-19.13 -21.80	-20.02	350.5 95.5
1.85	1.84 (V2)	1.20	1.50	-1.92	-19.20 -21.74	-20.05	350.2 95.2
1.90	1.77 (V2)	1.20	1.50	-2.06	-19.37 -21.78	-20.17	349.8 94.8
1.92	1.80 (V2)	1.30	1.53	-2.08	-18.68 -21.08	-19.48	350.9 96.1
1.95	1.77 (V2)	1.30	1.46	-2.08	-18.75 -21.15	-19.55	350.9 96.0

and minimal basis in Version 2. Our V2 calculations on ammonia provide no contradiction, for maxima and minima in the quadrupole moment, -2.96 to -.29 Buckinghams, are, if anything, closer to the V1 range, -2.76 to 0.30 Buckinghams, than to the M2 span of -3.29 to -1.16 Buckinghams. So too are dipole moment extrema, 0.13 to 2.60 D in NH_3 - V2, against -.26 to 2.12 D (V1) and 1.44 to 3.67 D (M2), while diamagnetic susceptibilities and diamagnetic shielding occupy a more median position.

Optimised exponents and calculated one-electron properties (Table III.2.6) are more indicative of the disparities arising from basis set truncation in Version 2, especially when the M2 and V2 results are compared at the common H1s exponent value of 1.2. As an example, absolute differences in quadrupole moments range from 0.36 to 0.64 Buckinghams, accompanying, and almost certainly dependent on, a decrease in N2p orbital exponent of 0.13 to 0.30. Less significant are small discrepancies between M2 and V2 in calculated diamagnetic susceptibilities, while any variation in σ^d_{av} (H) is effectively masked by an obvious dependence on nitrogen orbital exponents in the V2 set.

At H1s exponent 1.3, the V2 results may conveniently be compared with those from the V1 series, and it is there apparent that any variations occur only on a minor scale. Hence Version 1 and Version 2 are not considerably different in a valence basis.

III.2.J NH_3 - A summary

With the NH_3 series, we have once more succeeded in optimising orbital exponents to reproduce experimental values of one-electron properties. In two respects, these calculations proved slightly superior to the previous H_2O sets.

In the first instance, we have recorded that the orbital exponents resulting from optimisation in Version 1 were close to the unique set so obviously desirable (1 combination in M1, 2 almost equivalent in V1). Secondly, the final M2 exponents optimised over all one-electron properties, in contrast to the H_2O - M2 set, where circumstances dictated a dipole moment in error by 10%. However, it is only fair to point out that such 'successes' can be classified as such only with respect to the current precision of experimental measurement. This reservation is particularly relevant in view of the stratification observed in individual expectation values among the four procedures; the procedures remain viable only because the groupings all occur within the present experimental limits. It is therefore conceivable that any significant reduction in those limits would invalidate every hitherto 'allowed' exponent combination within a particular procedure. To illustrate this point, redetermination of the experimental quadrupole moment as, say, -1.3 ± 0.2 would invalidate all but the M2 set from our total list of optimised exponent combinations.

Some comment should be made on optimised Hls exponents, for we have recorded unique values of 1.3 in NH_3 - M1 and -V1, whereas a value of 1.2 was general throughout all H_2O calculations, as well as NH_3 - M2 and -V2. Although we are hesitant about generalising from the particular, these results argue that parameter transfer between molecular systems may not be made without some consideration for environmental similarities, at least within the confines of the Version 1 approach.

In summary, the calculations on ammonia have not added significantly to our information about the effects of basis set size (M *vs* V), nor of approximations in nuclear attraction integrals (Version 1 *vs* Version 2), nor, again, have they supplied criteria by which we can select a particular procedure as superior to the others. However, they have provided confirmation that small, but significant, differences may be associated with a particular approximation and/or basis set. Previously, we have recorded these differences primarily as they are reflected in the expectation values of one-electron properties. More properly, property variations are a direct consequence of the optimisation values of orbital exponents, and hence of relative expansion/contraction in the atomic orbitals.

In terms of this last concept, we may express our generalised observations as follows. Approximation of nuclear attraction integrals (Version 1) produces a relatively diffuse 2p orbital, irrespective of basis set size, whereas exact evaluation

(Version 2) favours a contracted distribution, noticeably more so when the inner shell 1s orbital is included in the basis. While the 2s exponent had lesser effects, in every instance, 2p and 2s orbitals operated in a complementary manner i.e. a small increase in 2p exponent (contraction) inevitably produced a decrease in the 2s exponent (expansion) of somewhat greater magnitude. On the few occasions where the particular procedure was favourable to multiple values in the H1s orbital exponent, the resultant expansion or contraction had little or no effect on the parameterisation of other orbitals.

The above is, perhaps, rather a simplistic picture, because there obviously exist other fundamental differences in the form of the optimised wavefunctions, i.e. in the orbital coefficients in the LCAO expansion. One could not, for instance, insert M1-optimised exponents into the M2 procedure, and expect satisfactory expectation values for one-electron properties calculated from the resultant wavefunction; obviously we need to examine the wavefunctions themselves, and this we do in Section III.3.

III.2.K H_2CO - M2

We have previously noted that exponent grid calculations on formaldehyde were performed with frozen 1s exponents on carbon, oxygen and hydrogen, and three values along each axis of variation in valence shell 2s and 2p exponents. Table III.2.7 summarises maxima and minima

Table III.2.7. Exponents and Expectation Value Variation in Grid Calculations - H_2CO (a)

Tpe	Grid No. 1		Grid No. 2		Expt.	
	Min.	Max.	Min.	Max.	Min.	Max.
$\zeta 2s(C), \zeta 2p(C)$	1.525	1.725	1.825	2.025		
$\zeta 2s(O), \zeta 2p(O)$	2.175	2.375	2.175	2.375		
μ (Debyes)	0.33	4.16	0.99	3.88	2.30	2.38(b)
θ_{xx} (Buckinghams)	- .01	1.17	- 1.03	- .28	- 2.25	- .45(c)
θ_{yy} "	- 4.94	- 1.74	- 1.21	1.01	- .35	1.45(c)
θ_{zz} "	1.50	4.07	0.02	1.56	- 1.59	0.02(c)
$\chi^d_{zz}-\chi^d_{yy}$ ($\times 10^{-6}$ erg G^{-2} $mole^{-1}$)	28.39	31.60	31.97	34.18	33.89	35.81(c)
$\chi^d_{xx}-\chi^d_{yy}$ ($\times 10^{-6}$ erg G^{-2} $mole^{-1}$)	4.26	6.74	7.32	9.02	8.35	9.53(c)
$\sigma^d_{av}(H)$	105.9	111.0	110.4	113.5	106	110(d)

(a) Atom coordinates (av) - C(0,0,0), O(0,0,2.2864), H_1(1.8141, 0, - 1.09003), H_2(- 1.8141, 0, - 1.09003)

(b) Refs. 59, 60

(c) Calculated with the data of Refs. 61, 62

(d) Refs. 63, 64

of calculated one-electron properties. Diamagnetic susceptibilities have been deliberately cast as differences, independent of absolute magnitudes, following a near-suggestion by Neumann and Moskowitz [64] that the experimental bulk susceptibility value of -15.015×10^{-6} erg G^{-2} $mole^{-1}$ [77] may be in error.

Exponent variations in Grid No.1 were chosen to neatly straddle the Slater values of 2.275 for oxygen, and 1.625 for carbon. Although calculated extrema of dipole moments (0.33 to 4.16D) and diamagnetic shielding (105.9 to 111.0ppm) overlap the measured values (2.34 $\pm$ .04D and 108 $\pm$ 2ppm), expectation values for quadrupole moments and the related suceptibility differences fall completely outside the corresponding experimental data ranges. Our analysis of property-exponent relationships made it abundantly clear that the desired corrections would only be attained by a dramatic increase in C2p exponent.

Grid No.2, therefore, was designed to span a new range of carbon exponents (1.825 to 2.025), whilst retaining oxygen parameterisation as originally specified. Even so, the improvement was not as great as anticipated, since θ_{zz}, for instance, achieves only marginal agreement (max (calc.) $\simeq$ min (expt.)), while σ^{d}_{av} (H), at 110.4 to 113.5ppm lies above the experimental upper limit of 110ppm. Following our previous experiences, in that optimised 2s and 2p exponents are not unduly affected by changes in H1s exponent, we have allowed the discrepancy in σ^{d}_{av} (H) to remain, in the anticipation that the

necessary corrections could be made by Hls exponent manipulation.

Grid refinement proved a much more complicated process in 4 dimensions than 3. Our graphical procedure for establishing common overlap areas is limited by projection in 2 dimensions, and, for optimum refinement, the relevant areas should be as small as possible, i.e. envelopes of experimental agreement should be projected in the plane of exponents to which the calculated properties are most sensitive. In common with H_2O and NH_3, the formaldehyde properties are strongly p-orbital dependent, and the O2p-C2p exponent variation axes therefore constitute the logical choice. Because 2 degrees of freedom still remain, O2p-C2p projections occur at each nodal point in the O2s-C2s variation plane, and, unfortunately for the optimisation process, the insensitivity to 2s exponents is such that common overlap areas likewise occur at every one of those nodes.

With the previously adopted assumption that experimental error in the dipole moment is absent, we selected only one point on each dipole locus as giving the closest approach to the experimental value for σ^{d}_{av} (H). As a result, from the optimisation process we obtained a unique O2p-C2p exponent combination at each nodal point of O2s-C2s variation, but beyond this level, further refinement is not possible. Optimised orbital exponent combinations in Table III.2.8 reflect just this limitation.

It is apparent in the expectation values of Table III.2.8 that individual variation over the range of optimised exponent

Table III.2.8. H_2CO - One-electron Properties and Optimised Exponents in the M2 Set.

Exponents			μ	θ_{xx}	χ^d_{xx}	χ^d_{av}	σ^d_{av} (C)
C2s	O2s	H1s		θ_{yy}	χ^d_{yy}	$\chi^d_{zz} - \chi^d_{yy}$	σ^d_{av} (O)
C2p	O2p			θ_{zz}	χ^d_{zz}	$\chi^d_{xx} - \chi^d_{yy}$	σ^d_{av} (H)
1.825	2.175	1.2	2.39	- .61	-50.41	-44.79	345.9
2.065	2.350			0.56	-58.92	33.90	458.2
				0.05	-23.03	8.51	112.4
1.925	2.175	1.2	2.49	- .76	-50.32	-44.79	346.4
2.055	2.345			0.71	-59.01	33.98	458.2
				0.05	-25.03	8.69	112.6
2.025	2.175	1.2	2.35	- .91	-50.30	-44.85	346.8
2.035	2.360			0.89	-59.18	34.11	458.3
				0.02	-25.08	8.88	112.9
1.825	2.275	1.2	2.36	- .73	-50.30	-44.75	345.9
2.095	2.315			0.66	-58.94	33.95	459.6
				0.07	-25.00	8.64	112.6
1.925	2.275	1.2	2.45	- .87	-50.21	-44.73	346.4
2.080	2.310			0.79	-59.00	34.02	459.6
				0.08	-24.99	8.79	112.7
2.025	2.275	1.2	2.40	-1.00	-50.18	-44.79	346.7
2.060	2.315			0.94	-59.15	34.12	459.5
				0.06	-25.03	8.96	112.9
1.825	2.375	1.2	2.40	- .81	-50.24	-44.73	345.8
2.110	2.270			0.68	-58.94	33.92	460.7
				0.13	-25.02	8.70	112.6
1.925	2.375	1.2	2.39	- .94	-50.14	-44.71	346.4
2.110	2.280			0.86	-59.02	34.05	461.0
				0.08	-24.97	8.88	112.8
2.025	2.375	1.2	2.39	-1.07	-50.11	-44.76	346.7
2.080	2.280			1.00	-59.15	34.14	460.9
				0.07	-25.01	9.04	113.0

combinations falls well within the span of experimental error limits. As examples, diagonal x and y components of the molecular quadrupole tensor calculate as (in Buckinghams) -.61 to -1.07 and 0.56 to 1.00, respectively, compared to the corresponding experimental values -1.30 and 0.55, both with error limits $\pm$0.90, nearly 4 times the calculated range. Even σ^d_{av} (H) spans only 0.6ppm, as opposed to experiment, $\pm$ 2ppm.

We have included in Table III.2.8 the absolute values for calculated diamagnetic susceptibilities. Median values are, approximately, X^d_{xx} = -50.2, X^d_{yy} = -59.0, X^d_{zz} = -25.0 and X^d_{av} = -44.7 in units of 10^{-6}erg G^{-2} $mole^{-1}$. Experimental values are much higher in absolute magnitude, at -61.8 $\pm$ .5, -70.7 $\pm$ .5, -35.9 $\pm$ .5 and -56.1 $\pm$ .5, in the same ordering and units. Our values are not too dissimilar from those calculated by McKoy et al with their [95/3] Gaussian set [73], viz., X^d_{xx} = -54.8, X^d_{yy} = -62.3, X^d_{zz} = -28.3 and X^d_{av} = -48.5 (x 10^{-6}erg G^{-2} $mole^{-1}$). With the experimentally derived value for X^p_{av} = -41.12 $\pm$ .03, and the values above, X_{av} calculates as -3.6 (this work) and -7.4 (McKoy et al), both of which compare unfavourably with the experimental value, -15.015 x 10^{-6}erg G^{-2} $mole^{-1}$ [77]. Similarly, the Neumann and Moskowitz [64] value of X^d_{av} = -47.9, implies a X_{av} = -6.9 x 10^{-6}erg G^{-2} $mole^{-1}$, and it was this discrepancy of ~8 x 10^{-6}erg G^{-2} $mole^{-1}$ which led them to question the accuracy of the experimental value.

While the formaldehyde calculations have demonstrated yet

again the success of exponent optimisation to one-electron properties (with allowance for σ^{d}_{av} (H)), deficiencies in the optimisation process have been brought into sharper focus through the difficulties we experienced in limiting the number of viable exponent combinations. Obviously, greater precision in experimental data measurement would provide some alleviation, but, beyond this, there will be perhaps insurmountable difficulties when the number of parameters exceeds the number of independent experimental properties. In retrospect, it is apparent that we should have allowed the Hls exponent free variation in a 5-dimensional grid, but refinement at this level would certainly be approaching the limits of practicability.

We therefore forsee a rather proscribed future for exponent optimisation to one-electron properties. Without doubt, extended basis sets, whether for small or large molecular systems, will prove difficult, if not impossible, to optimise at a useful level. In the absence of energy criteria, the future of SNE, and by extension, *ab initio* wavefunctions would appear to be tied to parameterisation from pilot calculations on small systems.

III.3 PROPERTIES OF OPTIMISED WAVEFUNCTIONS

In the previous section, we have reported our successes in exponent optimisation to one-electron properties; we now turn from the gross effects described there, to an examination of other properties, e.g. energy, and of the finer details of electron distribution at the

molecular orbital level. In each case, we have selected a representative wavefunction from those where orbital exponents have been optimised, and retaining, where possible, consistency in H1s exponent values as an aid to comparison.

III.3.A H_2O

Wavefunctions for H_2O in the four procedures M1, M2, V1 and V2 are listed serially in Tables III.3.1 to III.3.4. Total energies have not previously been scrutinised, and the greater stability afforded by Version 1 over Version 2 in the minimal bases (-75.5693au, M1 *vs* -75.3323au,M2) is representative of a general trend observed throughout the grid calculations. By comparison with the best *ab initio* minimal basis result of -75.7033au [57], neither value fares particularly well, but then, nor does the last figure in relation to the experimental value of -76.481 au. However, we are inclined to discount total energy as a criterion of assessment where Hamiltonian approximations exist. As for the valence basis results, in the absence of the dominant inner-shell O1s stabilisation, comparison is meaningful only between V1 and V2, and the respective values, -17.9429 au and -17.9244 au, probably reflect the rather smaller differences recorded for the one-electron properties in both procedures.

Experimental ionisation potentials for H_2O have been measured as (in au) 0.463 $\pm$ .004, 0.533 $\pm$ 0.011 and 0.595 $\pm$ 0.011 [78,79], and these are to be compared, via Koopman's Theorem, with

Table III.3.1 H_2O - M1 Optimised Wavefunction and Populations

AO Exponents		7.66	2.15	2.01	1.20
MO	Energy(au)	O1s	O2s	O2pz	H1s
$1a_1$	-20.9424	0.9983	-.0036	-.0065	0.0408
$2a_1$	- 1.4596	-.0224	0.8440	0.1578	0.3246
$3a_1$	- .5654	-.0022	-.2429	0.9610	0.0934
$4a_1$	0.8722	-.0537	-.4208	-.2270	0.6199

		O2py	H1s
$1b_2$	- .6370	0.6328	0.5475
$2b_2$	0.0695	0.7743	-.4474

		O2px
$1b_1$	- .5171	1.0000

Tot.	-75.56930

Löwdin Populations		
AO	Oxygen	Hydrogen
1s	1.994	0.831
2s	1.646	
2pz	1.897	
2py	0.801	
2px	2.000	
Σs	3.640	0.831
Σ2p	4.698	
Nett.	8.338	0.831

Bond Indices	
O	H1s
1s	0.004
2s	0.272
2pz	0.079
2py	0.480
Σs	0.277
Σ2pσ	0.559
Σσ	0.836
%2pσ	66.9

Table III.3.2. H_2O - M2 Optimised Wavefunction and Populations

AO Exponents		7.66	2.30	2.34	1.20
MO	Energy(au)	O1s	O2s	O2pz	H1s
$1a_1$	-20.1663	0.9982	0.0004	-.0048	0.0424
$2a_1$	- 1.2623	-.0340	0.8045	0.1533	0.4051
$3a_1$	- .3081	-.0077	-.3227	0.9239	0.1452
$4a_1$	0.7690	-.0490	-.4987	-.3505	0.5595

		O2py	H1s
$1b_2$	- .4054	0.7131	0.4957
$2b_2$	0.5593	-.7011	0.5042

		O2px
$1b_1$	- .2790	1.0000

Tot.	-75.33233

Löwdin Populations		
AO	Oxygen	Hydrogen
1s	1.995	0.865
2s	1.503	
2pz	1.754	
2py	1.017	
2px	2.000	
Σs	3.498	0.865
Σ2p	4.771	
Nett	8.269	0.865

Bond Indices	
O	H1s
1s	0.003
2s	0.311
2pz	0.154
2py	0.500
Σs	0.314
Σ2pσ	0.654
Σσ	0.968
%2pσ	67.5

Table III.3.3. H_2O - V1 Optimised Wavefunction and Populations

AO Exponents		2.01	2.00	1.20
MO	Energy(au)	O2s	O2pz	H1s
$2a_1$	- 2.1618	0.9430	0.0871	0.2272
$3a_1$	- .5503	-.1951	0.9267	0.2272
$4a_1$	0.7177	-.2697	-.3657	0.6299

		O2py	H1s
$1b_2$	- .6878	0.6801	0.5184
$2b_2$	0.3503	0.7331	-.4809

		O2px
$1b_1$	- .4747	1.0000
Tot.	-17.94288	

Löwdin Populations		
AO	Oxygen	Hydrogen
1s	(2.000)	0.744
2s	1.855	
2pz	1.733	
2py	0.925	
2px	2.000	
Σs	3.855	0.744
Σp	4.658	
Nett	8.513	0.744

Bond Indices	
O	H1s
(1s)	-
2s	0.115
2pz	0.212
2py	0.497
Σs	0.115
Σ2pσ	0.709
Σσ	0.825
%2pσ	86.0

Table III.3.4. H_2O - V2 Optimised Wavefunction and Populations

AO Exponents		2.05	2.12	1.20
MO	Energy(au)	O2s	O2pz	H1s
$2a_1$	- 2.1103	0.9388	0.0819	0.2366
$3a_1$	- .4728	-.2384	0.8557	0.3248
$4a_1$	0.5723	0.2487	0.5109	-.5818

		O2py	H1s
$1b_2$	- .5628	0.7653	0.4552
$2b_2$	0.5985	0.5109	-.5818

		O2px
$1b_1$	- .3819	1.0000
Tot.	-17.92442	

Löwdin Populations		
AO	Oxygen	Hydrogen
1s	(2.000)	0.737
2s	1.876	
2pz	1.478	
2py	1.171	
2px	2.300	
Σs	3.876	0.737
Σ2p	4.649	
Nett	8.525	0.737

Bond Indices	
O	H1s
(1s)	-
2s	0.084
2pz	0.354
2py	0.485
Σs	0.084
Σ2pσ	0.839
Σσ	0.923
%2pσ	90.9

our calculated orbital energies. M1 energies, 0.517 ($1b_1$), 0.565 ($3a_1$) and 0.637 au ($1b_2$) are slightly higher by 0.03 - 0.05 au, and the agreement is therefore quite reasonable, even without allowing for a displacement term* of ~0.04 au. Orbital energies in the M2 wavefunction deviate by larger amounts, 0.18 - 0.22 au, but the displacement is again reasonably constant. Less consistency is observed in the valence bases, for in Version 1, the excellent agreement achieved by the lower potentials at 0.475 and 0.550 au is marred by the highest value at 0.688 au, and, again, in Version 2, deviations in the $1b_1$ and $3a_1$ orbitals amount to 0.06 and 0.08 au respectively, but drop to 0.03 au for the $1b_2$ MO. Nevertheless, with the displacement terms accounted as a necessary consequence of integral approximation, all four procedures must be regarded as essentially correct in their prediction of experimental ionisation potentials.

Electron distributions in the molecular plane of H_2O are displayed in Figs. III.3.1 ff. Contour intervals are shown alternately as integers and overprinted characters (the representations are photographic reductions of computer printed output), where the density limits in any numbered region, n, follow from the formula $2^{2n} \leq \rho \times 10^3 < 2^{2n+1}$, eg region 0 implies $.001 \leq \rho < .002$.

---

* The average deviation from experimental values for the M1 set is 0·043 av. If we allow this as an empirical correction term to be subtracted from the M1 values, the resultant predicted ionisation potentials, 0.474, 0.522 and 0.594 av are all in very close accord with experiment.

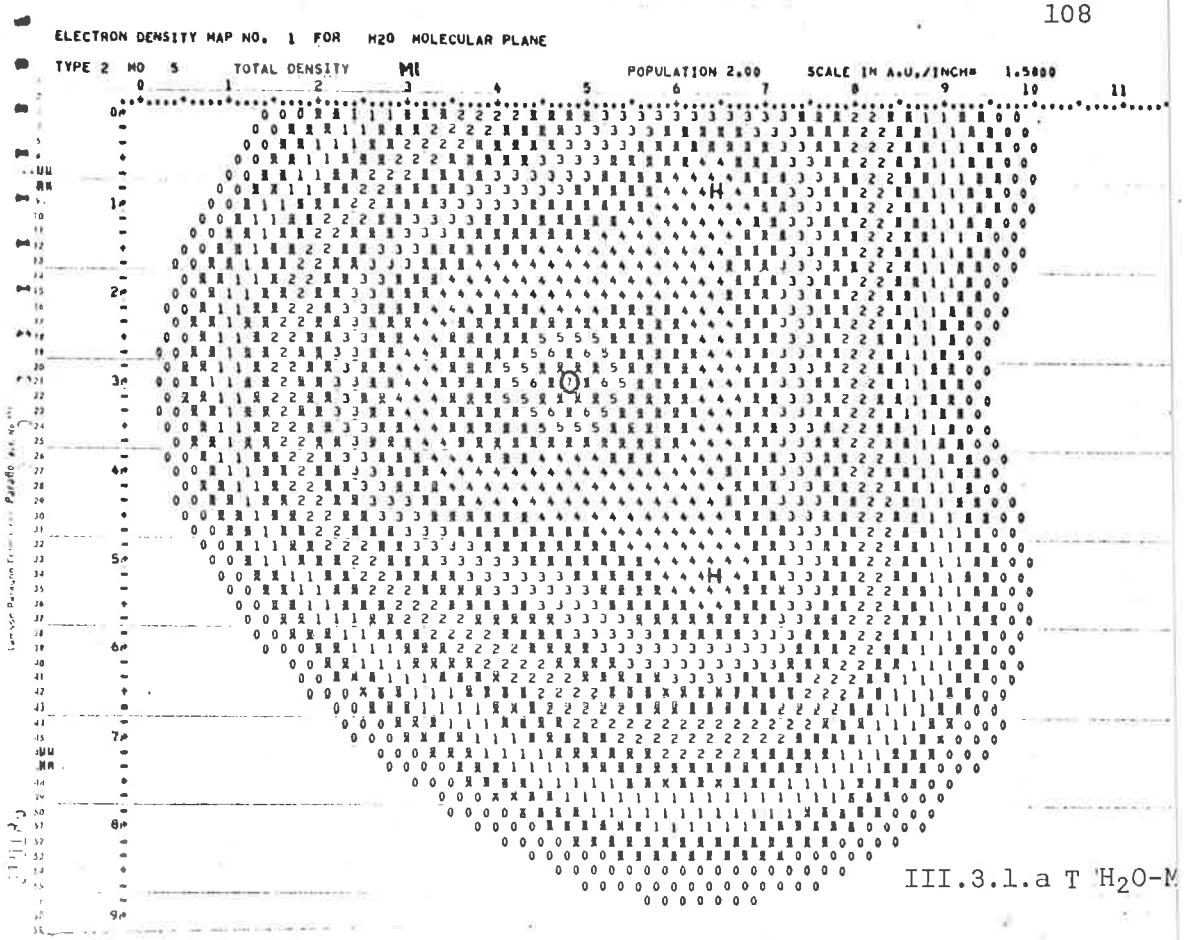

III.3.1.a T H_2O-M1

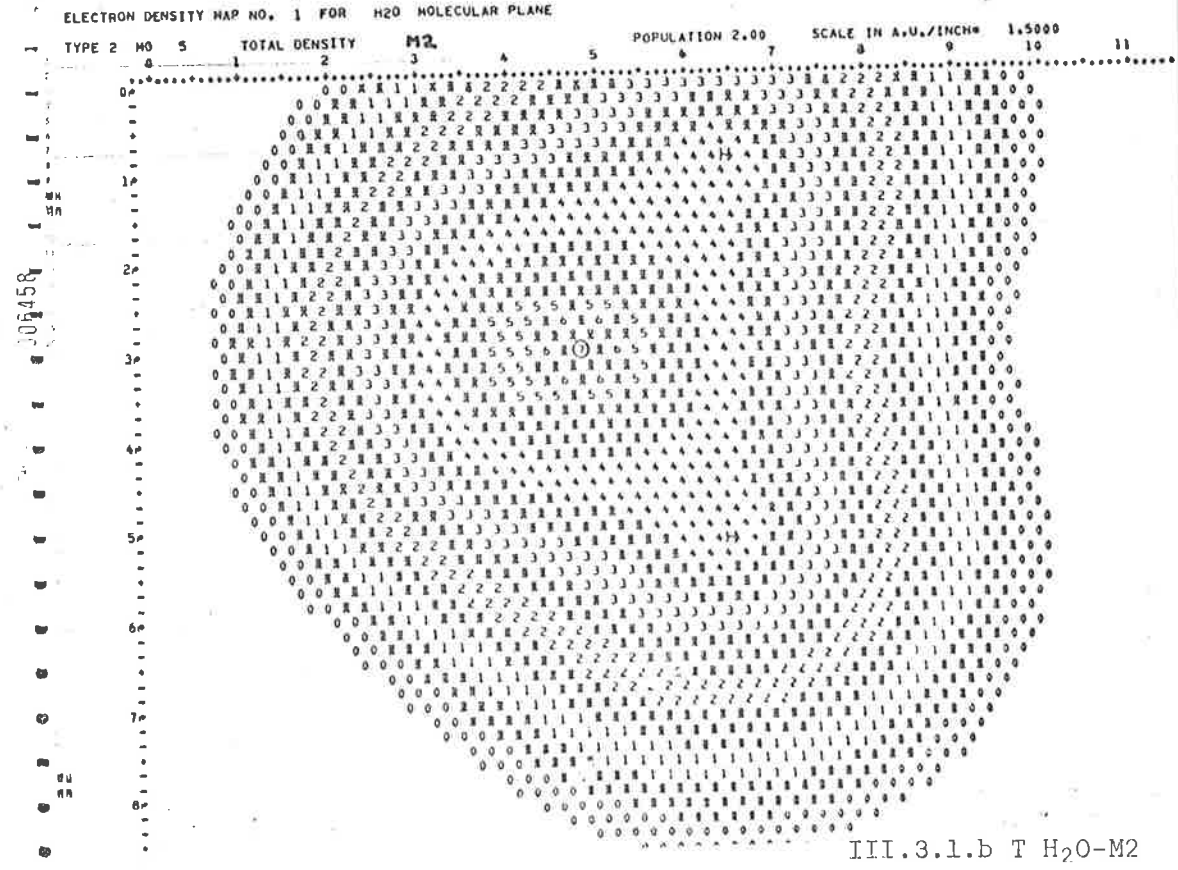

III.3.1.b T H_2O-M2

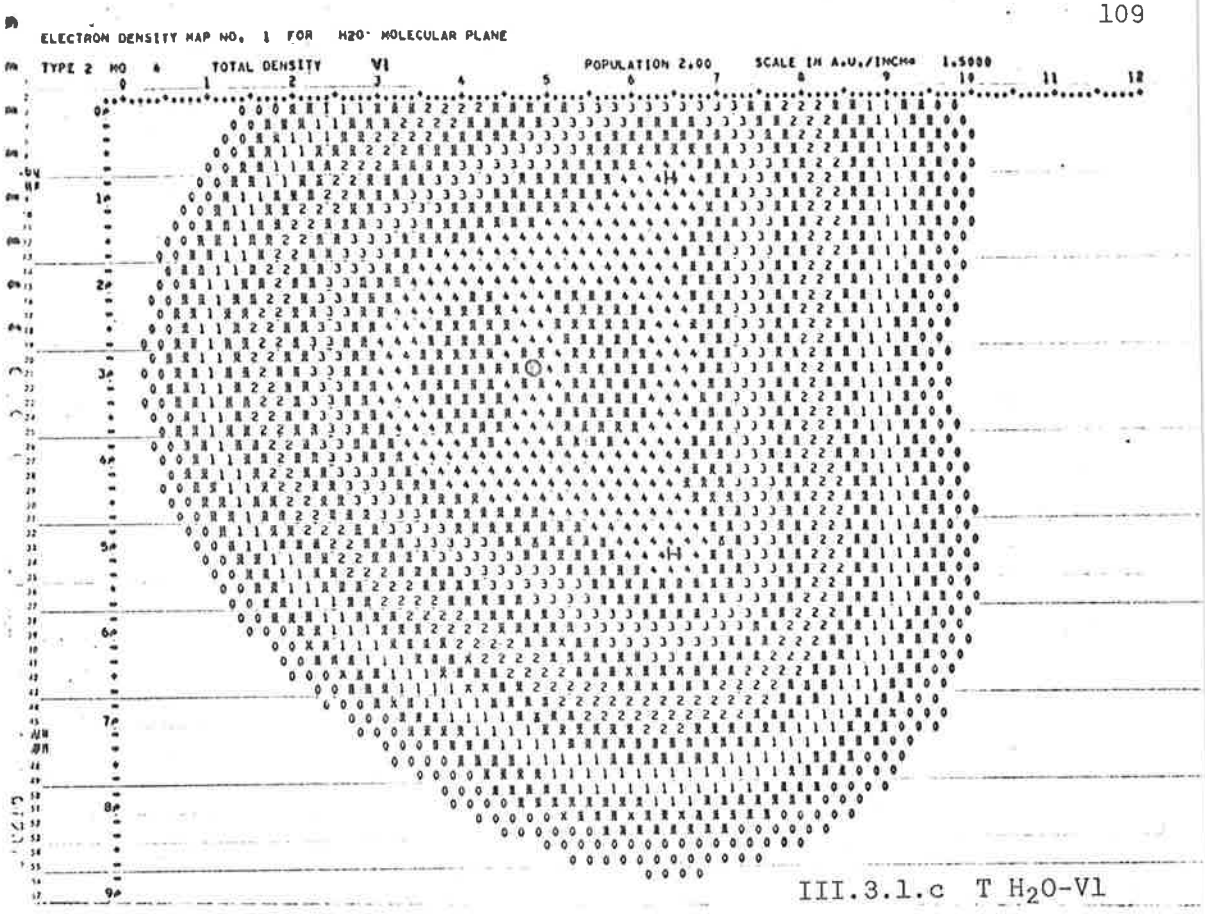

III.3.1.c T H_2O-V1

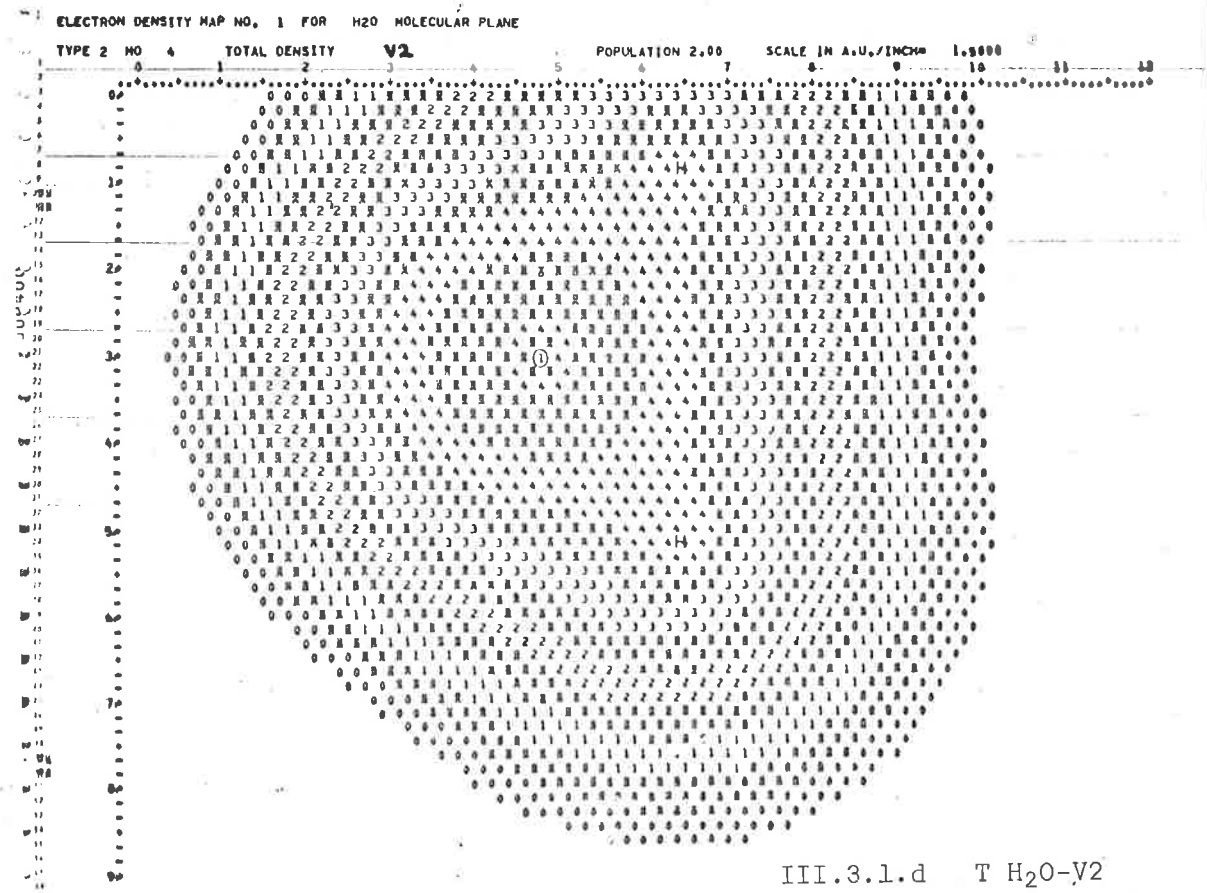

III.3.1.d T H_2O-V2

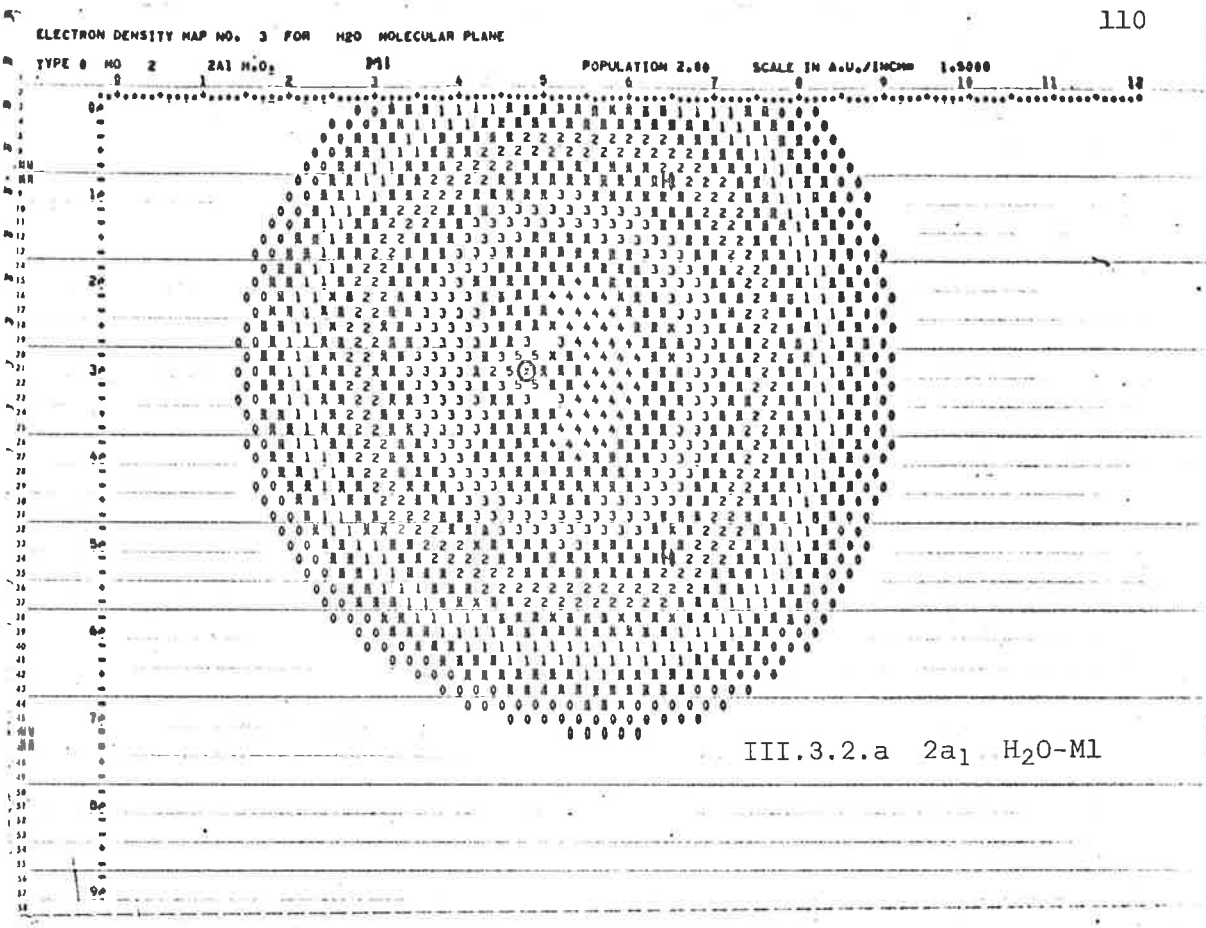

III.3.2.a $2a_1$ H_2O-M1

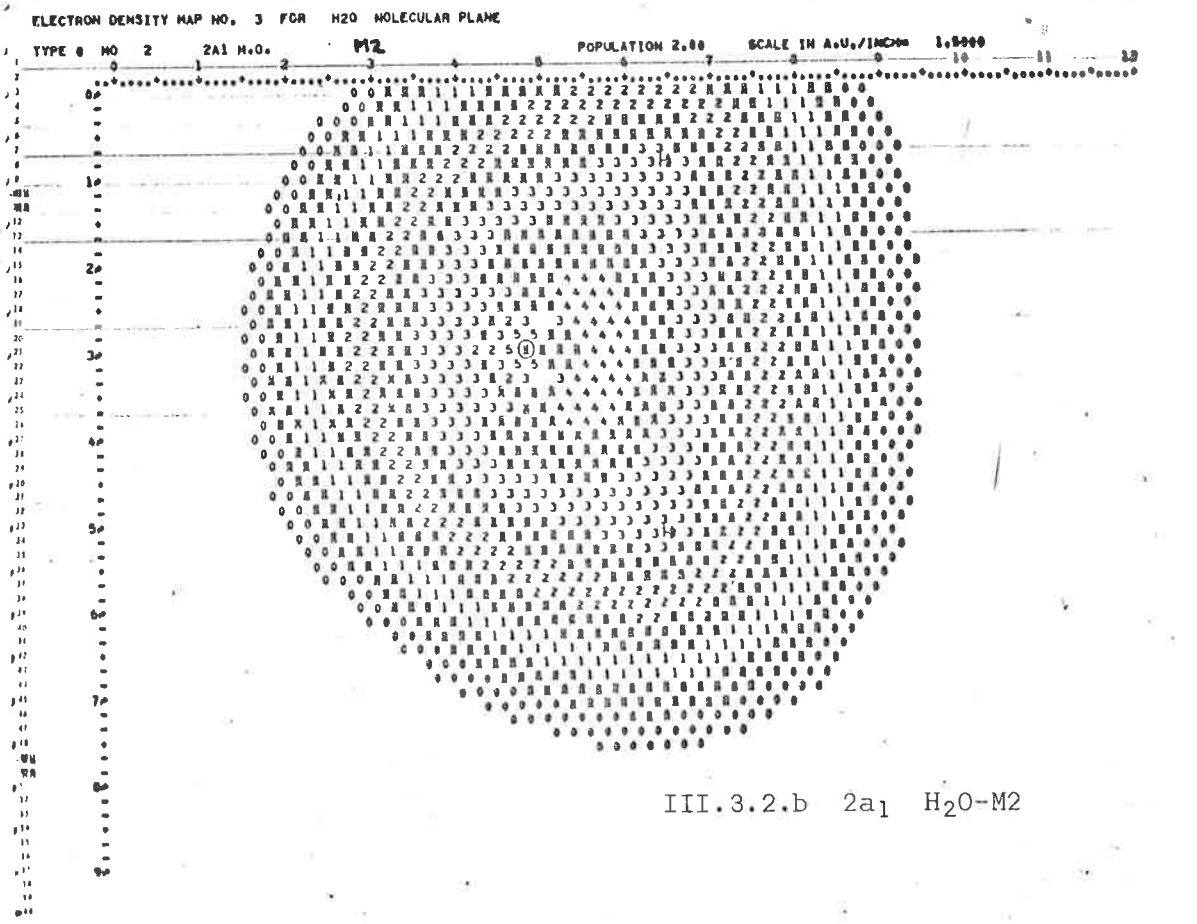

III.3.2.b $2a_1$ H_2O-M2

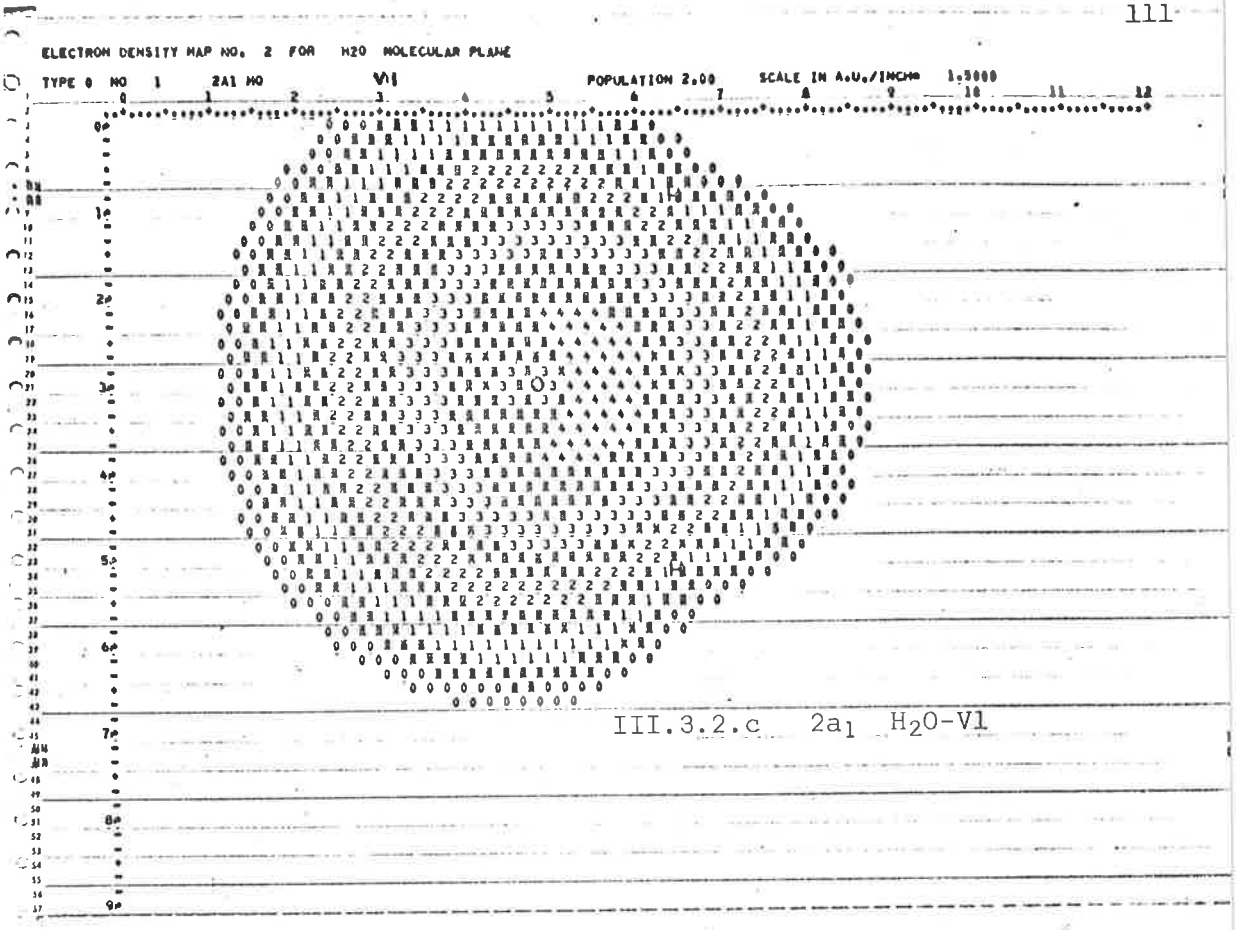

III.3.2.c $2a_1$ H_2O-V1

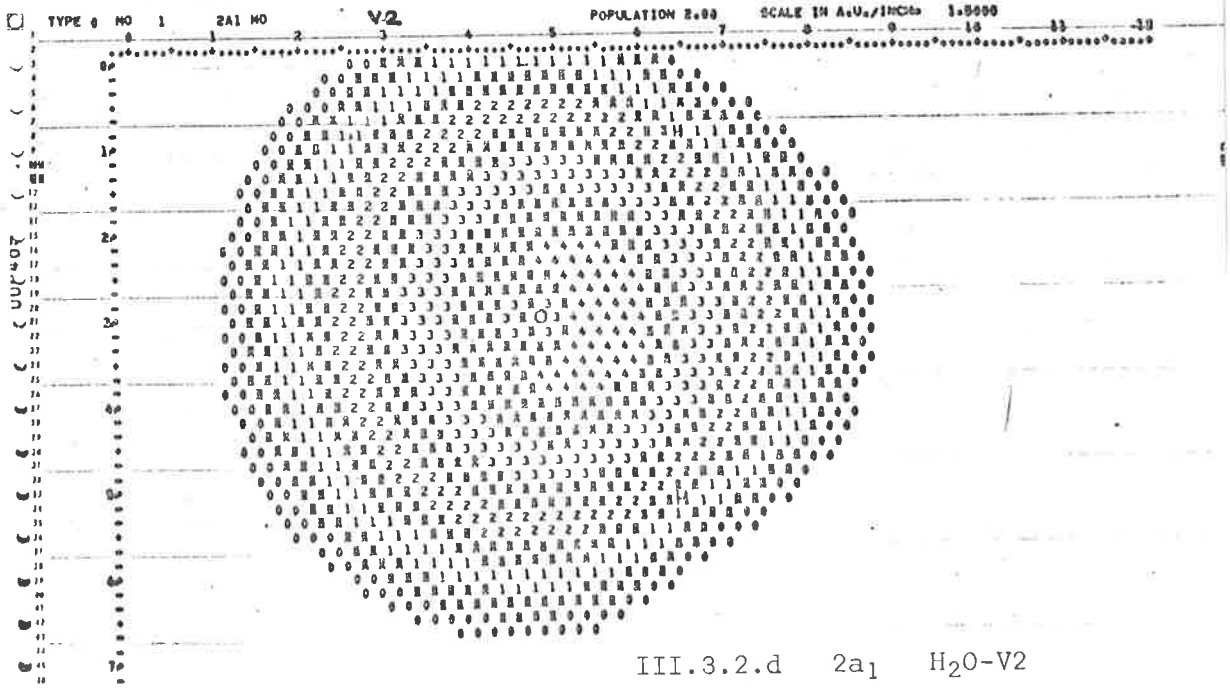

III.3.2.d $2a_1$ H_2O-V2

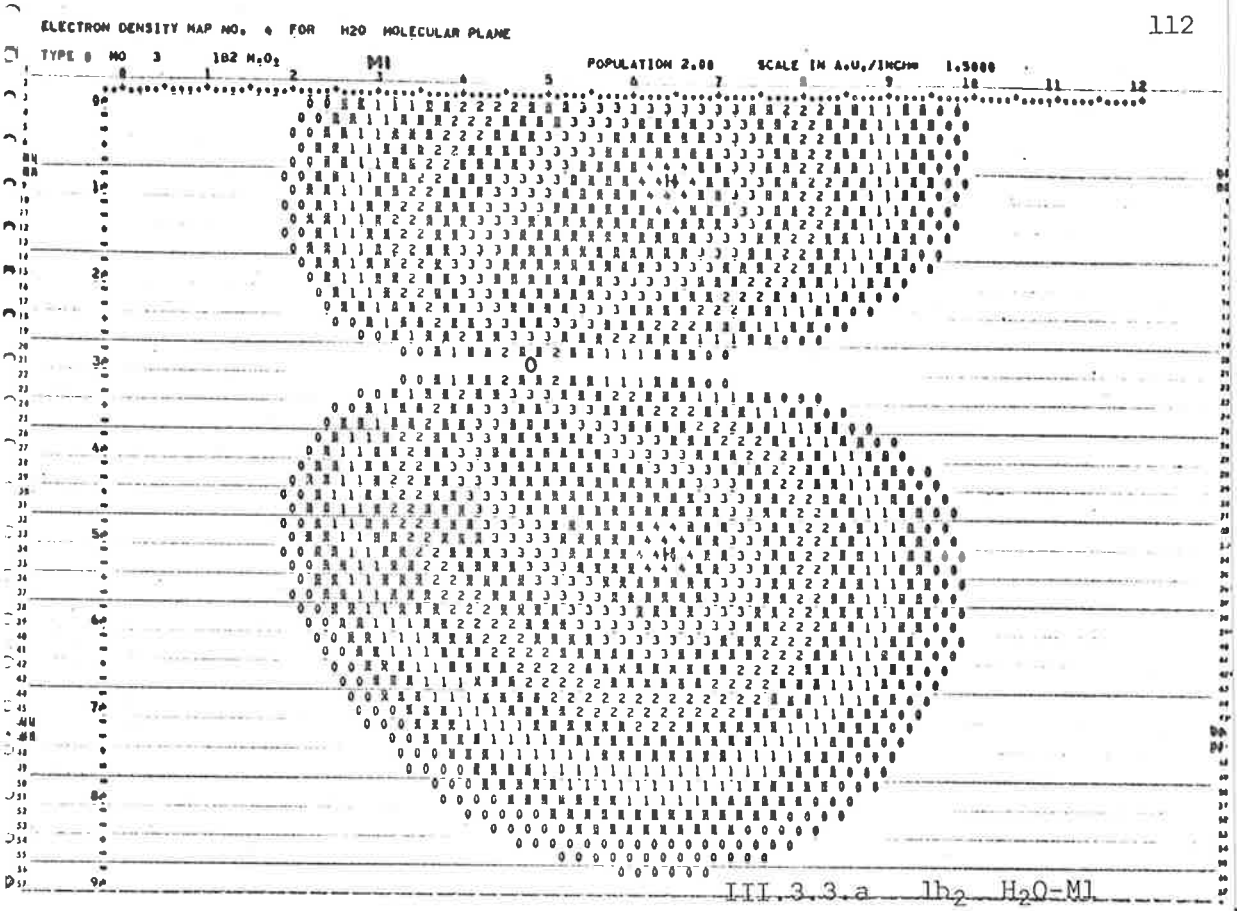

III.3.3.a $1b_2$ H_2O-M1

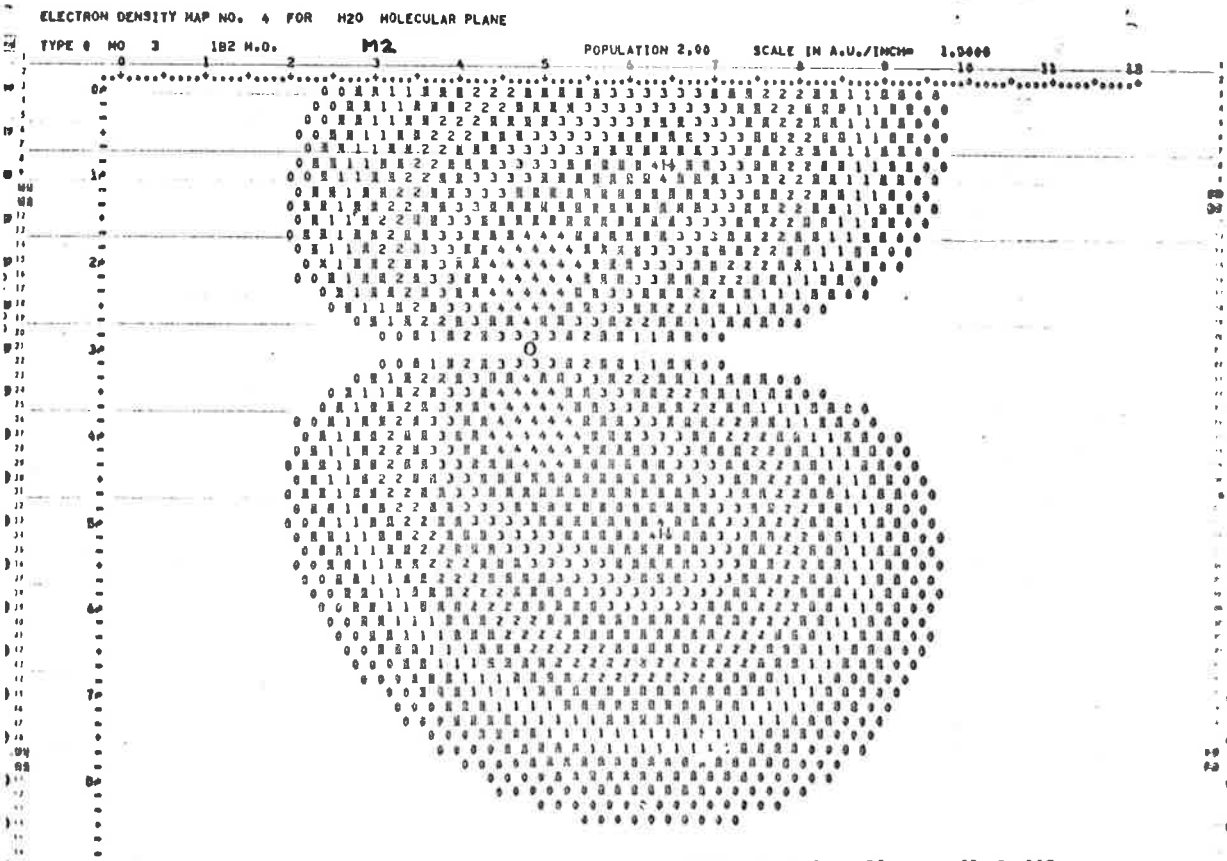

III.3.3.b $1b_2$ H_2O-M2

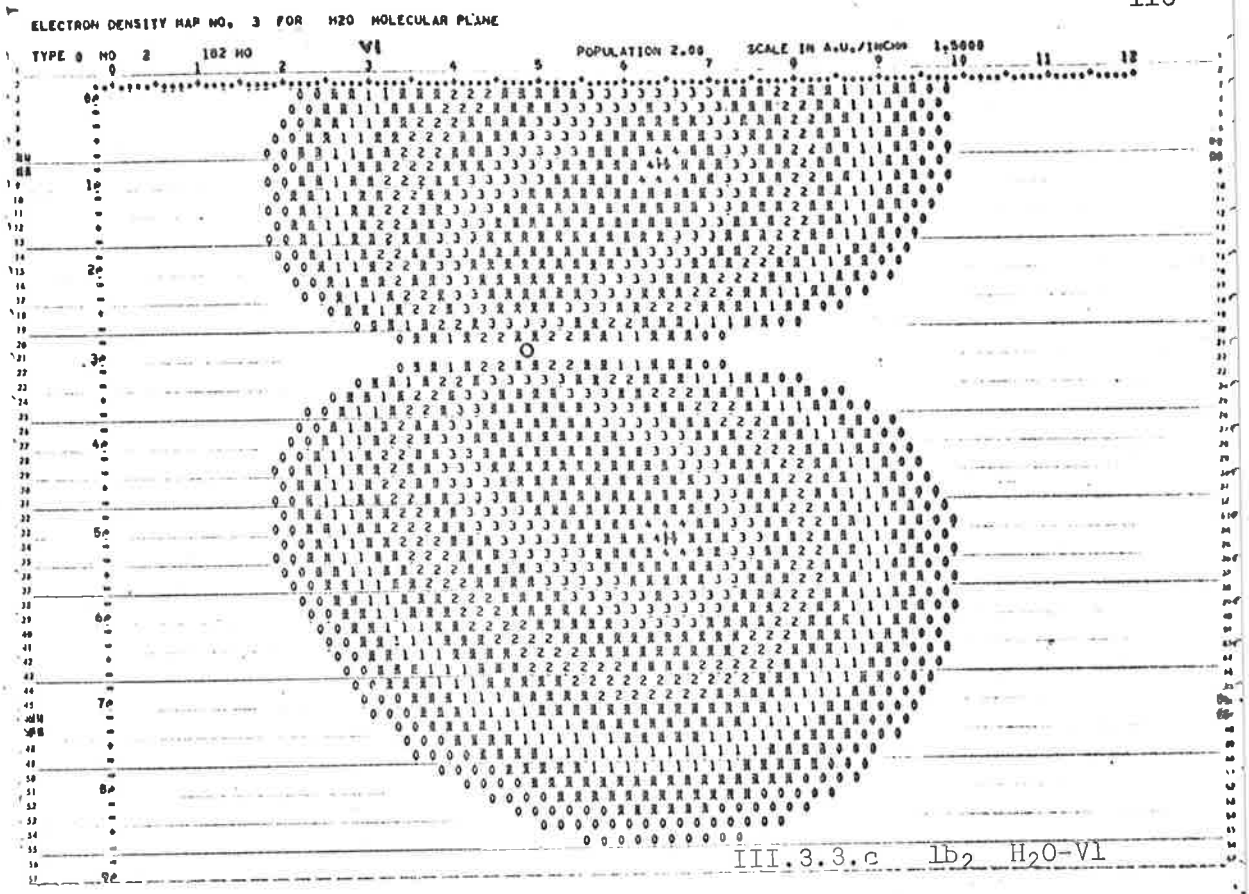

III.3.3.c $1b_2$ H_2O-V1

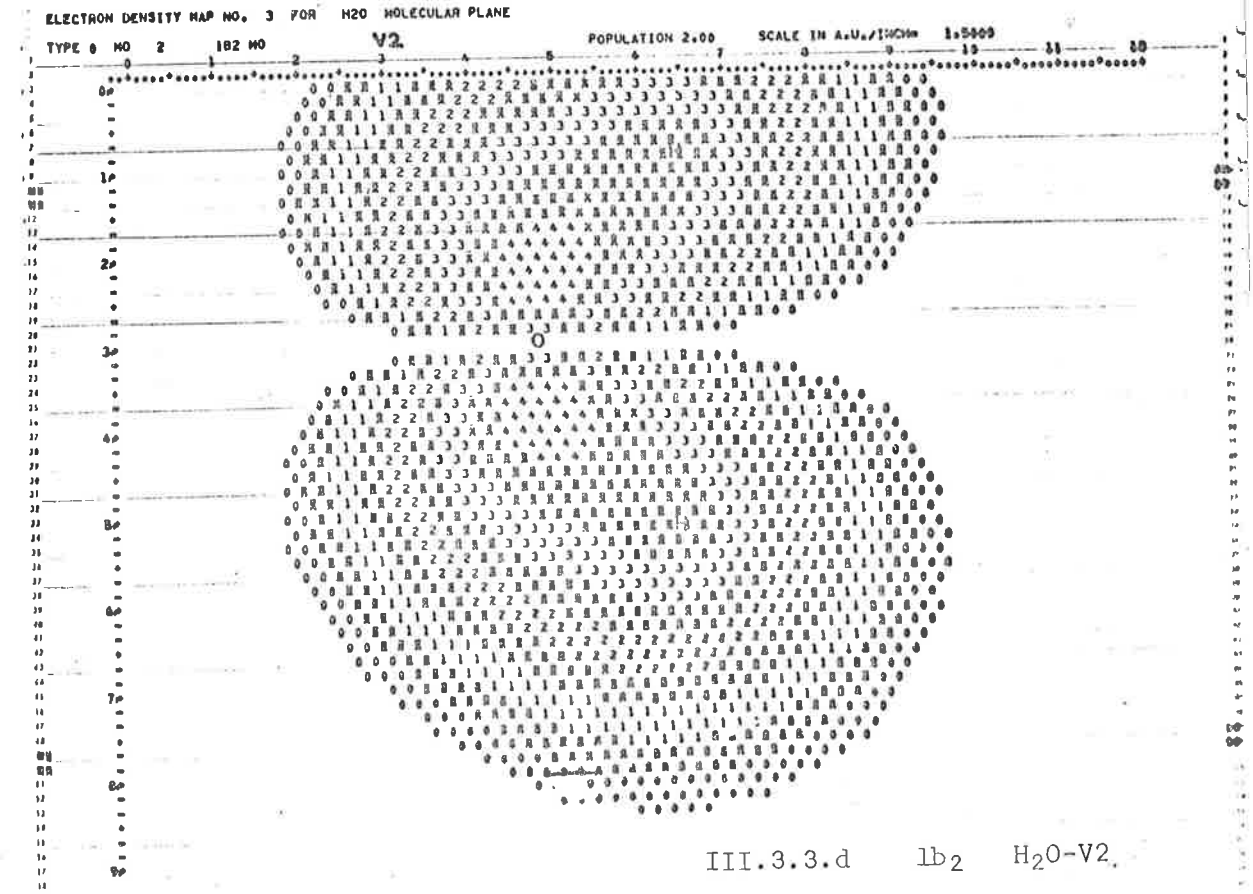

III.3.3.d $1b_2$ H_2O-V2

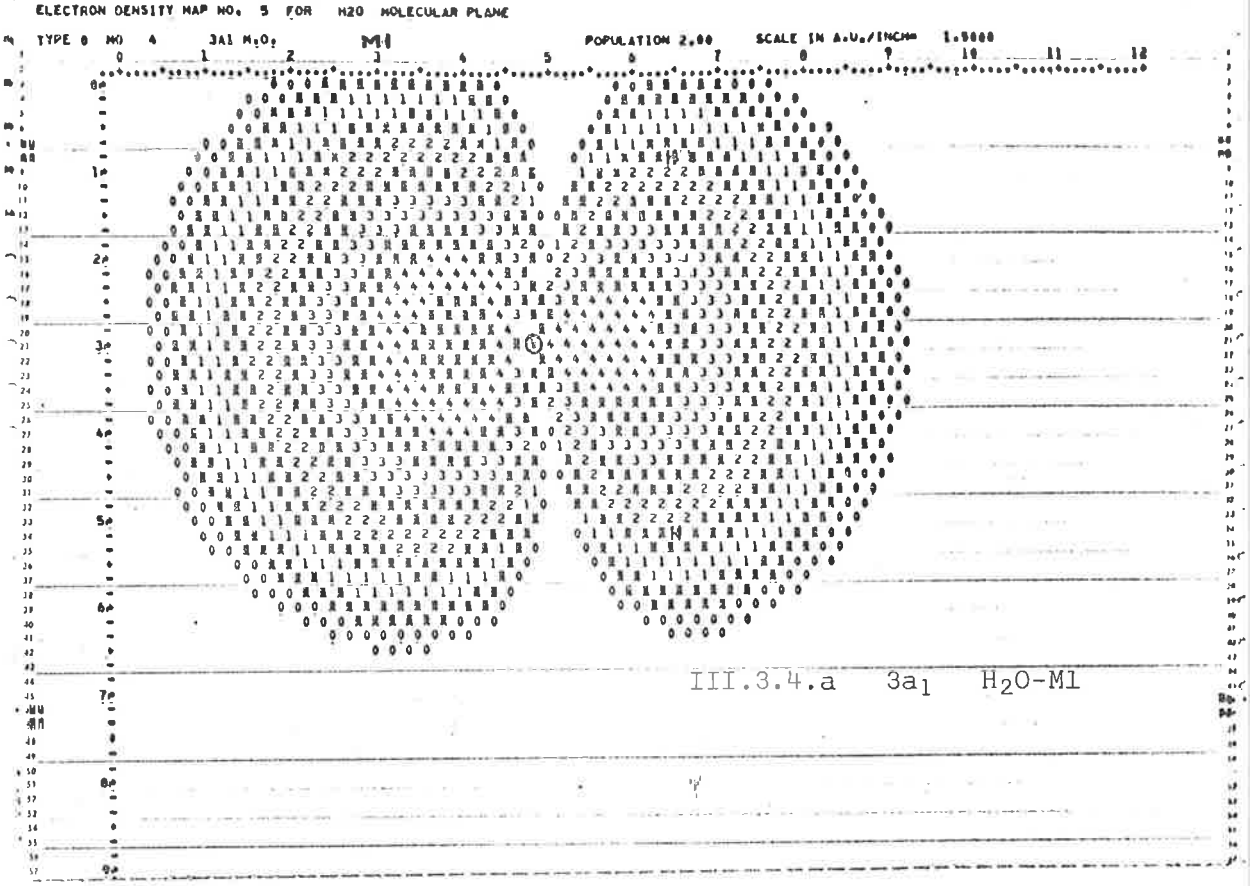

III.3.4.a $3a_1$ H_2O-M1

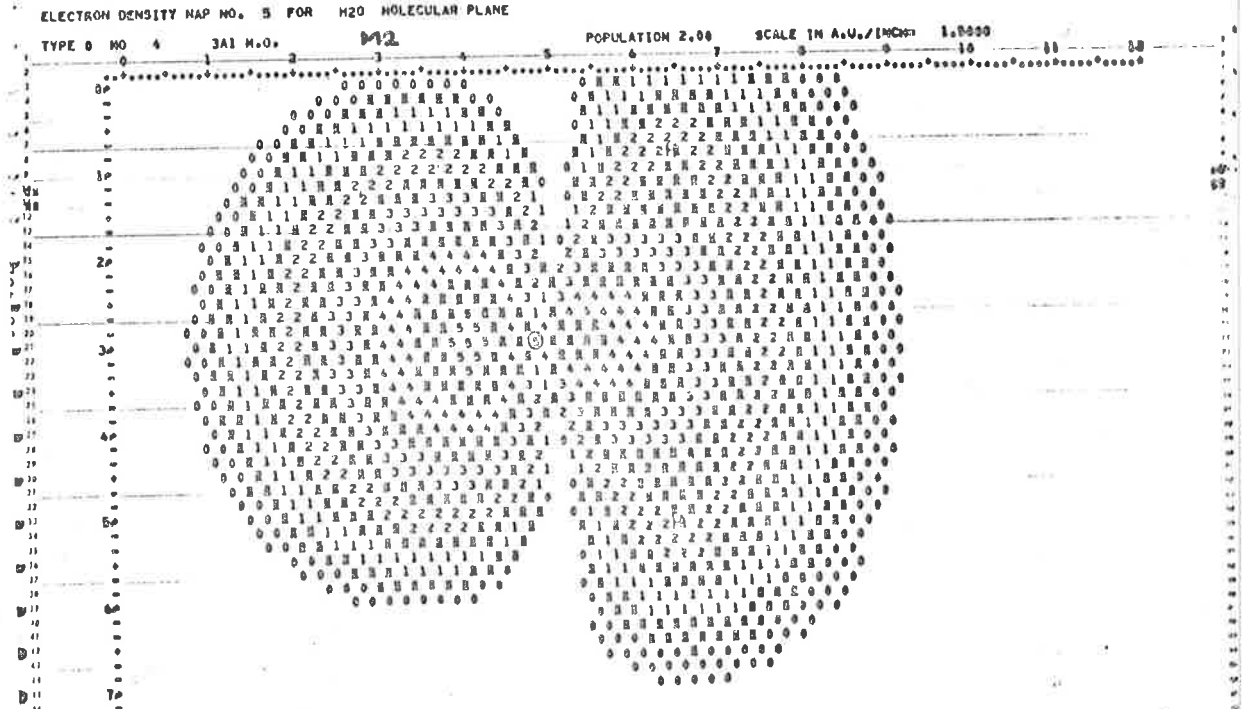

III.3.4.b $3a_1$ H_2O-M2

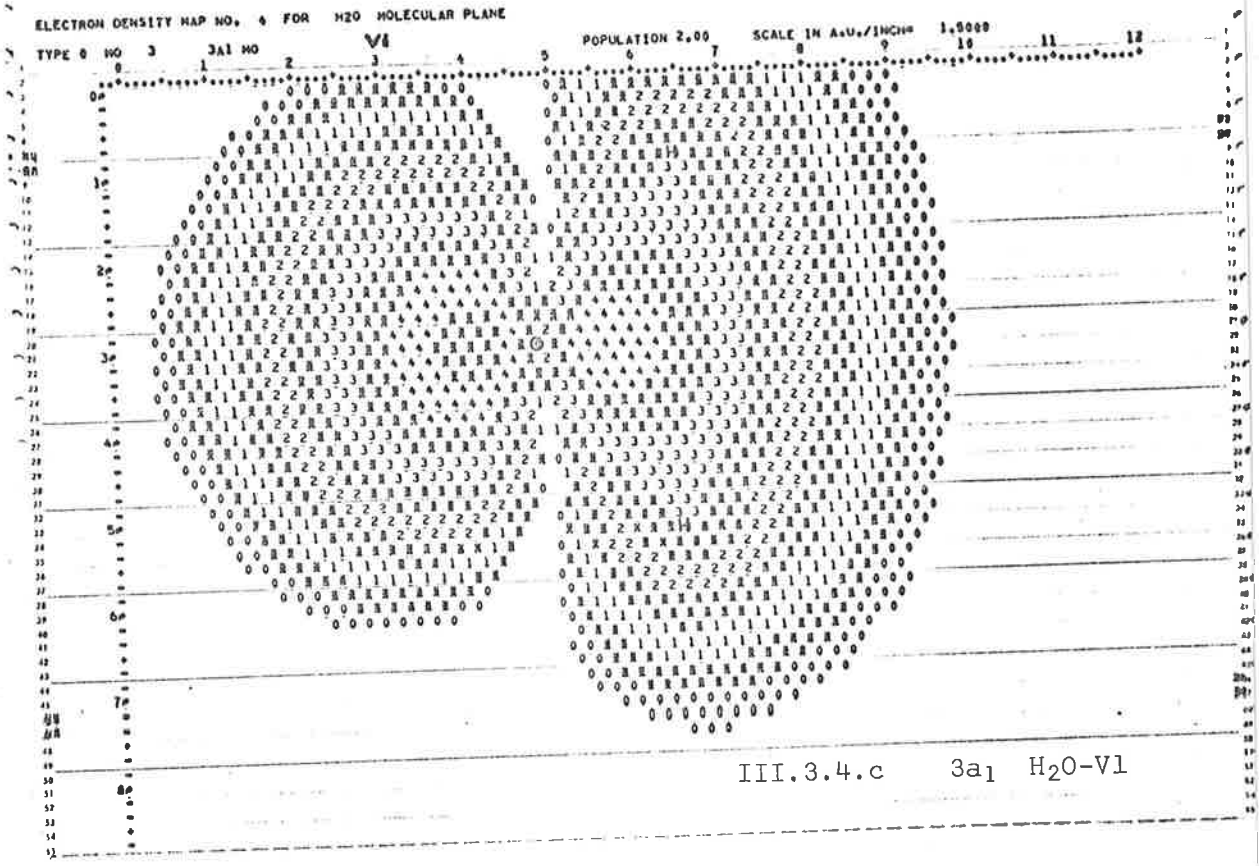

III.3.4.c $3a_1$ H_2O-V1

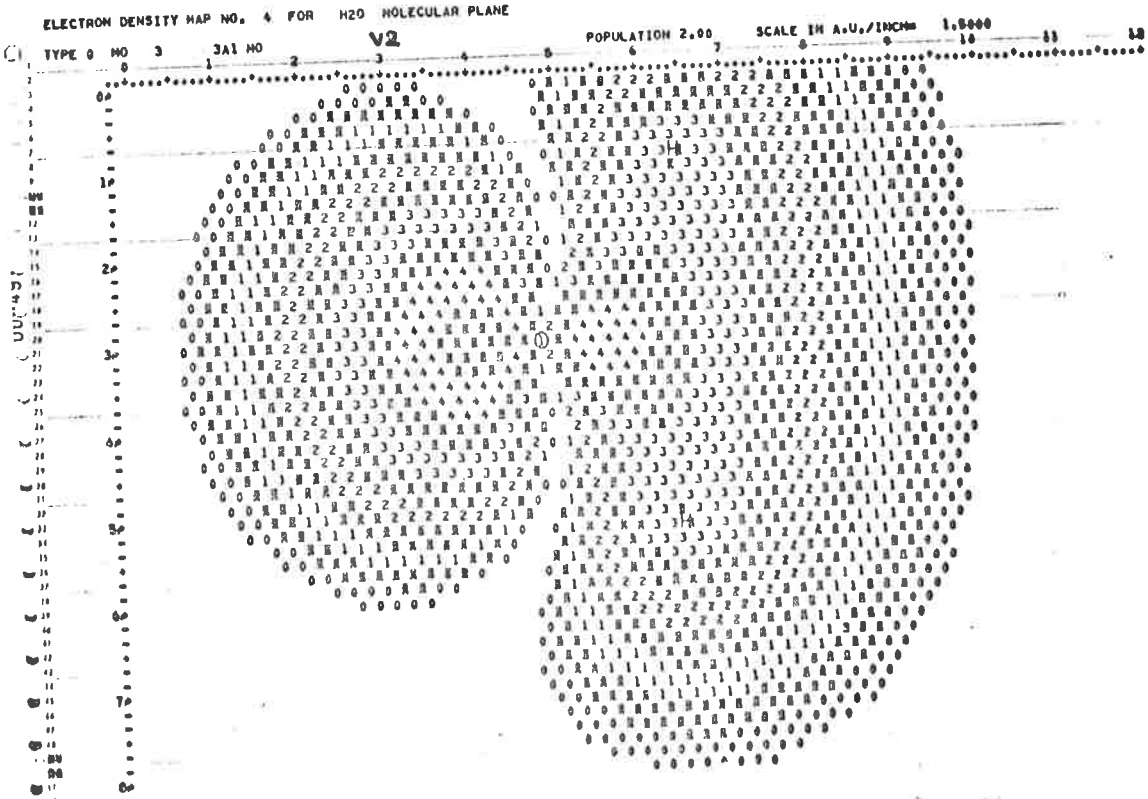

III.3.4.d $3a_1$ H_2O-V2

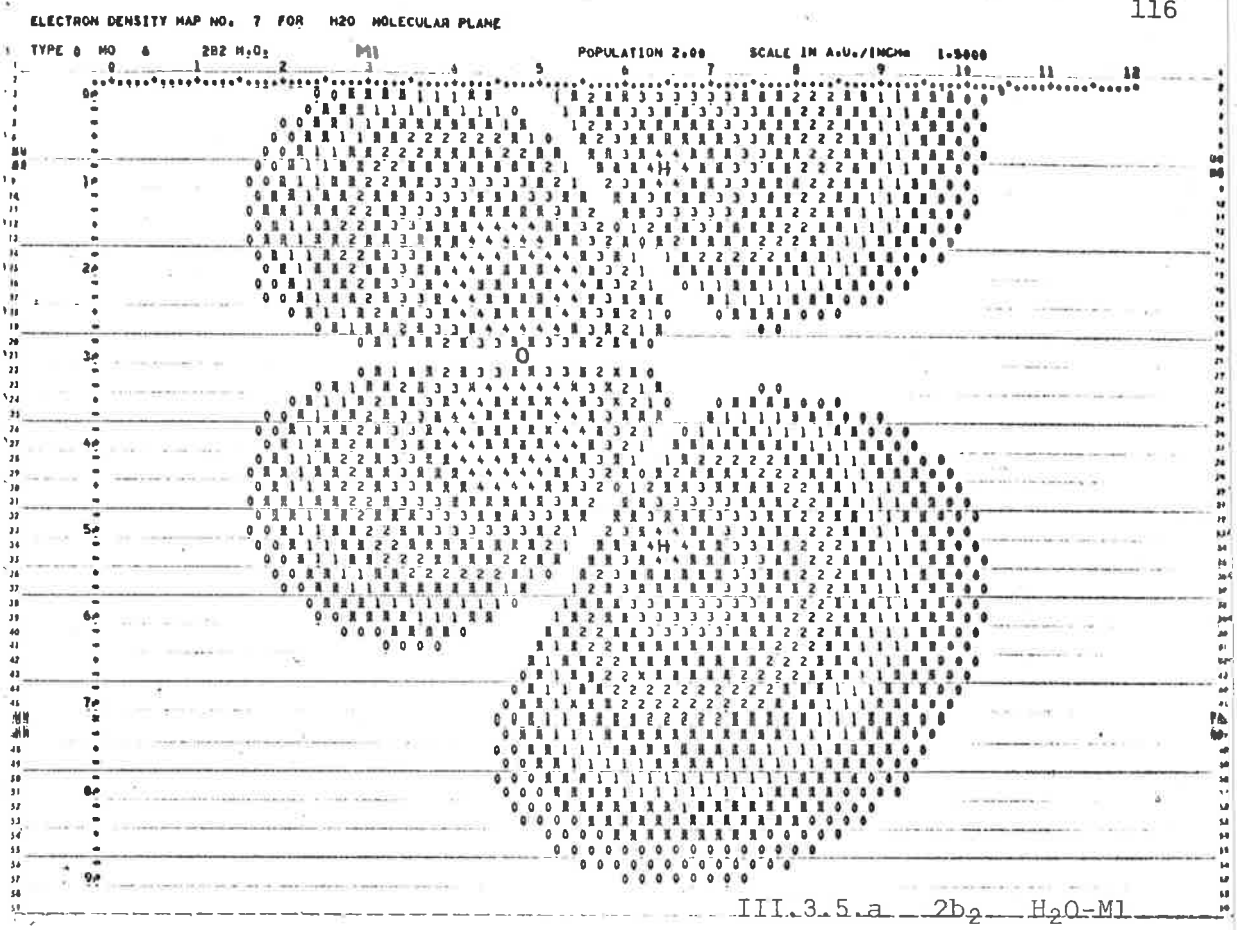

III.3.5.a $2b_2$ H_2O-M1

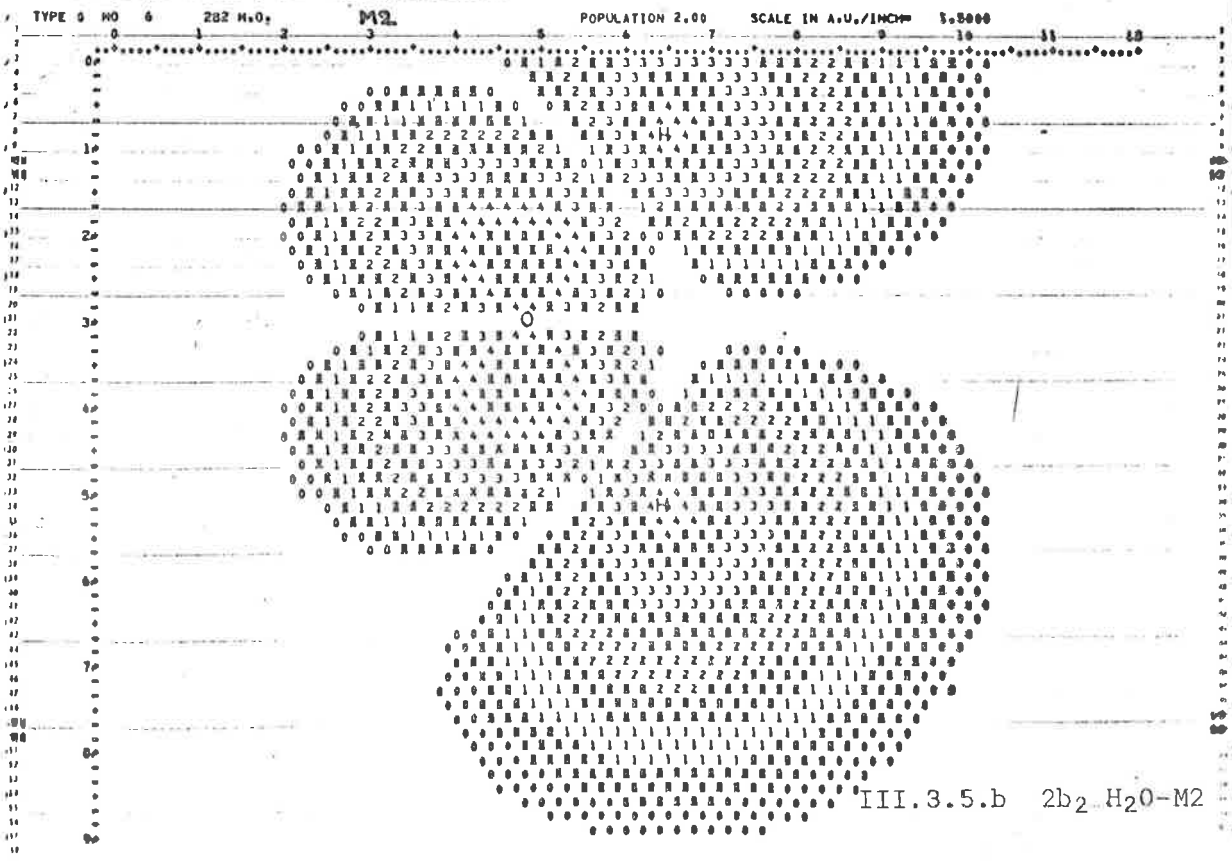

III.3.5.b $2b_2$ H_2O-M2

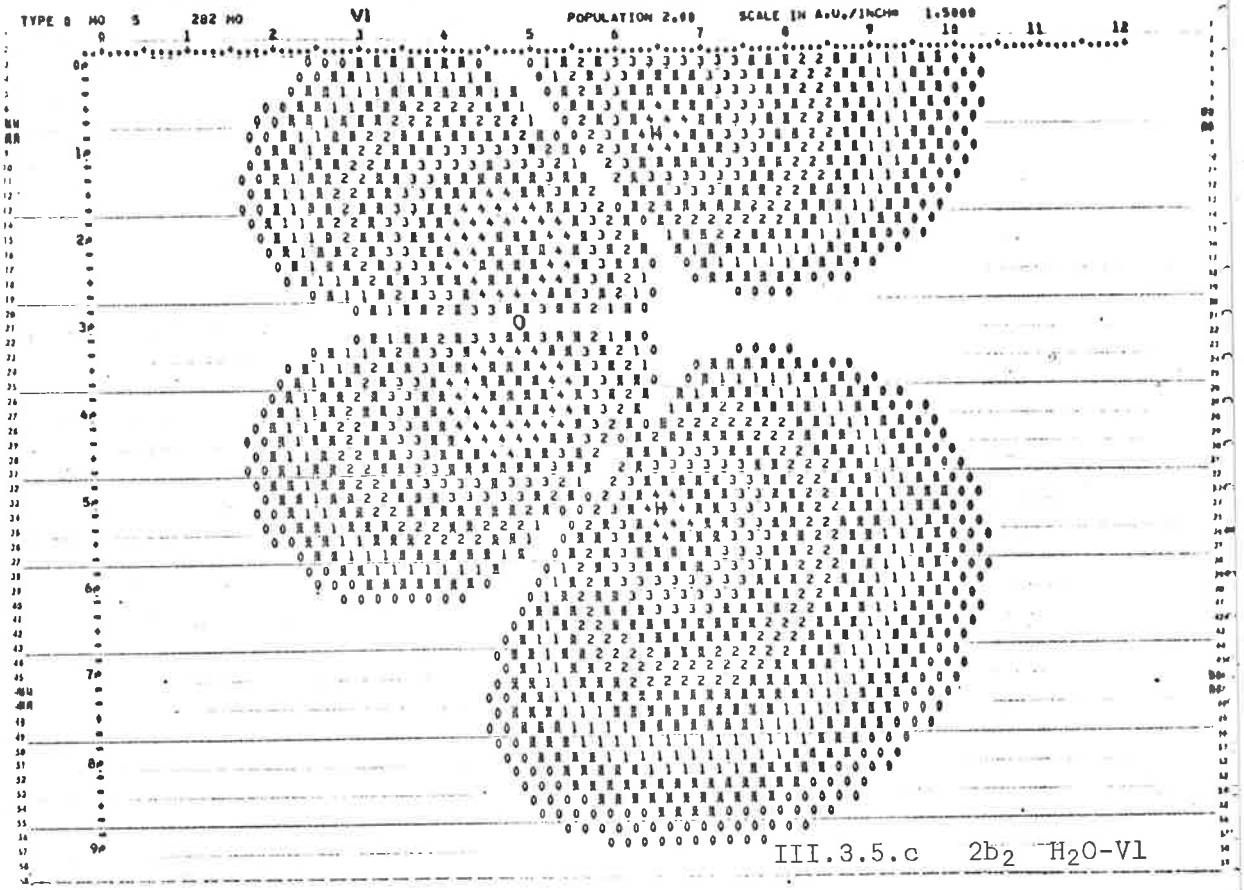

III.3.5.c $2b_2$ H_2O-V1

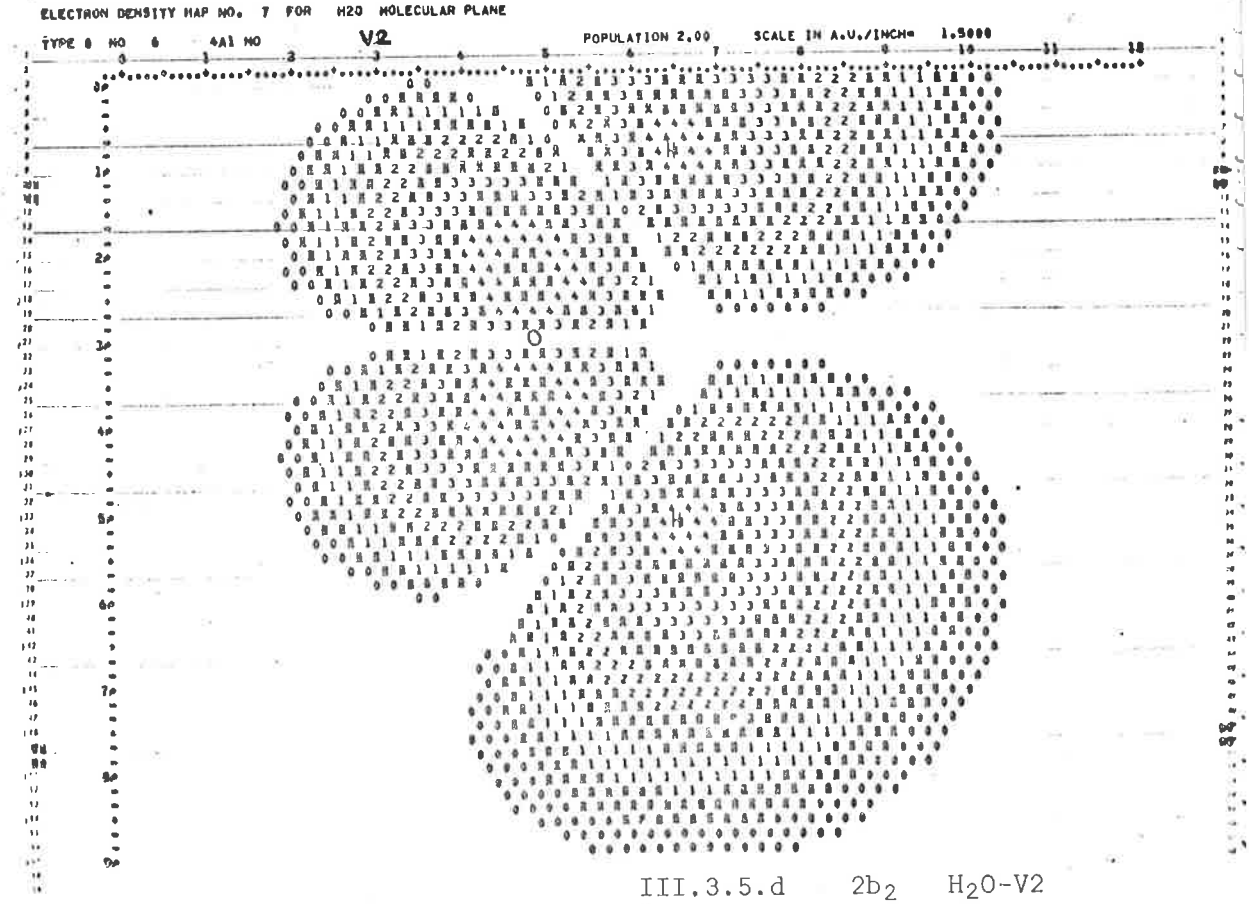

III.3.5.d $2b_2$ H_2O-V2

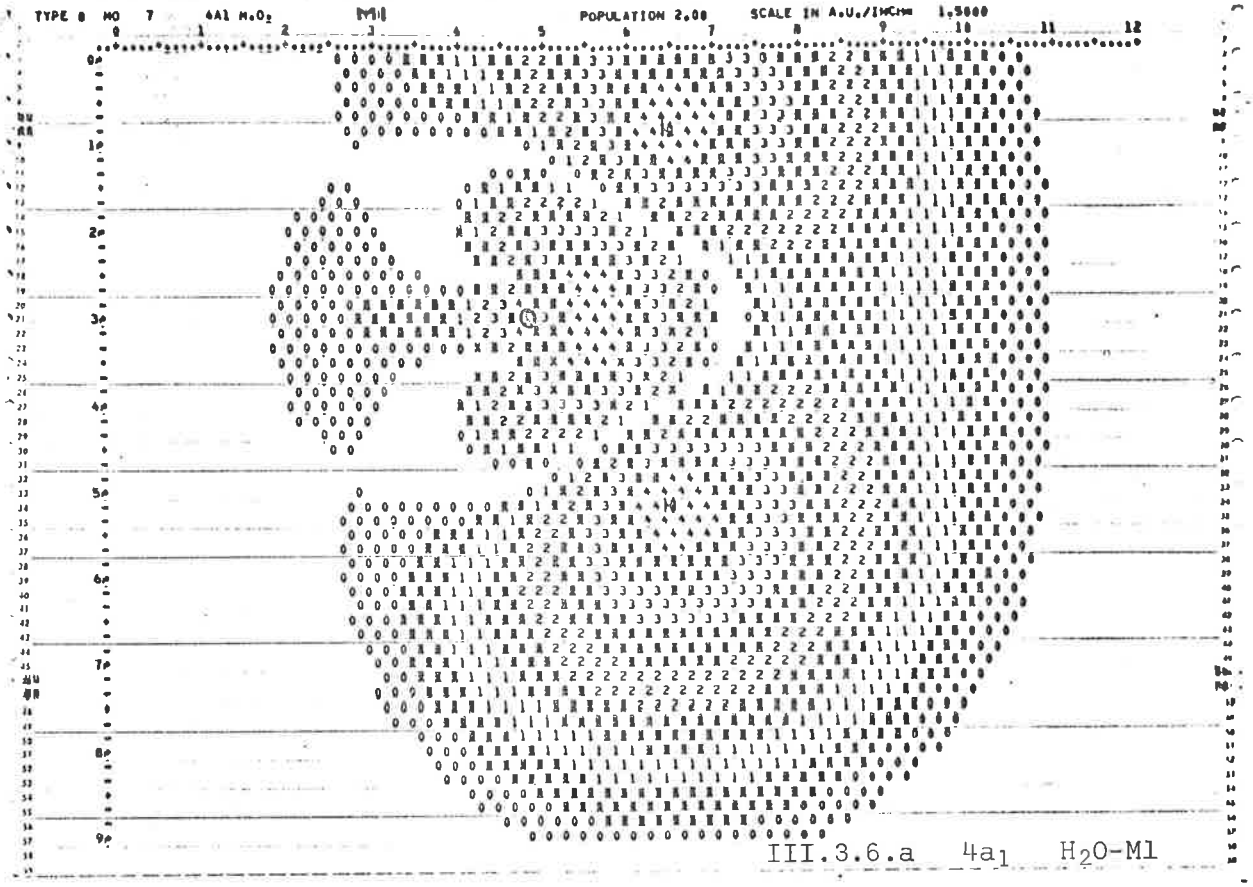

III.3.6.a $4a_1$ H_2O-M1

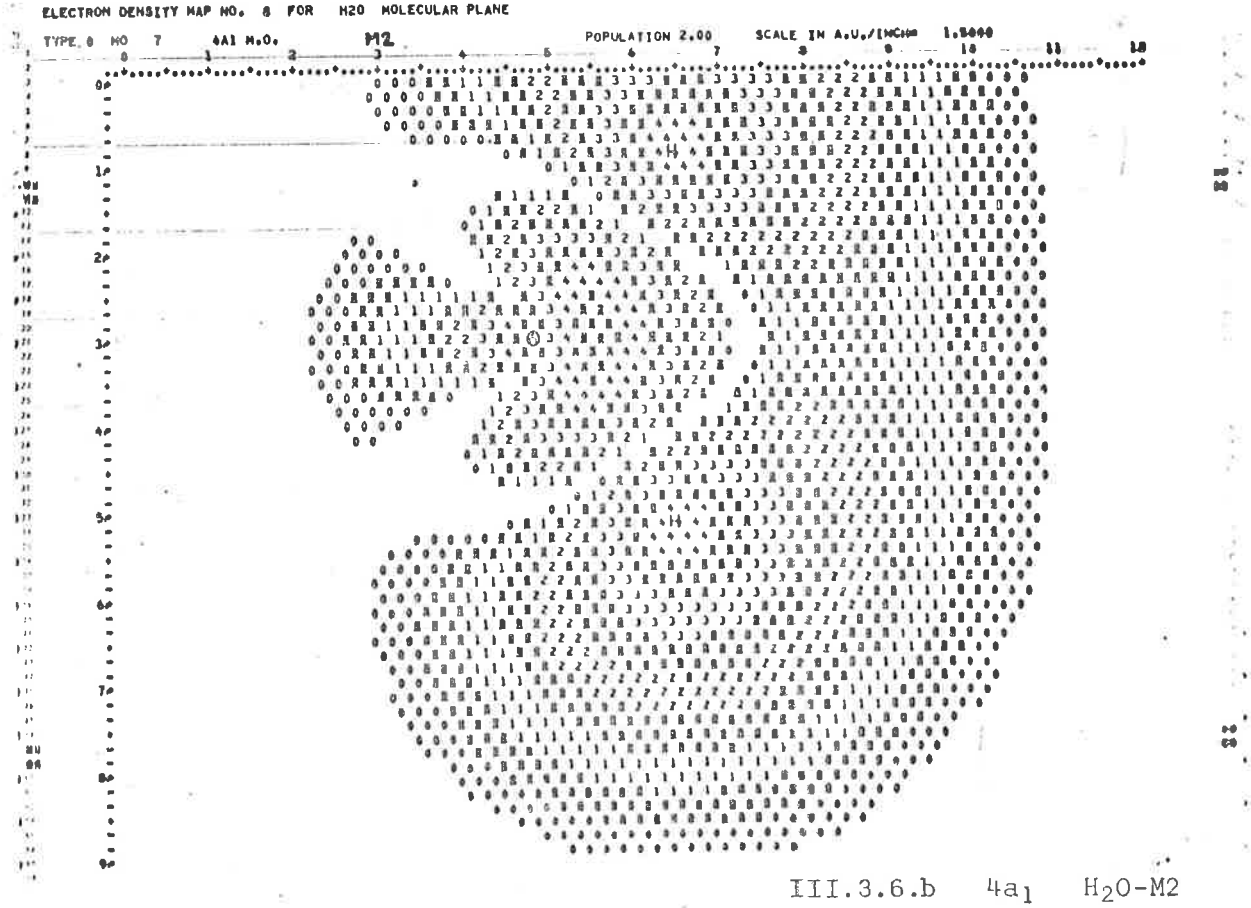

III.3.6.b $4a_1$ H_2O-M2

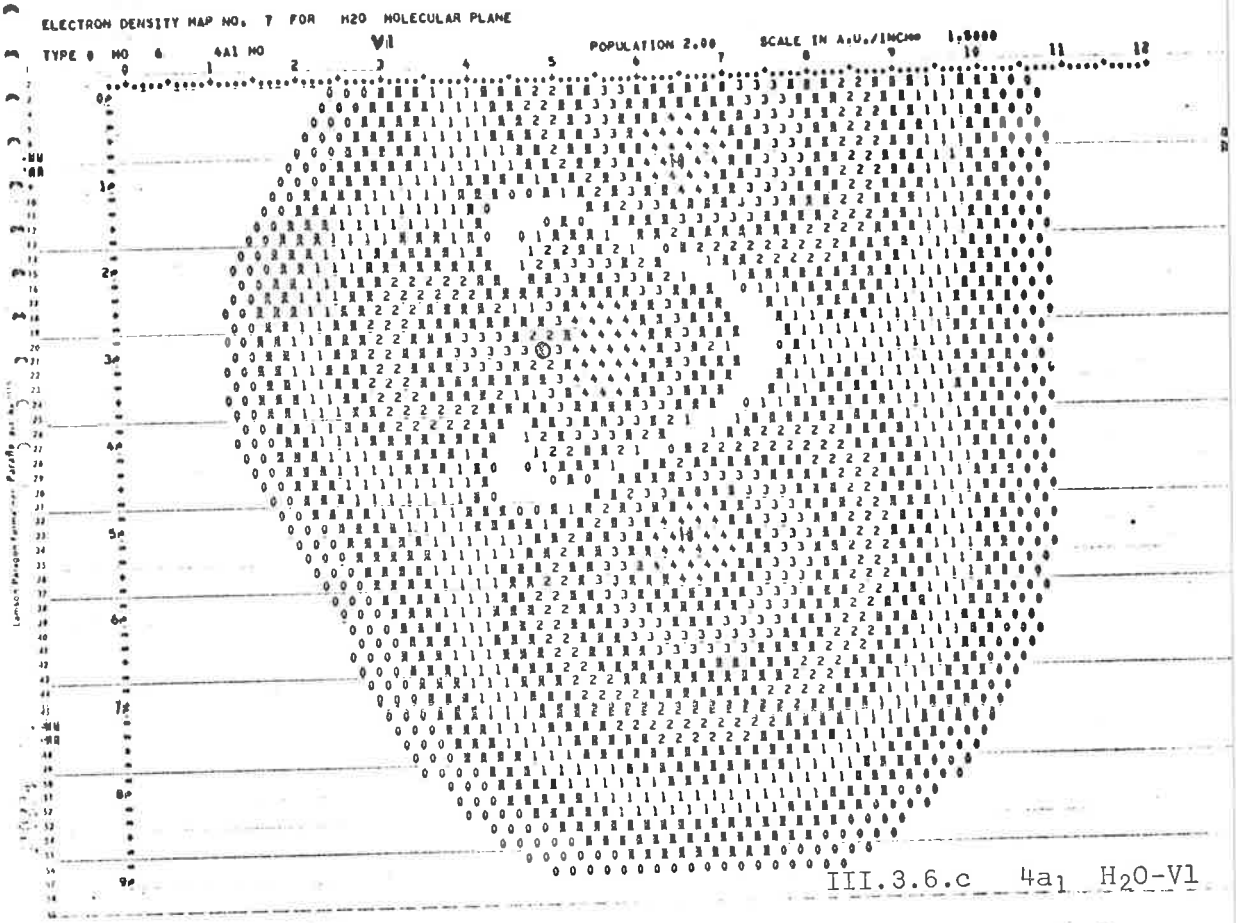

III.3.6.c $4a_1$ H_2O-V1

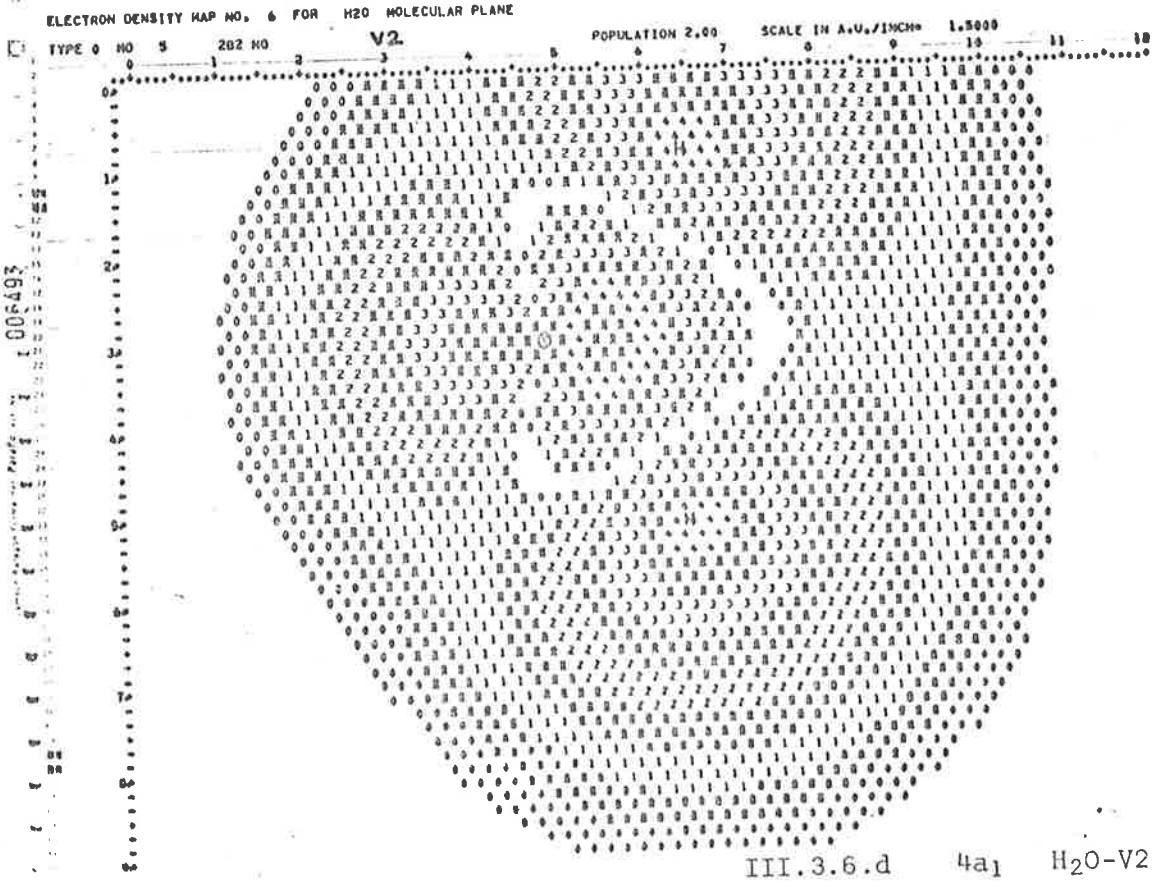

III.3.6.d $4a_1$ H_2O-V2

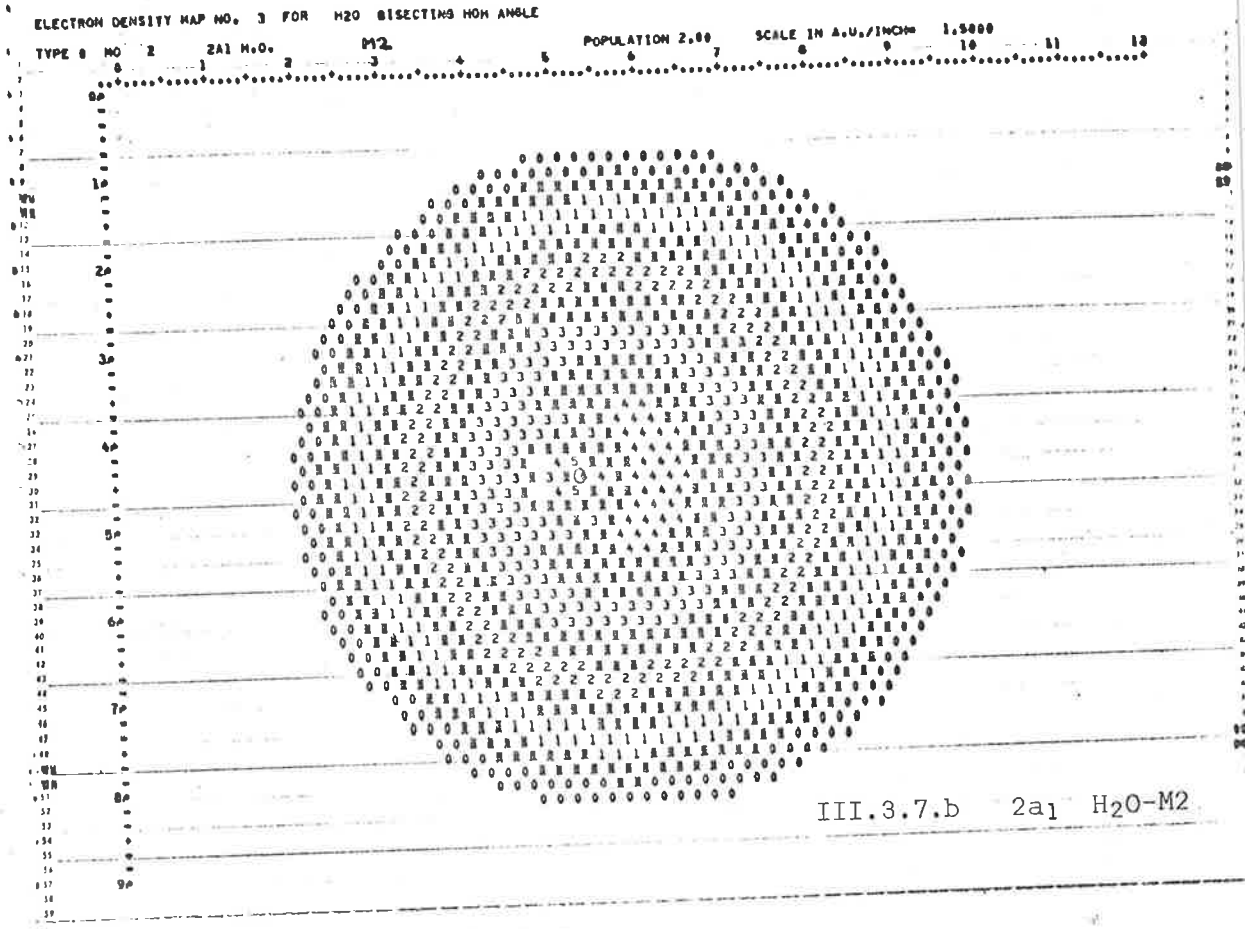

III.3.7.b $2a_1$ H_2O-M2

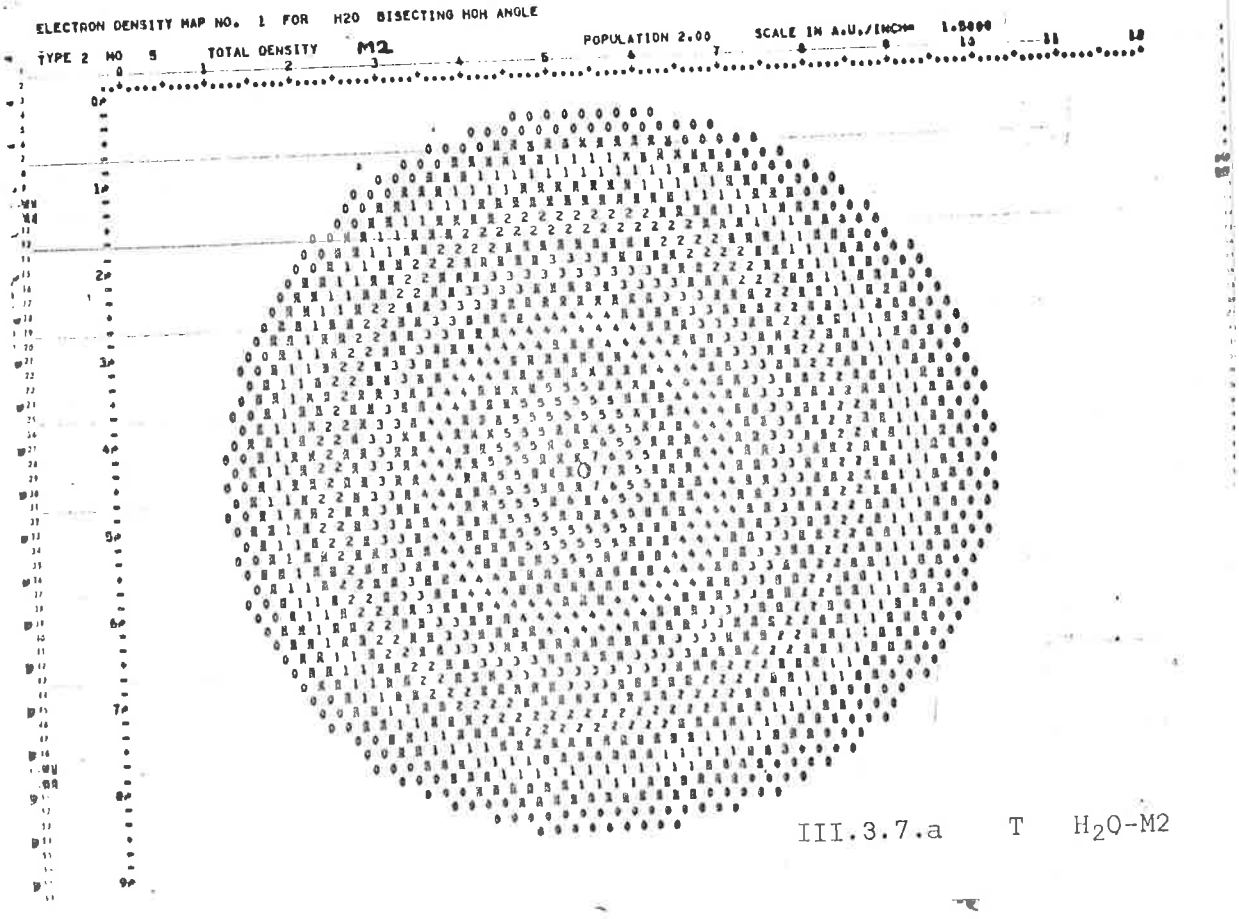

III.3.7.a T H_2O-M2

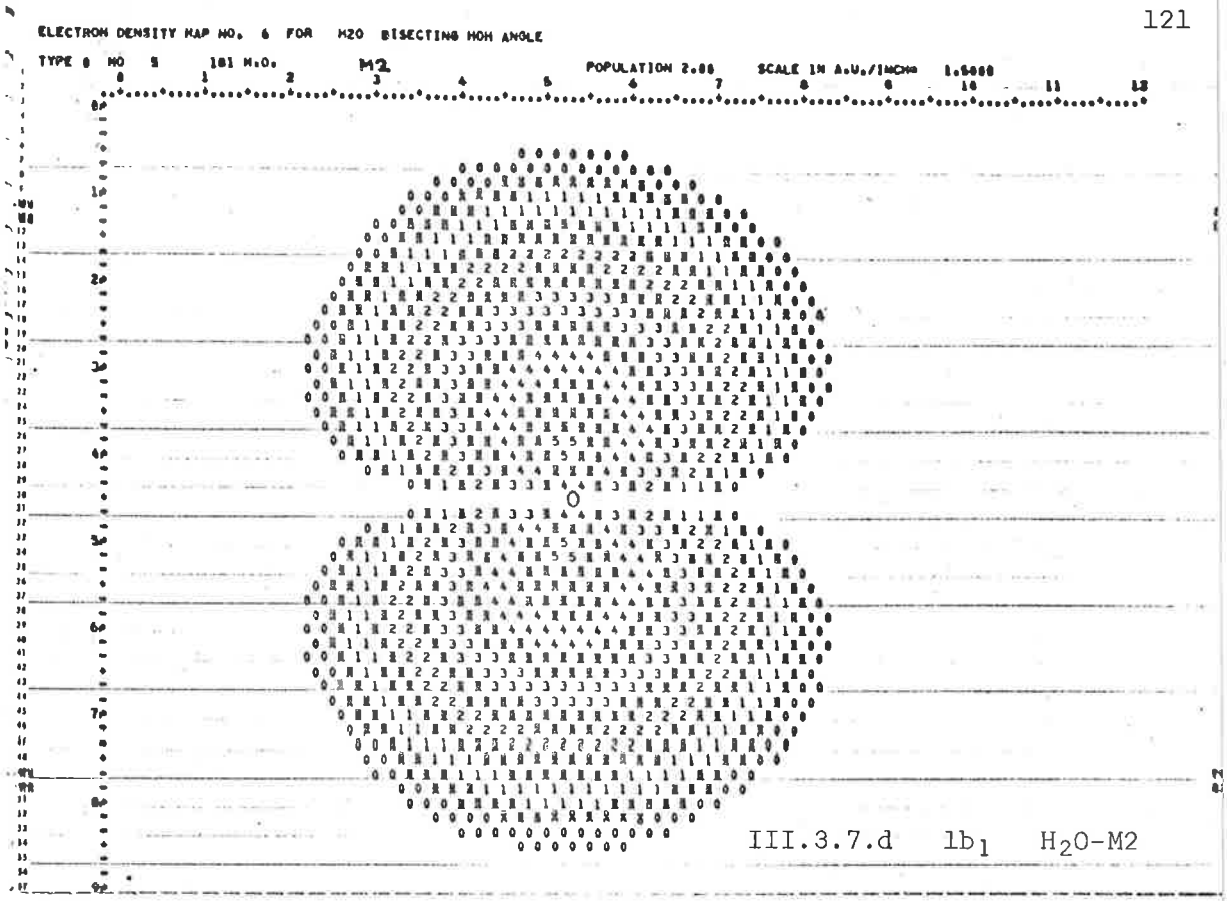

III.3.7.d $1b_1$ H_2O-M2

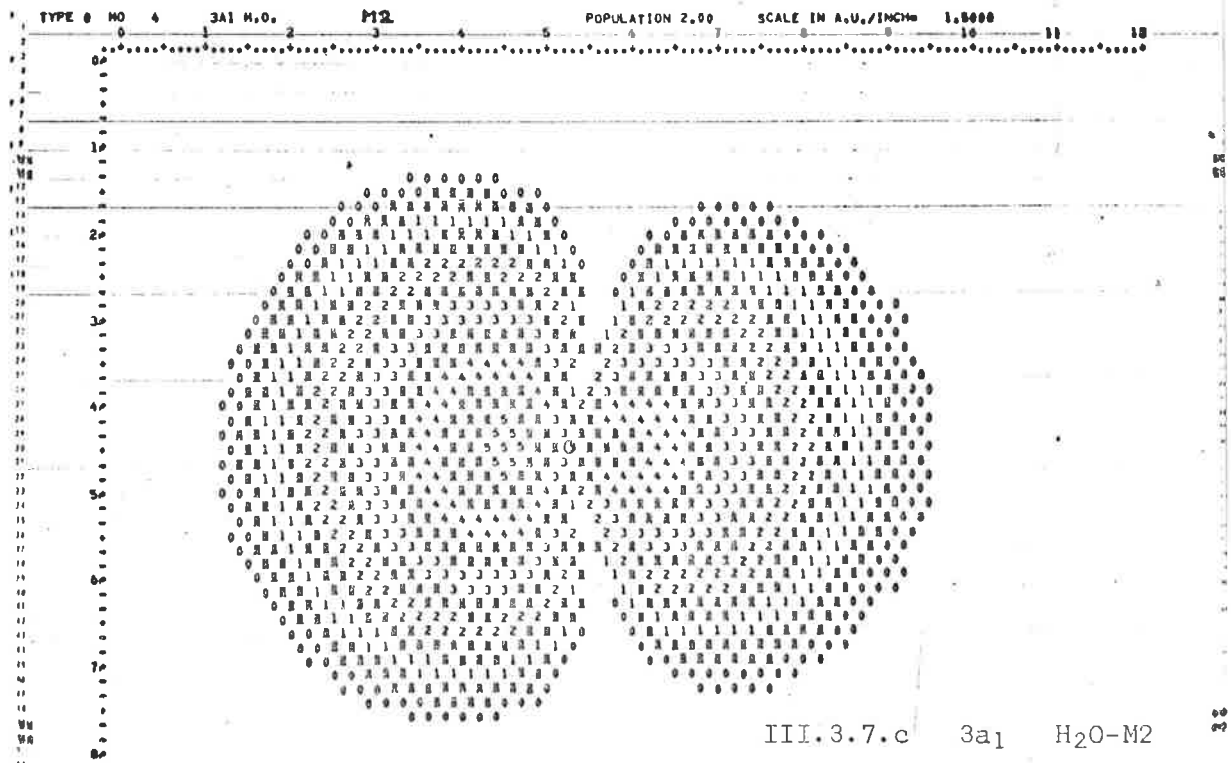

III.3.7.c $3a_1$ H_2O-M2

Perhaps the most striking feature of the total density maps in Fig. III.3.1 are the similarities displayed in the outer regions of the charge distributions. (Differences around the oxygen nucleus are quite prominent, but allowances must be made for the absence of O1s density in the valence basis density maps; 2p lobes, however, appear more distinct in Version 1). That near-identity should be sustained is not surprising, since one-electron properties associated with each distribution are in close accord with respect to experimental error. But it is surprising that Löwdin atomic populations (Table III.3.1-4) carry a suggestion of substantial variations. For instance, H populations calculated from the M2 and V2 wavefunctions are, respectively, 0.865 and 0.737, yet the density maps display no such obvious difference. Since we are inclined to favour the mapped distributions, it is our contention that direct comparisons between Löwdin populations should be treated with some caution.

It is also difficult to justify the bond index values contained in the same tables, since these, too, suggest significant electronic rearrangement between the minimal and valence bases. In both M1 and M2, σ hybridisation is close to the 67%p content of trigonal Sp^2-type, but rises abruptly to 86% and 91% p-character in the valence basis wavefunctions. No such trend is obvious from the density maps, which imply rather, that bond indices would group by version, and not by basis set.

While such effects are of interest, our main concern is with electron distribution at the molecular orbital level, and it is here that the wavefunctions and one-electron properties display most variation. In Table III.3.5, we have partitioned the one-electron properties into orbital contributions, and included those of a Gaussian [1062/42] wavefunction [80] for comparison.

Dipole moments, $\langle Z_o \rangle$, provide a convenient link between the pictorial display of electronic charge distributions and the numerical tabulation of orbital coefficients in the optimised wavefunctions. In the $2a_1$ MO, Hls contribution increases across the series V1 ≃ V2<M1<M2, a progression which is obvious also in the density maps (Fig. III.3.2), where the M2 density extends farthest into the region enclosed by the H atoms. Charge centroids $\langle Z_o \rangle$, Table III.3.5.a, follow the same pattern, with the small value of -.138 au in the valence bases reflecting predominant 02s character. Near incidence in the M1 and [1062/42] values, -.318 vs -.321au, in the $2a_1$ orbital is not sustained in the $1b_2$ MO, for there the M1 centroid at -.708 au is very much extended beyond the [1062/42] value of -.395 au. As a consequence of more dominant Hls contribution to $1b_2$ in the Version 1 wavefunctions, charge centroids are displaced more towards H than occurs in Version 2; relative positionings of the extensive 0.256 - 0.512 contour intervals (region 4) in the density maps of Fig. III.3.3 bear ample witness.

Displacement towards hydrogen of the charge centroid in the $3a_1$ MO across the series M1 (0.28), M2 (0.24), V1 (0.01) and V2 (-.16)

Table III.3.5.a. One-electron Expectation Values, H_2O - $\langle z_o \rangle$

MO	[1062/42]	M1	M2	V1	V2
$1a_1$	-.0004	0.0001	0.0000	-	-
$2a_1$	-.3213	-.3181	-.4102	-.1383	-.1378
$1b_2$	-.3949	-.7084	-.5399	-.6250	-.4484
$3a_1$	0.0858	0.2807	0.2440	0.0120	-.1606
$1b_1$	-.0728	0.0000	0.0000	0.0000	0.0000
Electronic	-1.407	-1.491	-1.412	-1.503	-1.494
Nuclear	2.192	2.219	2.219	2.219	2.219
Nett.	0.785	0.727	0.807	0.716	0.725

Table III.3.5.b One-electron Expectation Values, H_2O - θ_{xx}

MO	[1062/42]	M1	M2	V1	V2
$1a_1$	0.0075	0.0083	0.0084	-	-
$2a_1$	0.1728	-.0533	0.2264	-.0666	-.0439
$1b_2$	0.7511	1.2442	0.9734	1.1351	0.9138
$3a_1$	0.5793	0.4063	0.3686	0.5286	0.6655
$1b_1$	-.8879	-.7347	-.5401	-.7421	-.6596
Electronic	1.245	1.955	2.074	1.710	1.752
Nuclear	-3.047	-3.082	-3.082	-3.066	-3.066
Nett.	-1.801	-1.127	-1.008	-1.356	-1.315

Table III.3.5.c. One-electron Expectation Values, H_2O - θ_{yy}

MO	[1062/42]	M1	M2	V1	V2
$1a_1$	0.0075	0.0073	0.0072	-	-
$2a_1$	- .1789	-.0700	-.2307	0.0471	0.0273
$1b_2$	-1.1853	-1.6781	-1.3469	-1.5757	-1.3540
$3a_1$	0.3296	0.3942	0.2562	0.2845	0.0694
$1b_1$	0.4327	0.3789	0.2816	0.3826	0.3414
Electronic	-1.189	-1.936	-2.065	-1.723	-1.832
Nuclear	3.071	3.066	3.066	3.082	3.082
Nett.	1.882	1.131	1.001	1.358	1.250

Table III.3.5 d. One-electron Expectation Values, H_2O - θ_{zz}

MO	[1062/42]	M1	M2	V1	V2
$1a_1$	- .0149	-.0155	-.0155	-	-
$2a_1$	0.0061	0.0168	0.0043	0.0195	0.0166
$1b_2$	0.4343	0.4340	0.3734	0.4407	0.4402
$3a_1$	- .9090	-.8005	-.6248	-.8131	-.7349
$1b_1$	0.4552	0.3558	0.2585	0.3595	0.3183
Electronic	- .057	-.019	-.008	0.013	0.080
Nuclear	- .024	0.016	0.016	-.015	-.015
Nett.	- .081	-.003	0.007	-.002	0.065

Table III.3.5.e. One-electron Expectation Values, H_2O - $\langle x^2 \rangle$

MO	[1062/42]	M1	M2	V1	V2
$1a_1$	- .0177	- .0173	-.0175	(0.0000)	(0.0000)
$2a_1$	- .4929	- .5717	-.5569	-.5956	-.5723
$1b_2$	- .4249	- .5282	-.4416	-.5149	-.4897
$3a_1$	- .4701	- .3822	-.3101	-.4121	-.4497
$1b_1$	-1.3759	-1.1136	-.8216	-1.1247	-1.0010
Electronic	-5.563	-5.226	-4.295	-5.295	-5.025

Table III.3.5.f. One-electron Expectation Values, H_2O - $\langle y^2 \rangle$

MO	[1062/42]	M1	M2	V1	V2
$1a_1$	- .0177	- .0180	- .0183	(0.0000)	(0.0000)
$2a_1$	- .7274	- .6539	- .8616	- .5199	- .5249
$1b_2$	-1.7159	-2.4765	-1.9885	-2.3221	-2.0016
$3a_1$	- .6366	- .7902	- .3850	- .5749	- .8471
$1b_1$	- .4955	- .3712	- .2739	- .3749	- .3337
Electronic	-7.186	-7.820	-7.054	-7.584	-7.414

Table III.3.5.g. One-electron Expectation Values, H_2O - $\langle z^2 \rangle$

MO	|1062/42|	M1	M2	V1	V2
$1a_1$	- .0327	- .0332	- .0335	(-.0154)	(-.0154)
$2a_1$	- .6042	- .5960	- .7050	-.5383	- .5320
$1b_2$	- .6362	- 1.0684	- .8416	-.9778	- .8054
$3a_1$	- 1.4623	- 1.1867	- .9724	-1.3066	-1.3833
$1b_1$	- .4804	- .3866	- .2893	-.3903	- .3491
Electronic	- 6.431	- 6.542	- 5.683	-6.426	- 6.171

Table III.3.5.h. One-electron Expectation Values, H_2O -$\langle r^2 \rangle$

MO	|1062/42|	M1	M2	V1	V2
$1a_1$	- .0682	- .0686	- .0693	(-.0154)	(-.0154)
$2a_1$	- 1.8245	- 1.8217	- 2.1235	- 1.6538	-1.6292
$1b_2$	- 2.7770	- 4.0731	- 3.2717	- 3.8148	-3.2967
$3a_1$	- 2.5690	- 1.9590	- 1.6674	- 2.2936	-2.6861
$1b_1$	- 2.3518	- 1.8714	- 1.3848	- 1.8900	-1.6838
Electronic	-19.181	-19.587	-17.033	-19.304	-18.610

Table III.3.5.i. One-electron Expectation Values, H_2O - $\langle r_O^{-1} \rangle$

MO	[1062/42]	M1	M2	V1	V2
$1a_1$	- 7.6401	- 7.6522	- 7.6432	(-7.66)	(-7.66)
$2a_1$	- 1.1523	-1.1448	-1.1196	-1.0424	-1.0527
$1b_2$	- .8935	- .6463	- .7911	- .6815	- .7841
$3a_1$	- 1.0002	-1.0092	-1.1407	- .9345	- .9101
$1b_1$	- 1.0365	-1.0049	-1.1699	- .9999	-1.0599'
Electronic	-23.445	-22.915	-23.729	-22.636	-22.934
Nuclear	1.111	1.104	1.104	1.104	1.104
Nett	-22.334	-21.810	-22.625	-21.532	-21.829

Table III.3.5.j. One-electron Expectation Values, H_2O - $\langle r_H^{-1} \rangle$

MO	[1062/42]	M1	M2	V1	V2
$1a_1$	- .5556	- .5521	- .5521	(-.5522)	(-.5522)
$2a_1$	- .6292	- .5981	- .6233	-.5586	-.5622
$1b_2$	- .6935	- .7452	- .7140	-.7270	-.6748
$3a_1$	- .5287	- .4972	- .5090	-.5450	-.5654
$1b_1$	- .4907	- .4914	- .5066	-.4909	-.4972
Electronic	-5.795	-5.768	-5.810	-5.747	-5.703
Nuclear	4.794	4.766	4.766	4.766	4.766
Nett	-1.001	-1.002	-1.044	- .981	- .937

stems from an identical ordering recorded in H1s contributions. In the distribution maps, Fig. III.3.4, hydrogen nuclei fall in progressively more dense regions, ρ_{M1} = 0.004 - 0.008, ρ_{M2} = 0.008 - 0.016, ρ_{V1} = 0.016 - 0.032 and ρ_{V2} = 0.032 - 0.064 in accord with the above.

While this gradation is exactly the opposite to the sequence observed in the $2a_1$ MO, the orbitals of a_1 symmetry are not truly compensatory in their nett effect, for the total a_1 dipoles across the series sum as M1 = -.04, M2 = -.17, V1 = -.15 and V2 = -.30 au. Therefore, variations in electron distribution are not simply local effects occurring within a particular symmetry class, but function more or less independently over the whole set of occupied orbitals. We have previously noted the inconstancy in expectation values for the lone $1b_2$ orbital.

Since the dipole moment is non-vanishing only along the $Z(C_2)$ axis, we must turn to properties dependent on the operators y^2 or x^2 to examine electron distribution in other directions. Although molecular quadrupole moments have previously featured as optimisation criteria, second moments of the charge distribution offer conceptual advantages, and it is these which we shall use as a basis for further discussion. Tables III.3.5.e-h display the relevant second moments, but, for completeness, we include also molecular quadrupole moments in Tables III.3.5.b-d.

We have commented previously on a predominant 2s character in the $2a_1$ orbital of the valence basis wavefunctions, and second moments confirm an essentially spherical charge distribution. The greatest variation between $\langle x^2 \rangle$, $\langle y^2 \rangle$ and $\langle z^2 \rangle$ occurs in the V1 set and amounts to only 0.08 au. By contrast, expectation values in the minimal basis wavefunctions are indicative of considerable anisotropy, with M2 moments exaggerated over M1 in their minimum extension normal to the molecular plane (X) and maximum extension laterally (Y). In Fig. III.3.2, distortion of electron densities towards H is evident in both the M1 and M2 maps, but obviously more pronounced in the latter. Extension along the C_2 axis in confirmation of the condition $\langle z^2 \rangle > \langle x^2 \rangle$ is well illustrated in Fig. III.3.7.b, the M2 distribution mapped in the reflection plane bisecting the HOH angle. Variations among individual expectation values extend also to the [1062/42] wavefunction, and it is in line with our previous observations that any correspondence must be regarded as purely fortuitous.

As would be expected from the symmetry of the participant atomic orbitals, second moments of the $1b_2$ MO extend farthest in the Y-direction. On this occasion, substantial stratification occurs in the Version 1 and Version 2 expectation values; second moments associated with the former are of greater magnitude, implying a more diffuse charge distribution in accord with the smaller O2p orbital exponents characteristic of M1 and V1 wavefunctions. For the *ab initio* wavefunction, $\langle y^2 \rangle = -1.72$ au, which, in comparison with our M1 and

M2 values ($\langle y^2 \rangle$ = -2.48 and -1.99, respectively), argues a charge distribution considerably more compact than any of those found in the SNE procedures.

By contrast, second moments in the $3a_1$ MO indicate a more diffuse distribution for the [1062/42] wavefunction; the only exception occurs in the V2 expectation value for $\langle y^2 \rangle$, and it is evident from the mapped distribution in Fig. III.3.4 that the charge density therein is displaced more than occurs for other procedures.

Since the 02px orbital is unique in the $1b_1$ MO, expectation values arising therefrom are dependent on only two factors - the orbital exponent and distance from centre of mass. Because the centre of mass lies on the Z-axis, $\langle x^2 \rangle$ and $\langle y^2 \rangle$ provide a direct measure of vertical and lateral extension in the charge distribution, while $\langle z^2 \rangle$ differs from $\langle y^2 \rangle$ only by an additional $(\text{distance})^2$ term of 0.015 au.

Therefore, it is not surprising to find a distinct gradation in e.g. $\langle x^2 \rangle$, across the series M2, V2, M1, V1 in inverse relationship to 02p orbital exponent values. The *ab initio* wavefunction is more diffuse again.

Nett electronic second moments further provide correlations with relative charge distributions occurring in the total density maps. Normal to the molecular plane, the M2 distribution is most compact ($\langle x^2 \rangle$ = -4.30), whereas V2(-5.02), M1(-5.23), V1(-5.30) and [1062/42] (-5.56) group more or less together. In the SNE wavefunctions,

the progression above correlates with orbital exponent values.

Much the same effect is found in $\langle z^2 \rangle$, except that the *ab initio* expectation value of -6.43 au now lies within the range of M1, V1 and V2 results. Again, the M2 value, at -5.68 au, is well below all others, a characteristic, which, in the main, is preserved in passing to the operator y^2. A slight departure from the trends recorded for $\langle x^2 \rangle$ and $\langle z^2 \rangle$ places the expectation value of $\langle y^2 \rangle$ for the *ab initio* wavefunction close to the M2 result.

Since molecular quadrupole moments provide a measure of the shape, or deviation from spherical symmetry, of the total charge distribution, whereas second moments are simply a measure of the absolute size in each direction, the groupings reported above should be equally apparent in the nett values of θ_{xx}, θ_{yy} and θ_{zz}. In all cases, θ_{zz} values are small, ranging from -.081 au (*ab initio*) to 0.065 au (V2), indicative of very minor charge perturbations along the C_2 axis. By contrast, θ_{xx} (-1.80 au) and θ_{yy} (1.88 au) in the *ab initio* wavefunction reflect a considerable anisotropy in comparison with our results (e.g. M1: θ_{xx} = -1.13 au, θ_{yy} = 1.13 au), wherein a more spherical distribution is implied.

The operators r_O^{-1} and r_H^{-1} should be especially relevant to our discussion since Version 1 and Version 2 differ only in the methods used to evaluate the associated atomic integrals. However, expectation values which appear in Table III.3.5.i and j were all evaluated exactly, irrespective of whether the parent wavefunction belonged to

a Version 1 or Version 2 class. While this procedure was obviously necessary to ensure consistency in comparison of expectation values, it has the unfortunate consequence that those values do not relate directly to the energy variations from which stem the fundamental differences in final wavefunctions. We can therefore compare expectation values at no more than a superficial level.

For $\langle r_H^{-1} \rangle$, variations are relatively minor compared to those expectation values which we have previously examined. Agreement among nett electronic values is to be expected, since these are, after all, the exponent optimised diamagnetic shieldings, $\sigma_{av}^{d}(H)$. That agreement should continue at the MO level is unexpected, particularly in view of much greater deviations experienced with moment operators. It is to be noted that correspondence is more closely approached within a given basis, rather than within a particular method, with the M2 values closest to those of the [1062/42] wavefunction; the greatest deviation between those two amounts to only 0.02 au.

Expectation values for the operator, r_O^{-1}, show more scatter, but it is evident that the M2 set lies closest to *ab initio* values, while M1, V1 and V2 group more or less together. Although we can find no consistent pattern among individual orbital variations, values for the $1b_1$ MO grade in accordance with O2p optimised exponents, as would be expected.

In summarising our examination of one-electron and other properties of optimised wavefunctions in H_2O, it is apparent that very

little of a positive nature has emerged. We have established that Version 1 produces energetically superior wavefunctions, particularly with regard to absolute ionisation potentials, but, in defence of Version 2, calculated values there were incorrect only through a fairly constant displacement term. In both versions, minimal bases proved marginally more consistent than valence sets. As for total energy, the M1 result, while superior to M2, is still a long way from the best minimal basis *ab initio* energy.

We have shown that total electron distributions, whether measured by calculated one-electron properties, or by electron density mapping, are substantially the same throughout all four procedures*. At the molecular orbital level, all consistency in one-electron operators and electron density maps is lost, and we have related these variations to the LCAO expansion of each MO. Although individual groupings by version or basis set were sporadically observed among expectation values, there would appear to be no definite pattern which is maintained consistently over all operators and orbitals. Therefore, the results accrued in this phase of the examination must be accounted as of negative value only.

---

* The identity here is relative to experimental error; we have previously commented in Section III.2 upon the manner in which nett expectation values stratify at different levels within the experimental error range.

Comparisons with the *ab initio* [1062/42] Gaussian wavefunction were not particularly productive. No consistent similarities exist between [1062/42] expectation values and any one of the SNE optimised wavefunctions. Certainly some individual correlations occur, as with expectation values for $\langle r_o^{-1} \rangle$ in the M2 procedure, but such agreement fails to generalise over all one-electron properties. Second moments of the M2 distribution, for example, correlate poorly with *ab initio* values.

While it would be advantageous to find some direct relationship with *ab initio* calculations, our failure to do so implies no criticism of the SNE approach, for there is no guarantee that the 'exact' wavefunction in any way describes correctly the true molecular situation. Indeed, on the criteria of nett one-electron properties, the SNE results are, in general, superior in their representation of dipole (excepting M2) and quadrupole moments, and equivalent for diamagnetic shielding and susceptibilities.

III.3.B NH_3

In Tables III.3.6-9 we list wavefunctions for NH_3 in each of the procedures M1, M2, V1 and V2. As with the H_2O wavefunctions, these represent a selection from the optimised exponent combinations (Table III.2.5-6).

The experimental energy of NH_3 is -56.573 au [81]. In comparison, our calculated values for the M1 and M2 wavefunctions

Table III.3.6. NH_3 - M1 Optimised Wavefunction and Populations

AO Exponents		6.70	1.84	1.75	1.3
MO	Energy(au)	N1s	N2s	N2pz	H1s
$1a_1$	-15.7271	0.9974	-.0079	0.0068	0.0415
$2a_1$	- 1.2168	-.0291	0.8459	-.1496	0.2951
$3a_1$	- .4284	0.0006	0.2182	0.9729	-.0441
$4a_1$	1.2235	-.0666	-.4866	0.1761	0.4925

		N2py	N2px	$H^1$1s	$H^2$1s	$H^3$1s
1e	- .5859	0.6891	0.0001	0.5846	-.2922	-.2923
		-.0001	0.6891	-.0001	0.5063	-.5062
2e	0.2444	0.0001	-.7160	-.0001	0.4937	0.4936
		-.7160	-.0001	0.5700	-.2849	-.2850
Tot.	-55.92461					

Lowdin Populations		
AO	Nitrogen	Hydrogen
1s	1.991	0.865
2s	1.526	
2pz	1.938	
2py	0.975	
Σs	3.517	0.865
Σ2p	3.888	
NCH	7.405	0.865

Bond Indices	
N	$H^1$1s
1s	0.004
2s	0.230
2pz	0.030
2py	0.666
Σs	0.234
Σ2p	0.696
Nett	0.930
%2p	74.8

Table III.3.7. NH_3 - M2 Optimised Wavefunction and Populations

AO Exponents		6.70	1.90	2.06	1.20
MO	Energy(au)	N1s	N2s	N2pz	$H^1$1s
$1a_1$	-15.2360	0.9968	-.0075	0.0058	0.0462
$2a_1$	- 1.1166	-.0426	0.7758	-.1387	0.3545
$3a_1$	- .2723	0.0034	0.2434	0.9658	-.0514
$4a_1$	0.8225	0.0682	0.5820	-.2189	-.4504

		N2py	N2px	$H^1$1s	$H^2$1s	$H^3$1s
1e	- .4135	0.0011	0.7101	0.0009	0.4974	-.4983
		-.7101	0.0011	-.5749	0.2882	0.2866
2e	0.5273	0.0025	0.7041	-.0021	-.5011	0.5031
		0.7041	-.0025	-.5798	0.2917	0.2881
Tot.	-55.55944					

Löwdin Populations		
AO	Nitrogen	Hydrogen
1s	1.991	0.922
2s	1.322	
2pz	1.904	
2py	1.008	
Σs	3.313	0.922
Σ2p	3.921	
Nett	7.234	0.922

Bond Indices	
N	$H^1$1s
1s	0.004
2s	0.275
2pz	0.039
2py	0.667
Σs	0.279
Σ2p	0.706
Nett	0.984
%2p	71.7

Table III.3.8. NH_3 - V1 Optimised Wavefunction and Populations

AO Exponents		1.77	1.75	1.30
MO	Energy(au)	N2s	N2pz	$H^1$1s
$2a_1$	- 1.7578	0.9130	-.0819	0.2308
$3a_1$	- .4032	0.1829	0.9579	-.1278
$4a_1$	0.9587	-.3648	0.2752	0.5136

		N2py	N2px	$H^1$1s	$H^2$1s	$H^3$1s
1e	- .6079	0.7024	-.0002	0.5812	-.2907	-.2905
		0.0002	0.7024	0.0002	0.5032	-.5034
2e	0.5292	-.7117	-.0097	0.5734	-.2799	-.2935
		-.0097	0.7117	0.0078	-.5005	0.4927
Tot.	-12.44546					

Löwdin Populations		
AO	Nitrogen	Hydrogen
1s	(2.000)	0.815
2s	1.734	
2pz	1.848	
2py	0.987	
Σs	3.734	0.815
Σ2p	3.822	
Nett	7.556	0.815

Bond Indices	
N	$H^1$1s
2s	0.140
2pz	0.080
2py	0.666
Σs	0.140
Σ2p	0.746
Nett	0.887
%2p	84.2

Table III.3.9. NH_3 - V2 Optimised Wavefunction and Populations

AO Exponents		1.85	1.84	1.20		
MO	Energy(au)	N2s	N2pz	$H^1$1s		
$2a_1$	- 1.7843	0.9046	-.0840	0.2412		
$3a_1$	- .3383	0.2444	0.9054	-.2004		
$4a_1$	0.5768	-.3492	0.4161	0.4847		
		N2py	N2px	$H^1$1s	$H^2$1s	$H^3$1s
1e	- .4986	0.0000	0.7384	0.0000	0.4768	-.4768
		0.7384	0.0000	0.5506	-.2753	-.2753
2e	0.6314	-.0001	0.6744	0.0001	-.5222	0.5221
		-.6744	-.0001	0.6029	-.3013	-.3016
Tot.	-12.36165					

Löwdin Populations		
AO	Nitrogen	Hydrogen
1s	(2.000)	0.803
2s	1.756	
2pz	1.654	
2py	1.090	
Σs	3.756	0.803
Σ2p	3.834	
Nett	7.590	0.803

Bond Indices	
N	$H^1$1s
2s	0.115
2pz	0.163
2py	0.661
Σs	0.115
Σ2p	0.824
Nett	0.938
%2p	87.8

are -55.925 and -55.559 au respectively, while the geometry - (but not exponent -) optimised minimal basis STO wavefunction of Kaldor and Shavitt [81], gives -56.008 au. It is apparent that the NH_3 results parallel those observed for H_2O in the progression *ab initio* <M1 <M2. However, the separation between M1 and *ab initio* is not so marked in this instance. Also in accord with H_2O, V1 and V2 energies for NH_3 are almost equivalent with Version 1 marginally more stable (-12.445 au vs. -12.362 au).

Ionisation potentials for $3a_1$ and 1e orbitals have been experimentally measured as 0.380 and 0.549 au [82]. Calculated values and displacements, the latter in parentheses, are, in au: M1, 0.428 (.048),0.586 (.037); M2, 0.272 (-.108), 0.413 (-.136); V1, 0.403 (.023), 0.608 (.059); V2, 0.380 (-.042), 0.499 (-.050). With regard to absolute values, M1, V1 and V2 predictions must all be considered reasonable; if allowance is made for an average displacement, as we did for H_2O, then maximum separation occurs for the M1 wavefunction, but only by the small amount of 0.018 au, less than 0.5eV.

While the displacement term is undoubtedly convenient for illustrative purposes, there should be no illusions concerning its artificiality. However, it is obvious that some allowance has to be made in compensation for approximations in the Hamiltonian, and, in the absence of a quantitative estimate, the use of average displacement correction terms would appear to be justified.

Electron density maps for NH_3 appear in Figs. III.3.8-13, in the reflection plane, and Fig. III.3.14, in the plane normal to the C_3 axis passing through N. The first group includes all four procedures, M1, M2, V1 and V2, while the second group maps solely the M2 wavefunction.

It is apparent in the total density maps (Fig. III.3.8.a-d) that extension of the charge distribution along the C_3 axis, the traditional lone pair direction, varies in the order M1 ≃ V1>V2>M2, and since the N2pz orbital should contribute significantly to the density in that region, it is gratifying to note that 2pz orbital exponents are in the correct inverse order (M2>V2>V1 = M1)

By contrast, Löwdin populations for N2pz orbital progress as V2 = 1.66 .< V1 = 1.85 < M2 = 1.90 < M1 = 1.94, and it is obvious that those figures fail completely to correlate with the density maps. As occurred with the H_2O wavefunctions, hybridisation (via bond indices) varies greatly between the basis sets. With the minimal bases p- character in the N-H bond is intermediate between trigonal sp^2 and tetrahedral sp^3, as evinced in the calculated percentages for the M1 and M2 wavefunctions, respectively, 74.8 and 71.7%p. Valence basis results infer a much greater p-content, at 84.2% for V1 and 87.8% for V2. Again, we find it difficult to justify those values, for the density maps, excepting the area around the nitrogen centre, are very nearly identical in the bonding region. Likewise, no obvious differences are visible in the charge distribution around hydrogen, yet Löwdin

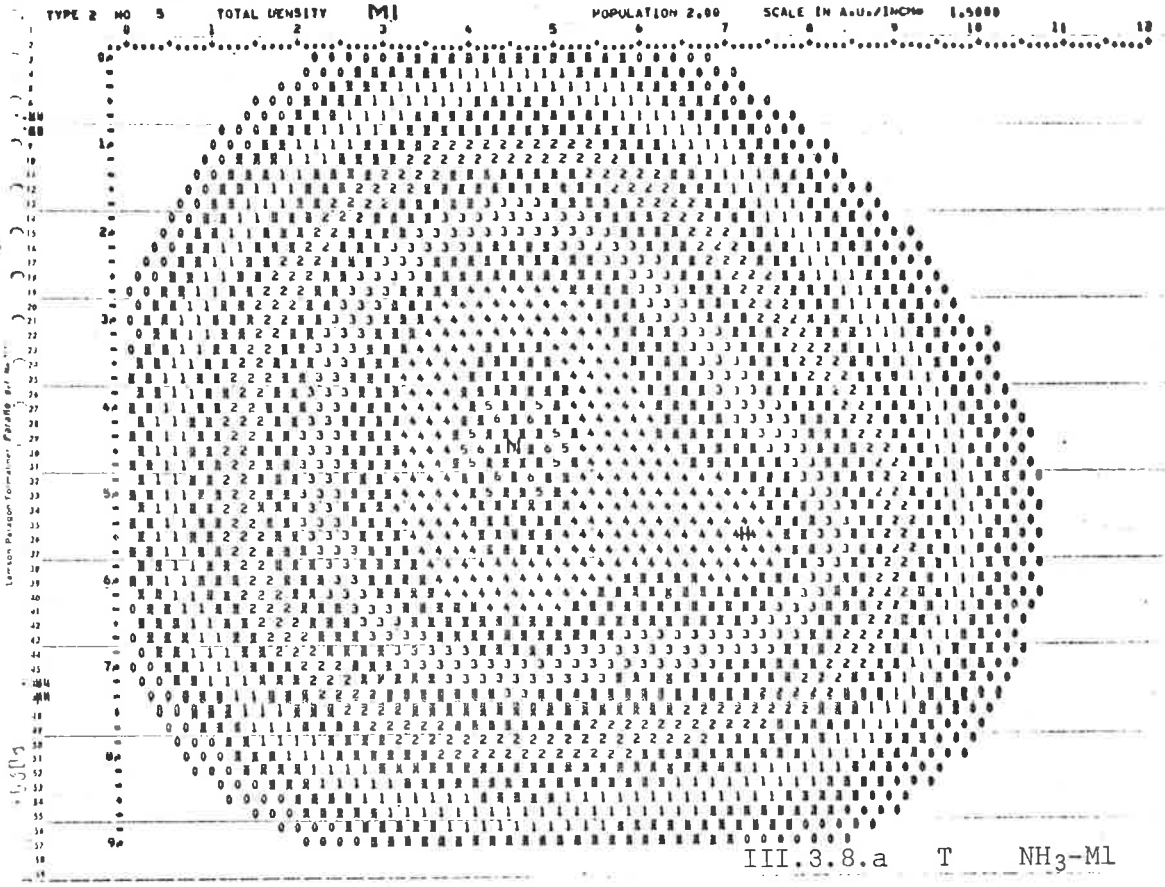

III.3.8.a T NH_3-M1

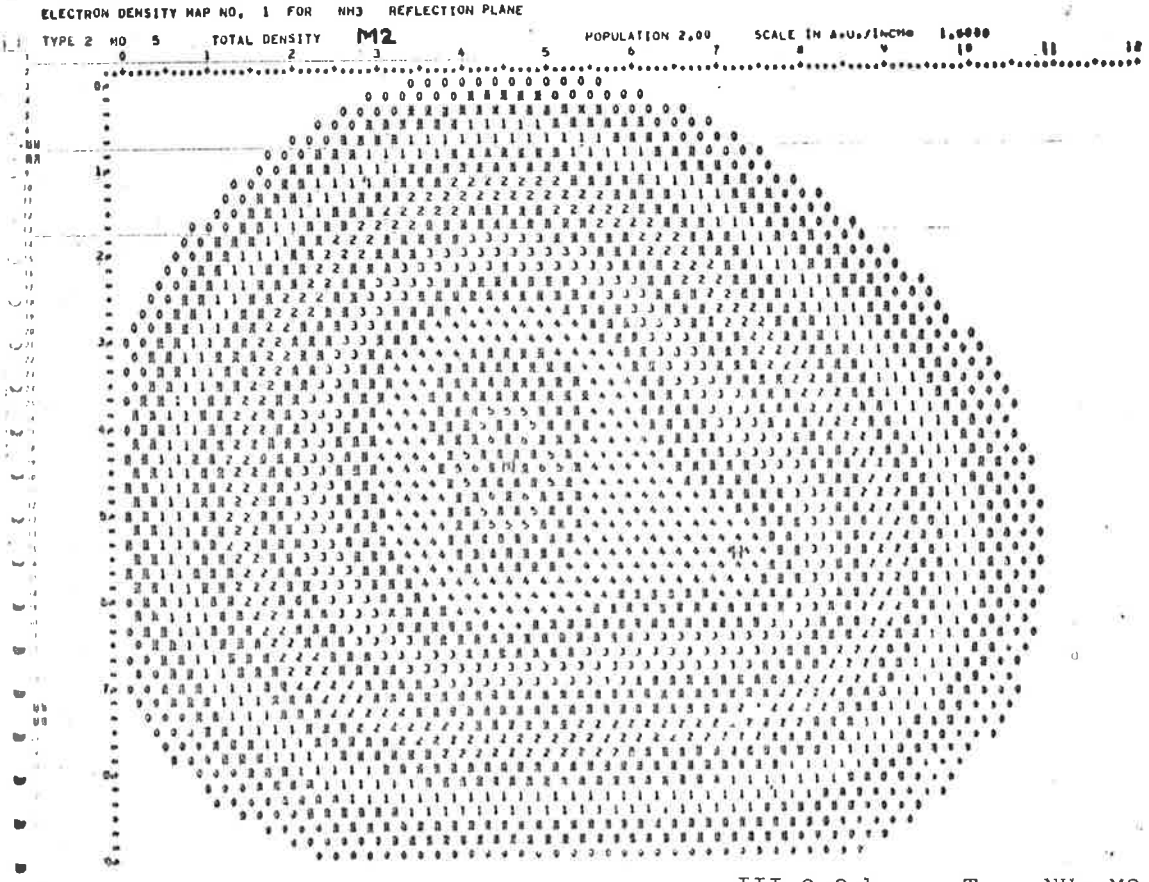

III.3.8.b T NH_3-M2

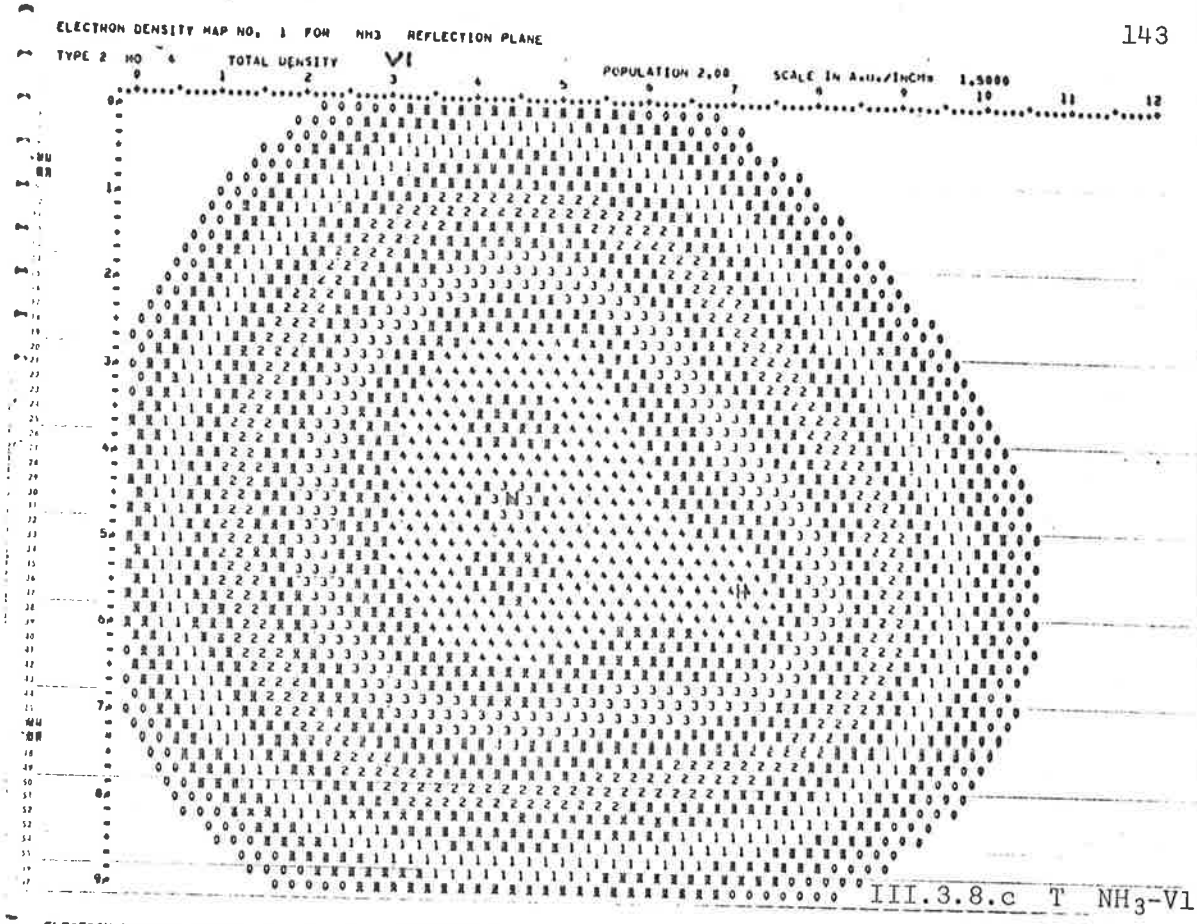

III.3.8.c T NH_3-V1

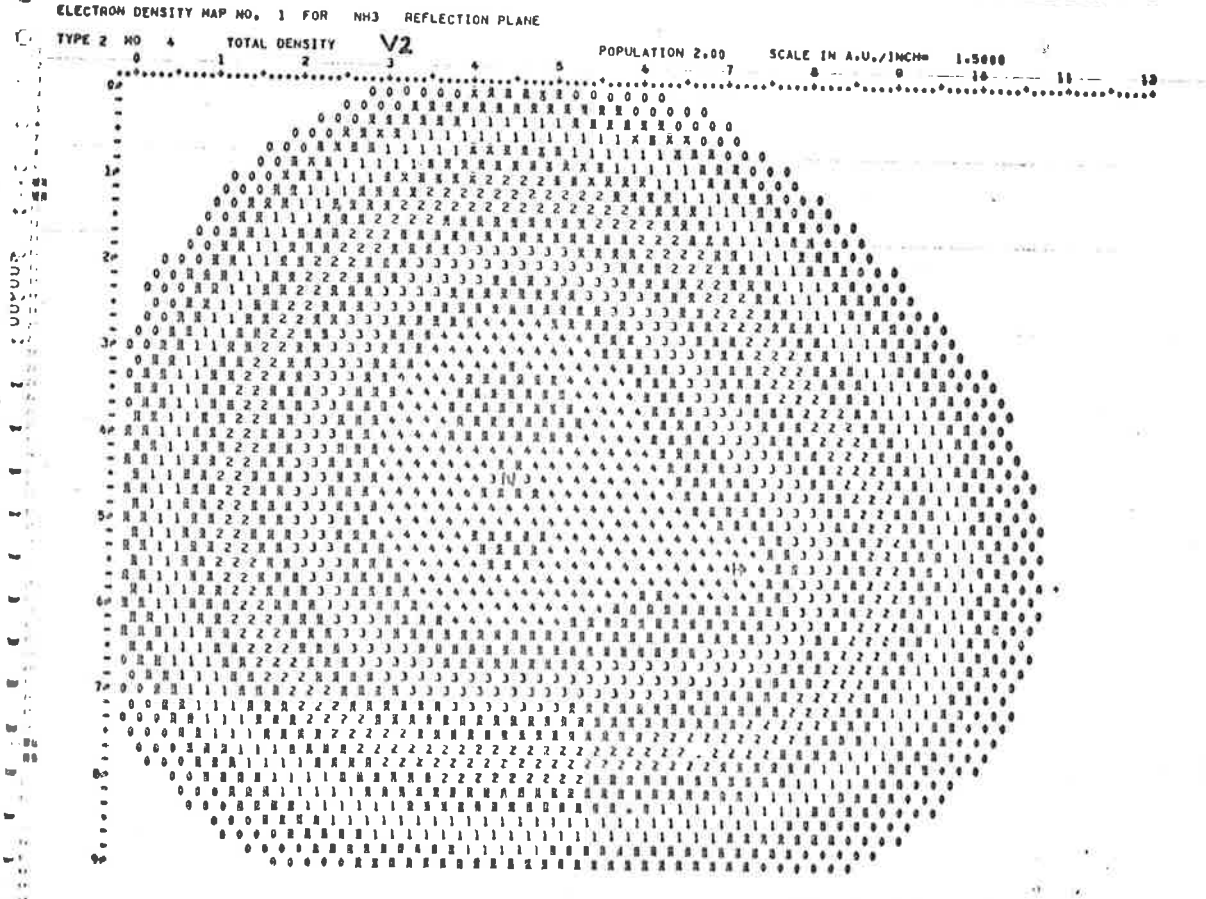

III.3.8.d T NH_3-V2

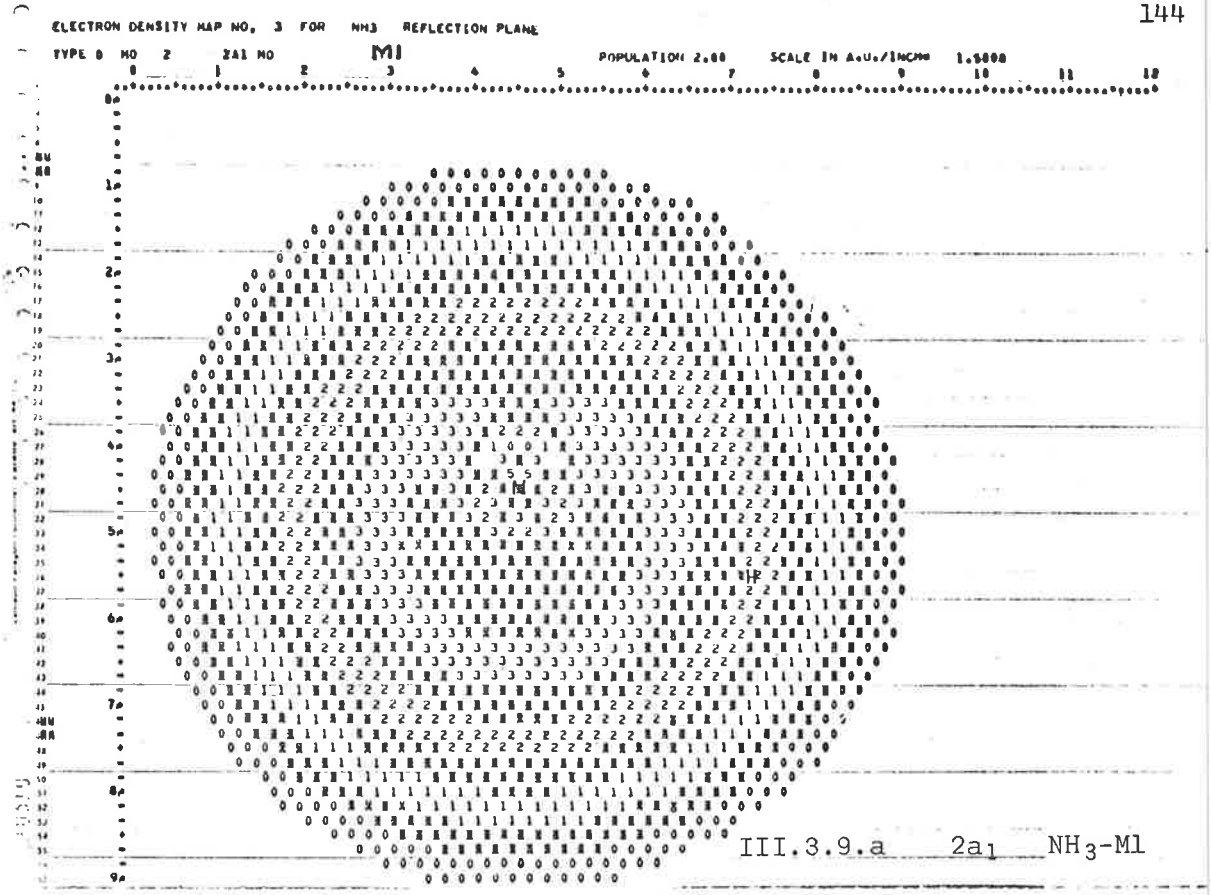

III.3.9.a $2a_1$ NH_3-M1

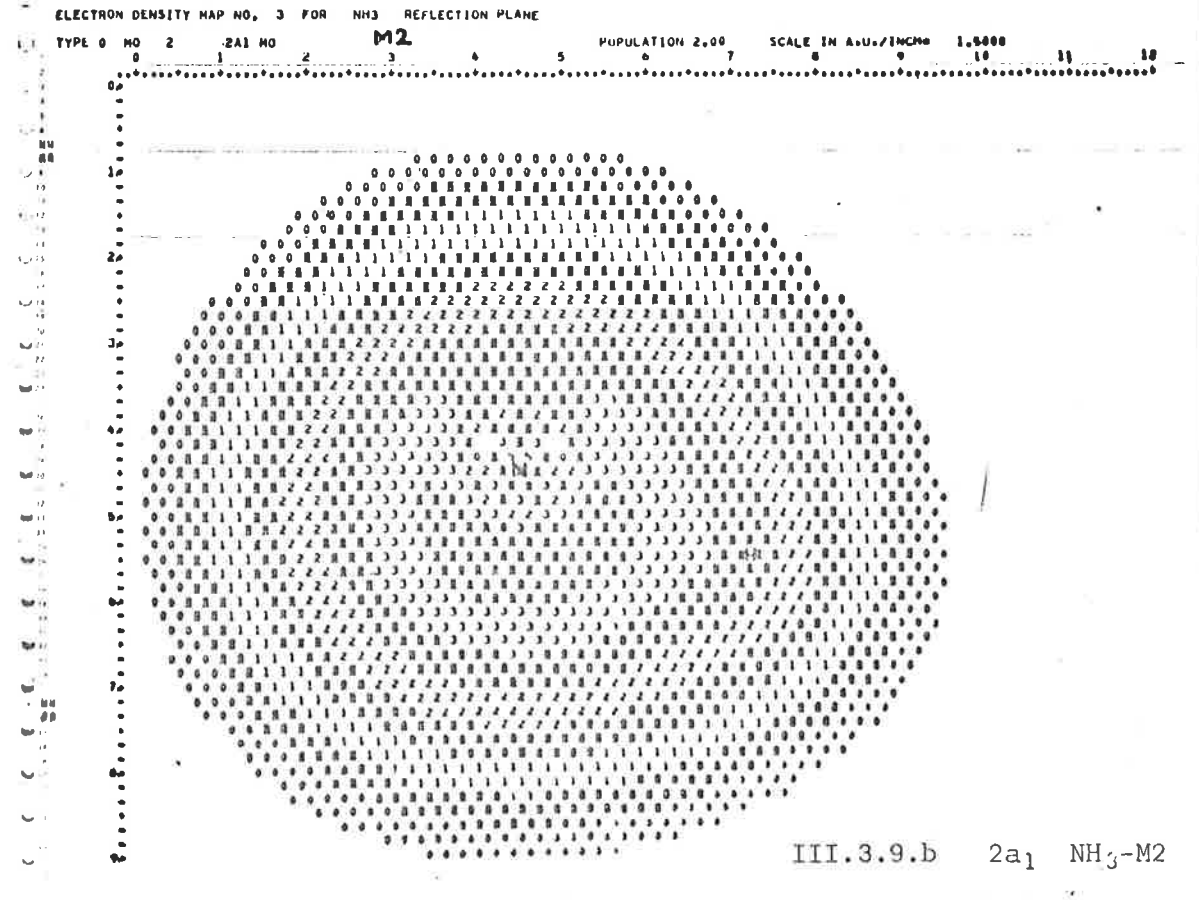

III.3.9.b $2a_1$ NH_3-M2

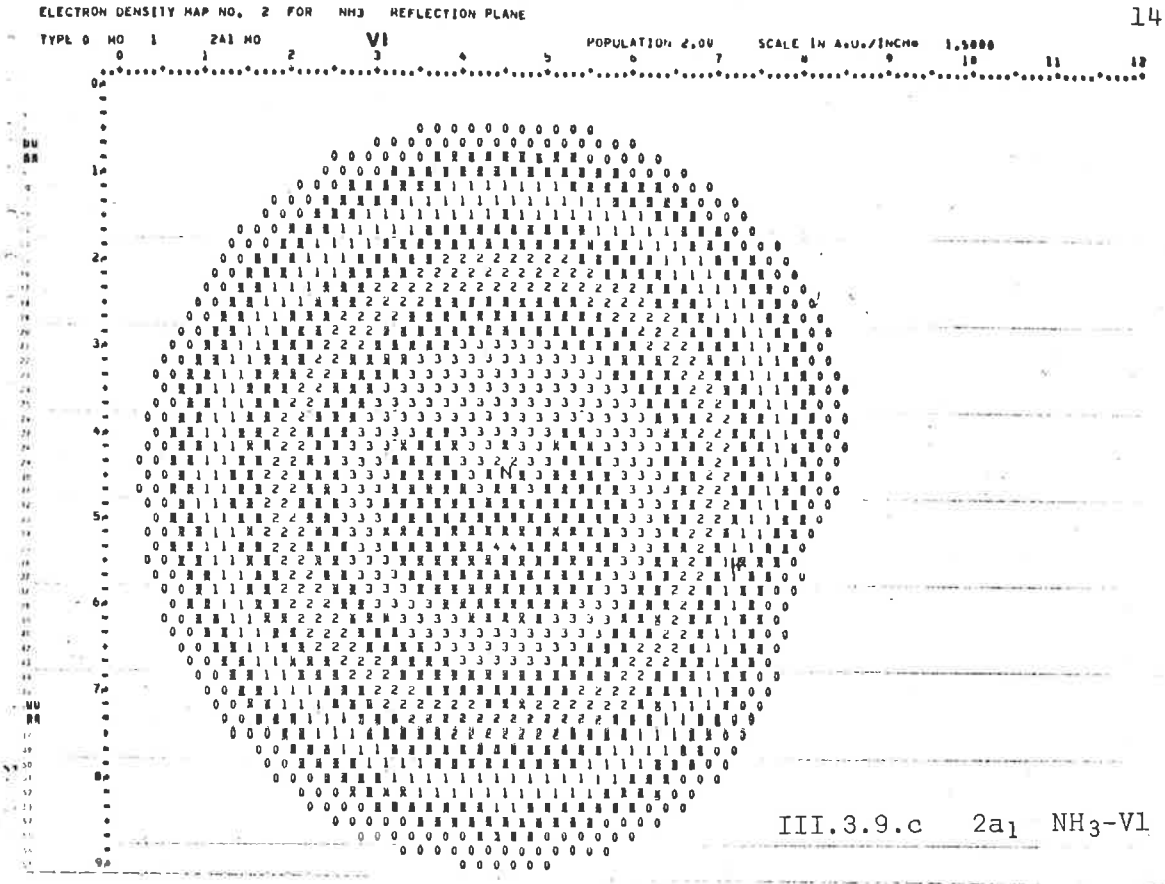

III.3.9.c $2a_1$ NH_3-V1

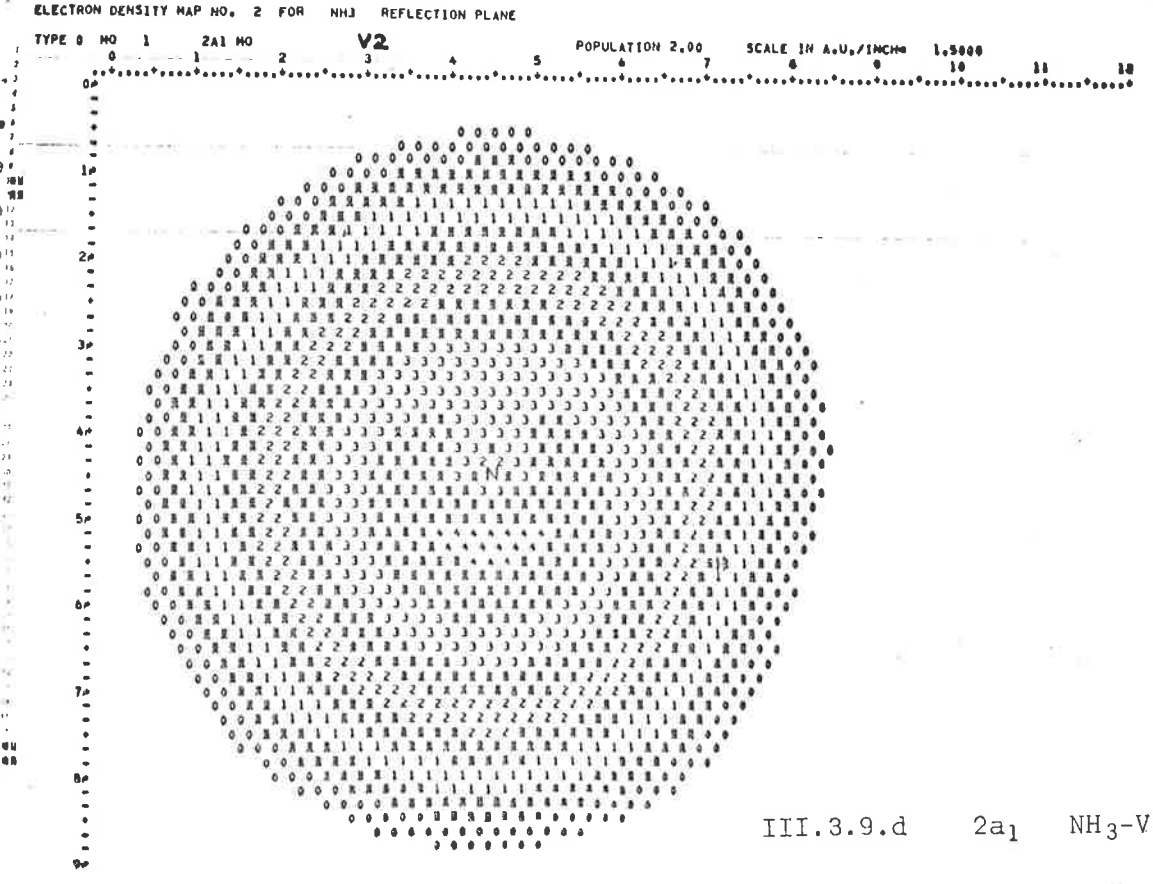

III.3.9.d $2a_1$ NH_3-V2

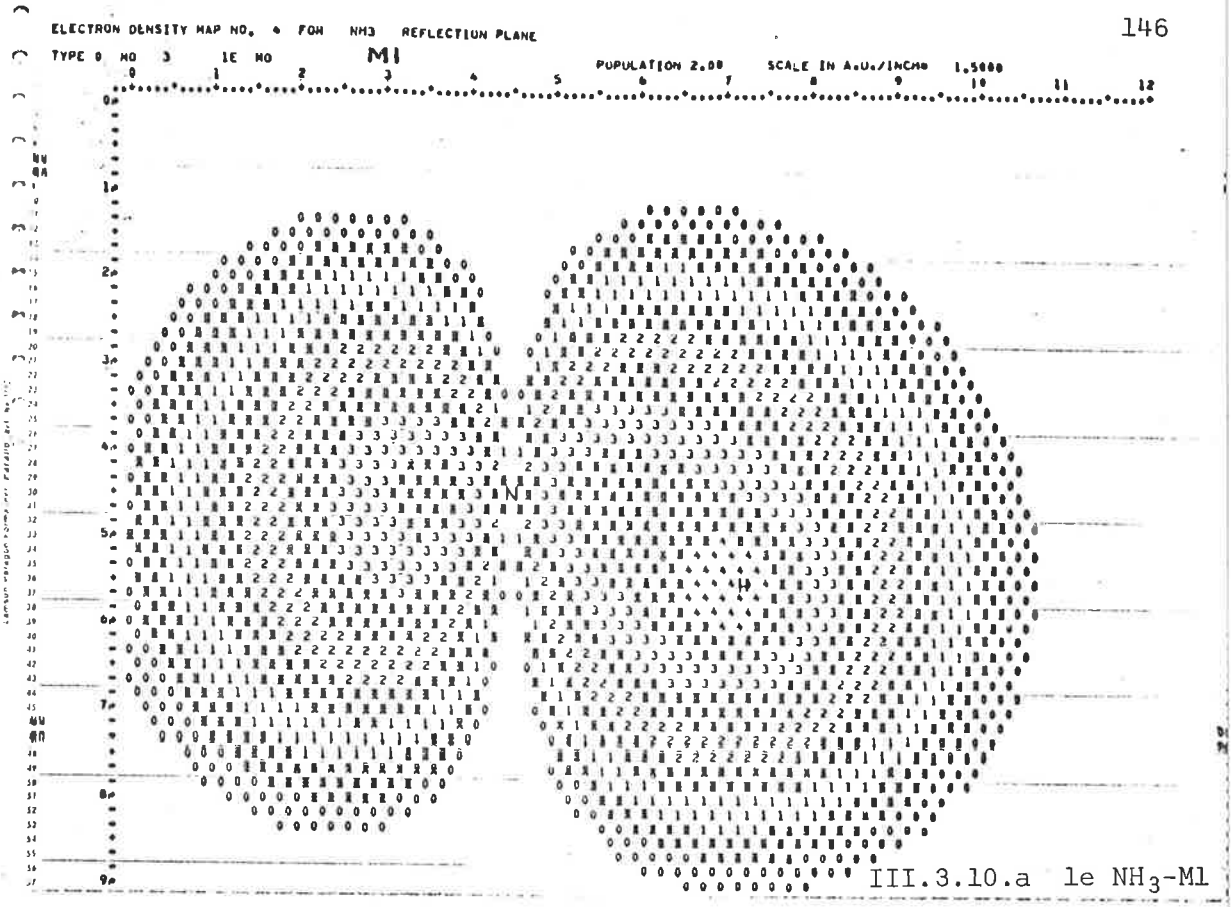

III.3.10.a le NH_3-M1

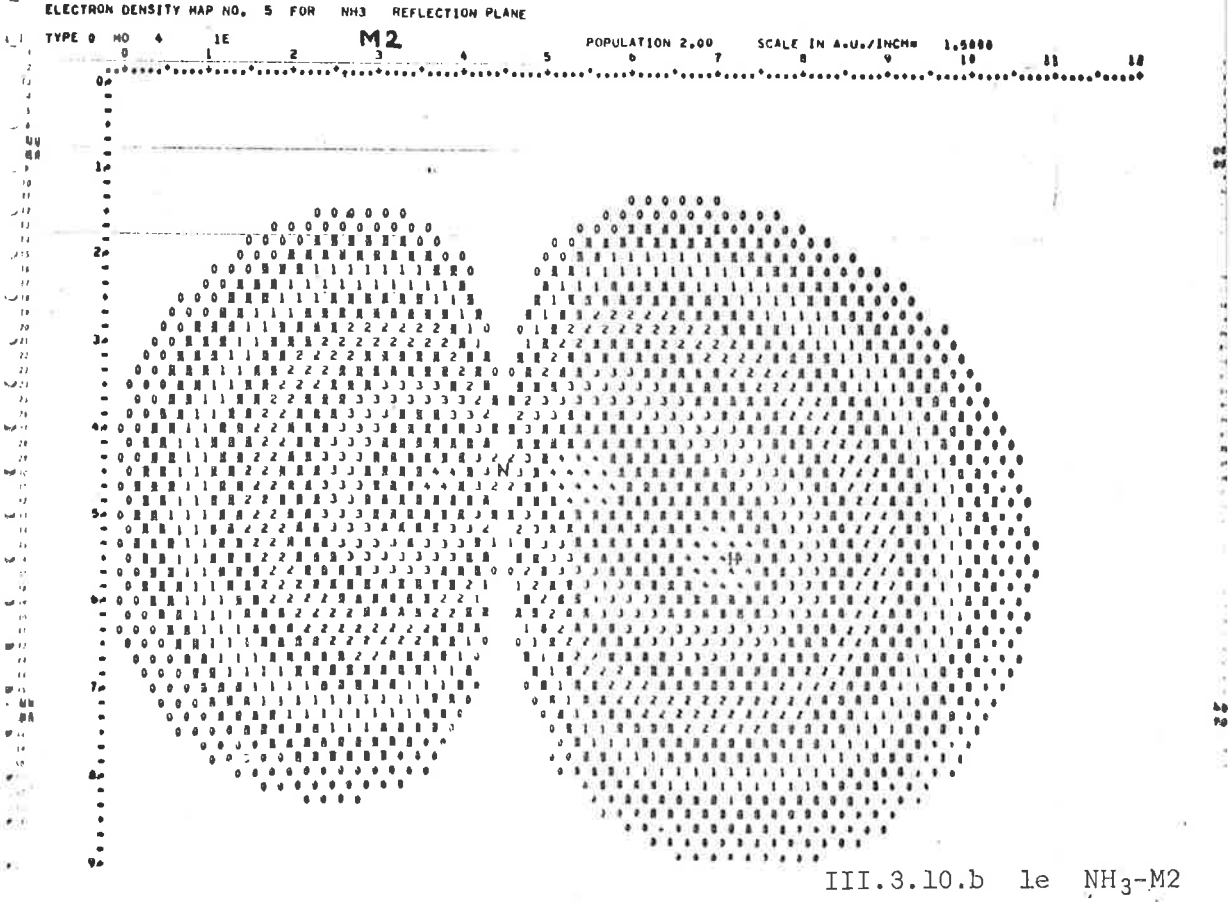

III.3.10.b le NH_3-M2

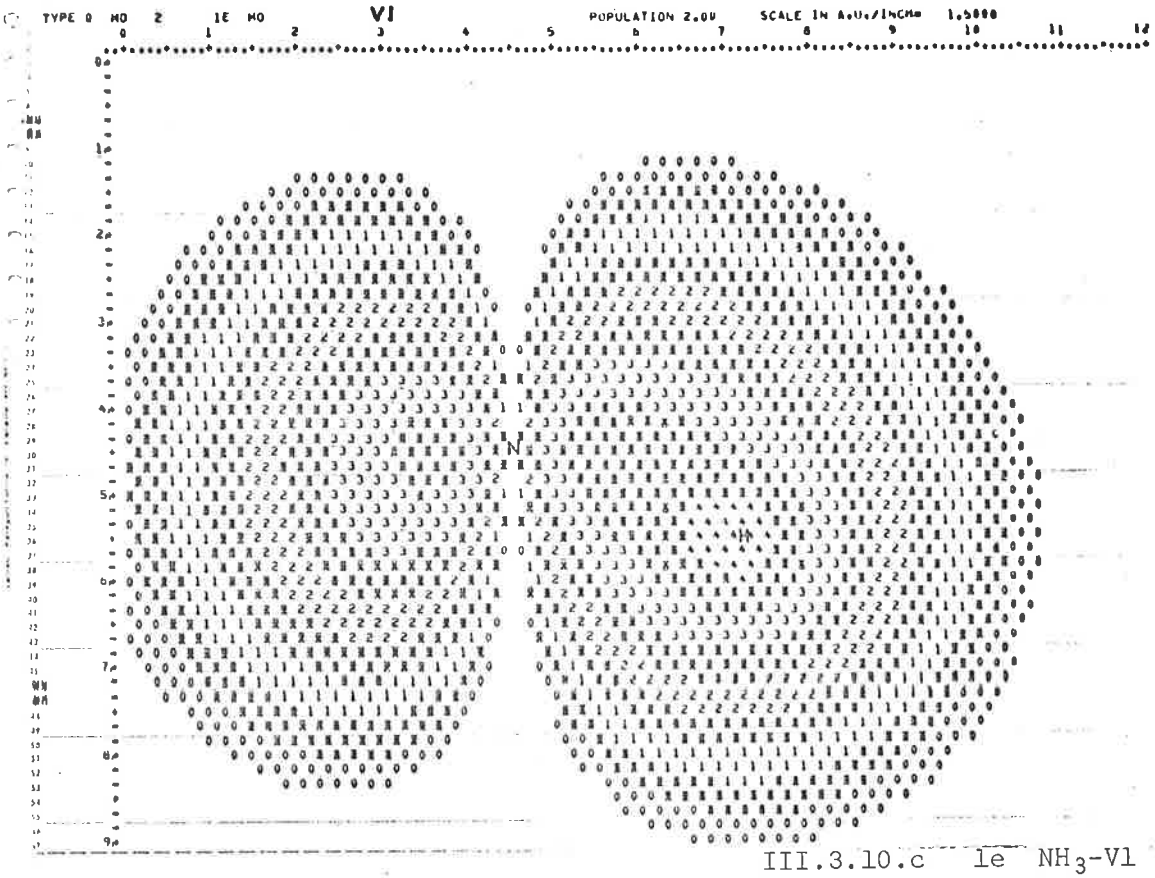

III.3.10.c le NH_3-V1

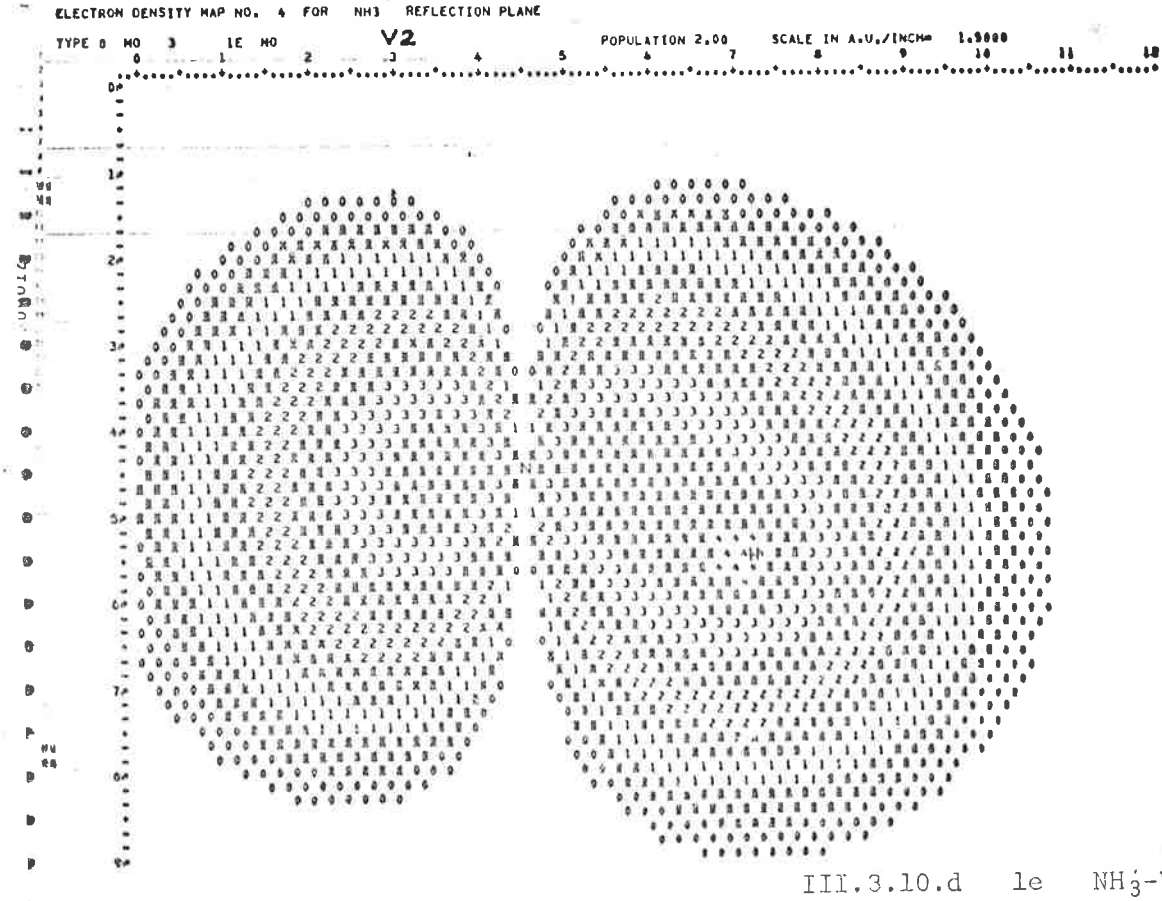

III.3.10.d le NH_3-V2

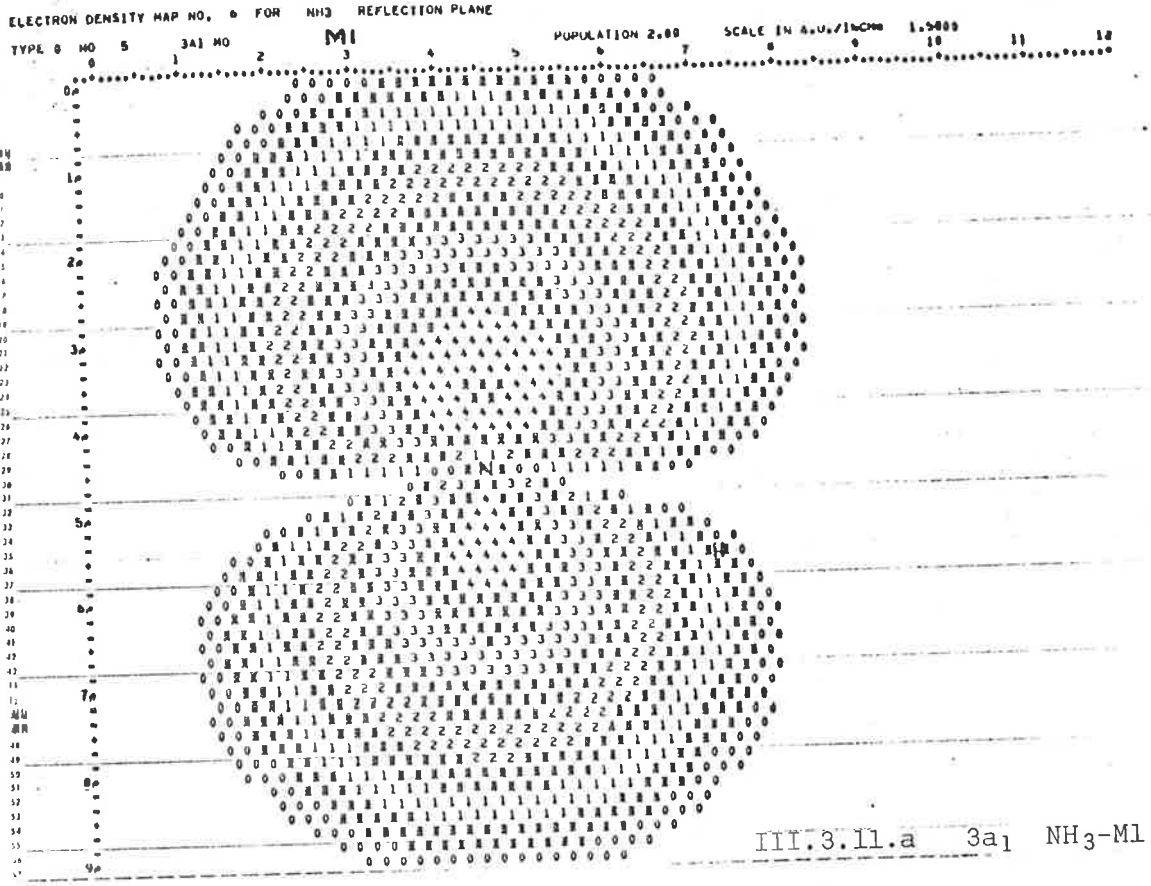

III.3.11.a $3a_1$ NH_3-M1

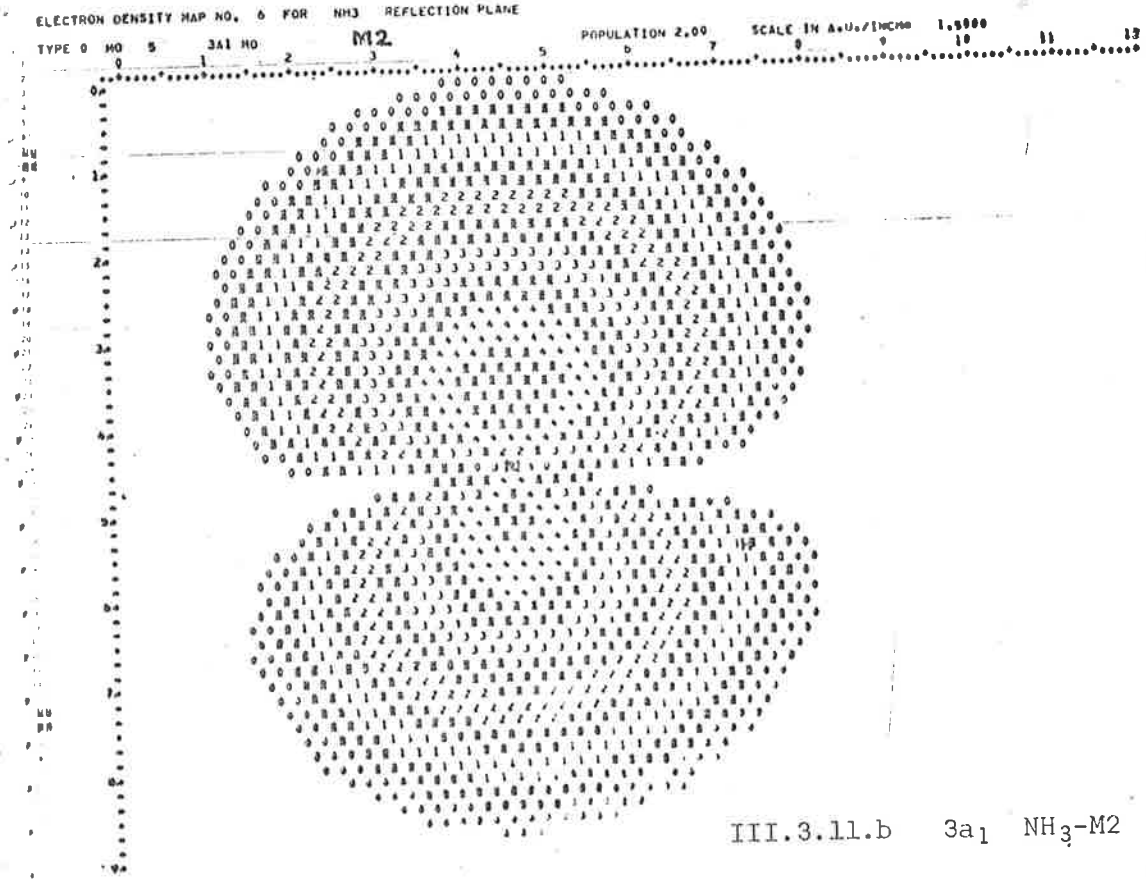

III.3.11.b $3a_1$ NH_3-M2

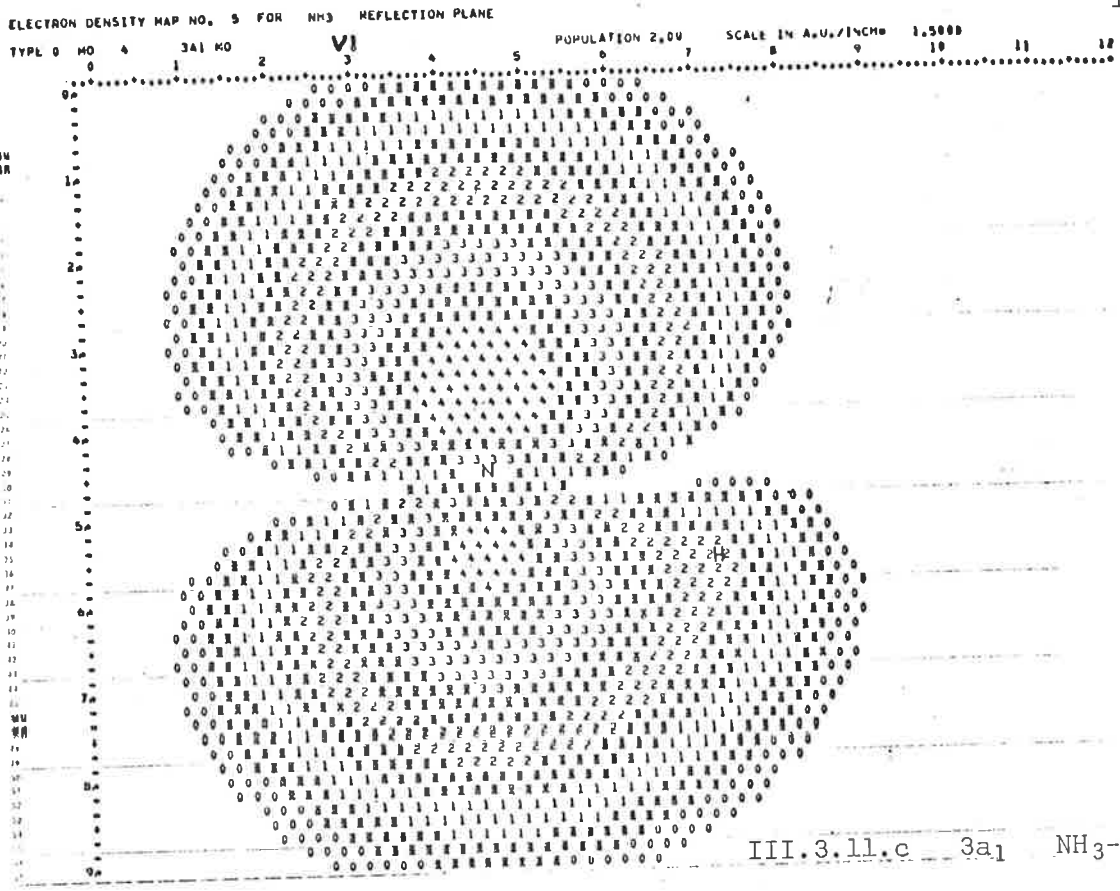

III.3.11.c $3a_1$ NH_3-V1

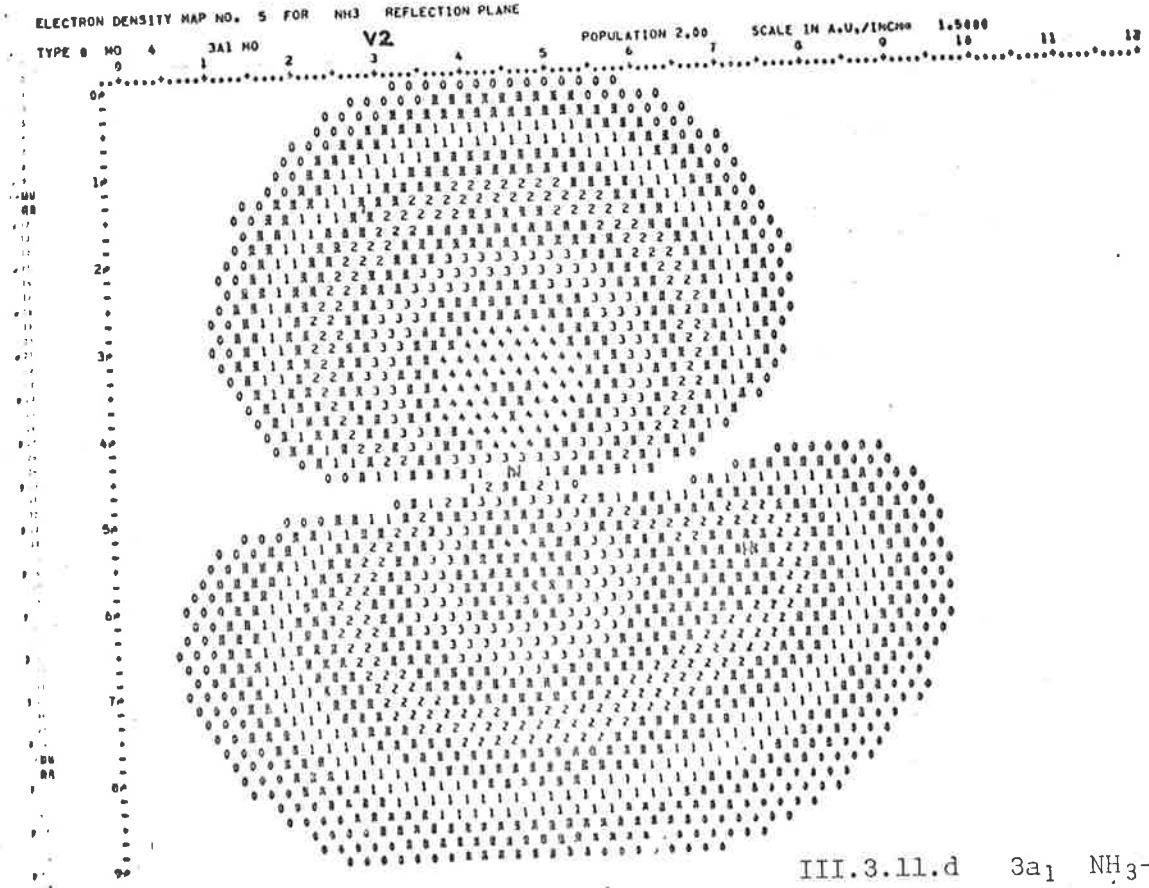

III.3.11.d $3a_1$ NH_3-V2

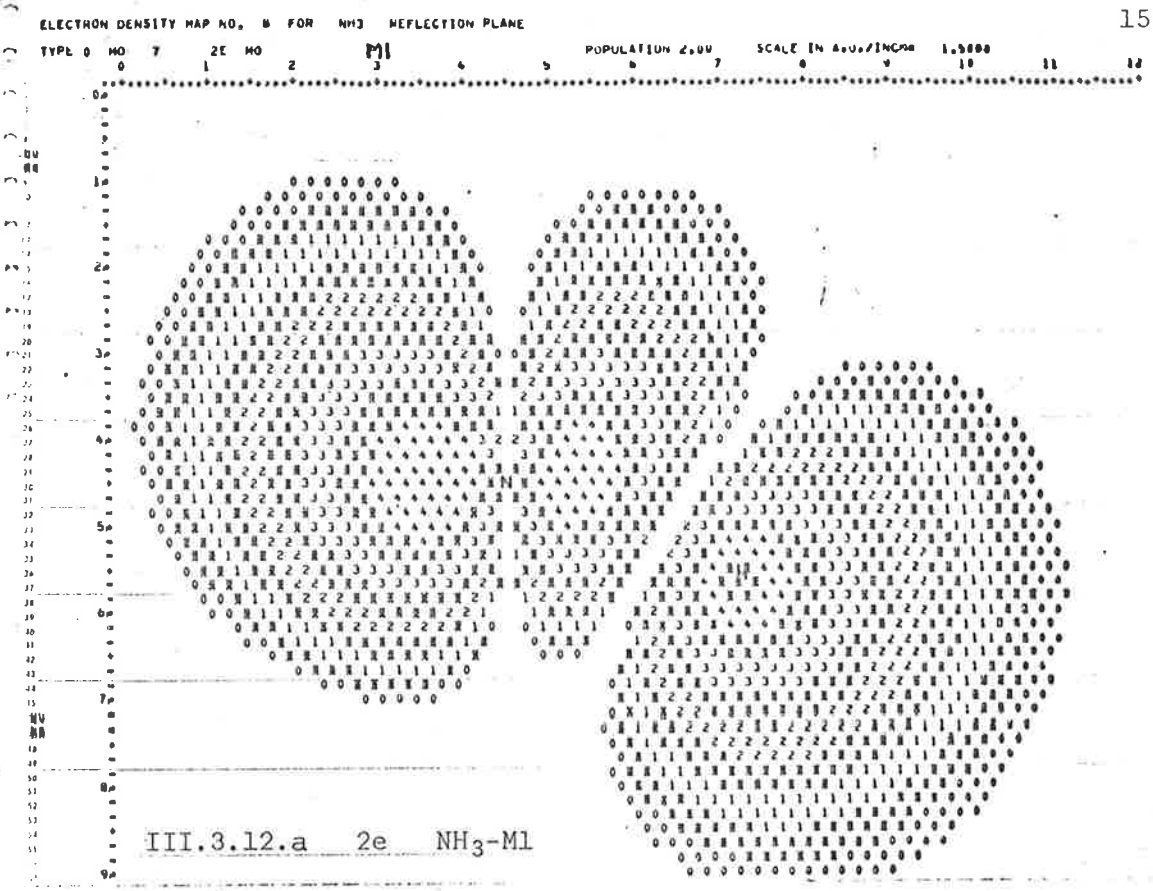

III.3.12.a 2e NH_3-M1

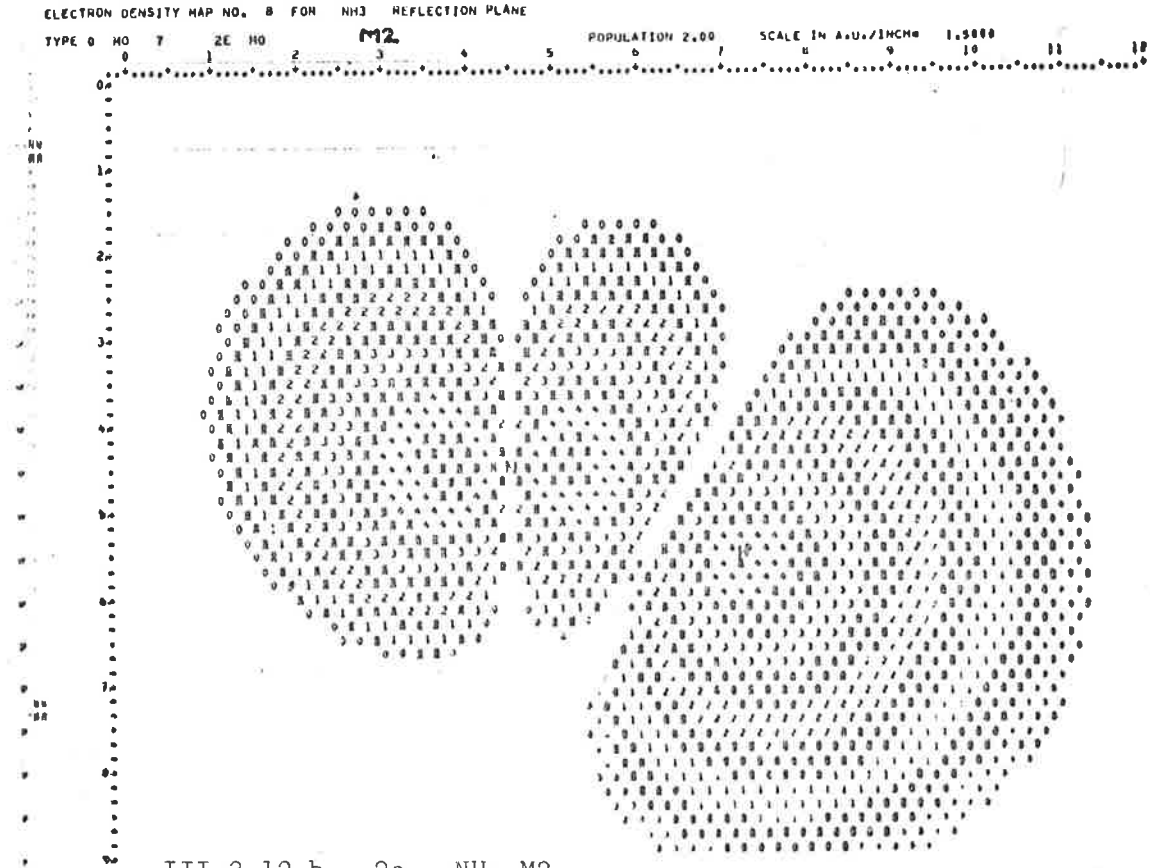

III.3.12.b 2e NH_3-M2

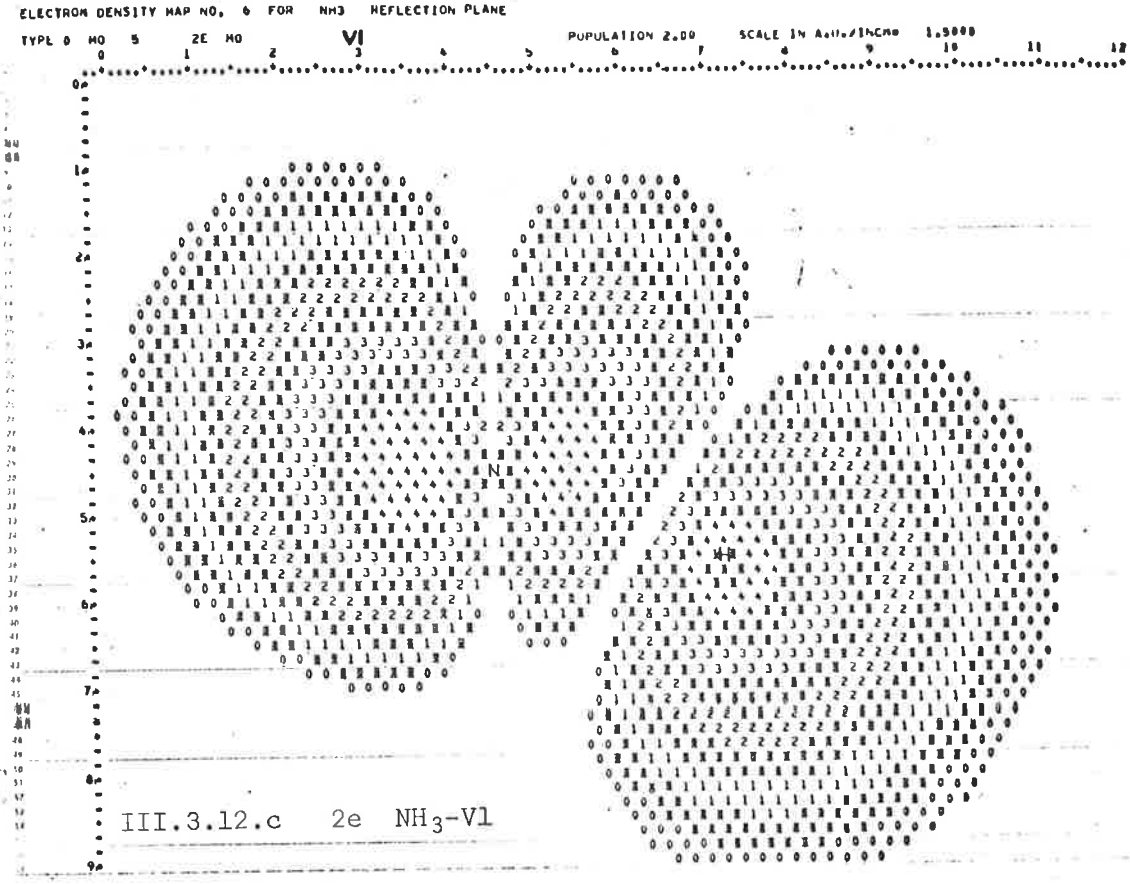

III.3.12.c 2e NH_3-V1

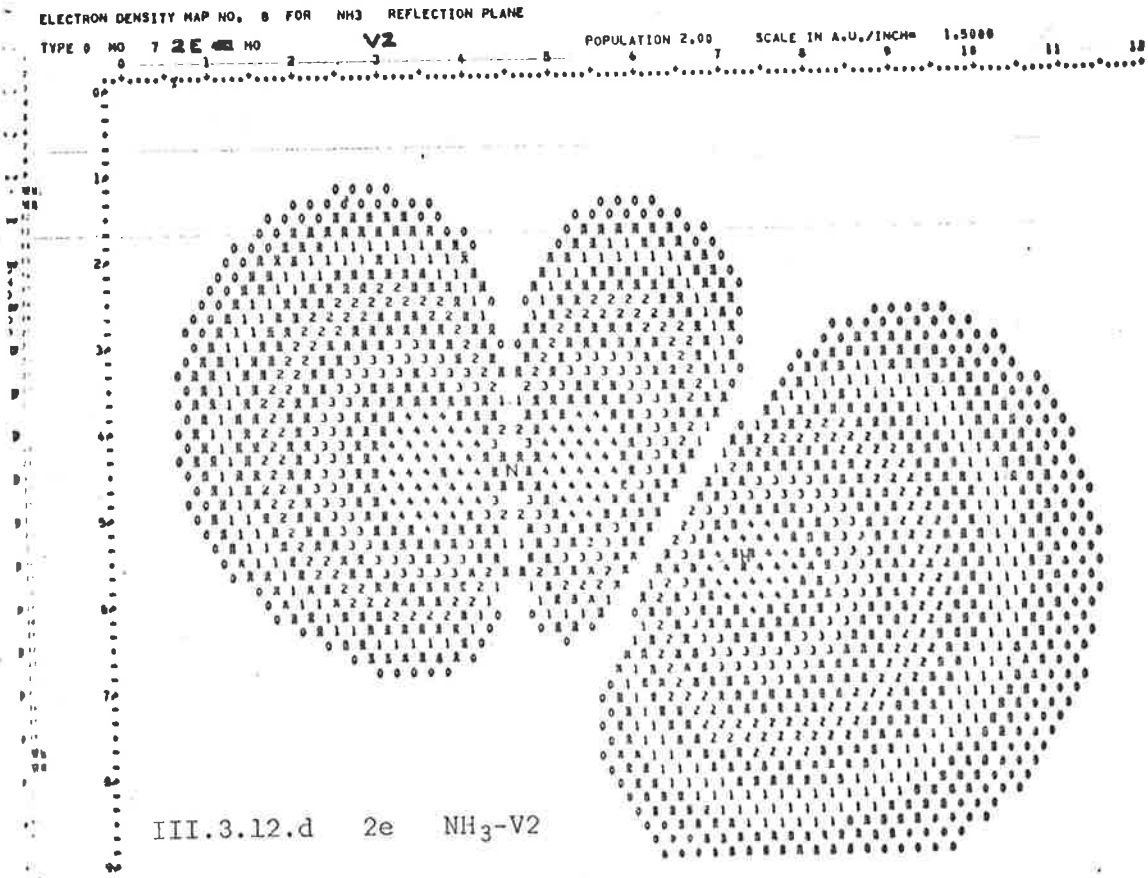

III.3.12.d 2e NH_3-V2

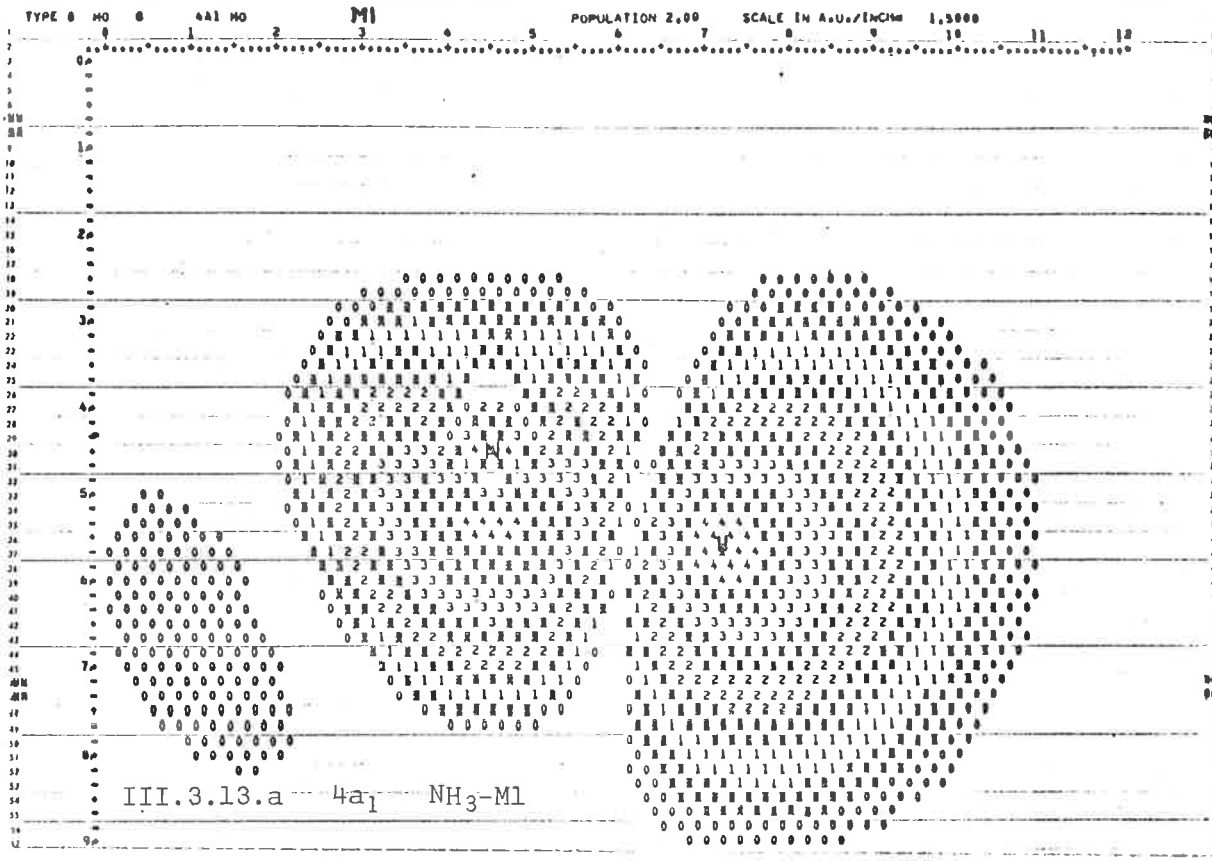

III.3.13.a $4a_1$ NH_3-M1

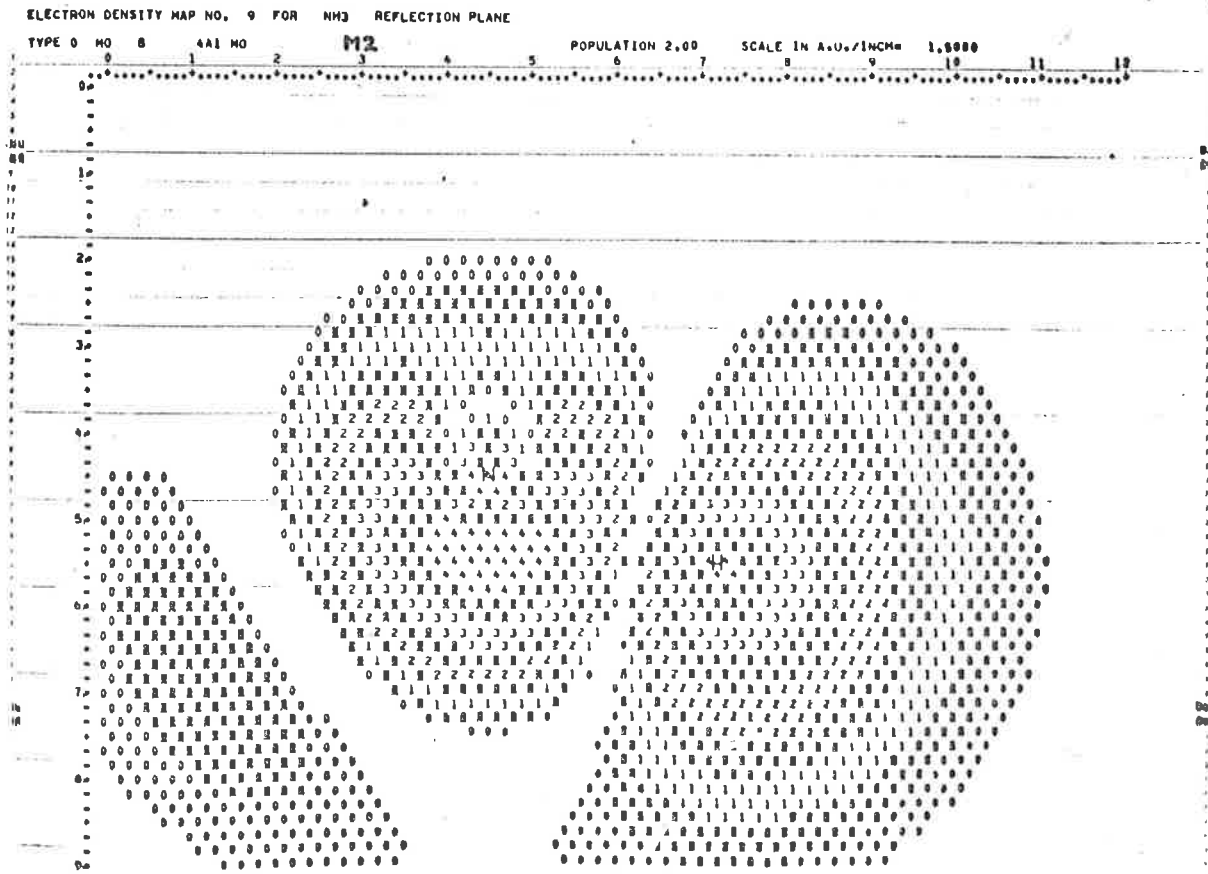

III.3.13.b $4a_1$ NH_3-M2

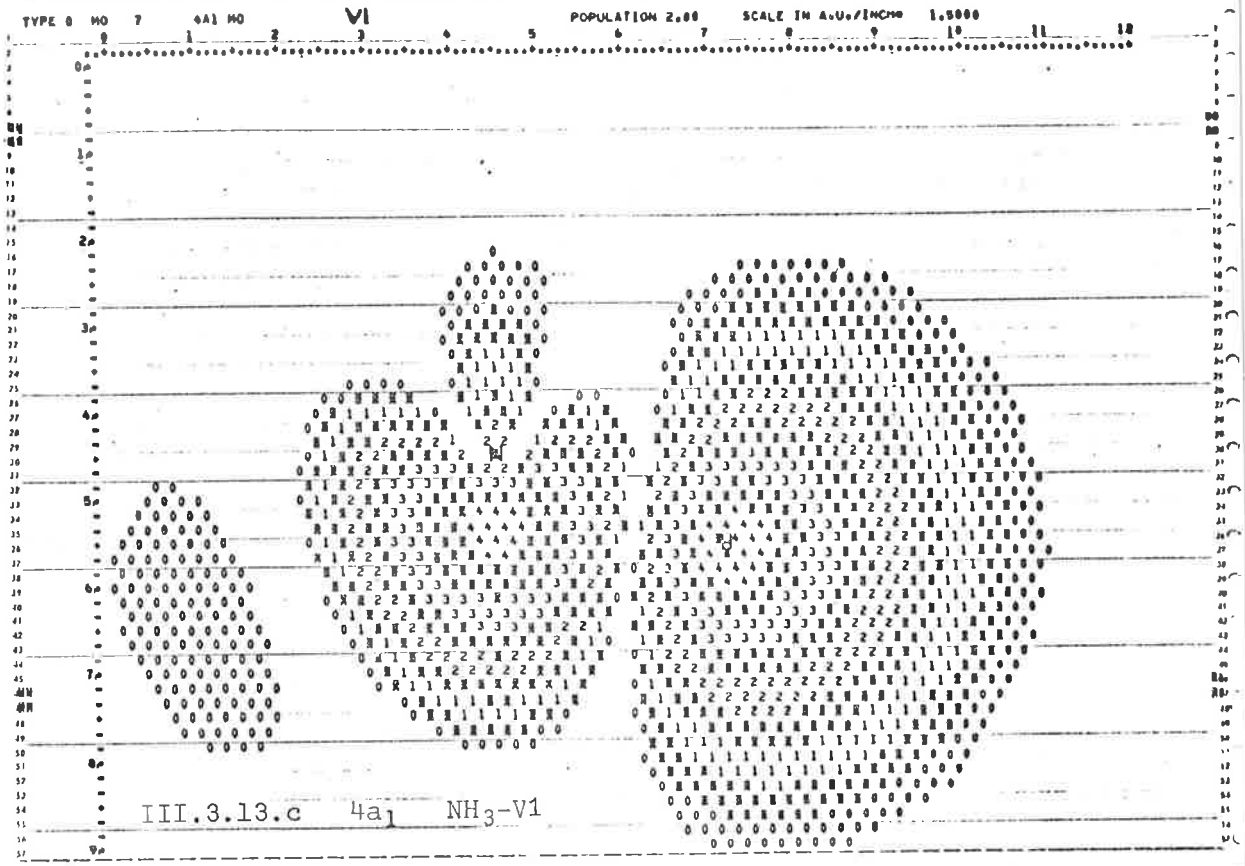

III.3.13.c $4a_1$ NH_3-V1

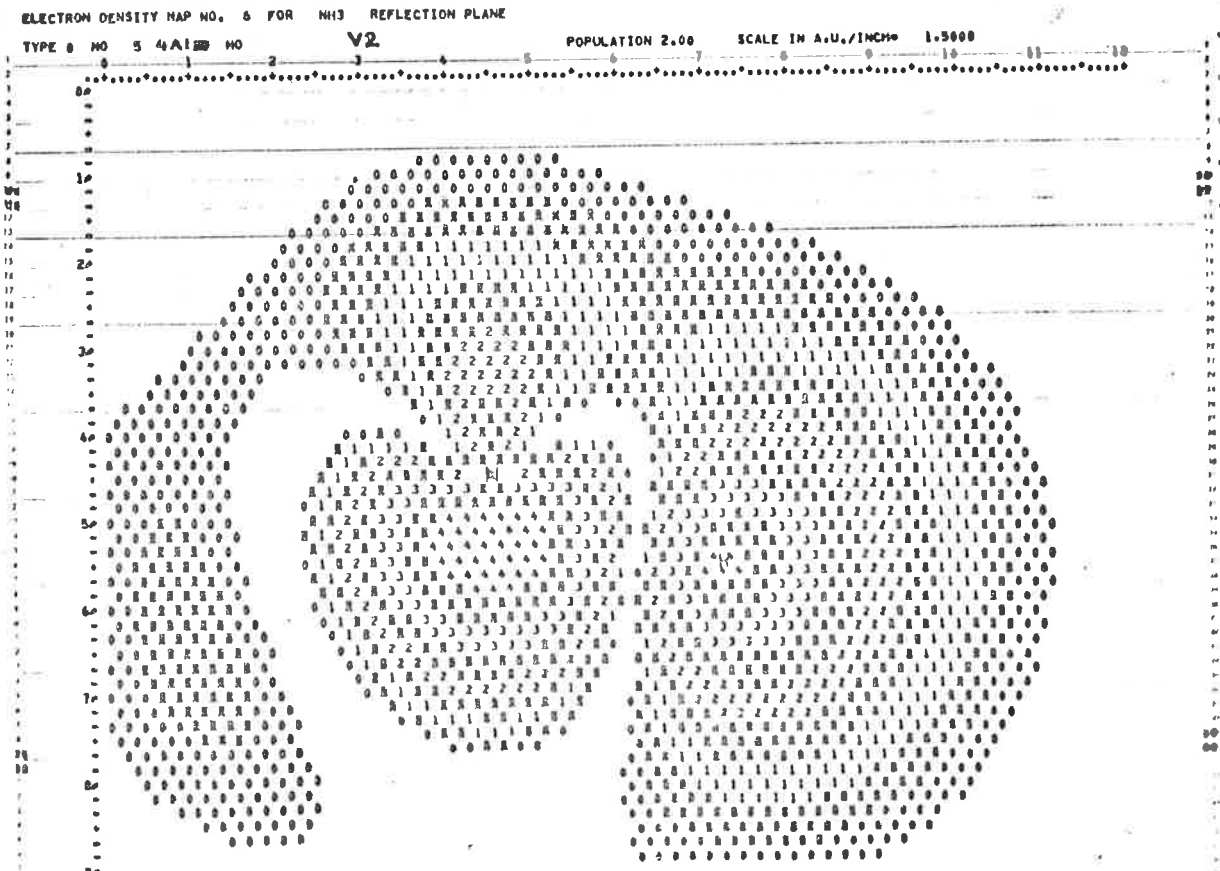

III.3.13.d $4a_1$ NH_3-V2

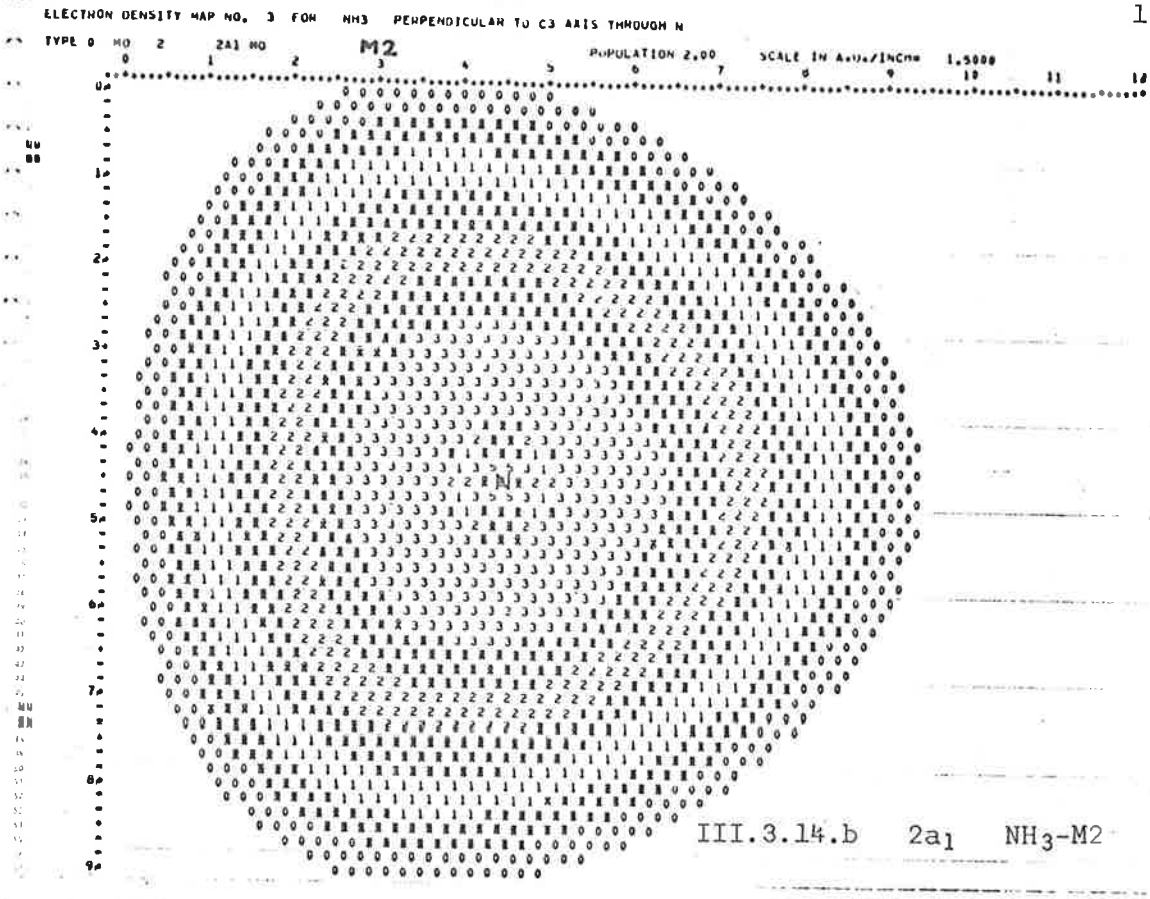

III.3.14.b $2a_1$ NH_3-M2

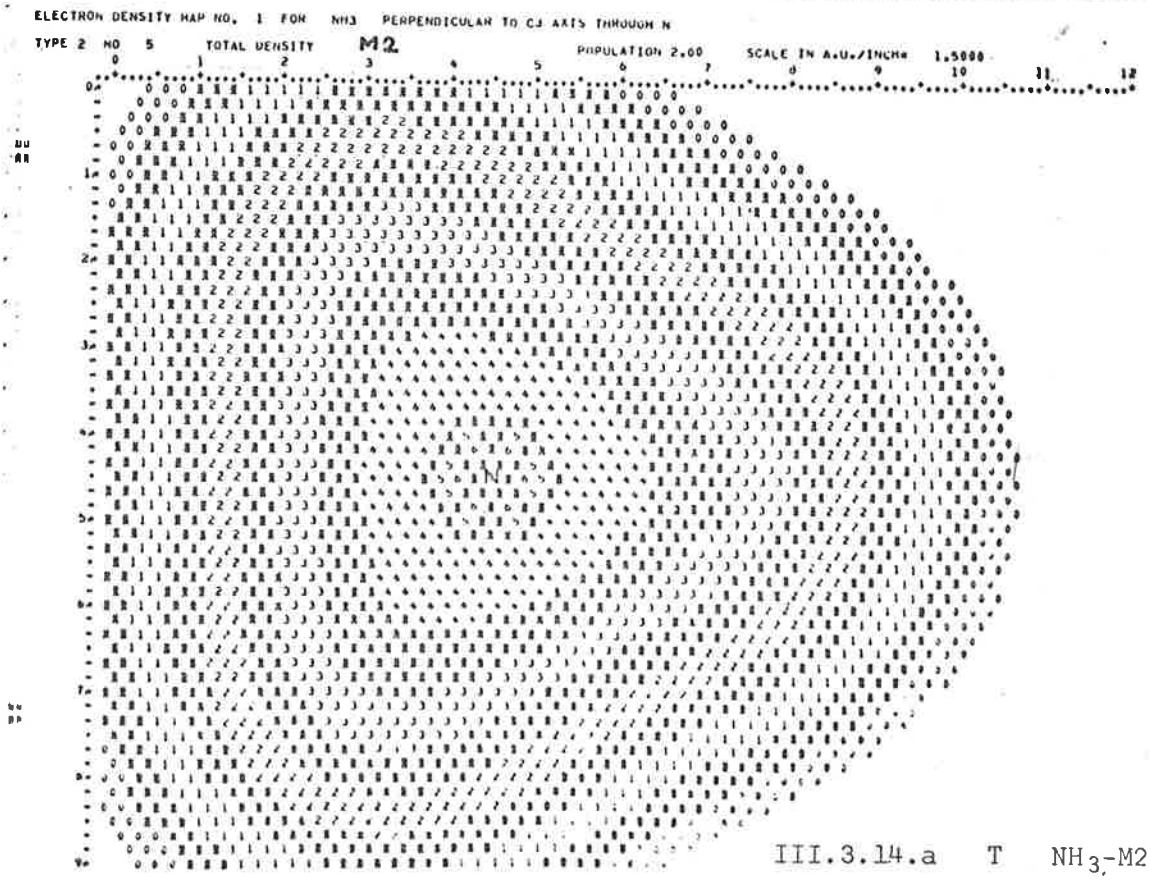

III.3.14.a T NH_3-M2

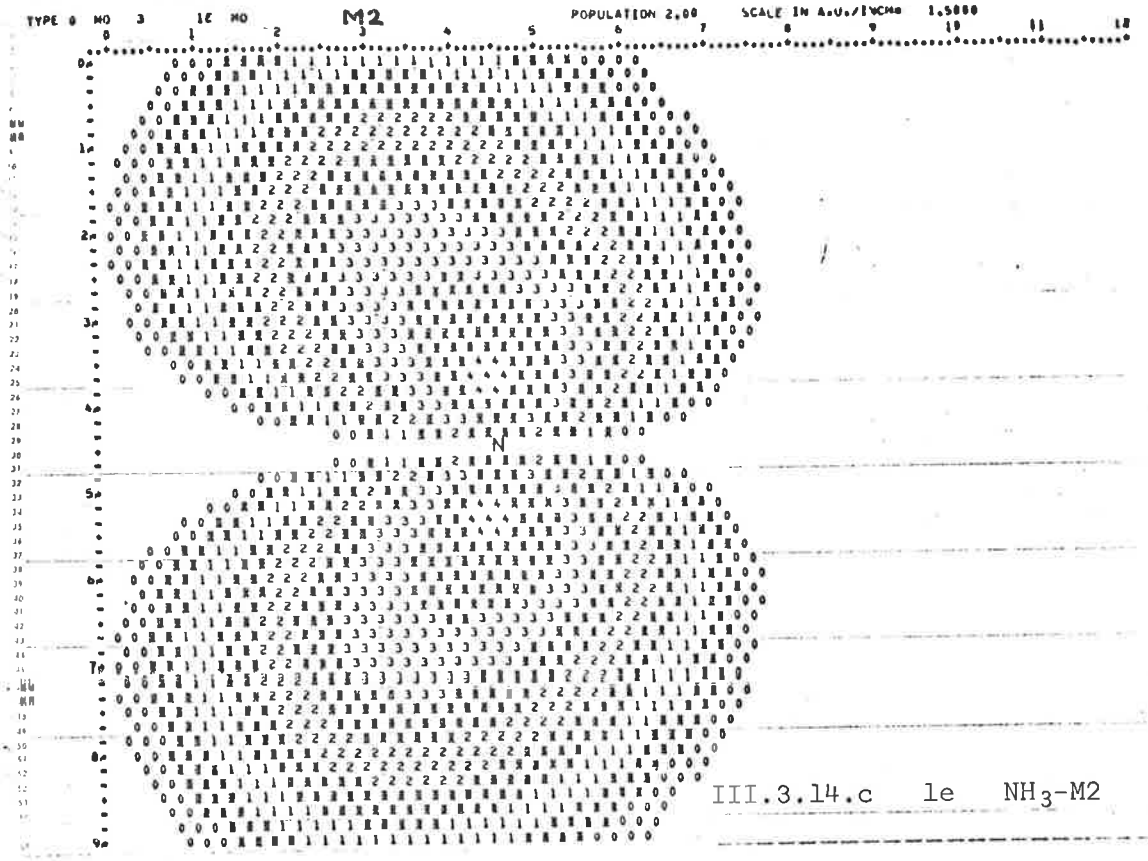

III.3.14.c le NH_3-M2

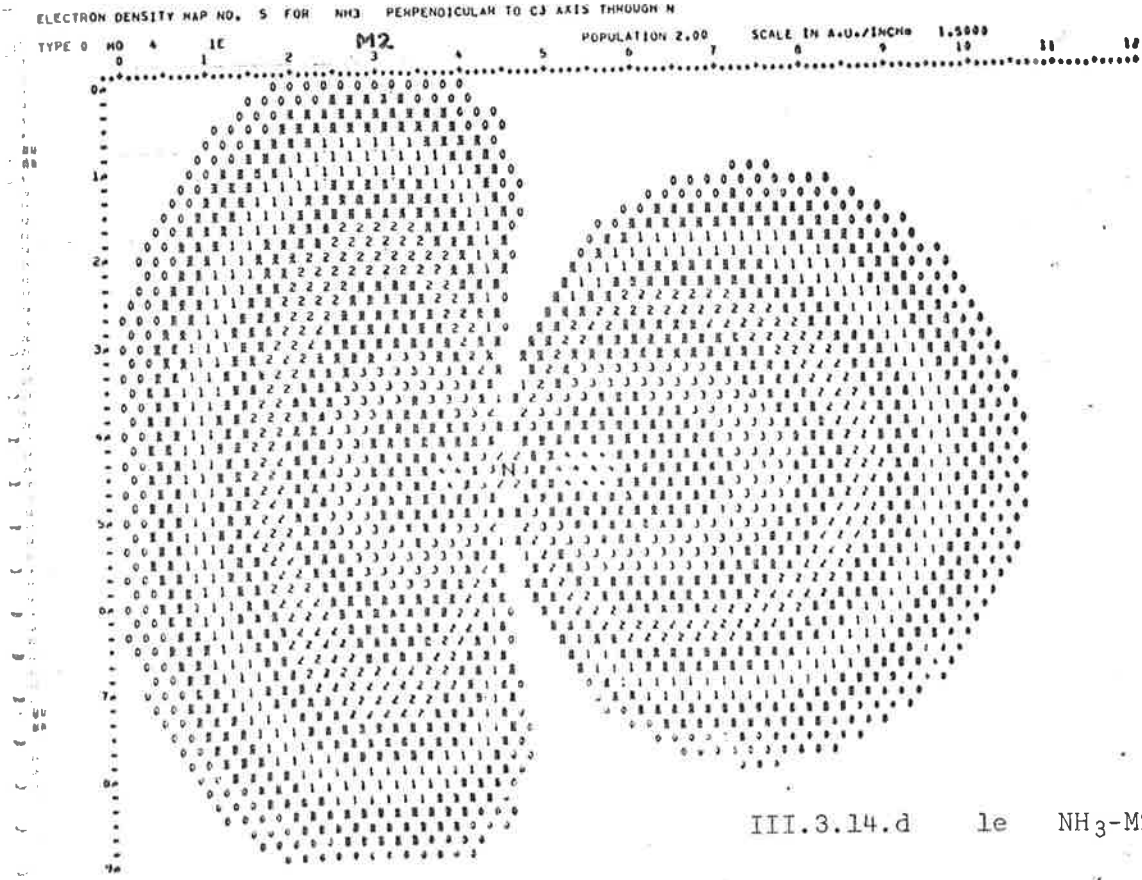

III.3.14.d le NH_3-M2

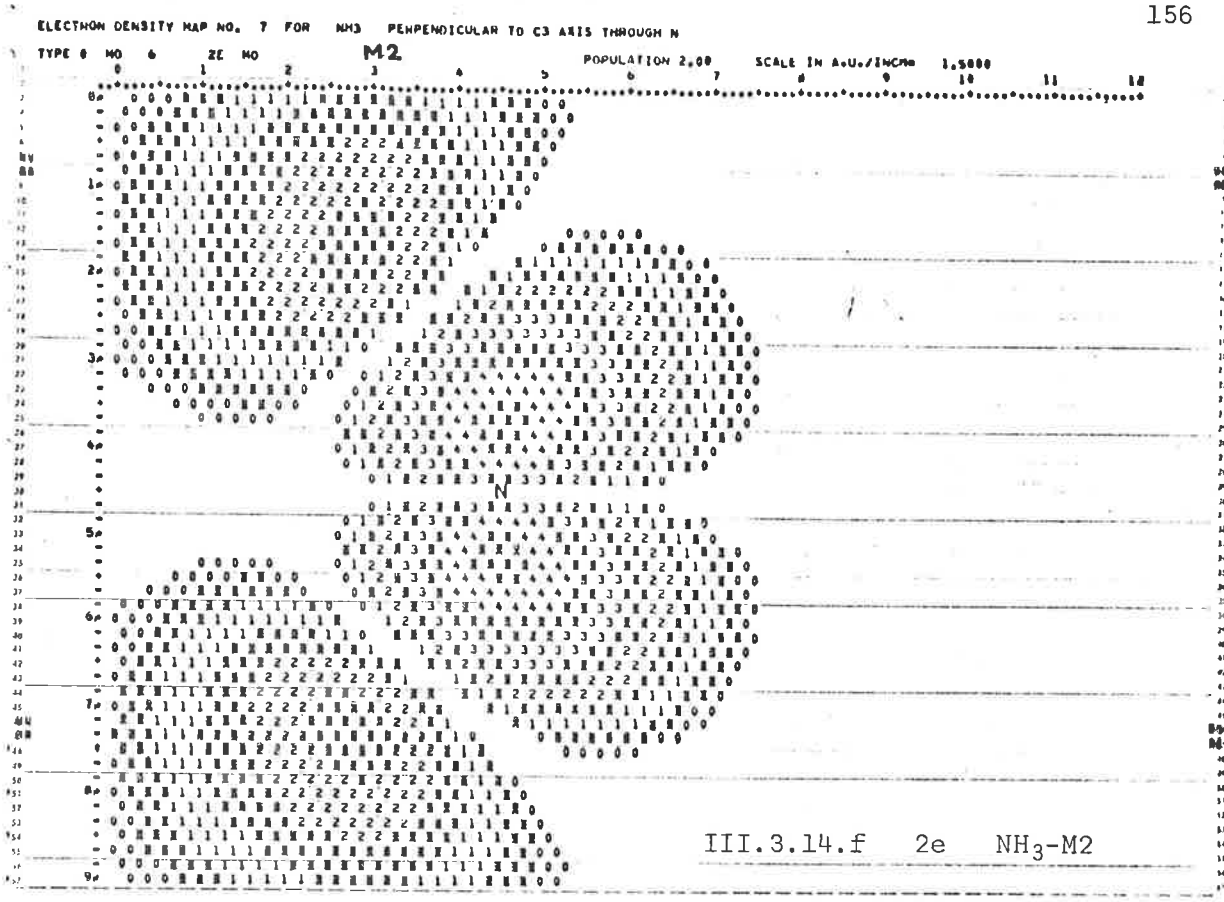

III.3.14.f 2e NH_3-M2

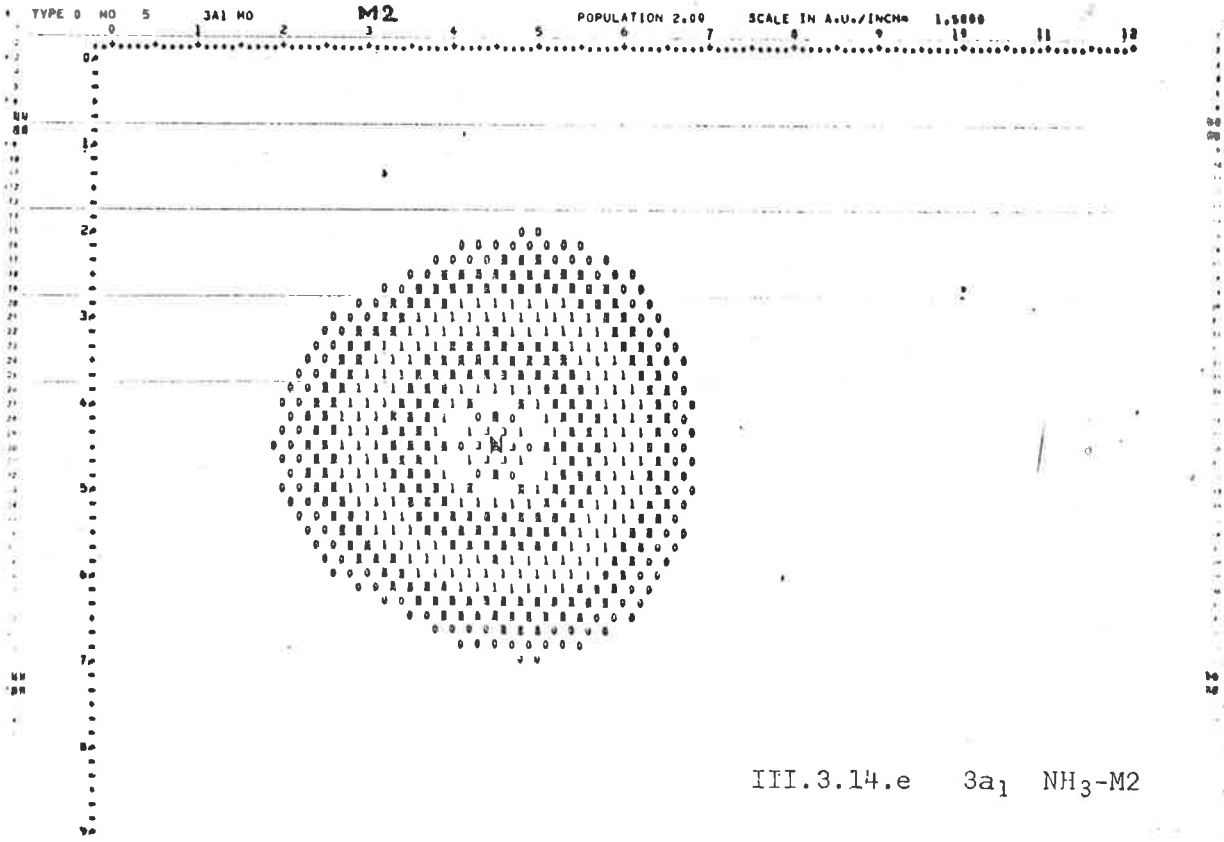

III.3.14.e $3a_1$ NH_3-M2

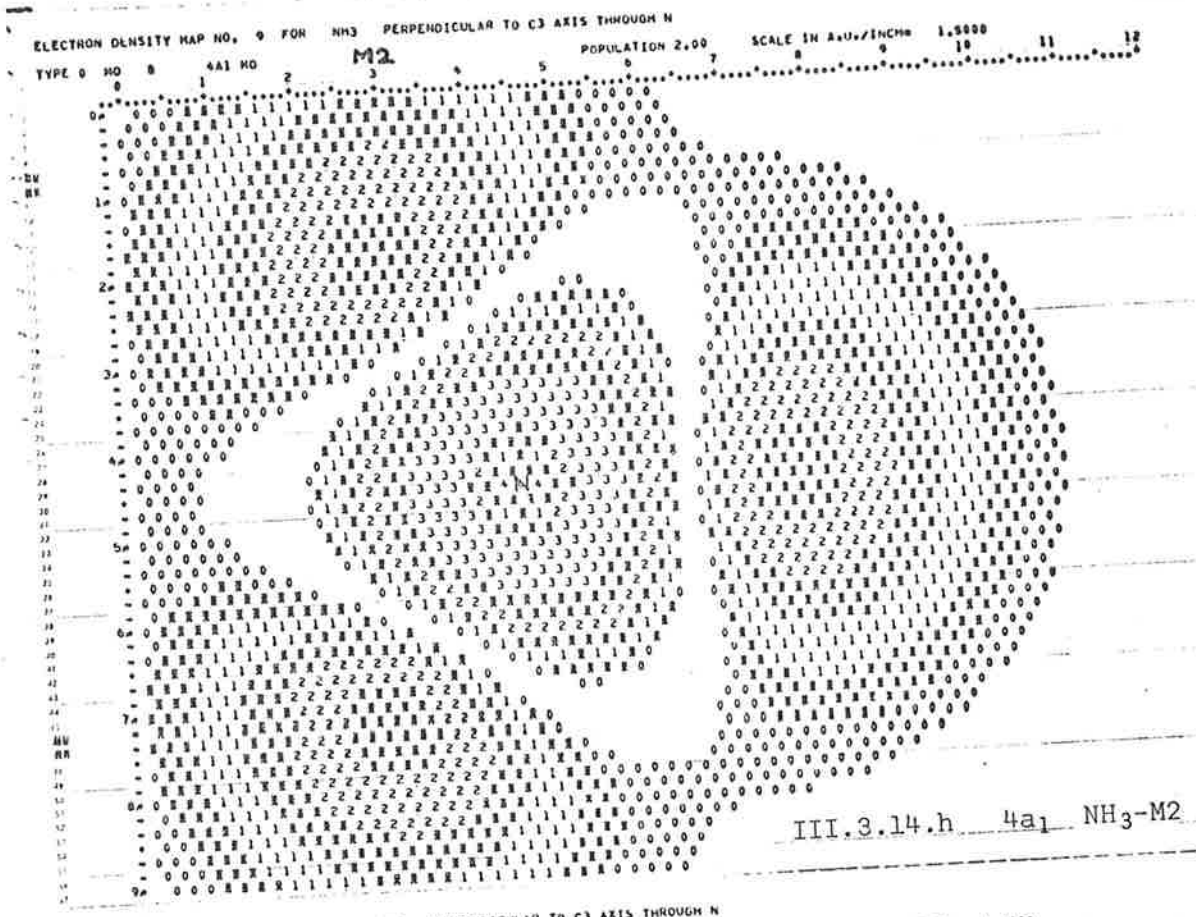

III.3.14.h $4a_1$ NH_3-M2

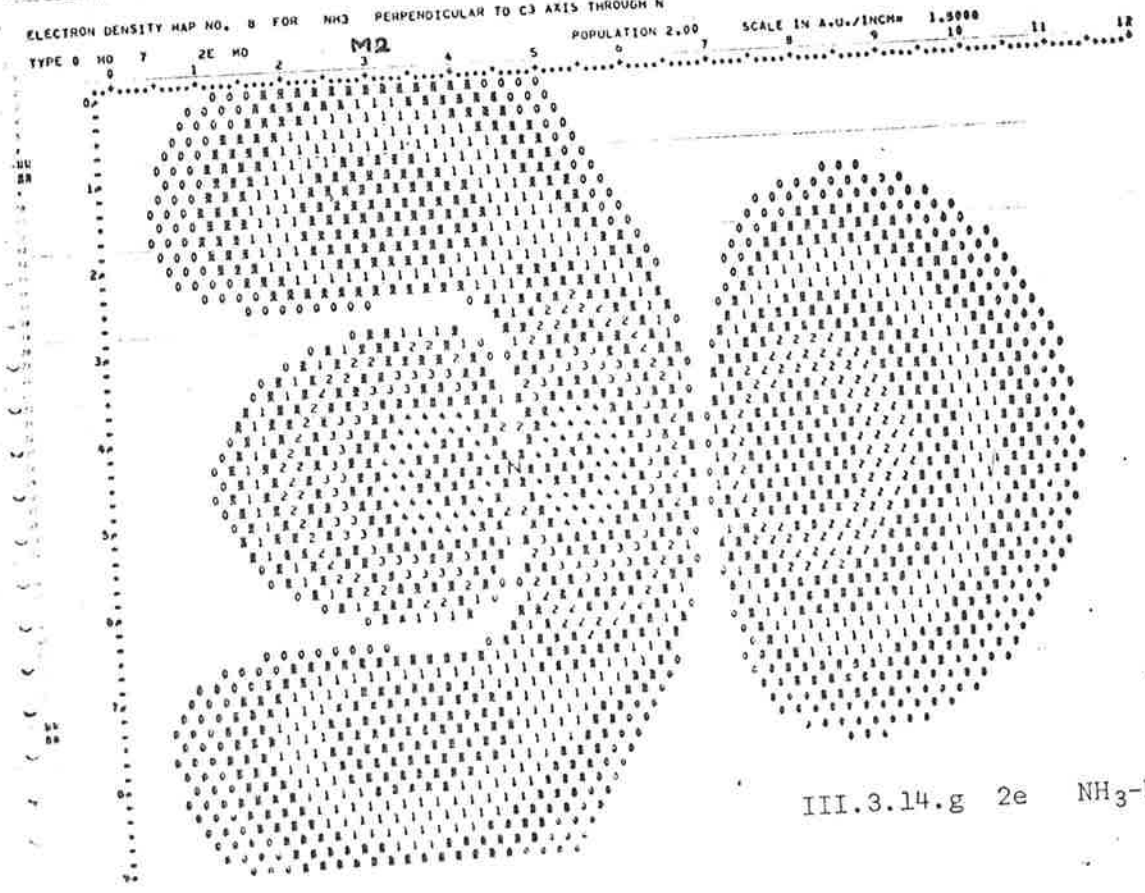

III.3.14.g 2e NH_3-M2

populations for Hls suggest that considerable fluctuations exist. Numerically, Hls populations are: M1 = 0.86, M2 = 0.92, V1 = 0.82, V2 = 0.80, and one would expect that variations of this magnitude should be quite apparent in the density maps. In the light of such obvious disagreement between mapped charge distributions and population/bond indices, we feel justified in our earlier contention that the latter are prone to give misleading results.

In analogy to our examination of the wavefunctions for H_2O, the NH_3 density maps prove extremely useful in illustrating comparative effects of atomic orbital contributions at the MO level. For the $2a_1$ MO (Fig. III.3.9) charge distributions in the minimal basis wavefunctions extend well towards the hydrogen centre, whereas V1 and V2 behave in a manner reminiscent of the corresponding H_2O maps (Fig. III.3.2.c-d), with a "pinch" around H. As a consequence, charge centroids (both at 0.16 au, Table III.3.10.a) are contracted towards N, relative to the M1 and M2 wavefunctions, wherein $\langle z_N \rangle$ occurs at 0.33 and 0.36 au, respectively.

Some compensation occurs in the $3a_1$ orbital, for there both minimal basis wavefunctions map as essentially N2pz orbitals, weighted away from H (Fig. III.3.11), as is evident in $\langle z_N \rangle$ values, -.32(M1) and -.30 au (M2). By contrast, the centroid in the V1 wavefunction is displaced only half that distance, (-·15 au), while, for V2, the expectation value of -.05 au indicates very little polarisation relative to N. These effects obviously stem from orbital coefficients

Table III.3.10.a. One-Electron Expectation Values, NH_3 - $\langle Z_N \rangle$

MO	M1	M2	V1	V2
$1a_1$	- .0002	0.0000	-	-
$2a_1$	0.3276	0.3567	0.1645	0.1639
1e	0.3933	0.3603	0.3879	0.3347
	0.3933	0.3603	0.3879	0.3347
$3a_1$	- .3150	- .2981	- .1487	- .0482
Electronic	1.598	1.558	1.583	1.570
Nuclear	-2.159	-2.159	-2.159	-2.159
Nett	- .561	- .601	- .576	- .589

Table III.3.10.b. One-Electron Expectation Values, NH_3 - $\langle \theta_{zz} \rangle$

MO	M1	M2	V1	V2
$1a_1$	- .0158	- .0155	-	-
$2a_1$	0.0750	0.2052	- .0482	- .0228
	1.0108	0.9201	1.0035	0.9318
1e	1.0108	0.9201	1.0035	0.9318
$3a_1$	-1.0376	- .7734	- .9853	- .7552
Electronic	2.087	2.513	1.947	2.171
Nuclear	-3.566	-3.566	-3.599	-3.599
Nett	-1.479	-1.053	-1.652	-1.427

Table III.3.10.c. One-electron Expectation Values, NH_3 - $\langle x^2 \rangle$

MO	M1	M2	V1	V2
$1a_1$	- .0235	- .0243	-	-
$2a_1$	- .8253	- .9913	- .6983	- .6581
1e	- .9044	- .8365	- .8982	- .8471
	-2.5042	-2.2926	-2.4903	-2.3621
$3a_1$	- .5021	- .3847	- .5684	- .7086
Electronic	-9.519	-9.059	-9.311	-9.152

Table III.3.10.d. One-electron Expectation Values, NH_3 - $\langle z^2 \rangle$

MO	M1	M2	V1	V2
$1a_1$	- .0393	- .0398	(- .0163)	(- .0163)
$2a_1$	- .7503	- .7861	- .7465	- .6809
1e	- .6935	- .6444	- .6908	- .6728
	- .6935	- .6444	- .6908	- .6728
$3a_1$	-1.5397	-1.1582	-1.5537	-1.4638
Electronic	-7.433	-6.546	-7.396	-7.013

Table III.3.10.e. One-electron Expectation Values, NH_3 - $\langle r^2 \rangle$

MO	M1	M2	V1	V2
$1a_1$	- .0863	- .0884	(- .0163	(- .0163)
$2a_1$	- 2.4009	- 2.7687	- 2.1432	- 1.9971
1e	- 4.1022	- 3.7736	- 4.0793	- 3.8820
	- 4.1022	- 3.7736	- 4.0793	- 3.8820
$3a_1$	- 2.5439	- 1.9276	- 2.6905	- 2.8811
Electronic	-26.471	-24.664	-26.017	-25.317

Table III.3.10.f. One-electron Expectation Values, NH_3 - $\langle r_N^{-1} \rangle$

MO	M1	M2	V1	V2
$1a_1$	- 6.6936	- 6.6901	(- 6.70	(- 6.70
$2a_1$	- .9897	- .9448	- .9196	- .9518
	- .6402	- .7134	- .6431	- .6850
1e	- .6402	- .7134	- .6431	- .6850
$3a_1$	- .8801	- 1.0228	- .8484	- .8426
Electronic	-19.687	-20.169	-19.508	-19.729
Nuclear	1.566	1.566	1.566	1.566
Nett	-18.122	-18.604	-17.942	-18.163

Table III.3.10.g. One-electron Expectation Values, NH_3 - $\langle r_H^{-1} \rangle$

MO	M1	M2	V1	V2
1a	- .5218	- .5218	(- .5219	(- .5219
21	- .5360	- .5440	- .5148	- .5204
1e	- .8256	- .7893	- .8222	- .7700
	- .3758	- .3888	- .3769	- .3885
3a	- .4490	- .4634	- .4667	- .4813
Electronic	-5.416	-5.414	-5.405	-5.364
Nuclear	4.303	4.303	4.303	4.303
Nett	-1.113	-1.111	-1.102	-1.061

in the $3a_1$ MO; common to all four procedures is a comparatively small contribution from N2s, but both valence basis wavefunctions are distinguished by a large admixture of H1s into what would otherwise be a predominantly N2pz distribution. The density maps illustrate this point well, and show, in addition, the gradation in z-extension previously mentioned in conjunction with total density.

As a consequence, nett polarisation, relative to N, in orbitals of a_1 symmetry, is very weak, amounting to 0.01 and 0.06 au in the minimal basis wavefunctions, and 0.01 and 0,12 au for V1 and V2. However, these values are not relative to the centre of nuclear charge, which occurs ~·24 au towards H on the C_2 axis. Therefore, the molecular effect is one of fairly strong polarisation away from the H atoms, with the principal contribution stemming from the high p-content in the $3a_1$ MO.

Whereas expectation values in the a_1 orbitals are inclined to classify as minimal or valence basis in their stratification pattern, charge centroids for the 1e MO's are more or less equivalent, with a tendency to group, rather, by Version. Both Version 1 wavefunctions are characterised by charge centroids well displaced towards H, (0.39 au), whereas, for Version 2, $\langle z_N \rangle$ is located at 0.36 au in M2, and 0.33 au in V2. The density maps of Fig. III.3.10 are illustrative (note particularly the extent of region 4, $0.256 < \rho < 0.512$) and recall similar behaviour in the $1b_2$ MO of H_2O. It is apparent that H_1 orbital coefficients are primarily responsible for the behaviour above,

for percentage contributions to the 1e MO are graded numerically in the same order as $\langle z_N \rangle$ viz. M1 (34.2%), V1 (33.7%), M2 (33.3%), V2 (30.4%).

Viewed as a whole, dipole moments, $\langle z_N \rangle$, do not fall into any pattern consistent with respect to version, basis set or orbital symmetry. Our examination of the H_2O wavefunctions likewise failed to reveal any consistency among orbital contributions to dipole moment, nor to other one-electron property expectation values. Therefore, we shall confine our further discussion of the NH_3 wavefunctions to a brief resumé of those aspects which have some significance or confirmatory value to the observations recorded for H_2O.

Second moments of the charge distribution, $\langle z^2 \rangle$ (Table III.3.10.d) afford, in their nett values, confirmatory evidence for the gradations in extension, along the C_3 axis, of the total charge distribution. It is apparent also that the principal contribution arises in the $3a_1$ MO, for expectation values there are the largest (viz. -1.16 (M2), -1.46 (V2), -1.54 (M1), -1.55 V1)), and additionally, grade in accordance with the nett values. Expectation values for the M1 and V1 wavefunctions show some tendency to group together, both here and also in the $\langle x^2 \rangle$ component (Table III.3.10.c). Moreover, there is evidence of stratification in molecular quadrupole moment, θ_{zz} (Table III.3.10.b), principally at the $3a_1$ and 1e levels, and including, in this instance, the M2 and V2 expectation values as a separate grouping rather than individual scattered results. However,

while the existing patterns intimate that differences among the four procedures may be greatest in the $2a_1$ MO, they are, themselves, insufficiently general to rate more than a passing mention.

As occurred with the H_2O wavefunctions, expectation values for the operator r_H^{-1} (Table III.3.10.g) are unique in that separations among the four procedures are consistently small over all molecular orbital levels. Largest discrepancy occurs in the degenerate le MO's, where M1 and V2 differ in their combined contributions by 0.04 au.

Scatter in expectation values of $\langle r_N^{-1} \rangle$ is more pronounced (Table III.3.11.f), as we found before for $\langle r_O^{-1} \rangle$, but, with the exception of the M2 wavefunction, still not great by comparison with, say, $\langle z_N \rangle$. A larger nett value in the M2 approach would seem characteristic (-18.60 au vs -18.12 au for M1), for a similar separation from the M1, V1 and V2 values occurs also in H_2O.

In summary, the optimised wavefunctions for NH_3 vary considerably in their ability to reproduce absolute energy values. Total energies are considerably higher than experiment, with Version 2 showing the greater deviation. In comparison with an equivalent, but unoptimised, *ab initio* wavefunction, the M1 energy is not greatly different. Calculated ionisation potentials are in very reasonable agreement with experimental values, provided one allows for an arbitrary displacement term. In the absence of any correction, the predicted values by Version 1 are slightly high, but in good accord, nevertheless; both wavefunctions in Version 2 underestimate ionisation

potentials, with the valence basis results the better of the two.

Total charge distributions among the four procedures are not greatly different, although electron density arising from the Version 1 wavefunction is more extended along the C_3 rotation axis. There is a strong correlation with N2p orbital exponents, in accord with our observation that the effect arises predominantly in the $3a_1$ MO, where the N2pz orbital is dominant.

It would appear that there exists no consistent pattern in the recorded groupings among expectation values when partitioned at the molecular orbital level. In some instances, e.g. second moments and diamagnetic shielding, calculated values for the M1 and V1 wavefunctions exhibited quite a close correspondence in the $1e$ and $3a_1$ MO's, but the similarity does not extend to the $2a_1$ orbital. By way of contrast, grouping in dipole moment expectation values was dependent on basis set rather than version.

Nor were we able to establish an independent basis for assessment of the four procedures M1, M2, V1 and V2, other than the criteria of one-electron properties which, by the optimisation process, they all satisfy. Had we been able to establish a strong correlation within a given basis or version, that would, at least, have provided a reference point for future work. As the situation stands, either basis set, or version, would appear to provide a viable combination.

III.3.C H_2CO

The wavefunction for formaldehyde listed in Table III.3.11 is one from the optimised exponent combinations recorded previously in Section III.2.K. The calculated total energy of -112.997 au, is within approx. $\pm$ 0.03 representative of the entire optimised series, and compares to the experimental value, -114.562 au. Neumann and Moskowitz [64] have obtained -113.892 au in a Gaussian [532/21] basis, and this appears to be the closest approach to the Hartree-Fock limit reported to date. Our wavefunction fails by ~0.9 au to achieve their result, and in view of our previous calculations and the larger basis set for H_2CO, this is about the magnitude that would be expected.

Experimental ionisation potentials for formaldehyde [64] are (in au) 0.399, 0.529 and 0.588, associated with ionisation from higher occupied orbitals of symmetry, in turn, b_2, b_1 and a_1. By comparison, our calculated values (Koopman's Theorem) at 0.259 ($2b_2$), 0.231 ($1b_1$) and 0.391 ($5a_1$), show the displacement which we have to come to associate with the M2 procedure. However, magnitude errors are 0.140 au at the $2b_2$ MO, rising to 0.298 au, $1b_1$, and dropping to 0.197 au at the $5a_1$ level. Such inconsistancy is due to the reversal of the $2b_2$ and $1b_1$ levels in our wavefunction, an error which occurred not only at all optimised exponent combinations, but as well in the exponent grid calculations, which, as previously recorded, embraced a very extensive range of exponent values. This failure to achieve the correct orbital sequence constitutes the most disappointing feature

Table III.3.11 H_2CO-M2 Optimised Wavefunction and Populations

AO Exponent		6.70	2.025	2.035	7.66	2.175	2.360	1.20
MO	Energy(au)	C1s	C2s	C2pz	O1s	O2s	O2pz	H1s
$1a_1$	- 20.1765	0.0020	0.0221	0.0347	0.9991	0.0060	0.0047	0.0037
$2a_1$	- 10.9753	0.9962	0.0022	0.0026	-.0025	0.0271	-.0334	0.0539
$3a_1$	- 1.1839	-.0462	0.2801	0.2985	-.0218	0.8686	-.1976	0.1347
$4a_1$	- .8410	-.0456	0.6565	-.1768	-.0093	-.3203	-.1074	0.4591
$5a_1$	- .3913	-.0049	0.0275	0.5440	-.0131	-.3308	-.7521	-.1186
$6a_1$	0.7127	0.0510	0.6400	-.2860	-.0007	0.0401	-.0434	-.5012
$7a_1$	0.8749	0.0288	0.2824	0.7076	-.0324	-.1764	0.6171	-.0539
		C2px	O2px	H1s				
$1b_2$	- .4208	0.6068	0.3533	0.5035				
$2b_2$	- .2587	-.1108	0.9246	-.2576				
$3b_2$	0.5254	0.7871	-.1422	-.4244				
		C2py	O2py					
$1b_1$	- .2306	0.6141	0.7892					
$2b_1$	0.3258	-.7892	-.6141					
Tot.	-112.99654							

Table III.3.11 (Cont'd)

	Löwdin Populations		
AO	Carbon	Oxygen	Hydrogen
1s	1.9931	1.9879	1.1315
2s	1.0213	1.9345	
2pz	0.8350	1.2347	
2px	0.7609	1.9596	
2py	0.7543	1.2457	
Σs	3.0144	3.9324	1.1315
Σ2pσ	1.5959	3.1943	
Σ2p	2.3502	4.4400	
MeH	5.3646	8.3724	1.1315

Bond Indices

C	H1s	Oσ	Oπ
1s	0.0029	0.0010	-
2s	0.4516	0.0885	-
2pz	0.0443	0.8829	-
2px	0.4464	0.0501	-
2py	-	-	-
			0.9396
Σs	0.4546	0.0895	
Σ2p	0.4907	0.9330	
Σσ	0.9453	1.0225	
%2pσ	51.9	91.2	

O	H1s	Cσ	Cπ
1s	0.0000	0.0024	-
2s	0.0005	0.0767	-
2pz	0.0005	0.8934	-
2px	0.0146	0.0501	-
2py	-	-	0.9396
Σs	0.0005	0.0790	
Σ2p	0.0151	0.9435	
Σσ	0.0156	1.0225	
%2pσ	-	92.3	

of our H_2CO calculations, for, while one can countenance departures from absolute energy values as a necessary evil of integral approximation, the perturbations arising therefrom should not be sufficient to destroy qualitative relationships.

However, one-electron properties are essentially correct, by virtue of the optimisation process, and it is of interest to examine them in relation to the wavefunction itself, electron density maps (Figs. III.3.15-17) and expectation values calculated from *ab initio* wavefunctions. For the last, we have selected the [95/3] Gaussian set of Dunning, Winter and McKoy [73] in preference to the Neumann and Moskowitz function [64], which included d orbitals not in our basis.

Total density is displayed in three views through the molecule in Figs. III.3.15.a (molecular plane), III.3.16.a (reflection plane) and III.3.17 (CH bond). The region around the H nucleus in the molecular plane is of interest, because it would appear by comparison with the corresponding H_2O density map (Fig. III.3.1.b) that the H atom in H_2CO is poorly endowed with electrons, an inference which is at variance with the H1s population value of 1.13. We are therefore disinclined to place too much faith in the Löwdin populations. Calculated bond indices are of some note, if only for the highly simplistic bonding electron arrangement which they indicate. According to the values in Table III.3.11, the C-O σ-bond is almost entirely formed through unperturbed 2pz orbitals on each atom, while

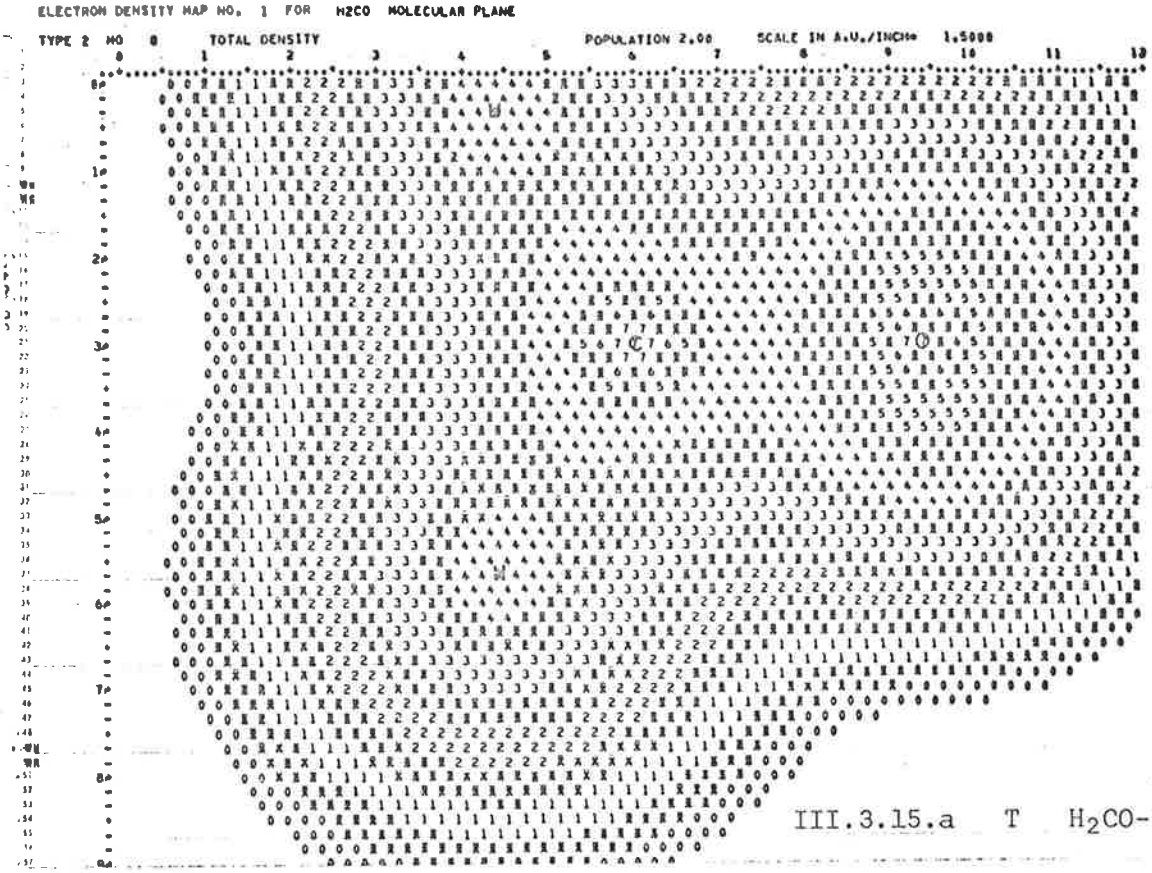

III.3.15.a T H_2CO-M2

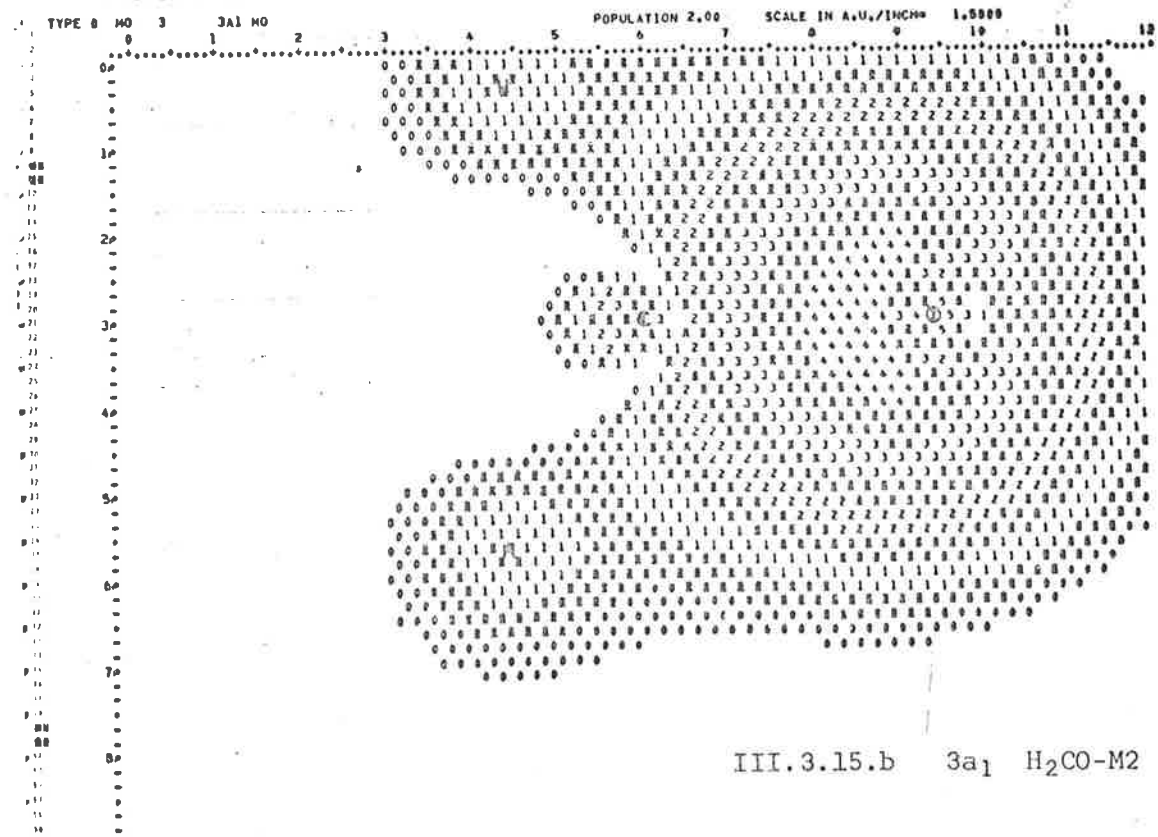

III.3.15.b $3a_1$ H_2CO-M2

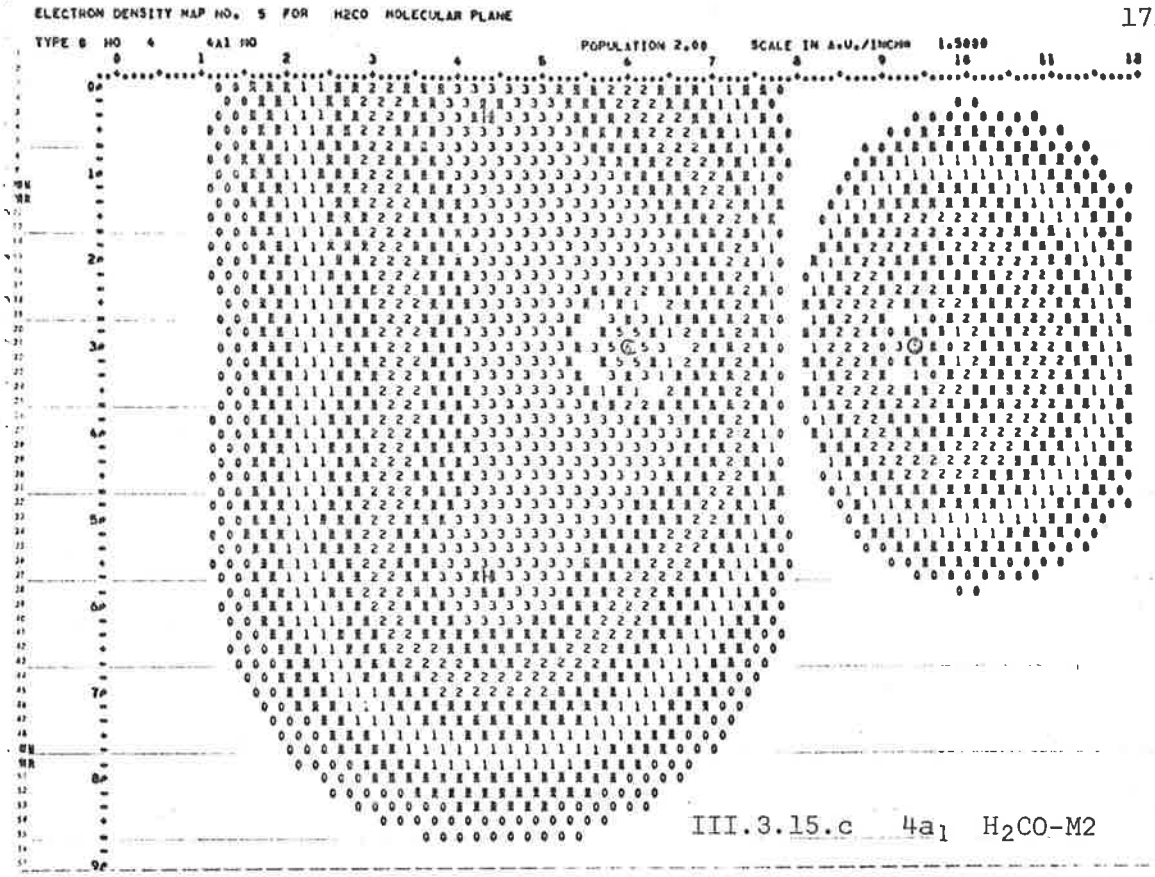

III.3.15.c $4a_1$ H_2CO-M2

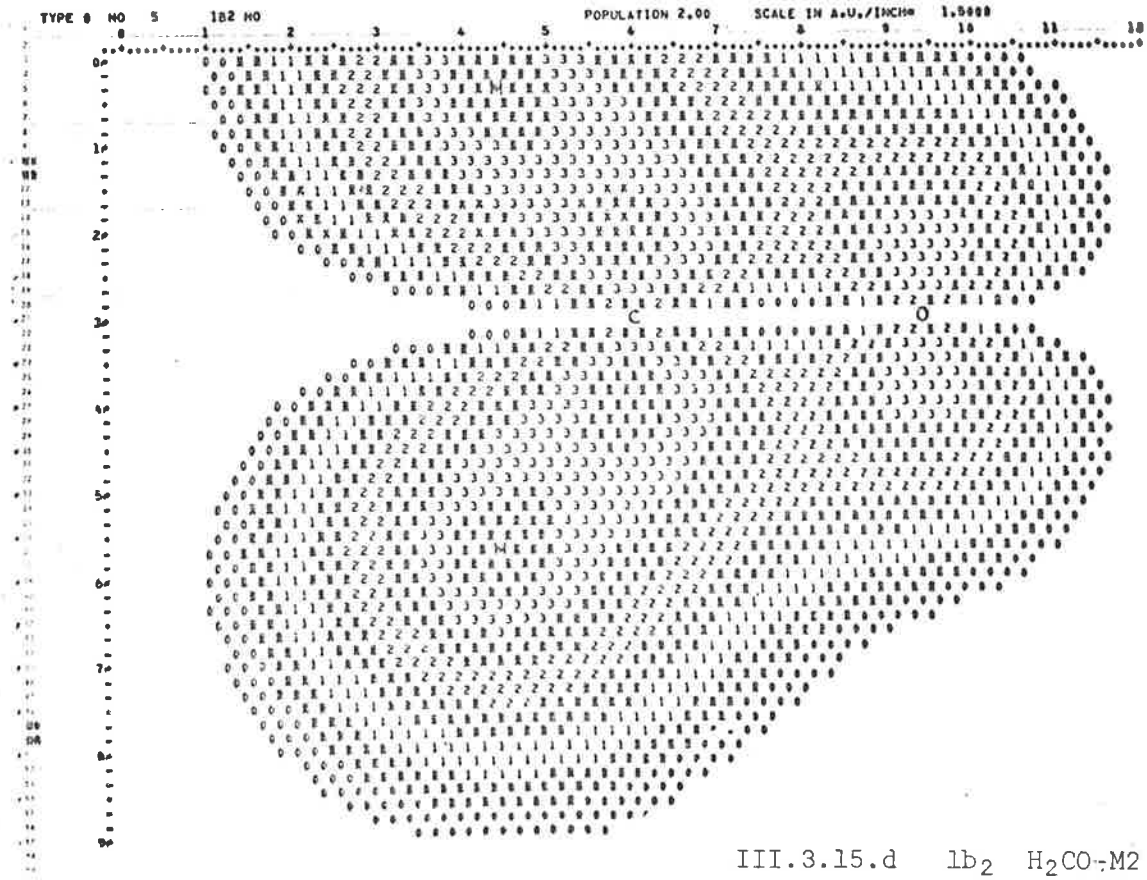

III.3.15.d $1b_2$ H_2CO-M2

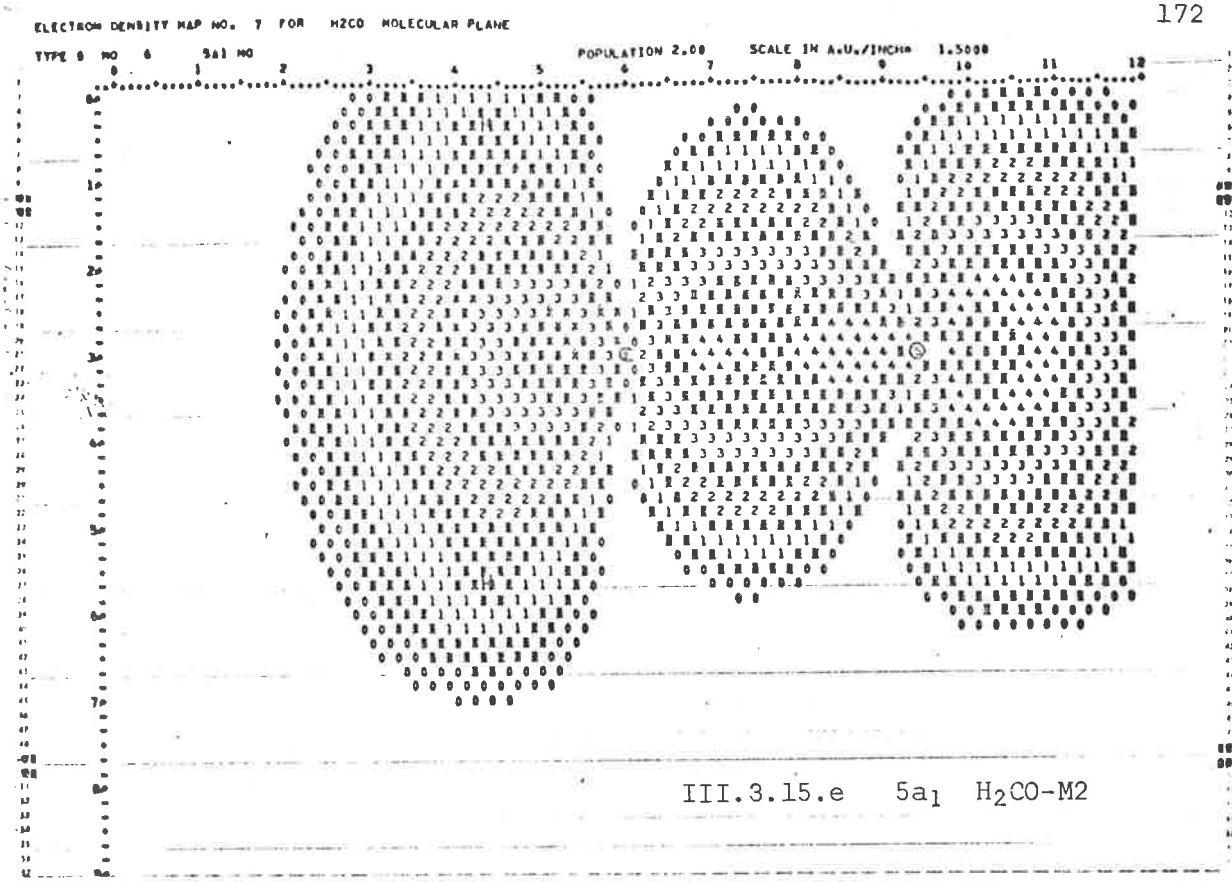

III.3.15.e $5a_1$ H_2CO-M2

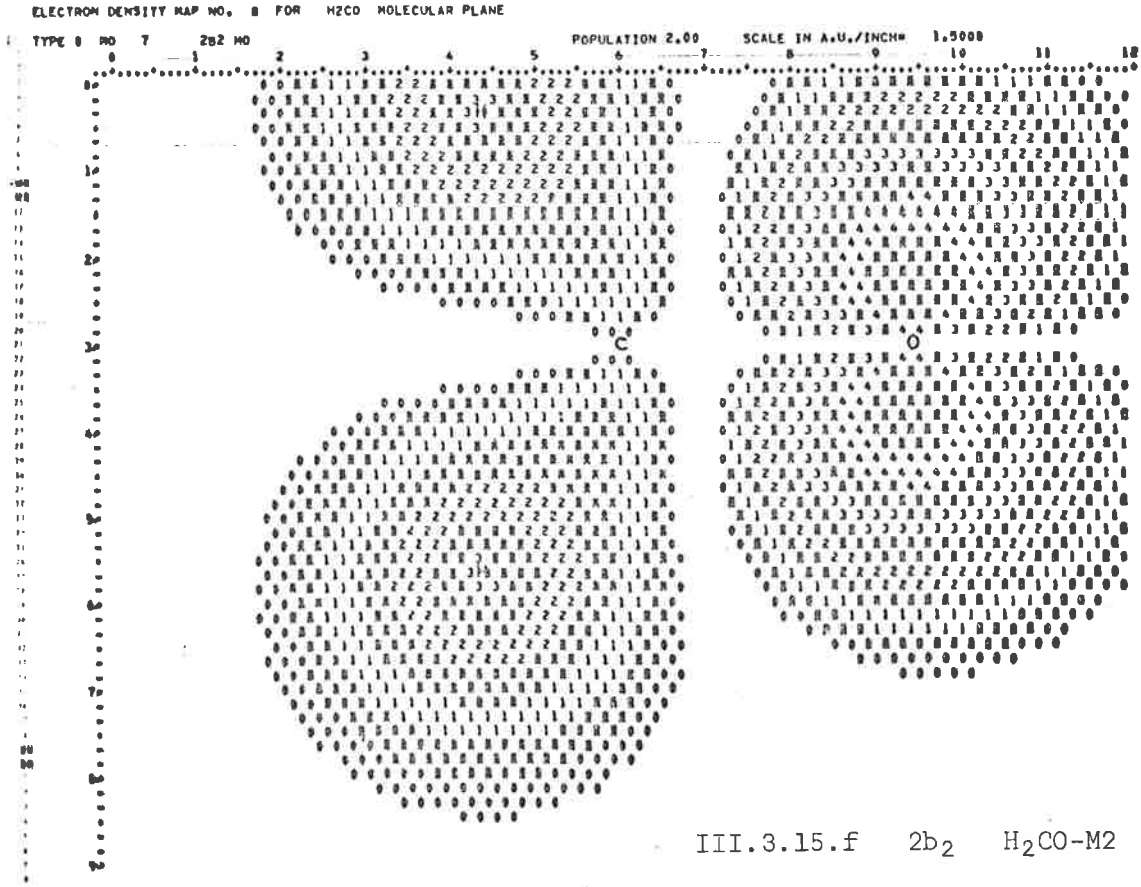

III.3.15.f $2b_2$ H_2CO-M2

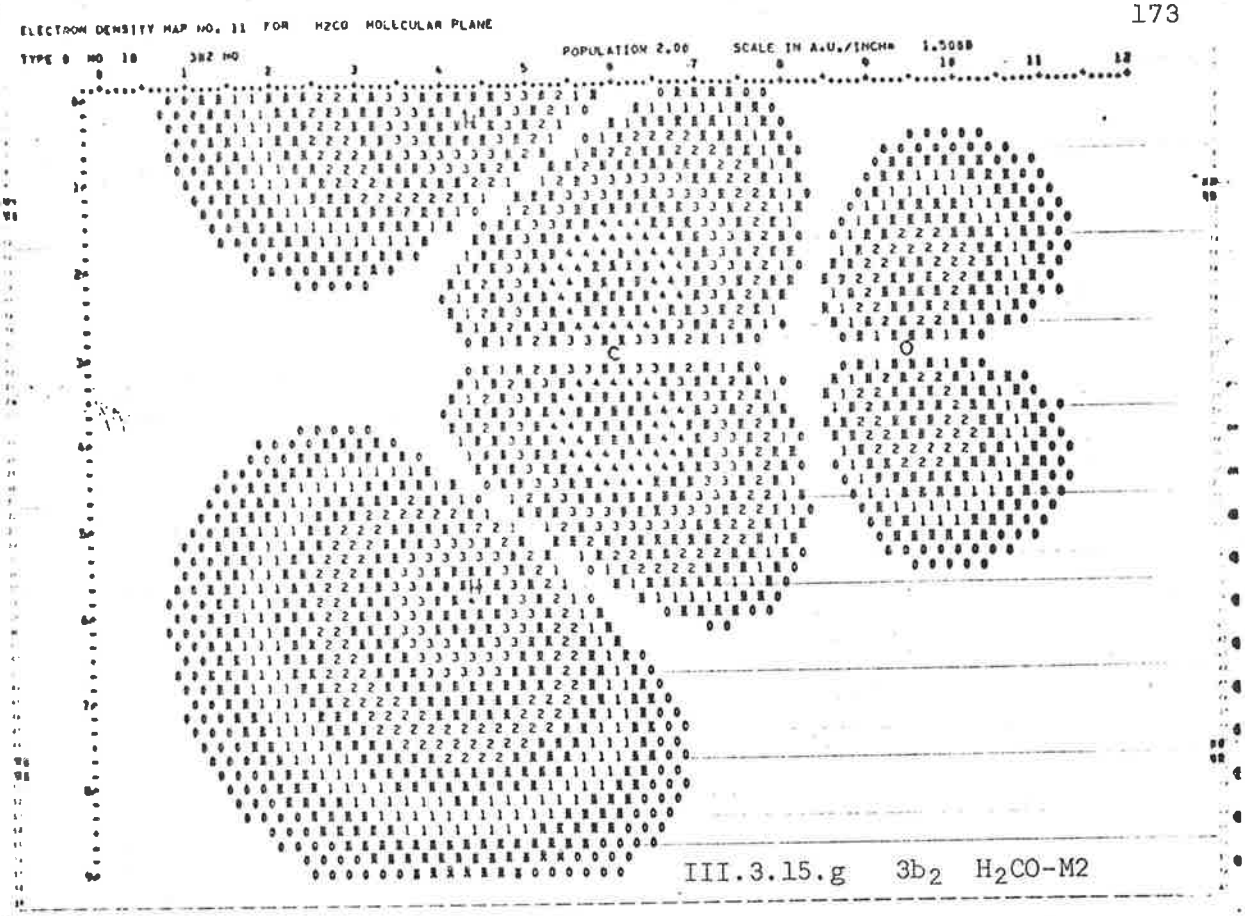

III.3.15.g $3b_2$ H_2CO-M2

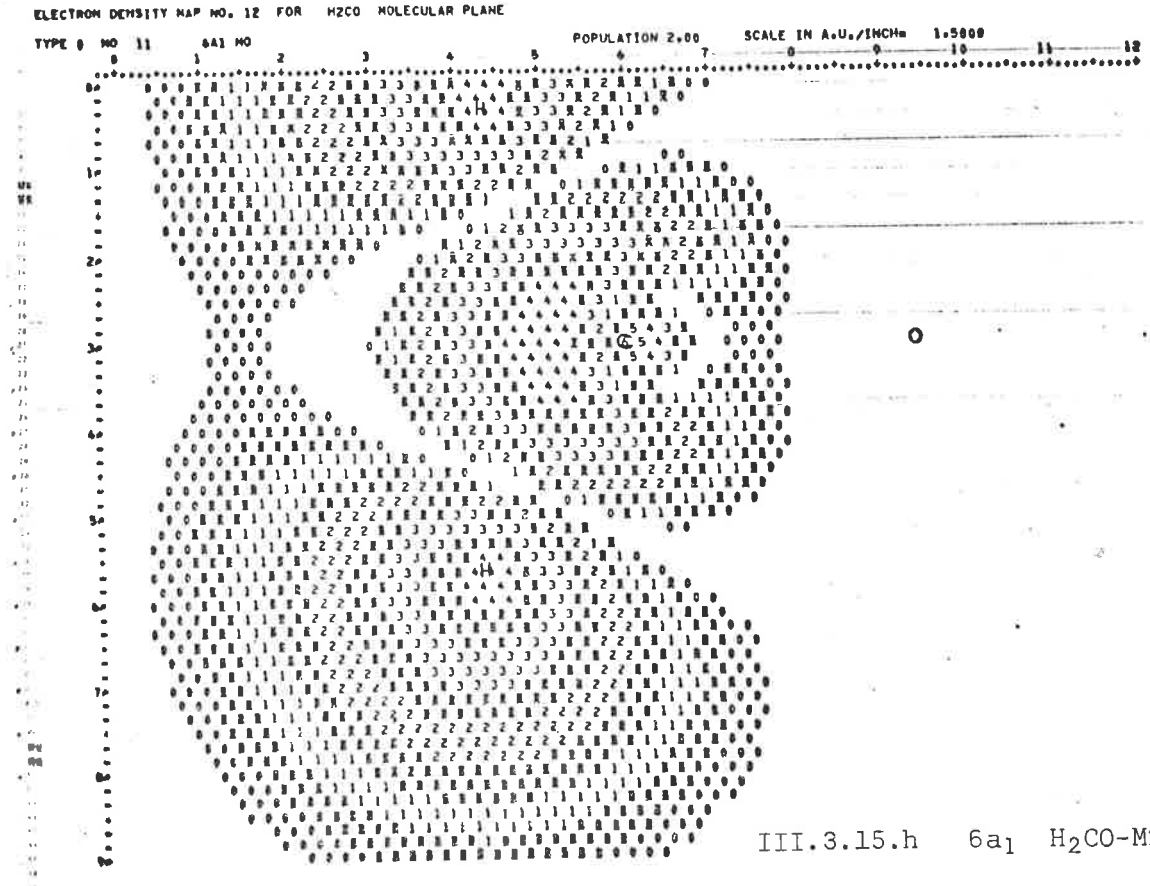

III.3.15.h $6a_1$ H_2CO-M2

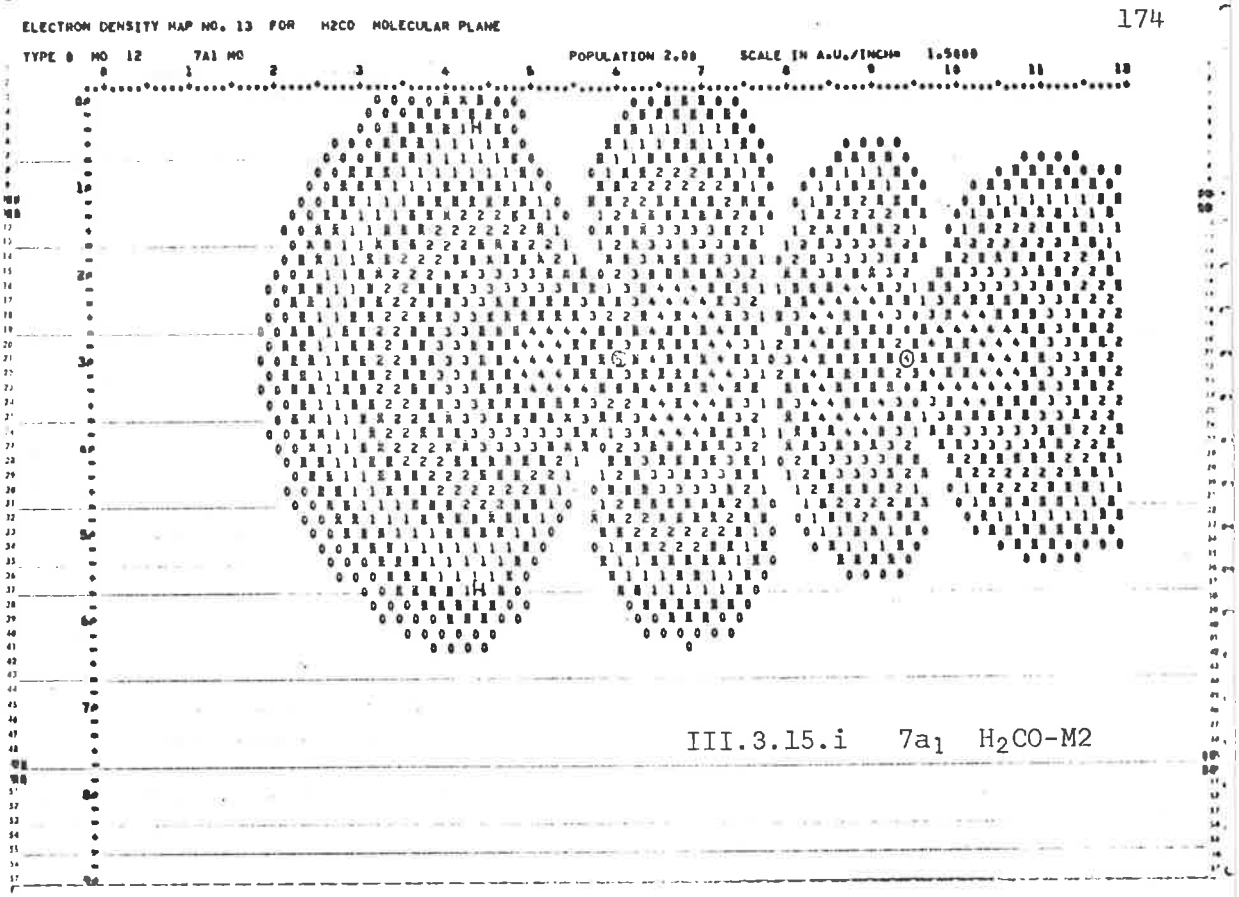

III.3.15.i $7a_1$ H_2CO-M2

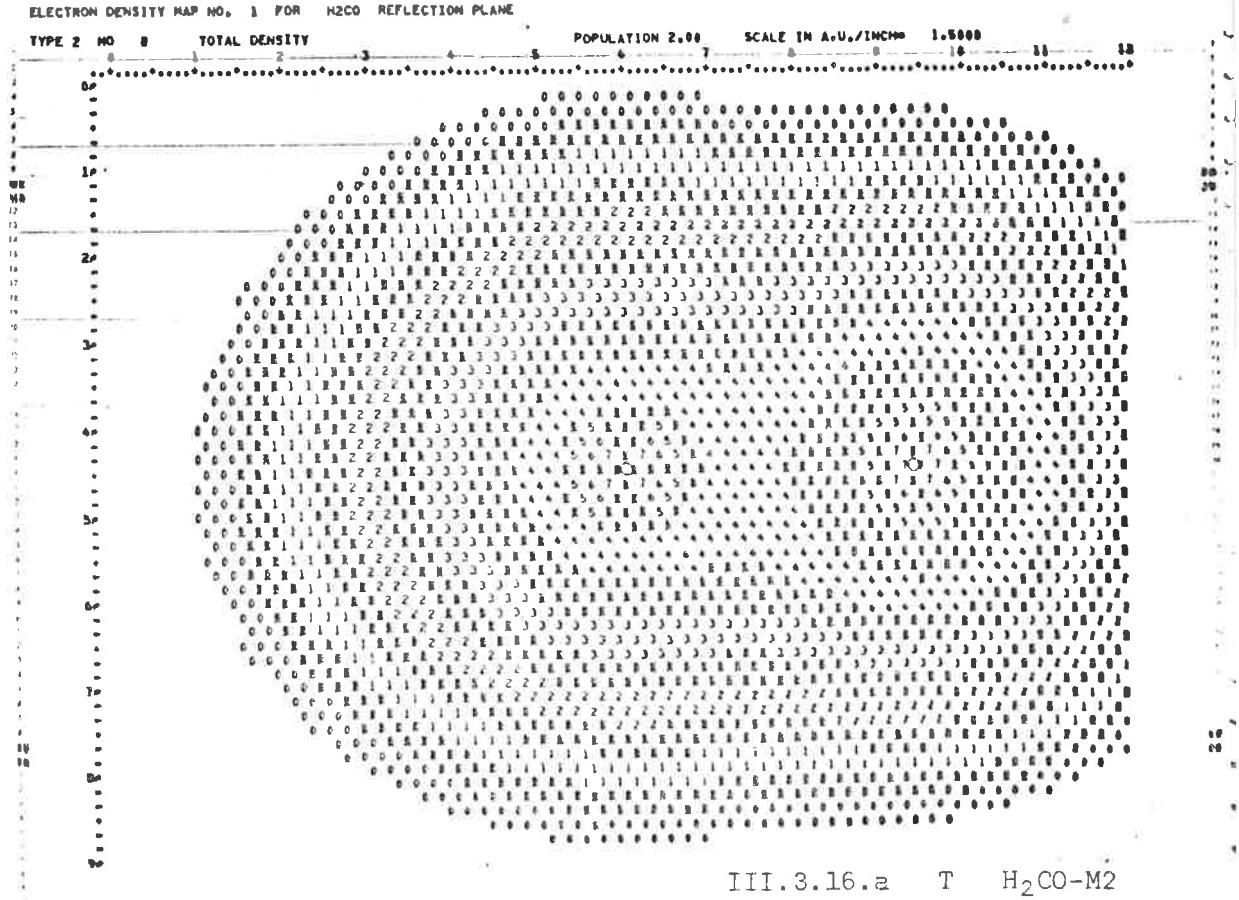

III.3.16.a T H_2CO-M2

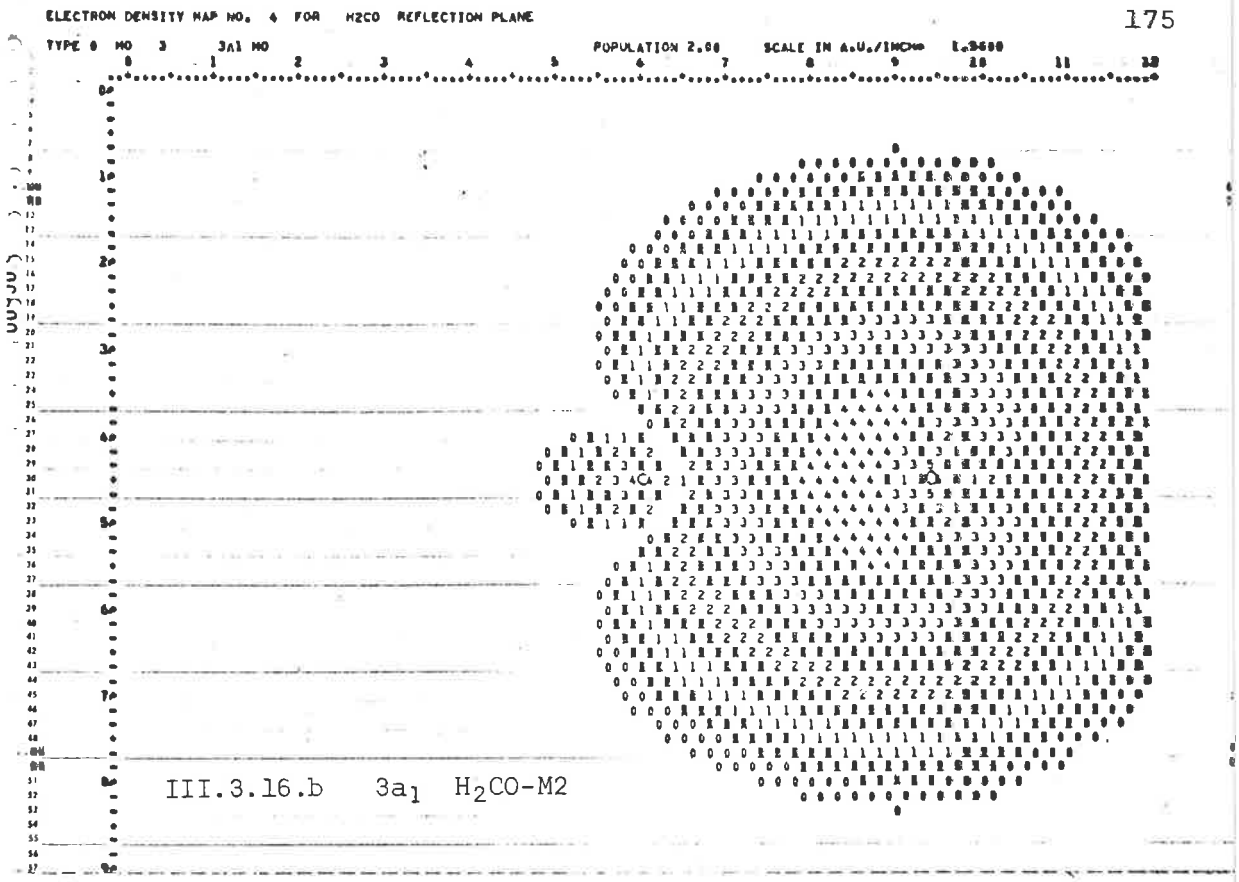

III.3.16.b $3a_1$ H_2CO-M2

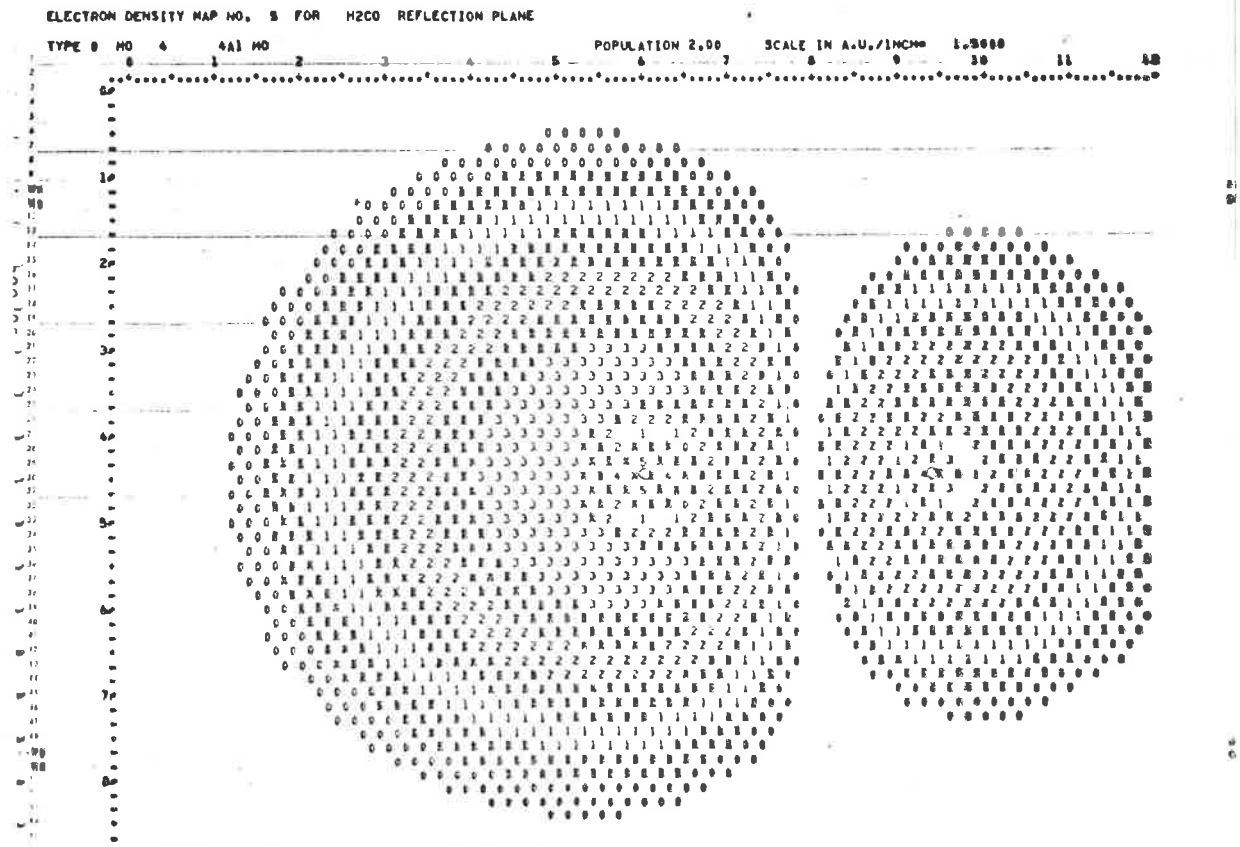

III.3.16.c $4a_1$ H_2CO-M2

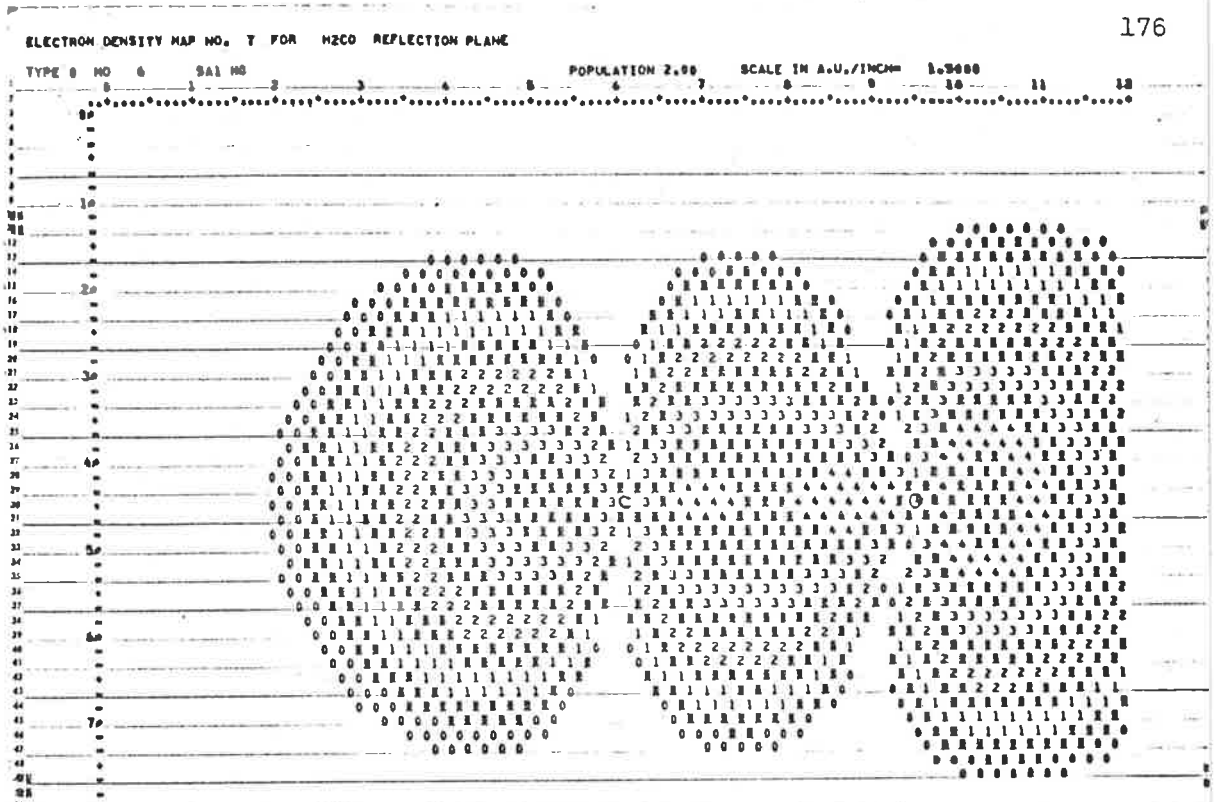

III.3.16.d $5a_1$ H_2CO-M2

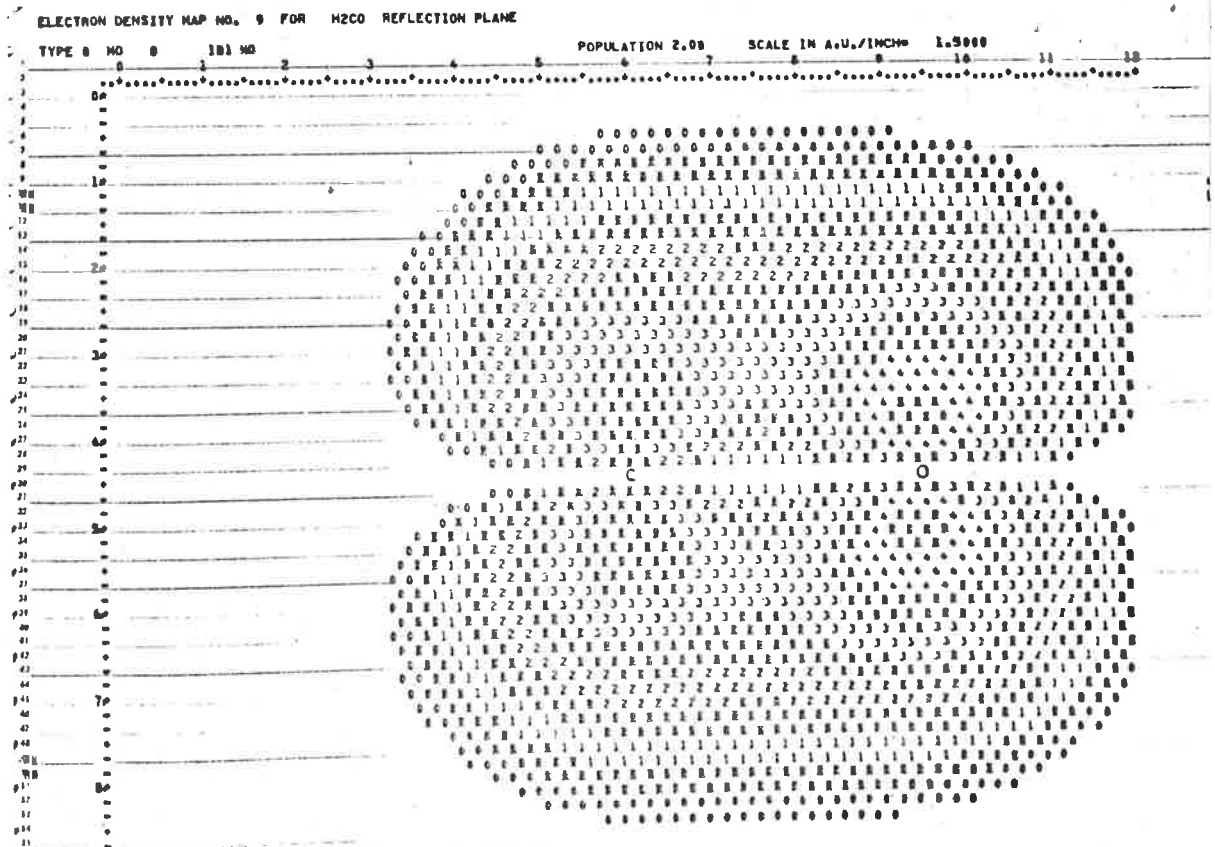

III.3.16.e $1b_1$ H_2CO-M2

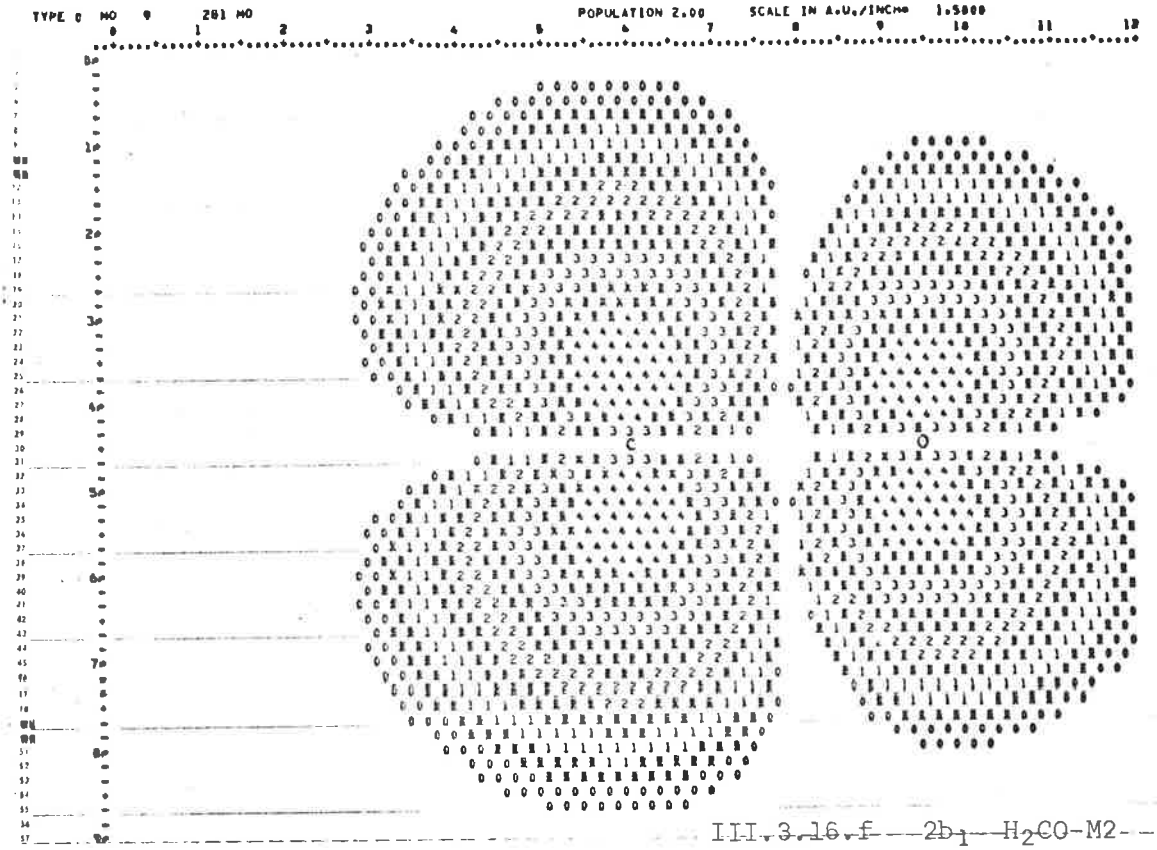

III.3.16.f ~~2b$_1$~~ H_2CO-M2

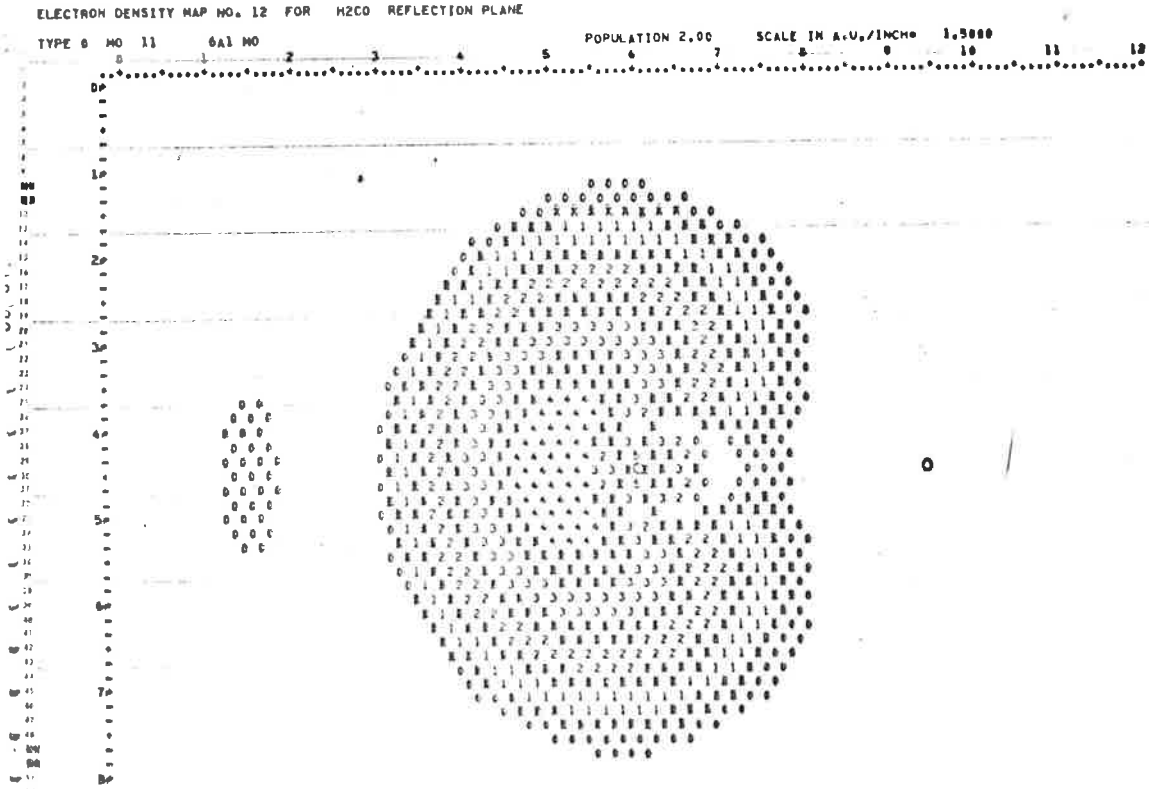

III.3.16.g $6a_1$ H_2CO-M2

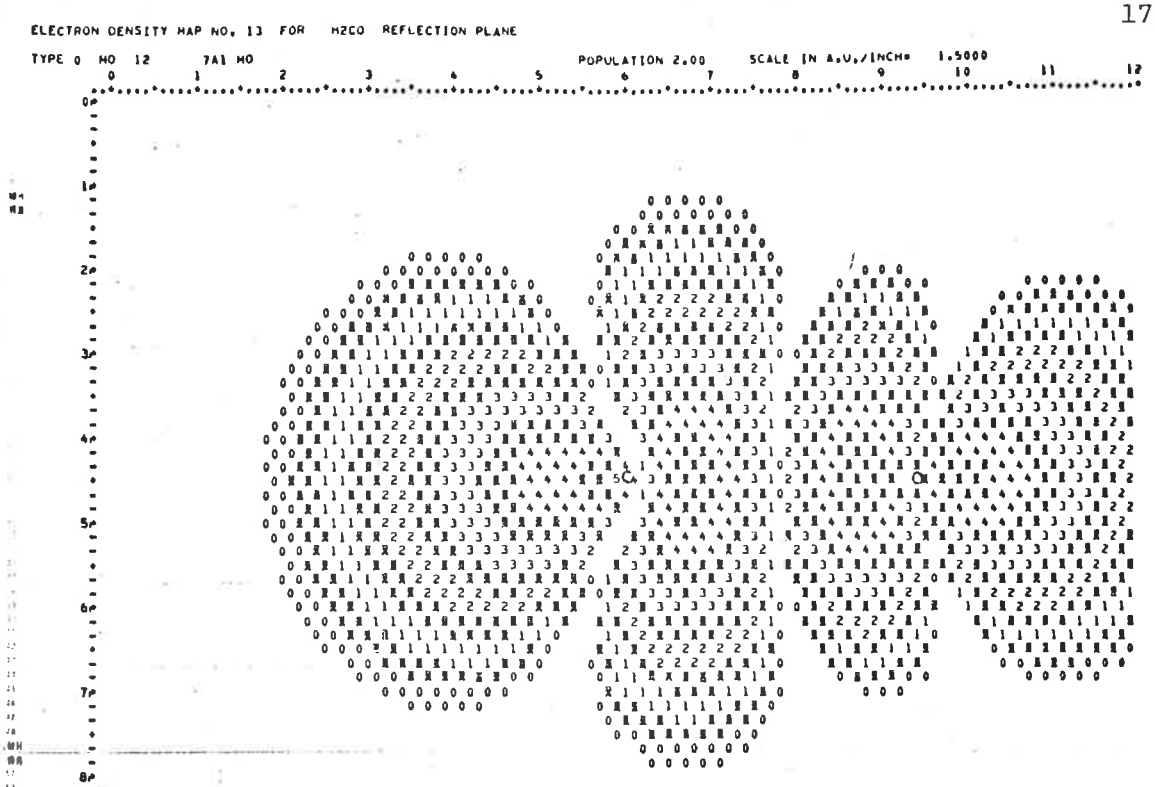

III.3.16.h $7a_1$ H_2CO-M2

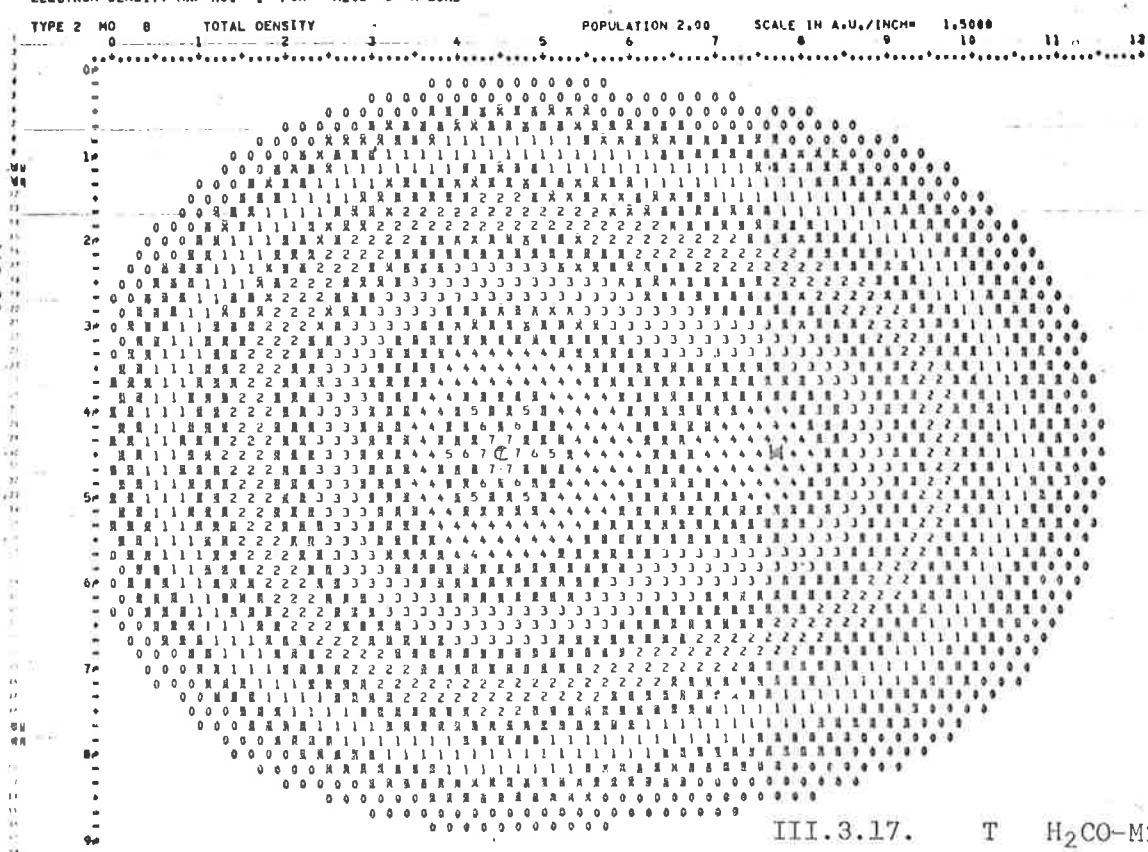

III.3.17. T H_2CO-M2

the π-bond, by symmetry, is composed of 2py orbitals. Presumably, O2s remains essentially non-bonding, while the 2px orbital on oxygen forms the traditional lone pair. As for the C-H bond, it would appear that the C2s and C2px orbitals admix to what is essentially an sp-hybrid, since the total p-content of the C-H bond index evaluates at 52%. While traditional valence theory can say little about finer details at the oxygen atom, it is generally held that C-H and C-O σ-bonds are of sp^2 character in keeping with the molecular geometry, and, therefore, in conflict with our bond index predictions. It is to be noted that there is no evidence in the density maps for the bent bonds one would associate with sp hybridisation.

Charge centroids for the M2 and *ab initio* [95/3] wavefunctions are listed in Table III.3.12.c. Orbitals $1a_1$ and $2a_1$ are obviously inner sehlls on oxygen and carbon. In the next higher orbital, $3a_1$, the charge centroid is located 0.8 au from the C atom towards H, in the M2 wavefunction, and at twice that distance, 1.63 au, by the *ab initio* results. It is evident in the corresponding density maps (Figs. III.3.15.b, III.3.16.b) that the O2s orbital is the main contributor, with only minor amounts entering from C and H orbitals.

By contrast, centroids for the $4a_1$ MC are not significantly different between the two wavefunctions, and both indicate a polarisation towards H(M2 = 0.29 au, [95/3] = 0.10 au). High contributions from Hls and C2s orbitals are responsible for the greater charge density in that region of the distribution maps (Fig. III.3.15c,

Table III.3.12.a. One-electron Expectation Values, H_2CO - θ_{xx}, θ_{yy}, θ_{zz}

	M2			[95/3]		
MO	θ_{xx}	θ_{yy}	θ_{zz}	θ_{xx}	θ_{yy}	θ_{zz}
$1a_1$	0.6515	0.6515	-1.3030	0.6506	0.6506	-1.3012
$2a_1$	0.6523	0.6578	-1.3101	0.6553	0.6553	-1.3106
$3a_1$	0.2328	0.3628	- .5956	0.1993	0.2245	- .4238
$4a_1$	0.5165	2.0587	-2.5752	1.0397	2.1008	-3.1405
$1b_2$	-.7062	2.6456	-1.9394	-.6622	1.7889	-1.1267
$5a_1$	1.2060	1.2877	-2.4937	1.3239	1.6662	-2.9902
$2b_2$	-.0117	1.4455	-1.4338	-.2996	2.1973	-1.8976
$1b_1$	0.8995	-.0632	-.8363	1.0857	-.5554	- .5303
Electronic	6.8814	18.0927	-24.9741	7.9853	17.4565	-25.4418
Nuclear	-7.5579	-17.4308	24.9887	-7.5579	-17.4308	24.9887
Nett	- .6766	0.6619	0.0146	0.4274	0.0257	-.4531

Table III.3.12.b. One-electron Expectation Values, H_2CO - $\langle x^2 \rangle$, $\langle y^2 \rangle$, $\langle z^2 \rangle$

	M2			[95/3]		
MO	$\langle x^2 \rangle$	$\langle y^2 \rangle$	$\langle z^2 \rangle$	$\langle x^2 \rangle$	$\langle y^2 \rangle$	z
$1a_1$	0.0174	0.0174	1.3203	0.0177	0.0177	1.3190
$2a_1$	0.0360	0.0324	1.3443	0.0325	0.0325	1.3431
$3a_1$	0.6384	0.5518	1.1907	0.5283	0.5115	0.9438
$4a_1$	1.7136	0.6855	3.7748	1.4190	0.7116	4.2057
$1b_2$	2.7504	0.5158	3.5725	2.1794	0.5453	2.4890
$5a_1$	0.3881	0.3336	2.8546	0.6737	0.4455	3.5497
$2b_2$	1.2807	0.3092	2.2287	2.1452	0.4807	3.2106
$1b_1$	0.3209	0.9627	1.4780	0.5470	1.6411	1.6244
Electronic	14.2909	6.8166	35.5279	15.0858	8.7717	37.3706

Table III.3.12.c. One-electron Expectation Values, H_2CO - $\langle r^2 \rangle$, $\langle z_c \rangle$

	M2		|95/3|	
MO	$\langle r^2 \rangle$	$\langle z_c \rangle$	$\langle r^2 \rangle$	$\langle z_c \rangle$
$1a_1$	1.3551	-2.2865	1.3544	-2.2858
$2a_1$	1.4126	- .0003	1.4082	-.0003
$3a_1$	2.3809	- .8108	1.9836	-1.6325
$4a_1$	6.1738	0.2911	6.3362	0.1039
$1b_2$	6.8388	- .2585	5.2137	- .4500
$5a_1$	3.5763	-1.7446	4.6689	-1.7584
$2b_2$	3.8186	-1.7821	5.8365	-1.1274
$1b_1$	2.7616	-1.4439	3.8125	-1.5015
Electronic	56.6354	-17.0373	61.2280	-17.3039
Nuclear		16.1111		16.1111
Nett		- .9261		-1.1928

Table III.3.12.d. One-electron Expectation Values, H_2CO - $\langle r_c^{-1} \rangle$, $\langle r_o^{-1} \rangle$, $\langle r_H^{-1} \rangle$

	M2			|95/3|		
MO	$\langle r_c^{-1} \rangle$	$\langle r_o^{-1} \rangle$	$\langle r_H^{-1} \rangle$	$\langle r_c^{-1} \rangle$	$\langle r_o^{-1} \rangle$	$\langle r_H^{-1} \rangle$
1a	- .4374	-7.6387	- .2609	- .4375	-7.6400	- .2609
2a	-5.6691	- .4375	- .4726	-5.6589	- .4375	- .4725
3a	- .5475	-1.1322	- .2976	- .6264	-1.0923	- .3098
4a	- .8570	- .4371	- .5544	- .6996	- .4828	- .5303
1b	- .6055	- .4510	- .6130	- .6036	- .5652	- .4912
5a	- .6033	- .9200	- .3230	- .5255	- .9025	- .3318
2b	- .4218	-1.0548	- .3380	- .4419	- .8082	- .4173
1b	- .6273	- .8745	- .3200	- .5320	- .8017	- .3039
Electronic	-19.5379	-25.8199	-6.3589	-19.0508	-25.4604	-6.2353
Nuclear	4.4440	3.1460	5.1978	4.4440	3.1460	5.1978
Total	-15.0939	-22.6739	-1.1611	-14.6069	-22.3144	-1.0375

III.3.16.c.). Again, both wavefunctions produce remarkably similar $\langle z_C \rangle$ expectation values in the $5a_1$ orbital, in this case located well past the mid-point of the C-O bond towards oxygen. The mapped distributions Figs. III.3.15.e and III.3.16.d are close to a classic cylindrical pz-pz overlap, with only minor distortion around the hydrogen nuclei, in accord with atomic orbital coefficients in that MO. In nett effects for all orbitals of a_1 symmetry, the M2 wavefunction is less polarised towards oxygen than is the Gaussian set; relevant values are -4.55 au, and -5.57 au, respectively.

Charge centroids in the $1b_2$ orbital are not greatly dissimilar, with expectation values -·258 au for the M2 wavefunction, and -·450 in the Gaussian basis as an indication of a small polarisation towards the oxygen nucleus. However, the M2 centroid in the $2b_2$ MO is obviously compensating for the lower nett polarisation in the a_1 orbitals, for the value of -1·782 au is well towards oxygen and far in excess of the [95/3] centroid, at -1.127 au. It is apparent from the form of the wavefunction that the 02px orbital is primarily responsible for this polarisation, and, in this aspect, the density map of Fig. III.3.15.f shows quite clearly the concentration of charge around the oxygen centre (note that the extensive distribution around the hydrogen atoms is very diffuse).

Charge distribution in the $1b_1$ orbital (Fig. III.3.16.e) is very much the classic π-type, with a surfeit of density surrounding oxygen. It is therefore not surprising to find the centroid located

at -1.444 au, past the C-O midpoint, in good agreement with the [1062/42] result, -1.502 au.

From dipole moments, we turn to second moments as a measure of electron distribution along axes in the plane normal to the molecular C_2 rotation axis. It is evident from the nett values in Table III.12.b that the *ab initio* wavefunction entails a distribution more diffuse than is the case with our M2 calculations. The difference is most obvious in extension above the molecular plane where $\langle y^2 \rangle$ expectation values are 8.77 and 6.82 au, respectively, and decreases only slightly for $\langle x^2 \rangle$, 15.09 *vs* 14.29 au.

Individual MO's are less consistent in their behaviour, for the M2 distribution is the more diffuse throughout the $3a_1$ orbital. Both of the $4a_1$ and $1b_2$ orbitals show variable behaviour; the M2 wavefunction exhibits greater lateral extension in the $4a_1$ MO ($\langle x^2 \rangle$ = 1.714 au *vs* 1.419 au) and again in the $1b_2$ MO ($\langle x^2 \rangle$ = 2.750 au *vs* 2.179), where it is also expanded along the C_2 axis ($\langle z^2 \rangle$ = 3.572 au *vs* 2.489 au). Elsewhere, the [1062/42] wavefunction is the more diffuse of the two. In particular, the M2 representation of the $1b_1$ orbital is very much contracted from expectation values recorded for the *ab initio* function. Whereas the M2 value for $\langle y^2 \rangle$, 0.963 au, is in excess of all other individual contributions (the next greatest is 0.686 au in $4a_1$), it represents only $^1/_7$ of the nett value, 6.817 au. In comparison, the *ab initio* value for $\langle y^2 \rangle$ is 1.641 au, more than twice the highest remaining contribution, and $^3/_8$ of the overall

electronic contributions. McKoy et al [73] have taken their comparative figures as an indication that the π-electrons($1b_1$ MO) are rather deeply embedded in the σ-density, and our results certainly do nothing to disprove their contention, as witness the electron density maps of Fig. III.3.16, where the vertical extent of the $1b_1$ MO may be gauged with respect to orbitals of a_1 symmetry. This relative contraction in the π-orbital for the M2 function, and indeed, the overall contraction from *ab initio* values, very probably stems from the high valence orbital exponents on the carbon atom. At 2.025 and 2.035, respectively, for the 02s and 02p orbitals, the optimised exponents are considerably removed from the Slater value at 1.625.

Agreement between M2 and [95/3] expectation values for the potential operators (Table III.12.d) is generally quite reasonable, with nett values in the M2 set slightly greater in magnitude. Since our calculated σ^d_{av} (H) is known to be too high with optimised exponents, the excessive value for $\langle r_H^{-1} \rangle$ is not surprising.

In the overall analysis of the formaldehyde results, one cannot discount that the optimisation process was successful. It is true that calculated average diamagnetic shielding did not optimise correctly, but, as we have pointed out, there is potential for improvement in adjustment of the Hls orbital exponent. In the finer analysis, incorrect ordering of energy levels must be held as a failing, and, although it has no bearing on the one-electron properties

as such, it does detract from the success which was achieved in this respect with the H_2O and NH_3 calculations. About the high values for carbon valence orbital exponents we are unsure. Undoubtedly, the contraction in overall charge distribution stems from those parameters, but with uncertainty surrounding the experimental bulk magnetic susceptibility value, we have no means of working back to absolute second moments values.

It is apparent that the optimised wavefunction bears only a superficial resemblance to the *ab initio* Gaussian set of McKoy et al [73] in its one-electron property expectation values. Following our experience with H_2O optimised wavefunctions, we could expect little else.

In furtherance of our formaldehyde calculations, we have used the optimised wavefunctions as basis for configuration interaction at various levels of excitation. The aim here was two-fold, partly to examine the extent of energy improvement by admixture of the ground state with di-excited configurations, and partly to introduce, however sketchily, one aspect of our work* which difficulties encountered in the optimisation process prevented us from exploring more completely.

---

* In fact the early aims of this project envisaged investigation of excited state properties via configuration interaction on exponent optimised wavefunctions. In this context the SNE method was viewed as little more than a vehicle to provide the required "zeroth level" wavefunctions.

Although CI calculations were performed with all nine of the exponent optimised wavefunctions for formaldehyde, the results were sufficiently alike to warrant examination of just one representative example, and we have chosen the first of those in Table III.2.8.

Energies and oscillator strengths for the few lowest singlet excited states in each symmetry class are listed in Table III.3.13. Column headings CI-1, CI-2 and CI-3 refer to the highest level of excitation allowed in each calculation. In the CI-1 set, only configurations resulting from single electron promotions were included. Di-excitations were added for the CI-2 set, and these included configurations in which the defining Slater determinants contain 0, 2 or 4 unpaired spin orbitals. This last restriction was maintained for the CI-3 series, where tri-excitation configurations were further added i.e. configurations involving 6 unpaired spin orbitals were not permitted.

Since our CI program was not sufficiently sophisticated to factorise by symmetry, the complete configuration list was energy sequenced and terminated at a maximum 125, from which the CI matrix was blocked out [83] and diagonalised. As a consequence of truncation, only a few of the triexcited configurations, and not all of the diexciteds, were sufficiently low in energy to qualify for inclusion in the CI matrix, and our CI-3 results, in particular, are probably not truly representative of the full effects arising from inclusion of higher excitations.

Table III.3.13. Configuration Interaction in Formaldehyde (a,b)

C.I. Level State	None (d)	CI - 1	CI - 2	CI - 3	Expt. (c)
$^1A_1$	ref.(2.39)	ref.(2.39)	-.146 au, ref.(1.58)	-.146 au, ref.(1.65)	ref. (2.39)
$^1A_1$	10.59	6.75(0.13)	7.64 ($\sim 10^{-4}$)	7.54 (4×10^{-4})	8.0($\sim$ 0.1)
$^1A_1$	11.27(di-)	-	10.43 (0.06)	10.54 (0.04)	$\sim$ 10($^1B_2$?)
$^1A_1$	12.69	12.61(0.13)	13.52 (0.001)	13.54 (0.003)	
$^1A_2$	2.68	2.84(o)	1.89(o)	1.89(o)	4.3($\sim 10^{-4}$)
$^1A_2$	8.88	8.84(o)	9.15(o)	9.14(o)	
$^1A_2$	9.20	9.43(o)	11.38(o)	11.38(o)	
$^1B_1$	5.93	5.65(0.003)	7.66 (0.008)	7.65 (0.008)	7.1(0.02)
$^1B_1$	13.01	13.33(0.013)	14.03 (0.021)	14.02 (0.021)	
$^1B_2$	14.02(di-)		13.89 (0.046)	13.83 (0.034)	$\sim$ 10($^1B_2$?)
$^1B_2$	14.20	13.75(0.09)	14.13 (0.013)	14.18 (0.023)	

(a) Values in eV, unless otherwise stated.

(b) ref. = reference ground state (dipole moment in Debyes), otherwise excitation energy (oscillator strength).

(c) Refs. 65 - 72.

(d) Entry di- indicates di-excited configuration.

Energy stabilisation afforded by inclusion of higher excited configurations amounts to 0.146 au, (~4eV), not a great improvement when compared to the 0.895 au destabilisation of the M2 ground state relative to the *ab initio* calculated energy. Moreover, the dipole moment drops from the optimised value of 2.39D to 1.65D (CI-3) or 1.58 (CI-2), indicative of substantial electronic re-arrangement which will undoubtedly have a deleterious effect on expectation values for other one-electron properties.

On the other hand, it is gratifying to note that excitation energies are in reasonable accord with experimental spectral assignments, although our oscillator strengths are generally too low.

The low energy calculated for the $^1A_2$ state (1.89 eV, c.f. expt. 4.3 eV) is amiss, but both the $^1B_1$ value of 7.65 eV, and $^1A_1$ at 7.54 eV are in very good agreement with the observed energies, 7.1 and 8.0 eV, respectively. Either of our calculated values, 13.83 eV for the lowest $^1B_2$ level, or 10.54 eV for the second $^1A_1$ excitation, correlate reasonably with the band at ~10eV, tentatively labelled $^1B_2$.

In contrast, energy levels in the CI-1 set are worse in their energy agreement, but better in oscillator strengths; it is apparent that the very large reductions in oscillator strengths in passing from CI-1 to CI-2 or -3 constitute an undesirable feature. The low values achieved by some di-excited levels, both before and after configuration interaction are of interest. In particular, the lowest $^1B_2$ configuration is in this categroy, and forms the major contributor

to the lowest $^1B_2$ state in the CI-2 and CI-3 calculations. Obviously, the optimised wavefunctions are not particularly stable to configuration interaction, for, while some energy improvement is experienced, it would appear that one-electron properties suffer considerably.

We must therefore leave the fate of our Simulated Non-Empirical scheme undecided. While the method itself is theoretically sound in its approximations and rotational invariance behaviour, it is obvious that the Ruedenberg expansion, whether applied solely to electron repulsion integrals, as in Version 2, or as well to nuclear attraction integrals (Version 1), introduces perturbations of considerable magnitude. Despite a searching analysis of optimised one-electron properties, calculated by the SNE method in its various forms, there appears to be no consistent relationship among these forms, nor, individually to *ab initio* wavefunctions.

Most of our observations on the complexities associated with exponent optimisation to one-electron properties we expect will be equally applicable to *ab initio* wavefunctions. It will be interesting to see if those expectations are fulfilled.

APPENDIX

A.1. EXTENSION OF FRAGA'S TABLES TO REAL ORBITALS

Table A.1.1. contains values of the ϕ-dependent part, $F(\phi)$, of the one-electron integral $\langle X_a|P|X_b\rangle$ in which the operator dependence is expressed as $f(\phi)$. The convention adopted for real orbitals is as below,

σ = s, p_z, d_{z^2}

π = p_x, d_{x^2} $\qquad$ $\bar{\pi}$ = p_y, d_{yz}

δ = $d_{x^2-y^2}$ $\qquad$ $\bar{\delta}$ = d_{xy}

For the original tabulation of complex orbitals, see ref. 45.

Table A.1.1. Table of $F(\phi)$

$X_a . X_b$ \ $f(\phi)$	1	$\cos\phi$	$\sin\phi$	$\cos^2\phi$	$\sin^2\phi$	$\sin\phi\cos\phi$
$\sigma\ \sigma$	+ 2	-	-	1	1	-
$\sigma\ \pi$	-	$+\sqrt{2}$	-	-	-	-
$\sigma\ \bar{\pi}$	-	-	$+\sqrt{2}$	-	-	-
$\sigma\ \delta$	-	-	-	$+1/\sqrt{2}$	$-1/\sqrt{2}$	-
$\sigma\ \bar{\delta}$	-	-	-	-		$+1/\sqrt{2}$
$\pi\ \pi$	+ 2	-	-	+3/2	+1/2	-
$\pi\ \bar{\pi}$	-	-	-	-	-	+1/2
$\pi\ \delta$	-	+ 1	-	-	-	-
$\pi\ \bar{\delta}$	-	-	+ 1	-	-	-
$\bar{\pi}\ \bar{\pi}$	+ 2	-	-	+1/2	+3/2	-
$\bar{\pi}\ \delta$	-	-	- 1	-	-	-
$\bar{\pi}\ \bar{\delta}$	-	+ 1	-	-	-	-
$\delta\ \delta$	+ 2	-	-	+ 1	+ 1	-
$\delta\ \bar{\delta}$	-	-	-	-	-	-
$\bar{\delta}\ \bar{\delta}$	+ 2	-	-	+ 1	+ 1	-

A.2. COMPUTER PROGRAMS

All wavefunctions were generated with the program system, SNEAZ (Simulated Non-Empirical, Adjustable Zeta), certain features of which have already been described in Chapter II. SNEAZ is a composite FORTRAN/COMPASS deck comprising some 15,000 statements, and sectioned into 18 overlays. Program arrangement and functionality is as below.

OVERLAY (0,0) - Sequencing of primary overlay execution

OVERLAY (1,0) - Data set input, also job termination

OVERLAY (2,0) - Sequencing of secondary overlay execution - in the main, ground state calculations, but some preparitive transformations for excited state studies.

OVERLAY (2,1) - All one-electron Hamiltonian integrals, including overlap, from initial diatomic axes evaluation through to Löwdin orthonormal basis.

OVERLAY (2,2) - Coulomb repulsion integrals in STO basis, molecular axis system.

OVERLAY (2,3) - Transformation of Coulomb repulsion integrals to Löwdin orthonormal basis.

OVERLAY (2,4) - Iterative self-consistent-field convergence procedure.

OVERLAY (2,5) - Generates two-electron integrals over MO's, ready for configuration interaction.

OVERLAY (2,6) - Using the Ruedenberg approximation for 2-centre dipole length integrals, dipole moment is evaluated, and moment integrals over MO's are generated ready for C.I.

OVERLAY (2,7) - As for (2,6), all atomic integrals evaluated exactly. (2,6) was not used in any of the calculations reported in the text.

OVERLAY (3,0) - Sets up singlet configurations to the requested excitation level, energy sequenced.

OVERLAY (4,0) - Blocks out the truncated (if necessary) CI-matrix.

OVERLAY (5,0) - Diagonalises the CI-matrix above, and produces Löwdin orbital populations for the CI ground and excited states.

OVERLAY (6,0) - Evaluates new dipole moment for ground state, plus transition moments to excited states.

OVERLAYS (7,0) to (10,0) - As for (3,0) to (6,0) above, for triplet states.

Apart from QCPE 61, GIVENS subroutine, all programs and routines in SNEAZ were written as part of this project. The matrix

diagonalisation routine, EVQR, is our recoded version of QRDIAG, kindly supplied by F.R. Burden, Monash University, and the integral evaluation routines package, QCPE 131, is a generalised adaption of OVERLAYS (2,1) and (2,2).

Various options on printout, restarting and convergence accuracy, make SNEAZ a flexible, yet extremely fast, program system. Other options include integral scaling, adjustment of orbital exponent values to allow for inner-shell contributions, or simply for exponent variation, recycling to recalculate integrals during the self-consistent procedure (Variable Electronegativity), and multiple configuration interaction passes. By this last option, the user may elect to sequentially add firstly di-excited configurations, and subsequently tri-excited, to an originally mono-excitation configuration interaction calculation. Binary magnetic tape output is in a readily accessible form suitable for use with either of the companion programs, MOMENT and DMAP.

All one-electron properties recorded in Chapter III were generated via program MOMENT. Input preparation is minimal, consisting essentially of binary record sequences whereby essential data may be located on the SNEAZ output tape. Atomic integrals are evaluated by algorithms adapted from QCPE 145 [52], and output is in the form of individual MO, nett electronic and nuclear contributions to each one-electron property.

Program DMAP produced the printer output density maps of

Chapter III. Again, input is kept to a minimum, and the user is required only to specify 3 points (to define the mapping plane) and rectangular grid dimensions, plus details of the pattern - which MO's are to be mapped, and binary record locations on the SNEAZ output tape. All transformations to the mapping plane are performed automatically, a feature we considered desirable partly to eliminate human error, but mainly because density maps will usually be required in the plane of 3 atoms, or 2 atoms and some other point, and these conveniently define the mapping plane input data.

Contour intervals increase exponentially as 0.001×2^n. This formulation provides well-delineated contours of approximately equal width, a feature necessary for ready visual perception, but not achieved with a simpler linearly incremental relationship. In the form presented, intermediate contours have been overprinted to heighten relief, and the numbering sequence has been restricted to alternate contour regions as described in the text of Chapter III.

BIBLIOGRAPHY

1. Roothaan, C.C.J.: Revs. Mod. Phys., 23, 69 (1951)
2. Cook, D.B., P.C. Hollis, and R. McWeeney: Mol. Phys., 13, 553 (1967)
3. Jug, K.: Theoret. chim. Acta 14, 91 (1969)
4. Goeppart-Mayer, M., and A.L. Sklar: J. Chem. Phys., 6, 645 (1938)
5. Parr, R.G.: "Quantum Theory of Molecular Electronic Structure" (Benjamin, New York, 1964)
6. Clementi, E.: "Tables of Atomic Functions," Special IBM Technical Report, IBM Research Laboratory, San Jose, Calif., (1965)
7. Löwdin, P.O.: J. Chem. Phys., 18, 365 (1950)
8. Fischer-Hjalmars, I.: "Modern Quantum Chemistry", Istanbul Lectures, Part I, 185 (Academic Press, New York, 1965)
9. McWeeny, R.: Proc. R. Soc., A 227, 288 (1953)
10. Roby, K.R.: Ph.D. Thesis, Monash University, Vic., Aust. (1968)
11. Hinze, J., and H.H. Jaffe: J. Chem. Phys., 38, 1834 (1963)
12. Sichel, J.M., and M.A. Whitehead: Theoret. chim. Acta, 7, 32 (1967)
13. Pople, J.A., D.P. Santry, and G.A. Segal: J. Chem. Phys., 43, S129 (1965)
14. Dahl J.P.: Acta chem. Scand., 21, 1244 (1967)
15. Dahl, J.P., and C.J. Ballhavsen: Advances Quantum Chem., 4, 170 (1968)
16. Ruttink, P.J.A.: Theoret. chim. Acta, 6, 83 (1966)
17. Santry, D.P., and G.A. Segal: J. Chem. Phys., 47, 158 (1967)

18. Santry, D.P.: J. Amer. Chem. Soc., 90, 3309 (1968)

19. Edmiston, C., and K. Ruedenberg: Revs. Mod. Phys., 35, 157 (1963)

20. Edmiston C., and K. Ruedenberg; J. Chem. Phys., 43, S 97 (1965)

21. Trindle, C., and O. Sinanoglu: J. Amer. Chem. Soc., 91, 853 (1969)

22. Jug, K: Internat. J. quant. Chem., 35, 241 (1969)

23. Del Bene, J., and H.H. Jaffe: J. Chem. Phys., 48. 1807 (1968)

24. Del Bene, J., and H.H. Jaffe: J. Chem. Phys., 48, 4050 (1968)

25. Del Bene, J., and H.H. Jaffe: J. Chem. Phys., 49, 1221 (1968)

26. Roothaan, C.C.J.: J. Chem. Phys., 19, 1445 (1951)

27. Wiberg, K.: Tetrahedron, 24, 1083 (1968)

28. Pople, J.A., and G.A. Segal: J. Chem. Phys., 43, S176 (1965)

29. Pople, J.A., and G.A. Segal: J. Chem. Phys., 44, 3289 (1966)

30. Segal, G.A.: J. Chem. Phys., 47, 1876 (1967)

31. Wiberg, K.: J. Amer. Chem. Soc., 90, 59 (1968)

32. Brown, R.D., and F.R. Burden: Theoret. chim. Acta, 12, 95 (1968)

33. Giessner-Prettre, C., and A. Pullman: Theoret. chim. Acta, 11, 159 (1968)

34. Stout, E.W., and P. Politzer: Theoret. chim Acta, 12, 379 (1968)

35. Ruedenberg, K.: J. Chem. Phys., 19, 1433 (1951)

36. Mulliken, R.S.: J. chim. Physique, 46, 497 (1949)

37. Pople, J.A., D.L. Beveridge, and P.A. Dobosh: J. Chem. Phys., 47, 2026 (1967)

38. Clementi, E.: Internat. J. quantum Chem., 1, S307 (1967)

39. McLean, A.D., and M. Yoshimine: IBM J. Res. Develop., 12, 206 (1968)

40. Csizmadia, I.G., M.C. Harrison, J.W. Moskowitz, and B.T. Sutcliffe: Theoret. chim. Acta, 6, 191 (1966)

41. Ruedenberg, K., C.C.J. Roothaan and W. Jaunzemis: J. Chem. Phys., 24, 201 (1956)

42. Roothaan, C.C.J.: J. Chem. Phys., 24, 947 (1956)

43. Wahl, A.C., P.E. Cade, and C.C.J. Roothaan: J. Chem. Phys., 41, 2578 (1964)

44. Fraga, S.: Can. J. Chem., 42, 2509 (1964)

45. Fraga, S.: File No. 18-95-393, Depository of Unpublished Data, National Research Council, Canada (1965)

46. Klimenko, N.M., and M.E. Dyatkina: J. Struct. Chem., 6, 573 (1965)

47. Klimenko, N.M., and M.E. Dyatkina: J. Struct. Chem., 6, 714 (1965)

48. Abramowitz, M., and I.A. Stegun, eds.: "Handbook of Mathematical Functions", AMS 55, Natl. Bur. Std. (U.S.)

49. Burden, F.R.: personal communication

50. Shavitt, I., and M. Karplus: J. Chem. Phys., 43, 398 (1965)

51. Kern, C.W., and M. Karplus: J. Chem. Phys., 43, 415 (1965)

52. Columbia University Molecular Property Program, QCPE 145.

53. Nelson, R.D., D.R. Lide, and A.A. Maryott: Natl. Std. Ref. Data Series, Natl. Bur. Std. (U.S.)(U.S. Government Printing Office, Washington, D.C., 1967), Vol. 10.

54. Kukolich, S.G.: J. Chem. Phys. 50, 3751 (1969)

55. Selwood, P.W.: "Magnetochemistry" (Interscience Publishers Inc., New York, 1956)

56. Harrison, J.F.: J. Chem. Phys., 47, 2990 (1967)

57. Aung, S., R.M. Pitzer, and S.I. Chan: J. Chem Phys., 49, 2071 (1968)

58. Gordy, W., W.V. Smith and R.F. Trambarulo: "Microwave Spectroscopy" (John Wiley and Sons Inc., New York, 1953)

59. Schoolery, J.N., and A.H. Sharbaugh: Phys. Rev., 82, 95 (1951)

60. Lawrance, R.B., and M.W.P. Strandberg: Phys. Rev., 83, 363 (1951)

61. Huttner, W., M. Lo, and W.H. Flygare: J. Chem. Phys., 48, 1206 (1968)

62. Oka, T.: J. Phys. Soc. Japan, 15, 2274 (1960)

63. Flygare, W.H., J.M. Pochan, G.I. Kerley, T. Caves, M. Karplus, S. Aung, R.M. Pitzer, and S.I. Chan: J. Chem. Phys., 45, 2793 (1966)

64. Neumann, D., and J.W. Moskowitz: J. Chem. Phys., 49, 2056 (1968)

65. Barnes,E.E., and W.T. Simpson: J. Chem. Phys., 39, 670 (1963)

66. McMurry, H.L.: J. Chem. Phys., 9, 231 (1941)

67. Udvarhazi, A., and M.A. El-Sayed: J. Chem. Phys., 42, 3335 (1965)

68. Johnson, W.C., and W.T. Simpson: J. Chem. Phys., 48, 2168 (1968)

69. Price, W.C.: J. Chem. Phys., 3, 256 (1935)

70. Fleming, G., M.M. Anderson, A.J. Harrison, and L.W. Pickett: J. Chem. Phys., 30, 351 (1959)

71. Pople, J.A., and J.W. Sidman: J. Chem. Phys., 27, 1270 (1957)

72. Dunning, T.H., and V. McKoy: J. Chem. Phys., 48, 5263 (1968)

73. Dunning, T.H., N.W. Winter, and V. McKoy: J. Chem. Phys., 49, 4128 (1968)

74. Burns, G.: J. Chem. Phys., 41, 1521 (1964)

75. Slater, J.C.: Phys. Rev., 36, 51 (1930)

76. Clementi, E., and D.L. Raimondi: J. Chem. Phys., 38, 2686 (1963)

77. Sauterey, R: Compt. Rend., 229. 884 (1949)

78. Price, W.C., and T.M. Sugden: Trans. Faraday Soc., 44, 108 (1948)

79. Samson, J.A.R., and G.R. Cook: Bull. Am. Phys. Soc., 4, 454 (1959)

80. Neumann, D., and J.W. Moskowitz: J. Chem. Phys., 49, 2056 (1968)

81. Kaldor, U., and I. Shavitt: J. Chem. Phys., 45, 888 (1966)

82. Frost, D.C., C.A. McDowell, and D.A. Vroom: Can. J. Chem., 45, 1343 (1967)

83. Roney, B.D., T.M. Spotswood and M.L. Heffernan: "Matrix Elements for Configuration Interaction" Rept. Organic Chemistry Dept., Univ. of Adelaide (Oct., 1967)

84. Roney, B.D., T.M. Spotswood, M.L. Heffernan, and P.H. James: "Integral Evaluation Routines Package" Rept. Organic Chemistry Dept., Univ. of Adelaide (May, 1968)

Report of Organic Chemistry Department, University of Adelaide, May 1968.

INTEGRAL EVALUATION ROUTINES PACKAGE

B.D. Roney[†], T.M. Spotswood[†], M.L. Heffernan[¶] and B.H. James[¶]

Abstract:- A series of interrelated routines for the computation of one- and two-electron integrals is described. Treated specifically are overlap, kinetic energy, exchange nuclear attraction and coulomb repulsion integrals; auxiliary functions provide the user with access to other types. The package is coded in FORTRAN IV, and operable on any installation possessing the appropriate compiler.

A. GENERAL

Theoretical calculations of molecular electronic structure in the LCAO-MO approximation require the computation of a large number of integrals over atomic orbitals. As basis functions, Slater-type orbitals (STO's) in real form are commonly employed, and analytic formulations in terms of a variety of auxiliary functions have been proposed for the evaluation of the resultant integrals.

The auxiliary function $C_{\alpha\beta}^{\gamma\delta\varepsilon}(\rho_a,\rho_b)$[1] is particularly convenient, due to its general applicability over a wide range of one- and two-electron operators.[1,2] The P-, Q- and R-functions of Klimenko and Dyatkina[3] provide a completely general method for the evaluation of the C-functions.

This report describes a series of integral evaluation routines based essentially on the C-function route,[3,4] but modified to satisfy the requirements

[†] Department of Organic Chemistry, University of Adelaide, South Australia.

[¶] Chemistry Department, Monash University, Clayton, Victoria.

of speed and accuracy. A limitation to STO's of principal quantum number, n, not greater than 3 has been arbitrarily imposed in the routines. Since the methods are of general application, extension to orbitals of higher integral n does not involve substantial alteration.

The one-electron integrals treated specifically are overlap, kinetic energy and exchange nuclear attraction; a single subroutine (SZE) evaluates all three types simultaneously, a feature we consider desirable. Coulomb repulsion integrals are generated by function reference (CALG4), and, of more general utility, C-, D- and I-functions (defined below) are calculated by specific subprograms.

B. ANALYTIC FORMS OF THE INTEGRALS AND AUXILIARY FUNCTIONS

χ_{nlm} or (nlm) is the Slater type orbital with parameters n, l, m and orbital exponent ξ.

I. One-electron Integrals:[1,4]

a. overlap

$$(nlm_a|nlm_b) = k_a.k_b.\nu^{n_{a+1/2}}.D^{\gamma\delta\varepsilon}_{\alpha\beta}(\rho_a,\rho_b)$$

b. kinetic energy

$$(nlm_a|-1/2\Delta|nlm_b) = -1/2\xi_a^2.k_a.k_b.\{\nu^{n_{a+1/2}}.D^{\gamma\delta\varepsilon}_{\alpha\beta}(\rho_a,\rho_b) - 2n_a.\nu^{n_{a-1/2}}.$$

$$D^{\gamma\delta\varepsilon}_{\alpha-1,\beta}(\rho_a,\rho_b) + (n_a + l_a).(n_a - l_a - 1).D^{\gamma\delta\varepsilon}_{\alpha-2,\beta}(\rho_a,\rho_b)\}$$

exchange nuclear attraction

c. $$(nlm_a|-\frac{Z_a}{r_a}|nlm_b) = -Z_a.\xi_a.k_a.k_b.\nu^{n_{a-1/2}}.D^{\gamma\delta\varepsilon}_{\alpha-1,\beta}(\rho_a,\rho_b)$$

d. $$(n\ell m_a|-\frac{Z_b}{r_b}|n\ell m_b) = -Z_b.\xi_a.k_a.k_b.\nu^{n_a-1/2}.D^{\gamma\delta\varepsilon}_{\alpha,\beta-1}(\rho_a,\rho_b)$$

with $m = m_a = m_b$

Z is nuclear charge

$$k_p = \frac{2^{n_p-\ell_p}.(2\ell_p)!(2\ell_p+1)^{1/2}}{\ell_p![(2n_p)!(\ell_p-|m|)!(\ell_p+|m|)!]^{1/2}}$$

$$\nu = \xi_a/\xi_b$$

$$\alpha = n_a-\ell_a, \quad \beta = n_b-\ell_b, \quad \gamma = \ell_a-|m|, \quad \delta = \ell_b-|m|, \quad \varepsilon = |m|$$

$$\rho_a = \xi_a.R, \quad \rho_b = \xi_b.R \quad (R = \text{internuclear distance})$$

e. $$D^{\gamma\delta\varepsilon}_{\alpha\beta}(\rho_a,\rho_b) = \sum_p \sum_q C^a_p.C^b_q.C^{\gamma-2p,\delta-2q,\varepsilon}_{\alpha+2p,\beta+2q}(\rho_a,\rho_b)$$

$$C_o = 1, \quad C_p = \frac{(\ell-|m|).(\ell-|m|-1)..(\ell-|m|-2p+1)}{2^1.2^2....2^p.(2\ell-1)(2\ell-3)...(2\ell-2p+1)}.(-1)^p$$

II. Coulomb Repulsion Integral.[1,4]

a. $$(n\ell m_a,n'\ell'm'_a|n\ell m_b,n'\ell'm'_b) = W_a.W_b \sum_{LM_a} \sum_{LM_b} a_{NLM_a}.a_{NLM_b}.[NLM_a|NLM_b]\ \delta_{M_a,M_b}$$

with $M = M_a = M_b$

$$W = \frac{(1+\tau)^{n+1/2}.(1-\tau)^{n'-1/2}}{[(2n)!(2n')!]^{1/2}}$$

$$\tau = \frac{\xi-\xi'}{\xi+\xi'}, \quad N = n+n'-1$$

$$a_{NLM} = (N+L+L)!a'_{LM}$$

The basic charge distributions and coefficients a'_{LM} from Table I of reference 4.

b. $[NLM_a|NLM_b] = K_{ab}\bar{\xi}_b \sum_p \sum_q C_p^a . C_q^b . I_{\lambda+2p,\beta+2q}^{\gamma-2p,\delta-2q,\varepsilon}(\rho_a,\rho_a^*,\rho_b)$

$K_{ab} = (2L_a)!(2L_b)!(2L_b+1)/L_a!L_b![(L_a-M)!(L_a+M)!(L_b-M)!(L_b+M)!]^{1/2}$

$\cdot(N_b+L_b+1)!$

$\bar{\xi} = 1/2(\xi+\xi')$

C_p, C_q as above, but defined by L, M rather than l,m.

$\rho_a = 0, \quad \rho_a^* = 2\bar{\xi}_a . R, \quad \rho_b = 2\bar{\xi}_b . R$

$\lambda = -2L_a, \quad \beta = N_b - L_b, \quad \gamma = L_a - |M|, \quad \delta = L_b - |M|, \quad \varepsilon = |M|$

c. $I_{\lambda\beta}^{\gamma\delta\varepsilon}(\rho_a,\rho_a^*,\rho_b) = (2\mu)^{-L_a}\{C_{\lambda\beta}^{\gamma\delta\varepsilon}(\rho_a,\rho_b) - \sum_{m=o}^{N_a+L_a} u_m (2\mu)^m C_{\lambda+m,\beta}^{\gamma\delta\varepsilon}(\rho_a^*,\rho_b)$

$\mu = \dfrac{\rho_a^*-\rho_a}{2\rho_b}$

$u_m = 1/m! \quad \text{for} \quad 0 \leq m \leq 2L$

$u_m = 1/m! - \dfrac{(N-L)!}{(N+L+1)!(m-2L-1)!} \quad \text{for} \quad 2L+1 \leq m \leq N+L$

III. C-Function[3]

a. $C_{\alpha\beta}^{\gamma\delta\varepsilon}(\rho_a,\rho_b) = \rho_b^{\alpha+\beta+\gamma+\delta+2\varepsilon+1} \sum_{r=0}^{\gamma+\delta+2\varepsilon} \sum_{s=0}^{\gamma+\delta+2\varepsilon-r} . a_{rs}^{\gamma\delta\varepsilon} . T_{\alpha+2r,\beta+2s}(\rho_a,\rho_b)$

b. $a_{rs}^{\gamma\delta\varepsilon} = \dfrac{(-1)^{\varepsilon}\gamma!\delta!\varepsilon!}{2^{\gamma+\delta+2\varepsilon}} \cdot \sum_{\gamma_2=0}^{\gamma} \sum_{\gamma_3=0}^{\gamma-\gamma_2} \sum_{\delta_2=0}^{\delta} \sum_{\delta_3=0}^{\delta-\delta_2} \cdot \sum_{\varepsilon_2=0}^{\varepsilon} \sum_{\varepsilon_3=0}^{\varepsilon-\varepsilon_2} \sum_{\varepsilon_4=0}^{\varepsilon-\varepsilon_2-\varepsilon_3}$

$\sum_{\varepsilon_5=0}^{\varepsilon-\varepsilon_2-\varepsilon_3-\varepsilon_4} \sum_{\varepsilon_6=0}^{\varepsilon-\varepsilon_2-\varepsilon_3-\varepsilon_4-\varepsilon_5} \cdot \dfrac{(-1)^{\gamma_3+\delta_2+\varepsilon_2+\varepsilon_3+\varepsilon_4} \cdot 2^{\varepsilon_2+\varepsilon_3+\varepsilon_4}}{\gamma_1!\gamma_2!\gamma_3!\delta_1!\delta_2!\delta_3!\varepsilon_1!\varepsilon_2!\varepsilon_3!\varepsilon_4!\varepsilon_5!\varepsilon_6!}$

with $\gamma_1+\gamma_2+\gamma_3 = \gamma$

$\delta_1+\delta_2+\delta_3 = \delta$

$\varepsilon_1+\varepsilon_2+\varepsilon_3+\varepsilon_4+\varepsilon_5+\varepsilon_6 = \varepsilon$

$r = \gamma_2+\delta_2+\varepsilon_2+\varepsilon_4+2\varepsilon_5$

$s = \gamma_3+\delta_3+\varepsilon_3+\varepsilon_4+2\varepsilon_6$

c. $$T_{ij}(\rho_a,\rho_b) = j! \sum_{k=0}^{j} \sum_{l=0}^{j-k} \frac{1}{\rho_b^{k+1}.l!(j-k-l)!}.\{(-1)^{j-k-l} e^{\rho_b} P_{i+l}(\rho_a,\rho_b)$$

$$+ e^{-\rho_b}(-1)^l P_{i+l}(\rho_a,\rho_b) - e^{-\rho_b} Q_{i+l}(\rho_a,\rho_b)\}$$

d. $$P_n(\theta) = \frac{1}{2^{n+1}} \int_2^\infty e^{-\frac{\theta}{2}x}.x^n dx$$

$$Q_n(\theta) = \frac{1}{2^{n+1}} \int_0^\infty e^{-\frac{\theta}{2}x}.x^n dx$$

$$R_n(\Phi) = \frac{1}{2^{n+1}} \int_0^2 e^{-\frac{\Phi}{2}x}.x^n dx$$

with $\theta = \rho_a + \rho_b$, $\Phi = \rho_a - \rho_b$

Analytic formulation of the integrals above (IIId) is deferred to Section D.

C. COMPUTATION OF THE INTEGRALS AND AUXILIARY FUNCTIONS

Efficient processing of the integrals and auxiliary functions is attained by expansion in terms of the basic P-, Q- and R-functions above.

The functions $a_{rs}^{\gamma\delta\varepsilon}$ are independent of orbital exponents and hence transferrable among the different types of integrals and auxiliary functions. In fact, the 9-stage summation which appears in their analytic form is such a time-consuming process that their generation and storage external to integral

computation is a necessary step if efficiency in their usage is to be realised. All of the integrals involving STO's of principal quantum $n < 3$ are calculable using a-functions with parameters r, s, γ, δ, ϵ limited to the range tabulated below:

Parameter	Min.	Max.
ϵ	0	4
γ	0	$4-\epsilon$
δ	0	$4-\epsilon$
r	0	$\gamma+\delta+2\epsilon$
s	0	$\gamma+\delta+2\epsilon-r$

Similarly, the individual P_n-, Q_n- and R_n-functions are usually required more than once in the computation of a given integral or auxiliary function. By contrast with the a-functions, they are not independent of the orbital exponents, so that each new case requires a different set, over, possibly, a new range of n. The range of n is simply determined from the parameters which define the integral (orbital quantum numbers) or auxiliary function (α,β etc.). The limits are tabulated below:

Integral or Auxiliary function	Parameters of P-,Q-,R-functions	Min(n)	Max(n)
One-electron integrals (overlap, kinetic energy, nuclear attraction)	ρ_a, ρ_b	0	$n_a+n_b+l_a+l_b$
Coulomb repulsion integral	ρ_a, ρ_b	$-2L_a^\dagger$	$N_b+L_b^\dagger$
	ρ_a^*, ρ_b	$-2L_a^\dagger$	$N_a+N_b+L_a^\dagger+L_b^\dagger$
$I_{\lambda\beta}^{\gamma\delta\varepsilon}(\rho_a,\rho_a^*,\rho_b)$	ρ_a, ρ_b	λ	$\lambda+\beta+2(\gamma+\delta+2\varepsilon)$
	ρ_a^*, ρ_b	λ	$\lambda+\beta+2(\gamma+\delta+2\varepsilon)+N_a+L_a^\dagger$
$C_{\alpha\beta}^{\gamma\delta\varepsilon}$ and $D_{\alpha\beta}^{\gamma\delta\varepsilon}(\rho_a,\rho_b)$	ρ_a, ρ_b	α	$\alpha+\beta+2(\gamma+\delta+2\varepsilon)$

$L^\dagger$ is the maximum value achieved by L over the range of charge distributions (NLM|.

An efficient computational form for the $I_{\lambda\beta}^{\gamma\delta\varepsilon}(\rho_a,\rho_a^*,\rho_b)$ functions is illustrated by the following expansion in terms of P-, Q-, and R-functions:

$$I_{\lambda\beta}^{\gamma\delta\varepsilon}(\rho_a,\rho_a^*,\rho_b) = (2\mu)^{-L_a}\,\rho_b^{\alpha+\beta+\gamma+\delta+2\varepsilon+1} \sum_{r=0}^{\gamma+\delta+2\varepsilon} \sum_{s=0}^{\gamma+\delta+2\varepsilon-r} \sum_{k=0}^{\beta+2s} \sum_{l=0}^{\beta+2s-k}$$

$$\frac{a_{rs}^{\gamma\delta\varepsilon}\cdot(\beta+2s)!}{l!\,(\beta+2s-k-l)!}\cdot\Big\{(-1)^{\beta+2s-k-l}\cdot e^{\rho_b}\,[P_{\lambda+2r+l}(\rho_a,\rho_b) - \sum_{m=0}^{N_a+L_a} u_m\,(\rho_a^*-\rho_a)^m P_{\lambda+2r+l+m}$$

$$(\rho_a^*,\rho_b)] + e^{-\rho_b}\,\big((-1)^l[R_{\lambda+2r+l}(\rho_a,\rho_b) - \sum_{m=0}^{N_a+L_a}(\rho_a^*-\rho_a)^m\cdot R_{\lambda+2r+l+m}(\rho_a^*\rho_b)] -$$

$$[Q_{\lambda+2r+l}(\rho_a,\rho_b) - \sum_{m=0}^{N_a+L_a} u_m\,(\rho_a^*-\rho_a)^m Q_{\lambda+2r+l+m}(\rho_a^*,\rho_b)]\big)\Big\}$$

The expressions enclosed by square brackets [] may be evaluated externally for each required value of the index $(\lambda+2r+7)$, thereby introducing a substantial saving in computation on each occasion that the particular summation is required. Coulomb repulsion integrals may be similarly treated, once the expansion into basic charge distributions $(NLM_a|NLM_b)$ has been made - N_a and L_a serve to define both the limits of the summation over m, and the function u_m.

D. EVALUATION OF THE FUNCTIONS $P_n(\theta)$, $Q_n(\theta)$ AND $R_n(\Phi)$

Several analytic forms[3] are available for the computation of the integrals IIId of section B. Most are stable over only a fairly limited range of the parameters θ or Φ. In our pilot calculations we considered θ and Φ in the range $\pm 0{,}001$ to ± 100, n in the range -8 to +18; the methods outlined below are the fastest, consistent with an error not greater than 1 in the 11th figure.†

I. $n > 0$

a. $P_n(\theta)$ by forward recurrence from $P_o(\theta) = \theta^{-1} e^{-\theta}$, $P_n = \theta^{-1} (e^{-\theta} + P_{n-1})$, all θ

b. $Q_n(\theta)$ by forward recurrence from $Q_o(\theta) = \theta^{-1}$, $\quad Q_n = n\theta^{-1} Q_{n-1}$, all θ

c. $R_n(\Phi) = Q_n(\Phi)$, $\Phi \geq 80$ $\quad (I_b;\ \theta \leftrightarrow \Phi)$

d. $R_n(\Phi)$ by forward recurrence from $R_o(\Phi) = \Phi^{-1}(1-e^{-\Phi})$, $R_n = \Phi^{-1}(nR_{n-1} - e^{-\Phi})$, $9 \leq \Phi < 80$ and $-40 < \Phi \leq -8$

e. $R_n(\Phi)$ by backward recurrance from $P_m(\Phi)$, m = most positive value of n,

---

† Calculations on CDC 6400 computer system, with 60-binary bit word, equivalent to approximately 14 significant digits.

$$R_m(\Phi) = \frac{m!\,e^{-\Phi}}{\Phi^{m+1}} \sum_{p=m+1}^{\infty} \frac{\Phi^p}{p!}, \quad R_{n-1} = n^{-1}(\Phi R_n + e^{-\Phi}), \quad -8 < \Phi < 9, \ \Phi \neq 0$$

f. $R_n(0) = 1/(n+1)$

g. $R_n(\Phi) = -P_n(\Phi)$, $\Phi \leq -40$ (I_a; $\theta \leftrightarrow \Phi$)

II. $n < 0$

m = most negative value of n

a. $P_n(\theta)$ by forward recurrence from $P_{-1}(\theta) = E_i(-\theta)$[4], $E_i(-\theta) = C + \ln\theta +$

$$\sum_{p=1}^{\infty} \frac{(-\theta)^p}{p.p!}$$ (C - Euler's constant) $P_{n-1} = n^{-1}(-e^{-\theta} + \theta P_n)$, $0 < \theta < 4$

b. $P_n(\theta)$ by backward recurrence from $P_m(\theta)$ by continued fraction[5] =

$$e^{-\theta}\left(\frac{1}{\theta -} \frac{m}{1 +} \frac{1}{\theta -} \frac{m-1}{1 +} \frac{2}{\theta -} \cdots\right), \quad P_n = \theta^{-1}(e^{-\theta} + nP_{n-1}) \quad \theta \geq 4$$

c. $$Q_n(\theta) = -\frac{(-\theta)^{-n-1}}{(-n-1)!}\left\{C + \ln + \sum_{p=0}^{-n-2} \frac{1}{n+p+1}\left(1 + \frac{(-n-1)!(-\theta)^{n+p+1}}{p!}\right)\right\}$$ all θ

d. $R_n(\Phi) = Q_n(\Phi)$ $\Phi \geq 40$ (II_c; $\theta \leftrightarrow \Phi$)

e. $$R_n(\Phi) = -\frac{(-\Phi)^{-n-1}}{(-n-1)!}\left\{C + \ln|\Phi| - E_i(-\Phi) + \sum_{p=0}^{-n-2}\left[\frac{1}{n+p+1}\left\{1 + \frac{(-n-1)!(-\Phi)^{n+p+1}}{p!}\right)\right.\right.$$

$$\left.\left. + e^{-\Phi}\,(-n-p-2)!\,.\,(-\Phi)^{n+p+1}\right]\right\}, \quad 2 \leq \Phi < 40$$

$E_i(-\Phi)$ by continued fraction[5]

$$= -e^{-\Phi}\left(\frac{1}{\Phi +} \frac{1}{1 +} \frac{1}{\Phi +} \frac{2}{1 +} \frac{2}{\Phi +} \frac{3}{1 +} \cdots\right)$$

f. $R_n(\Phi)$ by series expansion $R_n(\Phi) = \sum_{p=-n}^{\infty} \frac{(-\Phi)^p}{p!\,(n+p+1)}$ $\quad -2 < \Phi < 2,\ \Phi \neq 0$

g. $R_n(0) = 0$

h. $R_n(\Phi)$ in the range $-40 < \Phi < -2$ may be calculated by IIf, but the series becomes more slowly convergent as $|\Phi|$ increases. In this range $Q_n(\Phi)$ (IIc) is stable, and $P_n(\Phi)$ is stable to back recurrence (but not forward). The fastest procedure is (a) generate $R_m(\Phi)$ by IIf, and $Q_n(\Phi)$ over all $n < 0$, (b) $P_m(\Phi) = Q_m(\Phi) - R_m(\Phi)$, then (c) $R_n(\Phi)$, $(n > m)$ is evaluated by $R_n(\Phi) = Q_n(\Phi) - P_n(\Phi)$, with $P_n(\Phi)$ by back recurrence (IIb; $\theta \leftrightarrow \Phi$). Despite its complexity this method is considerably faster than IIf.

i. $R_n(\Phi) = -P_n(\Phi)$, $\Phi < -40$ (IIb; $\theta \leftrightarrow \Phi$). In normal usage, $\theta > 0$, and the θ, Φ interchange represents special cases of $\theta < 0$ which would never be otherwise encountered for the functions P_n and Q_n.

E. SPECIAL CASE OF ONE-CENTRE INTEGRALS (R=0)

The integrals and auxiliary functions for R=0 may be expressed, as in section D, in terms of the appropriate C-function,[1a] where

$$\lim_{\rho \to 0} \; C^{\gamma\delta\varepsilon}_{\alpha\beta}(\rho_a, \rho_b) = C^{\varepsilon}_{\gamma+\delta} \cdot (-1)^{\delta} \cdot (\alpha+\beta+\gamma+\delta+2\varepsilon)! \cdot \left(\frac{\xi_b}{\xi_a+\xi_b}\right)^{\alpha+\beta+\gamma+\delta+2\varepsilon+1}$$

with

$$C^{\varepsilon}_{\omega} = 0 \quad \text{for } \omega \text{ odd}$$

$$C^{\varepsilon}_{\omega} = 2^{2\varepsilon+1} \cdot \varepsilon!\,\omega!\,(\omega/2+\varepsilon)!\,/\,(\omega/2)!\,(\omega+2\varepsilon+1)! \quad \text{for } \omega \text{ even}$$

SUBROUTINE FACGEN

Purpose: Calculates in array BF the values of 0! to 99! Entry is by BF (I+1) = I!, i.e. 0! is stored in the first element of BF.

Calling Sequence: CALL FACGEN (BF)

Parameters: BF (100)

Language: FORTRAN IV

Author: B.D. Roney, Department of Organic Chemistry, University of Adelaide.

SUBROUTINE AGENT

Purpose: Stores in array AFUN the $a_{rs}^{\gamma\delta\varepsilon}$ functions, and in array INDA, a composite index required to enter AFUN. A particular $a_{rs}^{\gamma\delta\varepsilon}$ is placed in AFUN at location (r+1, s+1, IND), with IND=INDA (γ+1, δ+1, ε+1). The ranges of the parameters are as previously defined in section D. The actual computation of the a-functions is performed by function reference from AGENT to A(IR, IS, K, L, M) where

IR=r, IS=s, K=γ, L=δ, M=ε

Calling Sequence: CALL AGENT (INDA, AFUN)

Parameters: INDA(5, 5, 5), AFUN(9, 9, 55)

Timing: Approx. 11 seconds to compute all a-functions in the defined range.

Special Notes: AGENT is called external to the integral evaluation routines.

Language: FORTRAN IV.

Author: B.D. Roney, Department of Organic Chemistry, University of Adelaide.

SUBROUTINE PQRN

Purpose: To generate and store in arrays P, Q and R the P_n-, Q_n- and R_n-functions over a specified range of the parameter n, as defined by the parameters NMIN (most negative) and NMAX (most positive). An indexing parameter, IREF, is set to define the relationship between the particular P_n-, Q_n-, or R_n-function and its location in the corresponding array - note that NMIN must always be set zero or negative, since IREF = 1-NMIN, and in particular, the recurrence relations (section D) assume $n = 0$ as initial value for computation of the functions with $n > 0$. e.g. P_{nmin} is placed in location P(1), P_{nmax} in location P(NMAX-NMIN + 1).

Calling Sequence: CALL PQRN (RO, RT, NMIN, NMAX, P, Q, R, BF, IREF)

Parameters: RO is the parameter $\theta = \rho_a + \rho_b$

RT is the parameter $\Phi = \rho_a - \rho_b$

NMIN, NMAX, IREF as above

P, Q, R are each dimensioned at 40

BF (100) is array of factorials (see SUBROUTINE FACGEN)

Language: FORTRAN IV

Author: B.D. Roney, Department of Organic Chemistry, University of Adelaide.

FUNCTION A

Purpose: Generates the individual $a_{rs}^{\gamma\delta\epsilon}$-function, usually by call from SUBROUTINE AGENT. Alternatively, the integral evaluation routines may be modified to directly reference this function - unless only a few integrals are to be computed, the former procedure of external evaluation is strongly recommended.

Calling Sequence: X = A (IR, IS, IT, JT, MT)

Parameters: IR = r, IS = s, IT = γ, JT = δ, MT = ϵ

Common Usage: /FACL/BF (100)

Array of factorials, BF, is required in the labelled COMMON block, FACL.

Language: FORTRAN IV

Author; B.D. Roney, Department of Organic Chemistry, University of Adelaide.

SUBROUTINE SZE

Purpose: Generates the one-electron integrals, overlap, kinetic energy and exchange nuclear attraction (centres a and b). The method is based primarily on the expansion of the corresponding D-functions in terms of P-, Q- and R-functions, but coded to take maximum advantage of the similarities which exist. Subroutine PQRN is required, as also is the externally generated array of $a_{rs}^{\gamma\delta\epsilon}$-functions (see subroutine AGENT).

Calling Sequence: CALL SZE (S, E, ZA, ZB, NA, LA, MA, XA, CA, NB, LB, MB, XB, CB, ABK, INDA, AFUN).

Parameters: S contains the overlap integral

E contains the kinetic energy integral

ZA contains the exchange nuclear attraction integral, centre A

ZB contains the exchange nuclear attraction integral, centre B

Note: ZB is returned zero if both orbitals are on the same centre.

NA, LA, MA, XA, CA are respectively the parameters for orbital a:-

n, l, m, ξ and core charge of centre a.

NB, LB, MB, XB, CB ditto - orbital b.

ABK contains the product $k_a.k_b$ (see Section B)

INDA, AFUN are the storage locations of $a_{rs}^{\gamma\delta\epsilon}$ functions, dimensioned (5,5,5) and (9,9,55).

Common Usage: Two labelled COMMON areas are used - (a) /FACL/BF (100) contains factorials; (b) /CFUN/XXX (300), OD

XXX is split into arrays required by SZE;

OD is preset before calling with the internuclear distance.

Additional Routines: SUBROUTINE PQRN

Language: FORTRAN IV

Author: B.D. Roney, Department of Organic Chemistry, University of Adelaide.

FUNCTION C

Purpose: Evaluates the $C_{\alpha\beta}^{\gamma\delta\epsilon}$-function as an expansion in terms of P-, Q- and R-functions. Assumes $a_{rs}^{\gamma\delta\epsilon}$ functions calculated externally and stored in arrays INDA, AFUN.

Calling Sequence: X = C (I, J, K, L, M, XA, XB, INDA, AFUN)

Parameters: I = α, J = β, K = γ, L = δ, M = ϵ

XA and XB are the orbital exponents ξ_a and ξ_b

INDA, AFUN contain the preset $a_{rs}^{\gamma\delta\epsilon}$ functions

(SUBROUTINE AGENT).- dimensioned (5,5,5) and (9,9,55)

Common Usage: Two labelled COMMON areas are required

/FACL/BF (100) contains array of factorials

/CFUN/XXX (300), OD

XXX is split into arrays local to C

OD contains internuclear distance, and must be preset prior to function reference.

Additional Routines: SUBROUTINE PQRN

Language: FORTRAN IV.

Author: B.D. Roney, Department of Organic Chemistry, University of Adelaide.

FUNCTION D

Purpose: Evaluates the $D_{\alpha\beta}^{\gamma\delta\epsilon}$-functions by expansion into the P-, Q- and R-functions. Arrays INDA and AFUN are assumed preset to contain the $a_{rs}^{\gamma\delta\epsilon}$-functions (SUBROUTINE AGENT).

Calling Sequence: X = D (I, J, K, L, M, LA, MA, LB, MB, XA, XB, INDA, AFUN)

Parameters: I = α, J = β, K = γ, L = δ, M = ϵ

LA, MA are the parameters for orbital a, l_a, m_a

LB, MB ditto, orbital b.

XA and XB are the orbital exponents ξ_a and ξ_b.

INDA, AFUN are storage locations for the $a_{rs}^{\gamma\delta\epsilon}$-functions, dimensioned at (5,5,5) and (9,9,55)

Common Usage: Two labelled COMMON blocks are required.

(a) /FACL/BF (100) contains factorials.

(b) /CFUN/XXX (300), OD

XXX is split up into arrays local to D

OD must be preset before calling with the internuclear distance

Additional Routines: SUBROUTINE PQRN is required

Language: FORTRAN IV

Author: B.D. Roney, Department of Organic Chemistry, University of Adelaide.

FUNCTION EYE

Purpose: Evaluates the $I_{\lambda\beta}^{\gamma\delta\varepsilon}(\rho_a, \rho_a^*, \rho_b)$ functions by expansion into P-, Q- and P-functions. The $a_{rs}^{\gamma\delta\varepsilon}$ functions are assumed preset in arrays INDA and AFUN.

Calling Sequence: X = EYE (II, JJ, KK, LL, MM, NA, LA, XA, XAA, XB, INDA, AFUN)

Parameters: II = λ, JJ = β, KK = γ, LL = δ, MM = ε

NA, LA are the parameters N_a, L_a of the basic charge distribution $(NLM_a|$

XA = ρ_a, XAA = ρ_a^*, XB = ρ_b

INDA, AFUN are storage locations for the $a_{rs}^{\gamma\delta\varepsilon}$ functions - dimensioned at (5,5,5), (9,9,55)

Common Usage: Two labelled COMMON areas

(a) /FACL/BF (100) contains array of factorials

(b) /CFUN/XXX (300), OD

XXX is split into arrays local to EYE

OD is dummy, since XA, XAA, XB contain all the information required concerning internuclear distance.

Additional Routines: SUBROUTINE PQRN is required

Language: FORTRAN IV

Author: B.D. Roney, Department of Organic Chemistry, University of Adelaide.

FUNCTION CALG4

Purpose: Evaluates the Coulomb repulsion integral. CALG4 is a rather special routine, as its current form is coded for computation within a LCAO-SCF program, rather than for isolated integrals. Assumed preset are the $a_{rs}^{\gamma\delta\varepsilon}$ functions in arrays INDA and AFUN, and two indexing parameters LJLM and KLLM in COMMON block INLMD

Calling Sequence: X = CALG4 (IX, JX, KX, LX, INDA, AFUN)

Parameters: IX, JX, KX and LX are indices which define the location of four orbitals (see below).

INDA and AFUN contain the preset $a_{rs}^{\gamma\delta\varepsilon}$ functions.

Common Usage: Blank COMMON is ordered as INTX (160), RELX (10), LM (70), NQ (70), LQ (70), MQ (70).

INTX and RELX are dummay arrays - in normal usage then contain information for LCAO-SCF calculation.

NQ, LQ, MQ contain the orbital parameters n, l and m.

LM contains a series of indices uniquely based on the l,m parameters of the orbitals. Array LM is computed as LM (I) = LQ(I)* LQ(I) + LQ(I) + MQ(I) + 1 i.e. $(lm) = l^2 + l + m + 1$, and serves as an index for entry to other arrays.

Labelled COMMON areas are -

(a) /FACL/BF (100): BF contains factorials

(b) /CFUN/XXX (300), OD:

XXX is split into arrays local to CALG4

OD must be preset prior to CALG4 reference with the internuclear distance.

(c) /INLMD/IJLM,KLLM:

IJLM and KLLM are preset prior to CALG4 reference by FUNCTION INDLM, IJLM and KLLM are indices based on the LM values of the orbitals, and serve as entries to arrays ALM and LMA (see below)

(d) /CALG/LMA(2,5,45), ALM(5,45)

LMA contains the parameters L and M of the basic charge distribution (NLM|, ALM the coefficient. e.g. LMA(1, 3, IJLM) and LMA(2, 3, IJLM) return, respectively the L and M parameters of the third charge distribution in the linear combination thereof which arises from the orbitals IX and JX. ALM(3, IJLM) returns the corresponding coefficient a'_{LM} (cf. section B, IIa) Arrays LMA and ALM are preset by DATA declarative statements in the calling program.

(e) /ORX/OEX(70): OEX contains orbital exponents, ξ

Additional Routines: SUBROUTINE PQRN is required

Language: FORTRAN IV

Author: B.D. Roney, Department of Organic Chemistry, University of Adelaide.

PROGRAM COULOMB

Purpose: Functions as a driver program for CALG4 (Coulomb repulsion integrals). COULOMB is coded to set up and calculate a few coulomb integrals for testing purposes (specifically $(2px_a, 2px_a \mid 2px_b, 2px_b)$, with equal and differing $\overline{\xi}_a$ and $\overline{\xi}_b$, over one- and two-centres).

Common Usage: As for CALG4, but containing the declarative DATA statements for arrays LMA and ALM. Also, an additional labelled COMMON area is defined:

/LMG/LMG4(1035)

LMG4 is preset by DATA statement as a quick reference array which determines if a particular coulomb integral (one- or two-centre) vanishes by orbital symmetry.

Additional Routines: FACGEN - factorials generated in BF.

AGENT, A - $a_{rs}^{\gamma\delta\epsilon}$ function generators

INDLM - determines index for entry to LMG4, and sets IJLM, KLLM indices for CALG4.

CALG4 and PQRN

Language: FORTRAN IV.

Author: B.D. Roney, Department of Organic Chemistry, University of Adelaide.

PROGRAM COMPOS

Purpose: Drive program for SUBROUTINE SZE, (one-electron integrals - overlap, kinetic energy and exchange nuclear attraction). Also for $C_{\alpha\beta}^{\gamma\delta\varepsilon}$, $D_{\alpha\beta}^{\gamma\delta\varepsilon}$ and $I_{\lambda\beta}^{\gamma\delta\varepsilon}$ functions. The I-function is actually used to compute a coulomb integral $(2p\pi_a, 2p\pi_a | 2p\pi_b, 2p\pi_b)$ through FUNCTION REP.

Common Usage: As for SZE or any of the auxiliary function generators.

Additional Routines: FACGEN, AGENT, A, SZE, C, D, REP, EYE, PORM.

Language: FORTRAN IV.

Author: B.D. Roney, Department of Organic Chemistry, University of Adelaide.

Acknowledgements: Two of us (B.H.J. and B.D.R.) acknowledge the award of Postgraduate Studentships (Commonwealth of Australia).

Bibliography:

(1a) Ruedenberg, K., C.C.J. Roothaan, and W. Jaunzemis: *J.Chem.Physics*, *24*, 201 (1956).

(1b) Roothaan, C.C.J.: *J.Chem.Physics*, *24*, 947 (1956).

(2) Fraga, S.: *Can.J.Chem.*, *42*, 2509 (1964)

(3) Klimenko, N.M., and M.E. Dyatkina: *Zh.strukt.khimii.*, *6*, 573 (1965) (in Eng.)

(4) Klimenko, N.M., and M.E. Dyatkina: *Zh.strukt.khimii.*, *6*, 714 (1965) (in Eng.)

(5) Abramowitz, M., and I.A. Stegun, eds.: *"Handbook of Mathematical Functions"*. AMS 55, National Bureau of Standards.

Report of Organic Chemistry Department, University of Adelaide, Oct. 1967.

MATRIX ELEMENTS FOR CONFIGURATION INTERACTION

B.D. RONEY and T.McL. SPOTSWOOD,

Department of Organic Chemistry, University of Adelaide,

Adelaide, South Australia.

and M.L. HEFFERNAN,

Department of Chemistry, Monash University,

Clayton, Victoria.

Summary

Interconfigurational matrix elements among mono-, di-, and tri-excited configurations, which contain no more than four non-closed-shell spin orbitals in the defining Slater determinants, have been tabulated for singlet and triplet spin states; the presentation is in a form readily adapted to automatic digital computation.

General

For the purposes of computer programming, excited configurations are most conveniently indexed by the molecular orbitals involved in the electronic excitation, which usage has been adopted in the following tables. For clarity, the alphabetic characters h, i, j (or p, r, s)* have been reserved as indices for orbitals which are doubly occupied in the ground configuration; similarly, k, l, m (or t, u, v)* denote virtual orbitals. Thus the diexcited configuration

---

* The configurational functions Ψ_a, Ψ_b in the general matrix element $H_{ab} = \int \Psi_a H \Psi_b \, d\tau$ are defined by the index sets (h, i, j, k, l, m) for Ψ_a and (p, r, s, t, u, v) for Ψ_b. The formal correspondence between the two sets is shown by the permutations (hp), (ir), (js), (kt), (lu), (mv), i.e. $h \leftrightarrow p$, $i \leftrightarrow r$, ... $m \leftrightarrow v$.